Reactivity of P_4 butterfly complexes

Dissertation zur Erlangung des

Doktorgrades der Naturwissenschaften (Dr. rer. Nat.)

an der
Naturwissenschaftlichen Fakultät IV
– Chemie und Pharmazie –
der Universität Regensburg

vorgelegt von Rebecca Grünbauer

aus Neustadt a. d. Waldnaab

Mai, 2020

Diese Arbeit wurde angeleitet von Prof. Dr. Manfred Scheer.

Promotionsgesuch eingereicht am:	30.04.2020
Tag der mündlichen Prüfung:	29.05.2020

Vorsitzende:	Prof. Dr. Julia Rehbein
Prüfungsausschuss:	Prof. Dr. Manfred Scheer
	Prof. Dr. Henri Brunner
	Prof. Dr. Frank-Michael Matysik

Universität Regensburg

Eidesstattliche Erklärung

Ich erkläre hiermit an Eides statt, dass ich die vorliegende Arbeit mit dem Titel *„Reactivity of P_4 butterfly complexes*“ ohne unzulässige Hilfe Dritter und ohne Benutzung anderer als der angegebenen Hilfsmittel angefertigt habe; die aus anderen Quellen direkt oder indirekt übernommenen Daten und Konzepte sind unter Angabe des Literaturzitats gekennzeichnet.

_____

Rebecca Grünbauer

This thesis was elaborated within the period from December 2016 until April 2020 in the Institute of Inorganic Chemistry at the University Regensburg under the supervision of Prof. Dr. Manfred Scheer.

Next to the results presented in this thesis the author contributed to the following publication:

Isomerism and dynamic behavior of bridging phosphaalkynes bound to a dicopper complex

A. Nicolay, M. S. Ziegler, D. W. Small, R. Grünbauer, M. Scheer, T. D. Tilley, *Chem. Sci.* **2020**, *11*, 1607-1616.

Preface

In the beginning of this thesis, a general introduction about the element phosphorus, P_4 activation and the current state of the P_4 butterfly chemistry is given. In chapter 2, the research objectives are laid out.

The following chapters (3-6) are composed as self-contained drafts suitable for future publications. Therefore, all chapters are structured to that effect with the paragraphs being: “Abstract”, “Introduction”, “Results and Discussion”, “Conclusion”, “Supplementary Information”, “Author Contributions” and “References”. If some of the presented results have already been partly discussed in other theses, the respective information is given in the paragraph “Author Contributions”.

In addition, due to reasons of uniformity, all chapters have the same text settings and the layout may vary in respect to the published versions. The consecutive numbering of compounds, figures, schemes and tables begins anew in each chapter for reasons of future publishing. The depicted molecular structures may differ in style due to layout requests from different journals.

The results presented in this thesis are summarized in the following chapters:

Chapter 3 – The butterfly complex [{Cp*Cr(CO)$_3$}$_3$(μ,η$^{1:1}$-P$_4$)] as a versatile ligand and its unexpected P$_1$/P$_3$ fragmentation route

Herein, the reactivity of the title compound towards Lewis acidic [M(CO)$_4$] fragments [M = Cr, Mo, W] is reported and subsequent reactions of the obtained products are delineated.

Chapter 4 – The reactivity of the P$_4$ butterfly ligand [{Cp'''Fe(CO)$_2$}$_2$(μ,η$^{1:1}$-P$_4$)] towards Lewis acids: Coordination vs. rearrangement

In this chapter the reactivity of the iron P_4 butterfly compound [{Cp‴Fe(CO)$_2$}$_3$(μ,η$^{1:1}$-P$_4$)] towards different Lewis acids is reported.

Chapter 5 – Reactivity of P$_4$ butterfly compounds towards NHCs: Generation of a novel metal bridged P$_2$ dumbbell complex

The as yet unexplored reactivity of the P_4 butterfly unit towards nucleophiles is investigated in this chapter. Within the investigations special emphasis is laid on the reaction with *N*-heterocyclic carbenes.

Chapter 6 – The P$_4$ butterfly complex [{Cp*Cr(CO)$_3$}$_2$(μ,η$^{1:1}$-P$_4$)]: a starting material for P$_4$ transfer processes

The lability of the Cr–P bonds in [{Cp*Cr(CO)$_3$}$_3$(μ,η$^{1:1}$-P$_4$)] is utilized obtain different P_4 butterfly complexes by means of a novel substituent exchange reaction pathway.

The second to last chapter of this thesis contains a thesis treasury presenting preliminary results. Finally, a comprehensive conclusion of all results presented in this thesis is given at the last chapter.

Für den wichtigsten Menschen in meinem Leben

“What are the three most important rules of the chemist?”

“Label clearly. Measure twice. Eat elsewhere.”

- Patrick Rothfuss, *The Name of the Wind* -

Table of content

1.Introduction

1.1 Elemental phosphorus and its allotropes

Elemental phosphorus has always sparked great interest in the scientific community. Its discovery was part of the quest for the search of the philosopher's stone and even today new elemental modifications are reported quite frequently.[1] The German alchemist *Henning Brand* was the first to obtain elemental phosphorus while boiling down urine to find the mystically acclaimed source of immortality.[2] Hereby, the contained phosphates were reduced yielding white phosphorus (P_4) the most prominent modification of this element. White phosphorus consists of tetrahedral P_4 molecules (Scheme 1a) and due to the high tension in the condensed P_3 rings this scaffold is highly reactive. Moreover, P_4 displays blueish chemiluminescent properties upon the reaction with oxygen. Therefore, it was given the Greek name "Φωσφόρος" (phōsphóros), which means light-bearer and subsequently the term "phosphorescence" (which is now used in a different photochemical context) was created.[1] P_4, the only molecular modification of phosphorus, is mainly found in the gaseous phase when heating any source of phosphorus above 280.5 °C. However, crystalline P_4 can be obtained as well, displaying a temperature dependent rearrangement from α-P_4 (cubic) at room temperature to β-P_4 (triclinic) below -76.9 °C and γ-P_4 (distorted *bcc*) when decreasing the temperature below -115 °C.[3]

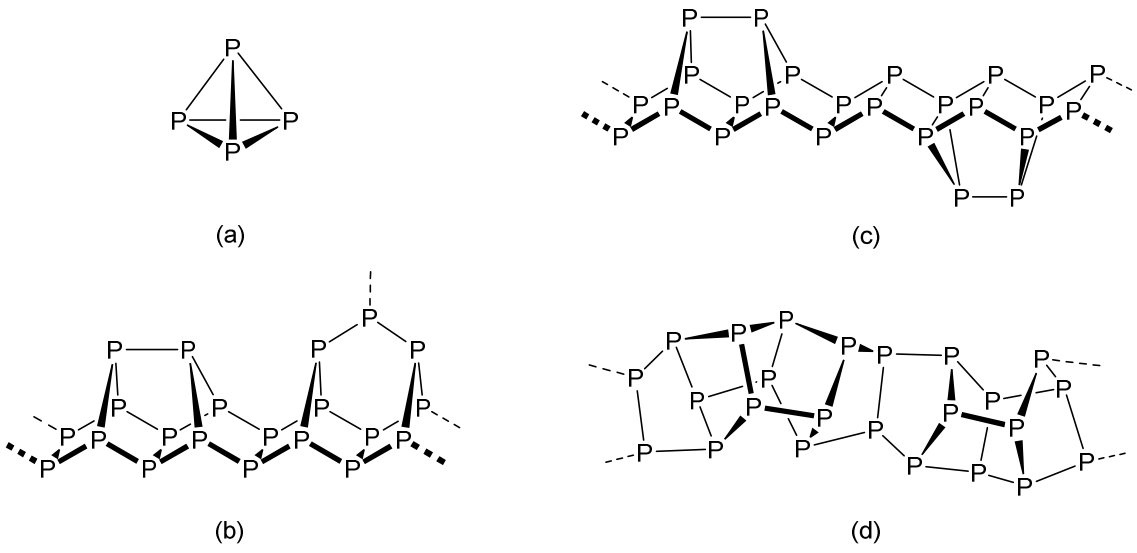

Scheme 1. Molecular structure of white phosphorus (a), the repetitive unit of the tubular allotrope found in violet and fibrous phosphorus (b) as well as the repetitive unit of two polymeric phosphorus strands isolated from a copper iodide matrix (c,d).

After the initial discovery of white phosphorus, more and more elemental modifications of phosphorus were identified and studied over the years. Different polymeric strand-like allotropes of phosphorus have been obtained by heating white phosphorus under the exclusion of oxygen. As phosphorus is highly oxophilic the exclusion of oxygen is of utmost importance. Otherwise, mere phosphorus oxide or phosphoric acid (in the presence of water) would be obtained from these reactions.[1a] The second most prominent phosphorus modification, the amorphous red phosphorus (P_{RED}), was first obtained by *A. Schrötter* and proved to be a

mixture of various polymeric phosphorus allotropes.[4] In 1947, *Roth et al.* reported that P_{RED} consists of different phases, of which Phase I, a mixture of different and not distinctly identifiable polymeric phosphorus allotropes, is classically referred to as P_{RED} nowadays.[5] By heating Phase I, four distinct phases (II, III, IV and V) could be isolated and subsequently studied in detail. However, Phase III is hitherto uncharacterized, which shows that there are still unanswered questions regarding the modifications of this essential element. The group of *Winchester* reported that Phase II incorporates unprecedented P-nanorods with a diameter of approx. 160 nm.[6] Phase IV and V both incorporate the same crosslinked phosphorus tubes, in which a zigzag-like P_2 ladder is capped by alternating P_8 and P_9 cages (Scheme 1b). Phase IV was first characterized by *Ruck et al.* and because of the parallel linkage of the phosphorus tubes (via the tips of the P_9 cages) this modification is also called fibrous phosphorus.[7] Phase V was first reported on by *J. W. Hittdorf* in 1865 and is called violet phosphorus or “Hittdorf´s phosphorus”.[8] Herein, the phosphorus tubes are connected in a perpendicular fashion in contrast to the parallel arrangement in fibrous phosphorus. Furthermore, the *Pfitzner* group could isolate two additional tube-like phosphorus allotropes from a copper iodide matrix.[9] These unprecedented phosphorus tubes are based on repetitive P_{12} motifs: one modification displays opposing P_8 cages on a zigzag-like P_2 band ($(CuI)_8P_{12}$—$^1_\infty$ [P8]P4(4)[, Scheme 1c), while in the other allotrope P_{10} cages are linked by P_2 dumbbells ($(CuI)_3P_{12}$—$^1_\infty$ [P10]P2[, Scheme 1d).

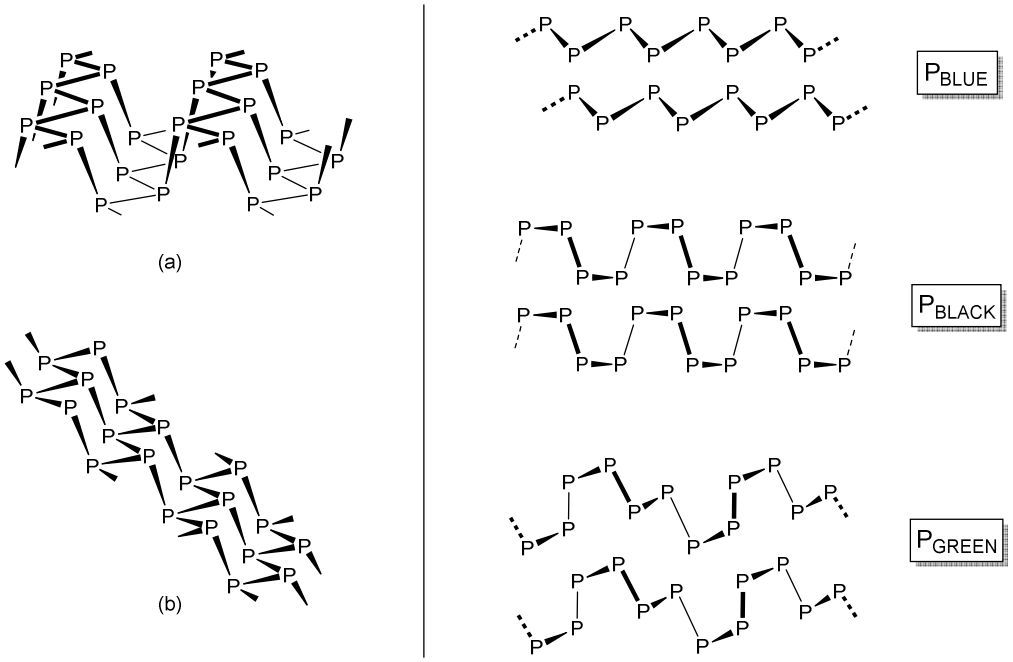

Scheme 2. Structural motifs found in layered allotropes of phosphorus; left: orthorhombic modification of P_{BLACK} at ambient conditions (a) and hexagonal modification of P_{BLACK} at high pressure (b); right: side view of monolayer stacking in P_{BLUE}, P_{BLACK} and P_{GREEN}.

Black phosphorus (P_{BLACK}), the thermodynamically preferred modification, was first isolated by *P. W. Bridgeman* in 1914. [10] Unlike the tube-like allotropes discussed before, it consists of monolayers of condensed P_6 rings in a chair-like conformation. In the orthorhombic sub-modification the P_6 rings are stacked in a parallel orientation (Scheme 2a), whereas at high pressure the P_6 rings are connected in a sloping fashion (Scheme 2b). This high-pressure structure is identical to the connectivity found in the grey arsenic allotrope,

the thermodynamically preferred modification of the heavier homologue of phosphorus.[1a] Recently, several groups reported on the extraction of thin monolayers from P_{BLACK}, called phosphorene, for optical as well as electronic investigations.[11] In contrast to the closely related graphene, phosphorene displays a thickness dependent band gap of 1.5 eV in the monolayer, while the band gap of bulk P_{BLACK} is given at 0.3 eV. Moreover, *Howard et al.* were able to synthetize phosphorene nanoribbons, which exhibit a range of unique chemical and physical properties.[12] Inspired by the fascinating properties of phosphorene, the study of new monolayered phosphorus allotropes has come to the attention of the scientific community. Two theoretically proposed representatives are the so called blue and green phosphorus, respectively.[13] In P_{BLUE} the P_6 rings are stacked in a narrow 2D zigzag honeycomb structure, whereas P_{GREEN} can be interpreted as the combination of P_{BLUE} and P_{BLACK} displaying an additional bend in comparison to the chair-like arrangement in P_{BLACK} (Scheme 2). Lastly, new approaches towards the isolation of unprecedented phosphorus modifications utilizing confined spaces inside carbon nanorods yielded various thin polyphosphorus strands and even rings consisting of 230 P atoms.[14] By high resolution transmission electron microscopy various strand types such as bead-like strung P_4 molecules, double stranded zigzag ladders and single stranded zigzag chains could be identified and characterized.[15] Consequently, the search for novel elemental phosphorus allotropes is still of great interest today and enables the investigation of fascinating materials with powerful properties.

1.2 The importance of phosphorus

Phosphorus is an essential element for all organisms because major groups of biomolecules like DNA, phospholipids or certain proteins rely on phosphate groups as key structural elements.[16] Moreover, the entire metabolic energy transfer is based on the release and storage of phosphate groups on ATP (adenosine triphosphate).[17] Due to its biological abundancy a so called phosphate cycle, very similar to the often discussed carbon cycle, can be observed on a global scale.[18] It describes the equilibrium between organic phosphates contained in biomolecules and inorganic phosphates stored in minerals. The biological importance of phosphorus is a strong incentive to examine its properties for the entire scientific community as biologically prominent elements often display a vast variety in reactivity.

Phosphorus itself is highly oxophilic and the reactive P_4 modification self-ignites upon contact with air.[1] Consequently, no natural reservoirs of elemental phosphorus can be found, but rather phosphate minerals, like apatite, or the aforementioned biomolecules. Due to its pyrophoric properties, P_4 was used as a chemical weapon and firebomb during World War II and in the production of lighter matches.[19] However, for security and health reasons the latter nowadays contain P_{RED}, as this modification is non-toxic and non-self-inflammable. Before the substitution, workers in matchstick factories in the 19th and early 20th century often suffered from the so called “phossy jaw”, a necrosis of the mouth tissue and jawbone due to the constant exposure to toxic P_4 vapor. Occasionally, small lumps of P_4 (liberated from broken World War II weapons) are washed ashore as P_4 is inert towards the reaction with water.[1] Unaware, people often mistake it for amber, which causes severe accidents, as the collected lumps of P_4 ignite spontaneously when drying.[20]

Despite its toxicity and flammability, P_4 is still the most common starting material in the synthesis of a variety of phosphorus containing compounds in academic and industry scale setups due to its incomparable reactivity. Usually, P_4 is obtained by reacting fluorapatite [$Ca_5(PO_4)_3$(OH, F, Cl)] with coal and quartz in an electric arc furnace under very harsh reaction conditions, producing gaseous P_2 which condenses as P_4 upon

cooling.[21] P_4 is then converted to a variety of different compounds like the chlorinating agents PCl_3 and $POCl_3$[22] or herbicides and fertilizers[23]. Hereby, the current large-scale reaction pathways require harsh reagents like chlorine gas and the subsequent workup often affords stochiometric amounts of waste. For example, the reaction of PCl_3 with Grignard reagents like RMgCl (R = organic residue) yields the desired phosphine PR_3 as well as three equivalents of undesired $MgCl_2$.[1b] Various phosphines obtained in this manner are crucial building blocks of chiral and highly selective catalytic compounds.[24] Consequently, phosphorus is an indispensable element not only in the synthesis of essential chemicals, but also extensively contributes to various fields of current research.

1.3 P_4 activation

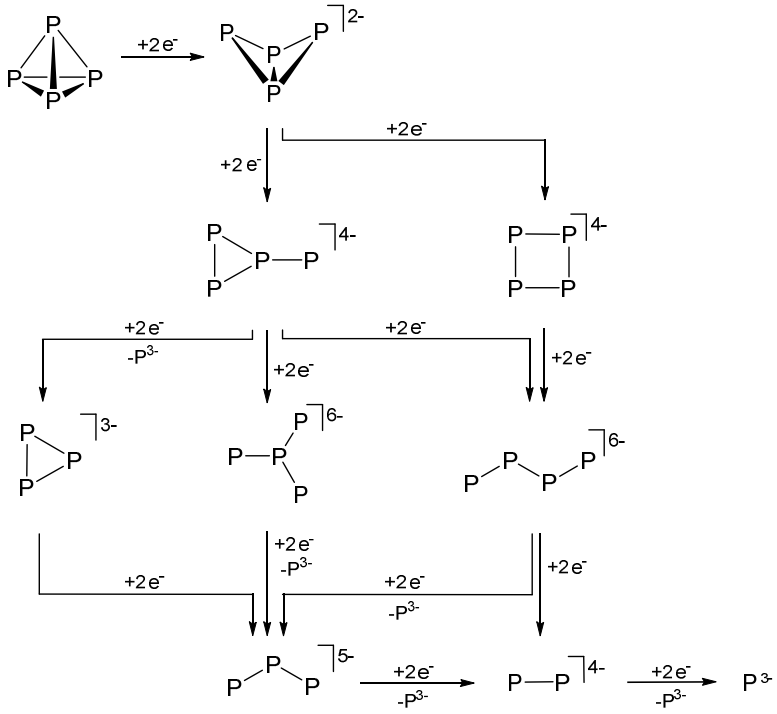

Scheme 3. P_n units (n≤4) obtained from the subsequent degradation of the P_4 tetrahedron during P_4 reduction.

The previously discussed molecular structure of P_4 gives insight into the high reactivity of the compound. With approx. 60° the P–P–P angles in the symmetric P_4 tetrahedron differ drastically from the energetically preferred angle for non-hybridized P atoms (approx. 90°).[3] However, the extraordinary reactivity of P_4 is also a drawback as in most reactions low selectivity is observed. In addition, the current synthetic routes converting P_4 to practical phosphorus containing compounds display major disadvantages (*vide supra*). Therefore, the investigation of the so called P_4 activation is of current interest.[25] Here, P_4 is reacted with organic or organometallic fragments to give a precast opening of the P_4 tetrahedron directing its reactivity in certain reaction pathways and decreasing energy barriers for subsequent reactions. Trough subsequent P–P bond cleavage and phosphide elimination a vast array of P_n fragments (n≤4) are obtained from the P_4 tetrahedron (Scheme 3). The classical definition of a P_n ligand states that all P atoms are exclusively linked to each other

and display only coordinative interactions with transition metals or main group elements.[25] Various P_n ligand systems have been studied until now and for each of the feasible P_n ligands exemplary compounds could be obtained, isolated and characterized.[25] Besides studies concerning the organic activation of P_4 and the conversion with main group elements, the classical approach to obtain P_n ligand complexes is the reaction of P_4 with unsaturated organometallic fragments. The P_n ligands obtained in this manner are consequently stabilized in the coordination sphere of these fragments.

The intact P_4 tetrahedron can coordinate in an *end-on* η^1-fashion promoted by one lone pair of electrons located on a P atom or in a *side-on* mode trough the σ-orbital of a P–P bond, respectively. With $[(np_3)Ni(\eta^1\text{-}P_4)]$ (np_3 = tris(2-diphenylphosphino-ethyl)amine, **A**, Scheme 4) the first example for an *end-on* coordination was reported by *Sacconi et al.* in 1979.[26] Subsequently, it took more than 20 years until *Krossing* first reported on the homoleptic $[Ag(\eta^2\text{-}P_4)_2]^+$ cation (**B**, Scheme 4) which bears two intact P_4 tetrahedra in a *side-on* coordination mode.[27] The first homoleptic P_4 complex **B** and the analog Cu[28] and Au[29] compounds display a D_{2h} symmetry which derives from an almost square planar coordination environment of the central metal ion.

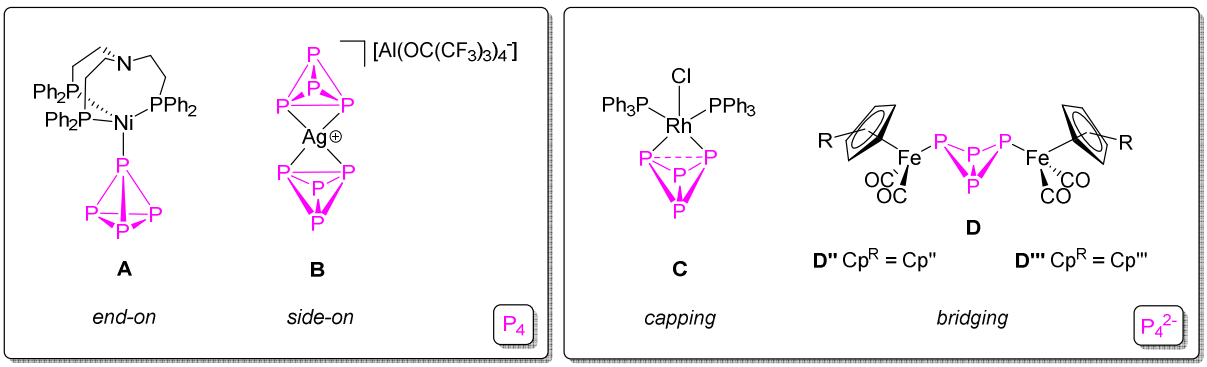

Scheme 4. Historical and most prominent compounds incorporating intact P_4 tetrahedra (left) and P_4 butterfly ligands (right).

The first step in the activation of P_4 is the selective reductive cleavage of one P–P bond affording the tetraphospha-*bicyclo*[1.1.0]butane (P_4^{2-}) unit, which is typically called P_4 butterfly motif due to its geometry (Scheme 4). The first example for this class of compounds was given by *Lindsell and Ginsberg* in 1971: $[(PPh_3)_2RhCl(\eta^{1:1}\text{-}P_4)]$ (**C**, Scheme 4).[30] The authors proposed at first that the P_4 tetrahedron stayed intact upon coordination with data collected from mass spectrometry and IR as well as Raman spectroscopic experiments. However, supplementary ^{31}P NMR spectroscopy clearly confirmed that one P–P bond of the P_4 tetrahedron was cleaved and the organometallic rhodium fragment is coordinated via the wing tip P atoms of the bidentate P_4^{2-} unit.[31] Next to this chelating coordination mode, a bridging coordination of the P_4^{2-} moiety is more commonly observed with $[\{Cp^RFe(CO)_2\}_2(\mu,\eta^{1:1}\text{-}P_4)]$ (**D**; Cp^R = Cp″ ($C_5H_3{}^tBu_3$, **D″**) or Cp‴ ($C_5H_2{}^tBu_3$, **D‴**), Scheme 4) being the most prominent example for this structural scaffold.[32] The reactivity of **D″** and **D‴** has been intensively studied under photolytic[32a] and thermolytic[32b] reaction conditions (*vide infra*) and therefore the P_4 butterfly moiety is an indispensable element in gaining insight in the mechanistic background of P_4 activation. Next to the well-studied organometallic P_4 butterfly compounds, only few examples are known for P_4 butterfly ligands with organic substituents. *Fluck et al.* reacted MesLi, MesBr and white phosphorus and

could therefore report on the first "*organo*-P_4 butterfly" compound [{sMes}$_2$(μ,η$^{1:1}$-P_4)] (**E**, sMes = 2,4,6-*tri*-^{t}Bu-phenyl) in 1985.[33]

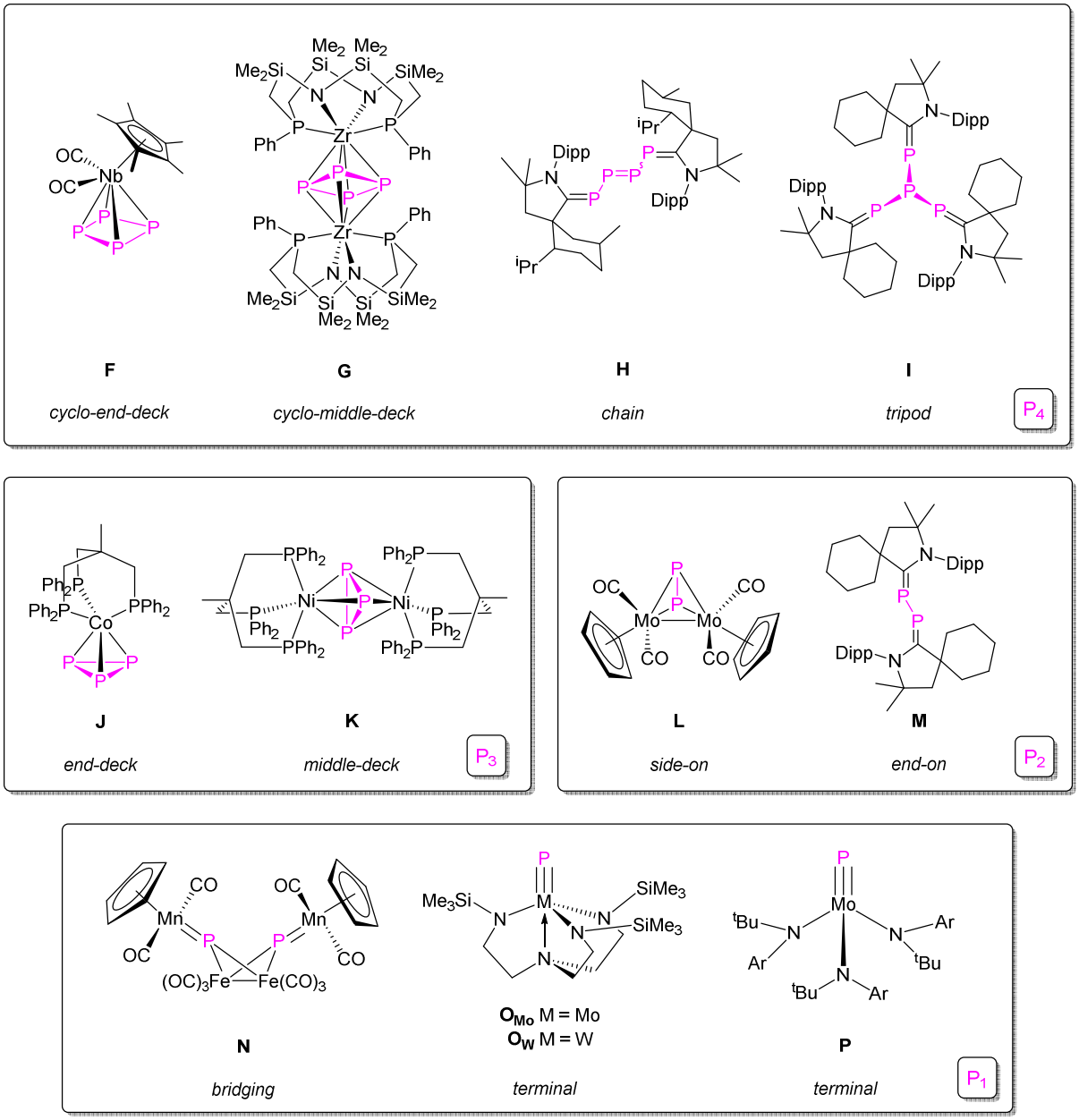

Scheme 5. Pioneer P_n ligand (n≤4) compounds.

A second step in the P_4 activation can be the selective cleavage of the P–P bond between the two bridgehead P atoms of the P_4 butterfly unit, yielding a *cyclo*-P_4 moiety. The first compound incorporating a rhomboidal distorted P_4 ring was [Cp*Nb(CO)$_2$(η^4-P_4)] (**F**, Scheme 5).[34] The first complex incorporating a *cyclo*-P_4 end-deck, was afforded by irradiating [Cp*Nb(CO)$_4$] in the presence of P_4. Complementary, *Fryzuk et al.* afforded [{Zr(PhP(CH$_2$SiMe$_2$NSiMe$_2$CH$_2$)$_2$-PPh)}$_2$(μ,η$^{4:4}$-P_4)] (**G**, Scheme 5), the first D_{2d} symmetric complex incorporating a square planar P_4^{4-} middle deck.[35]

Further reduction of the *cyclo*-P_4 unit generates P_4 chains which could first be isolated by the group of *Bertrand*. They obtained [(^{menthyl}CAAC)$_2$P$_4$] (menthyl = 2-CH_3,6-$CH(CH_3)_2C_6H_9$, **H**, Scheme 5) by reacting P_4 with a sterically demanding cyclic alkyl(amino)-carbene (CAAC, 1-[2,6-$(CH(CH_3)_2)_2C_6H_3$]-3,3-$(CH_3)_2$-pyrrolidine).^{31}P NMR spectroscopy reveals that the P_4 chain of **H** can be oriented in a cis or trans fashion in solution, while only the E-isomer crystallizes from slow evaporation. In contrast, the reaction with the sterically less demanding ^{cHex}CAAC (cHex = *cyclo*-hexane) affords [(^{cHex}CAAC)$_3$P$_4$] (**I**, Scheme 5) incorporating an *iso*-tetraphosphine moiety which is the last possible variation of a P_4^{x-} ligand.[36]

Sacconi et al. obtained the first *cyclo*-P_3 ligands from the reaction of P_4 with Co^{2+} and Ni^{2+} salts in the presence of the tridentate ligand L = $CH_3C(CH_2PPh_2)_3$.[37] Interestingly, the conversion with Co^{2+} affords [LCo(η^3-P$_3$)] (**J**, Scheme 5) displaying a terminal η^3-P_3 ligand, while the reaction with Ni^{2+} results in [{LNi}$_2$(μ,$\eta^{3:3}$-P$_3$)](BF$_4$)$_2$ (**K**, Scheme 5), a complex in which a bridging μ,$\eta^{3:3}$-P_3 coordination mode.

From the thermolysis of P_4 in the presence of [CpMo(CO)$_2$]$_2$, *Scherer et al.* afforded the first P_2 dumbbell incorporating complex: [{CpMo(CO)$_2$}$_2$(μ,$\eta^{2:2}$-P$_2$)] (**L**, Scheme 5)[38], which is currently used as a powerful building block in the formation of supramolecular aggregates in our group.[39] The herein observed μ,$\eta^{2:2}$-coordination mode of the P_2 unit is quite common. In contrast, *Bertrand et al.* obtained [(^{cHex}CAAC)P]$_2$ (**M**, Scheme 5), in which the P_2 dumbbell is stabilized in an end-on fashion by two carbenes, alongside **I**.[36]

Phosphido ligands (P^{3-}) represent the final stage of the P_4 activation after all six P–P bonds of the initial P_4 tetrahedron are reductively cleaved. The first example of a complex incorporating two trigonal planar coordinated μ_3-P^{3-} ligands was given by *Huttner et al.*: [{CpMn(CO)$_2$}$_2$(μ_3,$\eta^{1:1:1}$-P)$_2${Fe$_2$(CO)$_6$}] (**N**, Scheme 5).[40] After several theoretical proposals[41], *Scheer* and coworkers were the first to observe the terminal phosphide complex [(^{t}BuO)$_3$W≡P→Mo(CO)$_5$] in ^{31}P NMR spectroscopic studies and could confirm its identity via *in-situ* conversions with phosphaalkynes in 1995.[42] In the same year, the groups of *Cummins* and *Schrock* reported simultaneously on the terminal phosphido compounds [PM(Me$_3$SiNCH$_2$CH$_2$)$_3$N] (**O$_{Mo}$**: M = Mo; **O$_W$**: M = W, Scheme 5) and [PMo(N(^{t}Bu)Ar)$_3$] (**P**, Scheme 5), respectively.[43] These are the first structurally characterized representatives of compounds bearing a terminal P^{3-} ligand displaying exceedingly short P–M bond lengths (e.g. Mo–P = 2.11 Å in **O$_{Mo}$**), which indicate P≡M triple bonds. A shared feature of all phosphide compounds is the remarkably lowfield ^{31}P NMR chemical shift (e.g. δ = 977 ppm for **N**) caused by the tensed coordination geometry.

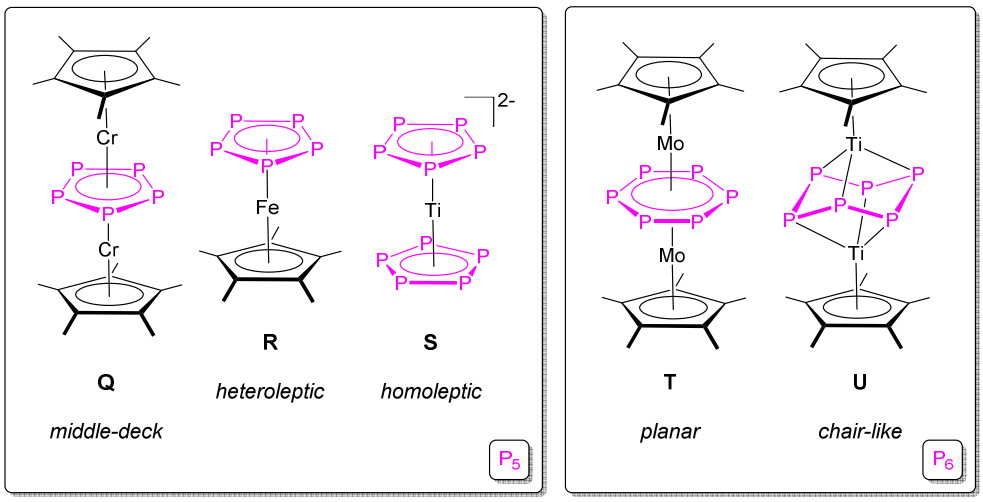

Scheme 6. Pioneer *cyclo*-P_5 and *cyclo*-P_6 compounds.

Besides the degradation of the P_4 tetrahedron during P_4 activation, aggregates with more than four phosphorus atoms can also be obtained from white phosphorus. If stabilizing organometallic fragments are scarce, intermediates of the P_4 activation process can accumulate providing greater polyphosphorus moieties. The group of *Scherer* took great interest in the synthesis of *cyclo*-P_5 and *cyclo*-P_6 units due to their isolobality to the 6π-electron donating cyclopentadienyl (Cp) and benzene ligands, respectively. In 1986, they reported on the first successful stabilization of a *cyclo*-P_5 moiety in the form of a middle deck in the triple decker $[(Cp^*Cr)_2(\mu_2,\eta^{5:5}\text{-}P_5)]$ (**Q**, Scheme 6) obtained from the thermolysis of $[Cp^*(CO)_2Cr]_2$ and P_4.[44] One year later, they could report on $[Cp^*Fe(\eta^5\text{-}P_5)]$ (**R**, Scheme 6), the first ever organometallic analog of ferrocene incorporating one planar *cyclo*-P_5 ligand.[45] Finally, almost 20 years later, *Ellis* and coworkers isolated the anionic complex $[Ti(\eta^5\text{-}P_5)_2]^{2-}$ (**S**, Scheme 6), which represents the first all-phosphorus sandwich complex.[46]

By incorporating the reliable thermolysis route, *Scherer* and coworkers obtained the triple-decker complex $[\{Cp^*Mo\}_2(\mu,\eta^{6:6}\text{-}P_6)]$ (**T**, Scheme 6), which bears the first inorganic benzene analog, from the reaction of $[Cp^*(CO)_2Mo]_2$ with P_4.[47] Two years after the report on **T**, the group published the synthesis of $[\{Cp^*Ti\}_2(\mu,\eta^{3:3}\text{-}P_6)]$ (**U**, Scheme 6), in which the *cyclo*-P_6 middle deck is arranged in a chair-like fashion.[48] For **T**, a D_{6d} symmetry was observed due to the planar geometry of the central *cyclo*-P_6 deck. The highly symmetric $\mu,\eta^{6:6}$-coordination mode found in **T** is in contrast to the $\mu,\eta^{3:3}$-coordination mode of **U** and the differing coordination spheres have strong influence on the electronic properties of the ligand. Hence, a drastic difference can be observed in the respective ^{31}P NMR chemical shifts: -315.6 ppm (**T**) vs. 386.7 ppm (**U**).

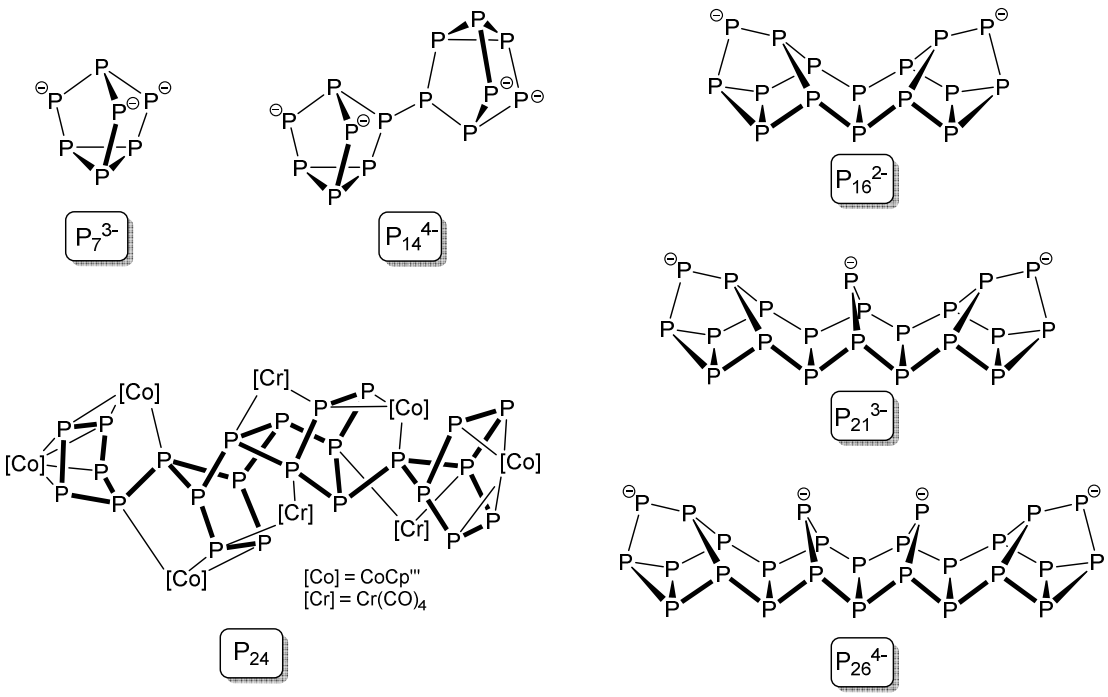

Scheme 7. Examples for large polyphosphoric aggregates.

Ultimately, even larger aggregates like the polyphosphide anions P_7^{3-}, P_{14}^{4-}, P_{16}^{2-}, P_{21}^{3-} and P_{26}^{4-} have been reported (Scheme 7).[49] The smaller anions are composed of P_7 cages, whereas the larger anions incorporate a zigzag-like P_2 band which is capped by bridging P atoms while condensed P_7 cages constitute the edges. In contrast, the P_{24} unit found in $[(Cp'''Co)_5P_{24}\{Cr(CO)_4\}_3]$ is the largest molecular neutral polyphosphorus

scaffold characterized by single crystal X-ray diffraction so far (Scheme 7).[50] The structure of the polyphosphorus core moiety can be interpreted as the result of a [4+2] cyclo-addition of two P_{12} repetitive units of Hittdorf´s phosphorus. Mass spectroscopy results indicate the presence of phosphorus aggregates made up of more than 60 phosphorus atoms, yet, so far, no structural characterization could be achieved.[51]

1.4 Reactivity of P_4 butterfly complexes

Scherer et al. first reported on the synthesis of the iron P_4 butterfly compounds [{Cp″Fe(CO)$_2$}$_2$(μ,η$^{1:1}$-P_4)] (**D″**) and [{Cp‴Fe(CO)$_2$}$_2$(μ,η$^{1:1}$-P_4)] (**D‴**) by applying irradiation or short term thermolysis to the corresponding [Cp^{R}Fe(CO)$_2$]$_2$ (Cp^R = Cp″ or Cp‴) dimer in presence of P_4.[32] The drastic reaction conditions induce decarbonylation, affording a number of byproducts which require subsequent chromatographic workup (Scheme 8). Surprisingly, our group discovered that these harsh reaction conditions are not required and a quantitative conversion can be observed almost instantly at room temperature.[52] This catapulted the yield and accessibility of **D‴** to a new level and consequently spiked interest in the implementation of this compound in novel reaction pathways.

1.4.1 Rearrangement processes

The stepwise decarbonylation of **D″** under photolytic conditions forces the P_4 butterfly ligand to rearrange in order to compensate for the electron deficiency accompanying the CO ligand dissociation.[32a] After the elimination of one CO ligand, [{Cp″Fe(CO)}(μ,η$^{2:1}$-P_4){Fe(CO)$_2$Cp″}] (**D$_A$**, Scheme 8) is obtained. In **D$_A$** the decarbonylated {Fe(CO)Cp″} fragment is coordinated by the two wing tip P atoms of the still intact P_4 butterfly moiety. Next in line is [{Cp″Fe}(μ,η$^{4:1}$-P_4){Fe(CO)$_2$Cp″}] (**D$_B$**, Scheme 8), which is afforded after the elimination of two CO ligands. In **D$_B$** the butterfly geometry is broken with the cleavage of the P–P bond between the former bridgehead P atoms due to the electron deficiency caused by the additional decarbonylation. The resulting distorted rhombic *cyclo*-P_4 moiety is substituted by one intact {Fe(CO)$_2$Cp″} fragment and coordinates in a η^4-fashion towards the fully decarbonylated {FeCp″} fragment. During the next decarbonylation step, the resulting {Fe(CO)Cp″} fragment inserts in the *cyclo*-P_4 ligand affording a ferra-tetraphospha-cyclopentadienyl ligand isolobal to the ferrole motif described for [{Fe(CO)$_3$}(η^4-C$_4$H$_4$Fe(CO)$_3$)].[53] Thus, [{Cp″Fe}(η^4-P$_4$Fe(CO)Cp″)] (**D$_C$**, Scheme 8) is obtained. Finally, [{Cp″Fe}$_2$(μ,η$^{4:4}$-P_4)] (**D$_D$**, Scheme 8), a sandwich complex with an open *cis*-P_4-chain middle deck, is obtained after the complete decarbonylation of **D″**. A fluctuation in the P–P bonds of the middle deck is suggested by ^{31}P NMR spectroscopy studies. For the AA′XX′ spin system of **D$_D$** two sets of signals could be observed at 185 K ($\delta_{AA'}$ = 302.5 ppm, $\delta_{BB'}$ = –143.2 ppm), while only one broad signal was recorded at room temperature, which displayed sharpening when heating the solution to 370 K. The authors proposed a *closo*-octahedral type complex with a closed *cyclo*-P_4 middle deck as a reasonable intermediate of the observed dynamic.

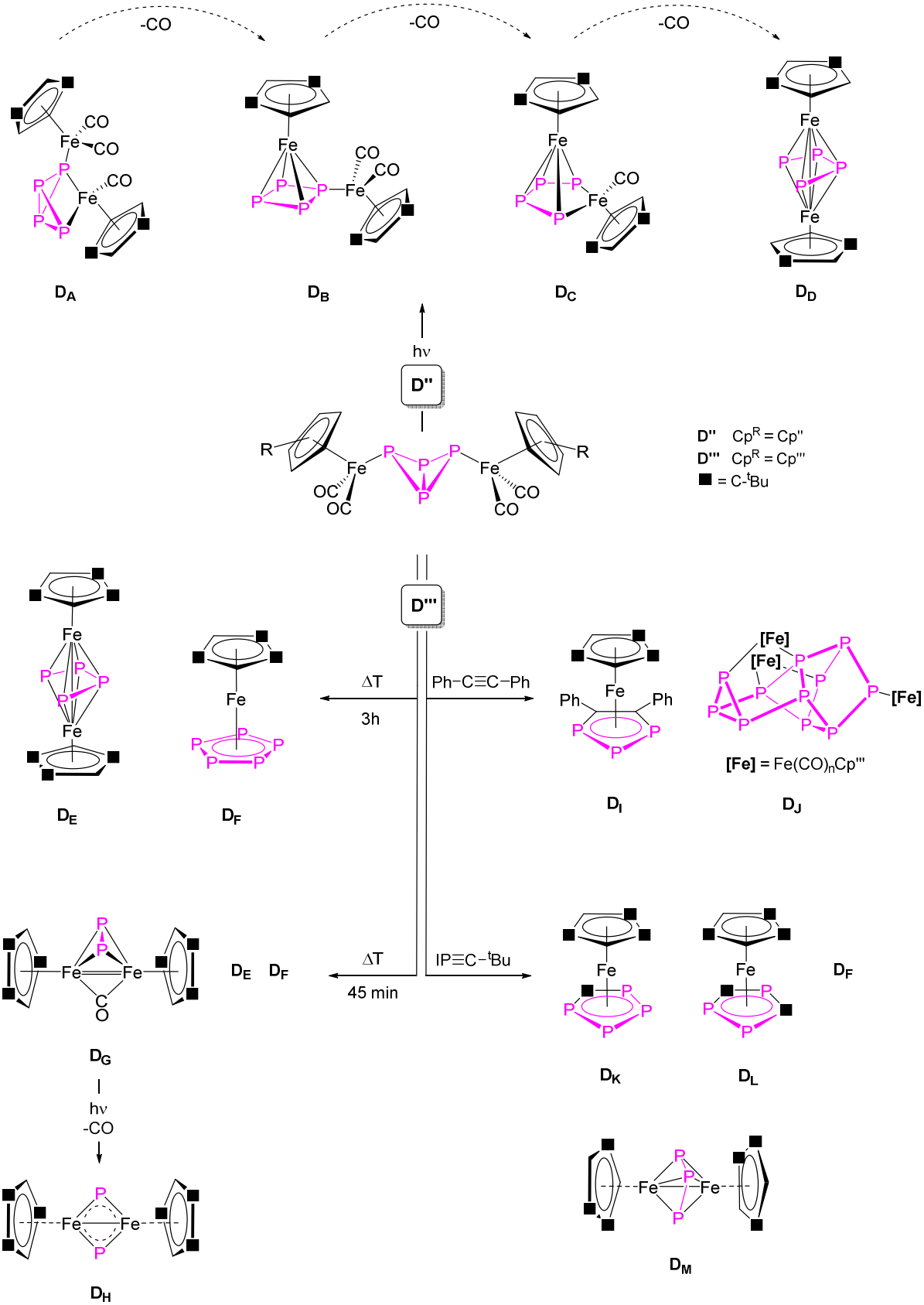

Scheme 8. Complexes obtained from **D″** and **D‴** under photolytic (top) and thermolytic (bottom left) reaction conditions as well as the conversion with Ph–C≡C–Ph and P≡C–^{t}Bu (bottom right).

Under thermolytic conditions, **D‴** decomposes to give only the P_4-chain incorporating [{Cp‴Fe}$_2$(μ,η$^{4:4}$-P_4)] (**D$_E$**, Scheme 8) alongside the pentaphosphaferrocene derivative [Cp‴Fe(η^5-P_5)] (**D$_F$**, Scheme 8).[32b] Obviously, the thermolysis in boiling decalin (190°C) for 3 hours is exceptionally harsher than UV irradiation for 20 minutes, leaving no carbonylated species behind. By decreasing the thermolysis time to 45 minutes the diphosphadiferratetrahedrane [{Cp‴Fe}$_2$(μ,η$^{2:2}$-P_2)(μ-CO)] (**D$_G$**, Scheme 8) which incorporates a Fe=Fe double bond can be isolated in reasonable yields alongside **D$_E$** and **D$_F$**.[54] Moreover, subsequent irradiation of **D$_G$** induces the release of the bridging carbonyl group and the cleavage of the P_2 dumbbell affording [{Cp‴Fe}$_2$(μ-P)$_2$] (**D$_H$**, Scheme 8) which incorporates a rhombic *cyclo*-Fe_2P_2 unit.[54] For **D$_G$** and **D$_H$** an almost planar arrangement of the two Cp‴ ligands in a nearly staggered conformation is reported.

In contrast to the pentaphosphaferrocene **D$_F$** obtained from **D‴** by decarbonylation induced rearrangement processes, the reaction of **D‴** with Ph–C≡C–Ph affords the sandwich complex [Cp‴Fe(η^5-$P_3C_2Ph_2$)] (**D$_I$**, Scheme 8) which incorporates a 1,2,3-triphospha-cyclopentadienyl ligand.[55] Additionally, the trinuclear iron complex [{Cp‴Fe(CO)$_n$}$_3$$P_{11}$] (**D$_J$**, Scheme 8) featuring a P_{11} scaffold could be isolated from this reaction. Most commonly the so called “ufosan” structure, which consists of six annulated P_5 rings, is observed for P_{11} scaffolds and was reported for Na_3P_{11}, $(Me_3EtN)_3P_{11}$, $(Me_3Si)_3P_{11}$ and $^iPr_3P_{11}$.[56] However, the polyphosphorus scaffold of **D$_J$** does not display this structural motif, but rather resembles a substructure motif of Hittorf´s phosphorus with an additional capping P atom on top of the P_2 band-like foundation.

Furthermore, **D‴** was reacted with the phosphaalkyne IP≡C–^{t}Bu, affording the sandwich complexes [Cp‴Fe(η^5-P_4C^tBu)] (**D$_K$**, Scheme 8) and [Cp‴Fe(η^5-$P_3(C^tBu)_2$)] (**D$_L$**, Scheme 8) next to the pentaphosphaferrocene derivative **D$_F$**.[57] The structural composition of the 1,2,3,4-tetraphospha-cyclopentadienyl and the 1,2,4-triphospha-cyclopentadienyl ligand incorporated by **D$_K$** and **D$_L$**, respectively, indicate a preliminary P_1/P_3 fragmentation of the starting material **D‴** followed by a subsequent reaction with one or two equivalents of IP≡C–^{t}Bu. Additionally, [{Cp‴Fe}$_2$(μ,η$^{3:3}$-P_3)] (**D$_M$**, Scheme 8) the first binuclear complex incorporating a triphosphaallyl unit could be isolated in small amounts from the reaction supporting the proposed P_1/P_3 fragmentation.

1.4.2 Coordination behavior

In the previously discussed reactions, the central P_4 butterfly moieties of [{Cp″Fe(CO)$_2$}$_2$(μ,η$^{1:1}$-P_4)] (**D″**) and [{Cp‴Fe(CO)$_2$}$_2$(μ,η$^{1:1}$-P_4)] (**D‴**) undergo structural transformations in response to the altered electronic structure caused by the applied reaction conditions. Another prominent feature of polyphosphorus ligand complexes is introduced by the coordinatively active lone pairs on each P atom: the coordination of the P_n ligand moiety towards various Lewis acidic compounds.[25] These coordination processes are observed for intact as well as rearranged or fragmented polyphosphorus scaffolds. Accordingly, DFT calculations were performed stating that a coordination of the intact P_4 butterfly moiety is feasible as well (Fig. 1).[58] For **D‴** the HOMO-1 (highest occupied molecular orbital) is concentrated on the wing tip P atoms, while the HOMO orbital is distributed over the entire P_4 butterfly scaffold. For the isoelectronic chromium compound [{Cp*Cr(CO)$_3$}$_2$(μ,η$^{1:1}$-P_4)] (**D***, Cp* = $C_5(CH_3)_5$) the order is reversed with the electron density of the HOMO being concentrated on the wing tip P atoms (Fig. 1). This difference in the electronic framework may induce differing reactivities for the analog P_4 butterfly complexes **D‴** and **D***. However, the lowest unoccupied molecular orbital (LUMO) is identical for the two compounds. It represents primarily the σ*-bonds between the wing tip P atoms and the respective organometallic substituents. Consequently, the wing tip P atoms

appear to be the pivotal points in respect to the coordination chemistry originating from the P_4 butterfly motif. Thus, the most preferred coordination mode for the P_4 butterfly unit is the chelating coordination via the two wing tip P atoms promoting the P_4 butterfly moiety to a bidentate ligand.

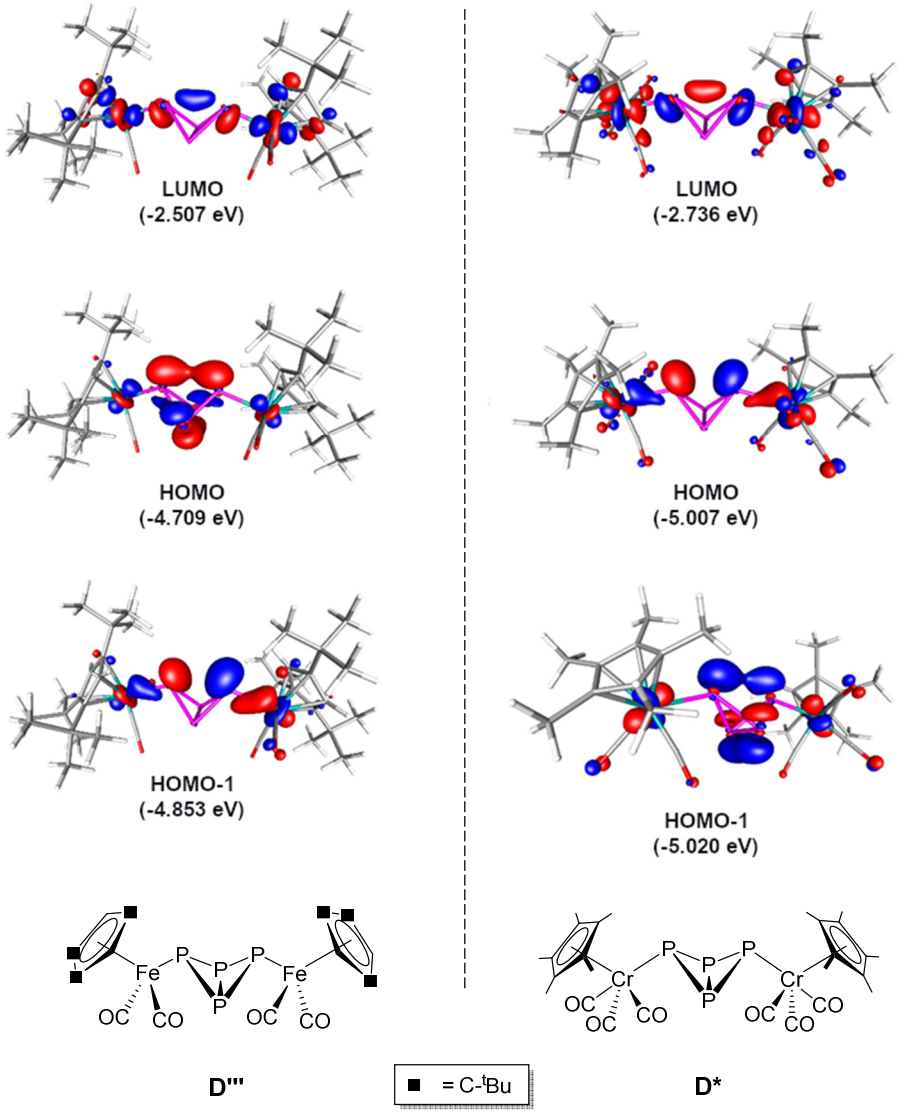

Figure 1. Frontier molecular orbitals of the isoelectronic P_4 butterfly compounds **D‴** and **D***; calculated at the BP86/def2-TZVP level of theory.[58]

In agreement with these computational results, the reaction of **D‴** with 1.0 eq. of $[Cu(CH_3CN)_4][BF_4]$ afforded $[\{Cp'''Fe(CO)_2\}_2(\mu_3,\eta^{1:1:1:1}\text{-}P_4)\{Cu(CH_3CN)\}][BF_4]$ (**D$_N$**, Scheme 9) in which the coinage metal salt is coordinated by the bidentate P_4 butterfly ligand.[58a] By a variation of the implied stoichiometry, $[\{(Cp'''Fe(CO)_2)_2\text{-}(\mu_3,\eta^{1:1:1:1}\text{-}P_4)\}_2Cu][BF_4]$ (**D$_O$**, Scheme 9), a homoleptic *spiro*-P_4-butterfly complex with a distorted tetrahedral coordination sphere of the central copper cation was obtained.[58a] In contrast, the reaction of **D‴** with 3.0 eq. of CuI gave the dimeric $[\{Cp'''Fe(CO)_2\}\{Cp'''Fe(CO)\}(\mu_4,\eta^{1:1:1:1:2}\text{-}P_4)\{CuI\}]_2$ (**D$_P$**, Scheme 9), for which an intricate coordination pattern can be observed.[59] Each of the two P_4 butterfly moieties is coordinated towards a Cu^+ cation and a $\{Fe(CO)_2Cp'''\}$ fragment in the *exo*-positions on the two wing tip P atoms, respectively. Additionally, a $\{Fe(CO)Cp'''\}$ fragment (obtained from the organometallic substituent after decarbonylation) is

coordinated in a chelating fashion by the two wing tip P atoms. Single crystal X-ray diffraction analysis indicates that the chelating coordination has only insignificant impact on the overall structure of the P_4 butterfly moiety. One observation is that the wing tip P atoms are slightly pulled inwards. The coordination process reduces the distance between the two wing tip P atoms (e.g. 2.96 Å in **D‴** and 2.8135(8) Å in $\mathbf{D_N}$) and the angle spanned by the two wing tip P atoms and one bridgehead P atom (e.g. 84° in **D‴** and 78° in $\mathbf{D_N}$).[32b,58a]

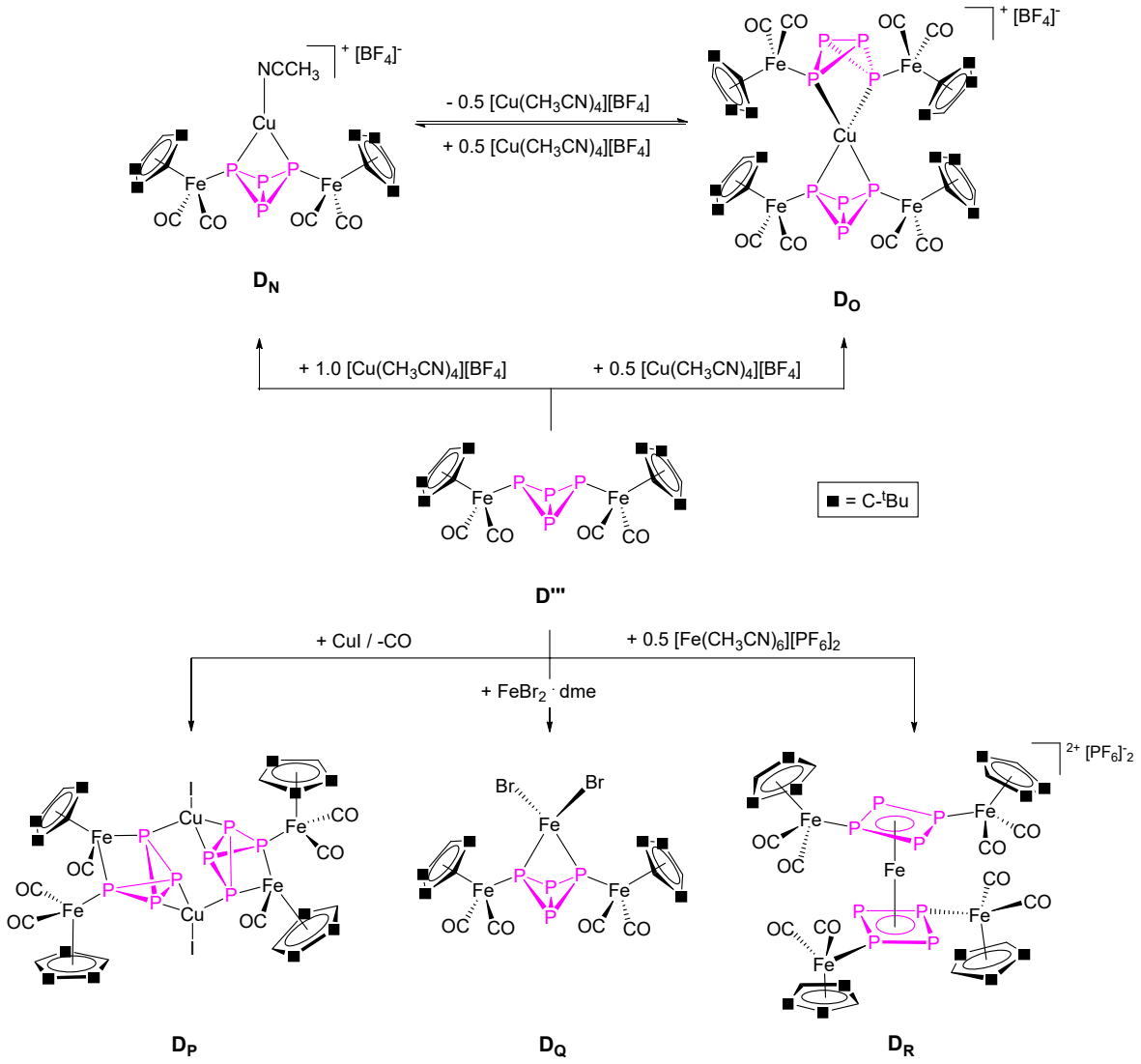

Scheme 9. Products obtained from the reaction of **D‴** with different Lewis acids.

Finally, the reaction of **D‴** with Fe(II) salts contributed an interesting facet to the reactivity of **D‴**. While the reaction with $FeBr_2$·dme (dme = 1,2-dimethoxyethane) gave the expected coordination adduct $[\{Cp'''Fe(CO)_2\}_2(\mu_3,\eta^{1:1:1:1}\text{-}P_4)\{FeBr_2\}]$ ($\mathbf{D_Q}$, Scheme 9), an isomerization yielding planar P_4^{2-} ligands was obtained when reacting **D‴** with $[Fe(CH_3CN)_6][PF_6]_2$.[60] Hence, $[\{(Cp'''Fe(CO)_2)_2(\mu_3,\eta^{1:1:4}\text{-}P_4)\}_2Fe][PF_6]_2$ ($\mathbf{D_R}$, Scheme 9), the first fully characterized carbon free sandwich complex with 6π-aromatic $P_4[Fe]_2$ ligands could be obtained. This puts emphasis to the fact that the nature of the involved Lewis acid strongly influences the reaction pathway.

1.5 Recent developments in the P_4 butterfly chemistry

Over the last years, our group was able to enlarge the library of P_4 butterfly compounds by utilizing different approaches. Cp^{BIG} (Cp^{BIG} = $C_5(4\text{-}^nBu\text{-}C_6H_4)_5$), a cyclopentienyl ligand derivative with an exceedingly large steric demand was employed to obtain the organometallic $[\{Cp^{BIG}Fe(CO)_2\}_2(\mu,\eta^{1:1}\text{-}P_4)]$ as well as the metal-free $[Cp^{BIG}{}_2(\mu,\eta^{1:1}\text{-}P_4)]$ via radical pathways.[61] With the help of a supporting Fe^{II}/Fe^{III} redox system, which promotes the formation of a Cp radical, several *organo*-P_4 butterfly compounds with less bulky Cp ligands ($[Cp^R{}_2(\mu,\eta^{1:1}\text{-}P_4)]$ with Cp^R = Cp*, Cp‴, Cp^{4iPr} ($C_5H^iPr_4$)) could be obtained.[61b] Lastly, the previously mentioned **D****, the isolobal chromium compound to **D″** and **D‴**, was prepared by the classical approach of reacting the dimeric $[Cp^*Cr(CO)_3]_2$ with white phosphorus.[62] Preliminary reactivity studies in our group demonstrated that **D**** affords the expected bidentate coordination pattern via the two wing tip P atoms analog to **D‴** but also displays unique reaction behavior.[58b] The previously discussed variations in the frontier molecular orbitals could be one explanation for these observations. Additionally, DFT calculations were performed on the BP86/def2-TZVP level, that illustrate that the P–Cr bond in **D**** is rather labile compared to the P–Fe bond in **D‴**.[58b] While a dissociation energy of 67.47 $kJ\cdot mol^{-1}$ is given for the P–Cr bond in **D****, the dissociation of the P–Fe bond in **D‴** is considerably more endothermic (142.91 $kJ\cdot mol^{-1}$). Consequently, **D**** is more prone to pursue rearrangement processes making it an interesting starting material for further investigations concerning the mechanisms behind the first steps in P_4 activation.

1.6 References

[1] (a) A. F. Holleman, N. Wiberg, E. Wiberg, *Lehrbuch für Anorganische Chemie*, 102. Edition, de Gryter, **2007**, 746-749.
(b) D.E.C. Corbridge, *Phosphorus: Chemistry, biochemistry & technology*, 6. Edition, CRC Press, **2013**

[2] F. Krafft, *Angew. Chem. Int. Ed. Engl.* **1969**, *8*, 660-671.

[3] (a) A. Simon, H. Borrmann, H. Craubner, *Phosphorus Sulfur Silicon Relat. Elem.* **1987**, *30*, 507-510.
(b) H. Okudera, E. Dinnebier Robert, A. Simon, *Z. Kristallogr*. **2005**, *220*, 259.

[4] A. Schrötter, *J. Prakt. Chem.* **1850**, *51*, 155-158.

[5] W. L. Roth, T. W. DeWitt, A. J. Smith, *J. Am. Chem. Soc.* **1947**, *69*, 2881-2885.

[6] R. A. L. Winchester, M. Whitby, M. S. P. Shaffer, *Angew. Chem. Int. Ed. Engl.* **2009**, *48*, 3616-3621.

[7] M. Ruck, D. Hoppe, B. Wahl, P. Simon, Y. Wang, G. Seifert, *Angew. Chem. Int. Ed. Engl.* **2005**, *44*, 7616-7619.

[8] W. Hittorf, Ann. Phys. Chem. **1865**, *126*, 193.

[9] A. Pfitzner, M. F. Bräu, J. Zweck, G. Brunklaus, H. Eckert, *Angew. Chem. Int. Ed. Engl.* **2004**, *43*, 4228-4231.

[10] P. W. Bridgman, *J. Am. Chem. Soc.* **1914**, *36*, 1344-1363.

[11] (a) L. Li, Y. Yu, G. J. Ye, Q. Ge, X. Ou, H. Wu, D. Feng, X. H. Chen, Y. Zhang, *Nat Nano* **2014**, *9*, 372-377.
(b) S. P. Koenig, R. A. Doganov, H. Schmidt, A. H. Castro Neto, B. Özyilmaz, *Appl. Phys. Lett.* **2014**, *104*, 103106.
(c) H. Liu, A. T. Neal, Z. Zhu, Z. Luo, X. Xu, D. Tománek, P. D. Ye, *ACS Nano* **2014**, *8*, 4033-4041.

[12] M. C. Watts, L. Picco, F. S. Russell-Pavier, P. L. Cullen, T. S. Miller, S. P. Bartu´s, O. D. Payton, N. T. Skipper, V. Tileli, C. A. Howard, *Nature **2019**, 568*, 216-220.

[13] (a) Z. Zhu, D. Tománek, *Phys. Rev. Lett.* **2014,** *112,* 176802.

(b) J. L. Zhang, S. Zhao, C. Han, Z. Wang, S. Zhong, S. Sun, R. Guo, X. Zhou, C. D. Gu, K. D. Yuan, Z. Li, W. Chen, *Nano Letters* ***2016****, 16* (8), 4903-4908.
(c) W. H. Han, S. Kim, I.-H. Lee, K. J. Chang, *J. Phys. Chem. Lett.* **2017,** 8, 4627-4632.
(d) E. Golias, M. Krivenkov, A. Varykhalov, J. Sánchez-Barriga, O. Rader, *Nano Lett.* **2018**, *18*, 6672-6678.

[14] (a) M. Hart, E. R. White, J. Chen, C. M. McGilvery, C. J. Pickard, A. Michaelides, A. Sella, M. S. P. Shaffer, C. G. Salzmann, *Angew. Chem. Int. Ed.* **2017**, *56*, 8144.
(b) J. Zhang, D. Zhao, D. Xiao, C. Ma, H. Du, X. Li, L. Zhang, J. Huang, H. Huang, C.-L. Jia, D. Tománek, C. Niu, *Angew. Chem. Int. Ed.* **2017**, *56*, 1850.

[15] M. Hart, J. Chen, A. Michaelides, A. Sella, M. S. P. Shaffer, C. G. Salzmann, *Inorg. Chem.* **2019**, *58* (22), 15216-15224.

[16] (a) F. H. Westheimer, *Science* **1987**, *235*, 1173-1178.
(b) J. M. Berg, L. Stryer, J. Tymoczko, G. Gatto, *Biochemistry*, 9. Edition, WH Freeman, **2019**.

[17] (a) K. Lohmann, *Naturwissenschaften* **1929**, *17*, 624-625.
(b) F. Lipmann, *Adv. Enzymol* **1941**, *1*, 99-162.
(c) J. Baddiley, A. M. Michelson, A. R. Todd, *J. Chem. Soc.* **1949**, 582-586.

[18] (a) M. Steiner, *Naturwissenschaften* **1938**, *6*, 723-724.
(b) P. N. Froelich, M. L. Bender, N. A. Luedtke, G. R. Heath, T. DeVries, *Am. J. Sci.* **1982**, *282*, 474-511.
(c) K. B. Föllmi, *Earth-Sci. Rev.* **1996**, *40*, 55-124.
(d) J. Elser, E. Bennett, *Nature* **2011**, *478*, 29-31.
(e) D. Cordell, S. White, *Sustainability* **2011**, *3*, 2027-2049.
(f) Z. Yuan, S. Jiang, H. Sheng, X. Liu, H. Hua, X. Liu, Y. Zhang, *Environ. Sci. Technol.* **2018**, *52*, 2438-2450.

[19] (a) J. P. W. Hughes, R. Baron, D. H. Buckland, M. A. Cooke, J. D. Craig, D. P. Duffield, A. W. Grosart, P. W. J. Parkes, A. Porter, *Br. J. Ind. Med.* **1962**, *19*, 83-99.
(b) E.-C. Koch, *Propellants Explos. Pyrotech.* **2008**, *33*, 165-176.

[20] U. Aviv, R. Kornhaber, M. Harats, J. Haik, *Disaster Mil. Med.* **2017**, *3*, 6.

[21] (a) J. B. Readman, *J. Chem. Technol. Biotechnol.* **1890**, *9*, 163-211.
(b) A. D. F. Toy **1973**, „The Chemistry of Phosphorus“: Pergamon Press, Oxford.
(c) G. Villalba, Y. Liu, H. Schroder, R. U. Ayres, *J. Ind. Ecol.* **2008**, *12*, 557-569.

[22] (a) S. Hoerold, A. Ratcliff, *J. Pyrotech.* **2001**, *13*, 54-63.
(b) T. J. Connolly, M. Matchett, P. McGarry, S. Sukhtankar, J. Zhu, *Org. Process Res. Dev.* **2006**, *10*, 391-397.
(c) L. Chen, X. Li, Y. Pang, L. Li, X. Zhang, L. Yu, *J. Mater. Sci. Mater. Med.* **2007**, *18*, 2199-2203.

[23] M. A. Dhansay, P. W. Linder, R. G. Torrington, T. A. Modro, *J. Phys. Org. Chem.* **1990**, *3*, 248-254.

[24] J. H. Downing, M. B. Smith, *Comprehensive Coordination Chemistry II* **2003**, *1*, 253-296.

[25] (a) B. M. Cossairt, N. A. Piro, C. C. Cummins, *Chem. Rev.* **2010**, *110*, 4164-4177.
(b) M. Caporali, L. Gonsalvi, A. Rossin, M. Peruzzini, *Chem. Rev.* **2010**, *110*, 4178-4235.
(c) M. Scheer, G. Balázs, A. Seitz, *Chem. Rev.* **2010**, *110*, 4236-4256.
(d) N. A. Giffin, J. D. Masuda, *Coord. Chem. Rev.* **2011**, *255*, 1342-1359.

[26] P. Dapporto, S. Midollini, L. Sacconi, *Angew. Chem. Int. Ed. Engl.* **1979**, *18*, 469.

[27] (a) I. Krossing, *Chem. Eur. J.* **2001**, *19*, 4603-4604.
(b) I. Krossing, L. van Wüllen, *Chem. Eur. J.* **2002**, *8*, 700-711.

[28] G. Santiso-Quinones, A. Reisinger, J. Slattery, I. Krossing, *Chem. Comm.* **2007**, 5046-5048.

[29] L. C. Forfar, T. J. Clark, M. Green, S. M. Mansell, C. A. Russell, R. A. Sanguramath, J. M. Slattery, *Chem. Comm.* **2012**, *48*, 1970-1972.

[30] A. P. Ginsberg, W. E. Lindsell, *J. Am. Chem. Soc.* **1971**, *93*, 2082-2084.

[31] W. E. Lindsell, *J. Chem. Soc., Chem. Commun.* **1982**, 1422-1424.

[32] (a) O. J. Scherer, G. Schwarz, G. Wolmershäuser, *Z. Anorg. Allg. Chem* **1996**, *622*, 951-957.
(b) O. J. Scherer, T. Hilt, G. Wolmershäuser, *Organometallics* **1998**, *17*, 4110-4112.

[33] R. Riedel, H.-D. Hausen, E. Fluck, *Angew. Chem. Int. Ed. Engl.* **1985**, *24*, 1056-1057.

[34] O. J. Scherer, J. Vondung, G. Wolmershäuser, *Angew. Chem. Int. Ed.* **1989**, *28*, 1355-1357.

[35] W. W. Seidel, O. T. Summerscales, B. O. Patrick, M. D. Fryzuk, *Angew. Chem. Int. Ed. Engl.* **2009**, *48*, 115-117.
[36] O. Back, G. Kuchenbeiser, B. Donnadieu, G. Bertrand, *Angew. Chem. Int. Ed. Engl.* **2009**, *48*, 5530-5533.
[37] M. Di Vaira, C. A. Ghilardi, S. Midollini, L. Sacconi, *J. Am. Chem. Soc.* **1978**, *100*, 2550-2551.
[38] O. J. Scherer, H. Sitzmann, G. Wolmershäuser, *J. Organomet. Chem.* **1984**, *268*, C9-C12.
[39] (a) J. Bai, E. Leiner, M. Scheer, Angew. Chem. Int. Ed. 2002, 41, 783-786.
(b) M. Scheer, L. J. Gregoriades, M. Zabel, J. Bai, I. Krossing, G. Brunklaus, H. Eckert, *Chem. Eur. J.* **2008**, *14*, 282-295.
(c) S. Welsch, M. Bodensteiner, M. Dušek, M. Sierka, M. Scheer, *Chem. Eur. J.* **2010**, *16*, 13041-13045.
(d) B. Attenberger, S. Welsch, M. Zabel, E. Peresypkina, M. Scheer, *Angew. Chem. Int. Ed.* **2011**, *50*, 11516-11519.
(e) M. Fleischmann, S. Welsch, E. V. Peresypkina, A. V. Virovets, M. Scheer, *Chem. Eur. J.* **2015**, *21*, 14332-14336.
(f) M. E. Moussa, B. Attenberger, E. V. Peresypkina, M. Fleischmann, G. Balázs, M. Scheer, *Chem. Commun.* **2016**, *52*, 10004-10007.
(g) M. Fleischmann, J. S. Jones, G. Balázs, F. P. Gabbaï, M. Scheer, *Dalton Trans.* **2016**, *45*, 13742-13749.
[40] H. Lang, L. Zsolnai, G. Huttner, *Angew. Chem. Int. Ed. Engl.* **1983**, *22*, 976-976.
[41] (a) M. L. Ziegler and H.-P. Neumann, *Chem. Ber.* **1989**, *122*, 25-30.
(b) F. P. Arnold, D. P. Ridge and A. L. Rheingold, *J. Am. Chem. Soc.* **1995**, *117*, 4427-4428.
(c) M. H. Chisholm, K. Folting and J. W. Pasterczyk, *Inorg. Chem.* **1988**, *27*, 3057-3058.
(d) M. H. Chisholm, J. C. Huffman and J. W. Pasterczyk, *Inorg. Chim. Acta* **1987**, *133*, 17-18.
(e) G. Becker, W. Becker, R. Knebl, H. Schmidt, U. Hildenbrand and M. Westerhausen, *Phosphorus and Sulfur* **1987**, *30*, 349-352.
(f) P. Binger, *Multiple Bonds and Low Coordination in Phosphorus Chemistry*, ed. M. Regitz, 0. J. Scherer, Thieme, Stuttgart, **1990**, p. 100.
(g) J. F. Nixon, *Chem. Rev.* **1988**, *88*, 1327-1362.
[42] M. Scheer, K. Schuster, T. A. Budzichowski, M. H. Chisholm, W. E. Streib, *Chem. Commun.* **1995**, 1671-1672.
[43] (a) C. E. Laplaza, W. M. Davis, C. C. Cummins, *Angew. Chem. Int. Ed. Engl.* **1995**, *34*, 2042-2044.
(b) N. C. Zanetti, R. R. Schrock, W. M. Davis, *Angew. Chem. Int. Ed. Engl.* **1995**, *34*, 2044-2046.
[44] O. J. Scherer, J. Schwalb, G. Wolmershäuser, W. Kaim, R. Gross, *Angew. Chem. Int. Ed. Engl.* **1986**, *25*, 363-364.
[45] (a) O. J. Scherer, T. Brück, *Angew. Chem. Int. Ed. Engl.* **1987**, *26*, 59-59.
(b) O. J. Scherer, T. Brück, G. Wolmershäuser, *Chem. Ber.* **1988**, *121*, 935-938.
[46] E. Urnèžius, W. W. Brennessel, C. J. Cramer, J. E. Ellis, P. v. R. Schleyer, *Science* **2002**, *295*, 832-834.
[47] O. J. Scherer, H. Sitzmann, G. Wolmershäuser, *Angew. Chem. Int. Ed. Engl.* **1985**, *24*, 351-353.
[48] O. J. Scherer, H. Swarowsky, G. Wolmershäuser, W. Kaim, S. Kohlmann, *Angew. Chem. Int. Ed. Engl.* **187**, *26*, 1153-1155.
[49] (a) M. Baudler, H. Ternberger, W. Faber, J. Hahn, *Z. Naturforsch.* **1979**, *B34*, 1690-1697.
(b) M. Baudler, T. Pontzen, J. Hahn, H. Ternberger, W. Faber, *Z. Naturforsch.* **1980**, *B35*, 517-521.
(c) M. Baudler, W. Faber, *Chem. Ber.* **1980**, *113*, 3394-3395.
(d) M. Baudler, *Angew. Chem.* **1982**, *94*, 520-539; *Angew. Chem. Int. Ed. Engl.* **1982**, *21*, 492-512.
(e) M. Baudler, O. Exner, *Chem. Ber.* **1983**, *116*, 1268-1270.
(f) M. Baudler, D. Düster, K. Langerbeins, J. Germeshausen, *Angew. Chem.* **1984**, *96*, 309-310; *Angew. Chem. Int. Ed. Engl.* **1984**, *23*, 317-318.
(g) M. Baudler, R. Heumüller, D. Düster, J. Germeshausen, J. Hahn, *Z. anorg. allg. Chem.* **1984**, *518*, 7-13.
(h) M. Baudler, R. Becher, J. Germeshausen, Chem. Ber. 1986, 119, 2510-2516.

(i) S. Du, J. Hu, Z. Chai, W.-X. Zhang, Z. Xi, *Chin. J. Chem.* **2019**, *37*, 71-75.

[50] F. Dielmann, M. Sierka, A. V. Virovets, M. Scheer, *Angew. Chem.* **2010**, *122*, 7012-7016; *Angew. Chem. Int. Ed. Engl.* **2010**, *49*, 6860-6864.

[51] L. Mu, S. Yang, X. Bao, H. Yin, X. Kong, *J. Mass Spectrom.* **2015**, *50*, 1352-1357.

[52] C. Schwarzmaier, A. Y. Timoshkin, G. Balázs, M. Scheer, *Angew. Chem. Int. Ed. Engl.* **2014**, *53*, 9077-9081.

[53] G. Dettlaf, E. Weiss, *J. Organomet. Chem.* **1976**, *108*, 213-223.

[54] C. Eichhorn, O. J. Scherer, T. Sögding, G. Wolmershäuser, *Angew. Chem. Int. Ed.* **2001**, *40*, 2859-2861.

[55] O. J. Scherer, T. Hilt, G. Wolmershäuser, *Angew. Chem. Int. Ed. Engl.* **2000**, *39*, 1425-1427.

[56] (a) W. Wichelhaus, H. G. von Schnering, *Naturwissenschaften* **1973**, *60*, 104.
(b) N. Korber, J. Daniels, H. G. von Schnering, *Angew. Chem. Int. Ed. Engl.* **1996**, *35*, 1107-1110.
(c) H. G. von Schnering, D. Fenske, W. Hönle, M. Binnewies, K. Peters, *Angew. Chem. Int. Ed. Engl.* **1979**, *18*, 679-680.
(d) M. Baudler, H. Jachow, J. Germershausen, *Z. Anorg. Allg. Chem*. **1987**, *553*, 15-23.
(e) K.-F. Tebbe, *Z. Anorg. Allg. Chem.* **1989**, *572*, 115-125.

[57] M. Scheer, S. Deng, O. J. Scherer, M. Sierka, *Angew. Chem. Int. Ed.* **2005**, *44*, 3755-3758.

[58] (a) **D‴**: C. Schwarzmaier, S. Heinl, G. Balázs, M. Scheer, *Angew. Chem. Int. Ed. Engl.* **2015**, *54*, 13116-13121.
(b) **D***: R. Grünbauer, *Master Thesis*, University of Regensburg (Regensburg), **2016**.

[59] M. Eberl, *Ph. D. Thesis*, University of Regensburg (Regensburg), **2011**.

[60] J. Müller, S. Heinl, C. Schwarzmaier, G. Balázs, M. Keilwerth, K. Meyer, M. Scheer, *Angew. Chem. Int. Ed.* **2017**, *56*, 7312-7317.

[61] (a) S. Heinl, M. Scheer, *Chem. Sci.* **2014**, *5*, 3221-3225.
(b) S. Heinl, S. Reisinger, C. Schwarzmaier, M. Bodensteiner, M. Scheer*, Angew. Chem. Int. Ed.* **2014**, *53*, 7639-7642.

[62] C. Schwarzmaier, A. Y. Timoshkin, G. Balázs, M. Scheer, *Angew. Chem. Int. Ed.* **2014**, *53*, 9077-9081.

2. Research objectives

Understanding the fundamental processes of P_4 activation could propose new pathways in the generation of phosphorus containing compounds ultimately rendering the current toxic, uneconomical and wasteful approach as obsolete. Intrigued by previous results, synthetic pathways originating from P_4 butterfly compounds are a fascinating possibility to obtain new P_n ligand complexes and furthermore gain insight in the subsequent processes of P_4 activation. Therefore, the isolobal compounds [{Cp‴Fe(CO)$_2$}$_2$(μ,η$^{1:1}$-P$_4$)] (**1**) and [{Cp*Cr(CO)$_2$}$_3$(μ,η$^{1:1}$-P$_4$)] (**2**) are chosen as starting materials to investigate the reactivity potential of P_4 butterfly compounds. On the one hand their isolobality suggests a rather similar reaction behavior, whereas the differing nature of the organometallic substituents is expected to promote unique reactivities as well. Hence, the combination of the two starting materials is predestined to evaluate the influence of the organometallic substituent on the reactivity of the P_n ligand complex.

Previously, the coordination behavior of **1** towards different Lewis acids has been investigated resulting in coordination processes as well as novel rearrangement pathways. However, the reactions were mostly limited to small Lewis acids like coinage metal or Fe(II) salts. Hence tasks of this thesis are:

- Investigating the relatively unknown reactivity of **2** towards different Lewis acids.
- Expanding the reactivity of **1** towards more elaborate Lewis acidic metallcarbonyles.

In contrast to the reactivity towards Lewis acids, the reactivity of P_4 butterfly complexes towards nucleophiles has not been studied to date. Therefore, another task of this thesis is:

- Investigating the reactivity of **1** and **2** towards different nucleophiles.

Lastly, the rather labile P–Cr bond in **2** suggest the possibility of selective bond cleavage ultimately yielding an unsubstituted P_4 butterfly motif which could be available for the reaction with newly introduced substituents. Consequently, the generation of novel P_4 butterfly complexes could be achieved. Therefore, the final task of this thesis is:

- Utilizing **2** in the selective transfer of the P_4 butterfly unit to obtain novel P_4 butterfly complexes.

3. The butterfly complex [{Cp*Cr(CO)$_3$}$_2$(μ,η$^{1:1}$-P$_4$)] as a versatile ligand and its unexpected P$_1$/P$_3$ fragmentation route

Rebecca Grünbauer, Gábor Balázs and Manfred Scheer

3.1 Abstract

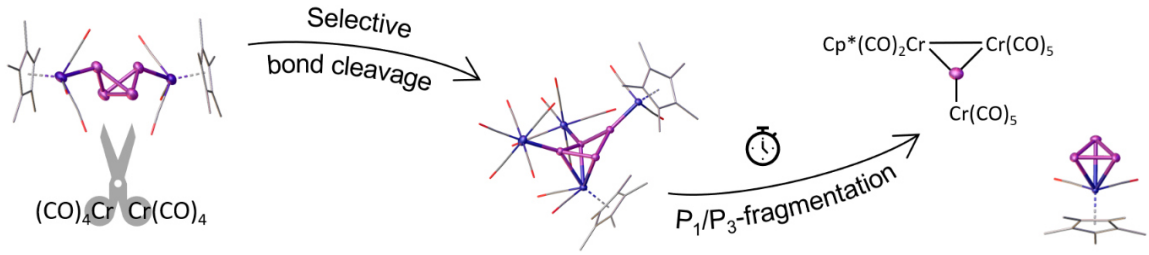

*The versatile coordination behavior of the P$_4$ butterfly complex [{Cp*Cr(CO)$_3$}$_2$(μ,η$^{1:1}$-P$_4$)] (**1**) towards Lewis acidic pentacarbonyl compounds of Cr, Mo and W is reported. The reaction of **1** with [W(CO)$_4$(nbd)] (nbd = norbornadiene) yields the complex [{Cp*Cr(CO)$_3$}$_2$(μ$_3$,η$^{1:1:1:1}$-P$_4$){W(CO)$_4$}] (**2**), in which **1** serves as a chelating P$_4$ butterfly ligand. In contrast, reactions of **1** with [M(CO)$_4$(nbd)] (M = Cr (**a**), Mo (**b**)) result in the step-wise formation of [{Cp*Cr(CO)$_2$}$_2$(μ$_3$,η$^{3:1:1}$-P$_4$){M(CO)$_5$}] (**3**) and [{Cp*Cr(CO)$_2$}$_2$(μ$_4$,η$^{3:1:1:1}$-P$_4$){M(CO)$_5$}$_2$] (**4**), which contain a folded cyclo-P$_4$ unit. **4a** undergoes an unprecedented P$_1$/P$_3$-fragmentation yielding the cyclo-P$_3$ complex [Cp*Cr(CO)$_2$(η^3-P$_3$)] (**5**) and the yet unknown phosphinidene complex [Cp*Cr(CO)$_2$(Cr(CO)$_5$)$_2$(μ$_3$-P)] (**6**). The identity of **6** is confirmed by spectroscopic methods and by the in-situ formation of [{Cp*Cr(CO)$_2$(^{t}BuNC)}P{Cr(CO)$_5$}$_2$(^{t}BuNC)] (**7**). DFT calculations shade light in the bonding situation of the reported products.*

3.2 Introduction

The activation of small molecules is currently of great importance, as hereby uneconomical industrial scale reactions can be improved by making them more atom-efficient, clean, sustainable and inexpensive.[1] Within this field, the investigations considering the activation of P_4 describe the subsequent P–P bond cleavage of the tetrahedral P_4 molecule of white phosphorus.[2] Ultimately, the goal of these studies is to achieve insight in controlling the remarkable reactivity of P_4 and eventually obtain organo-phosphorus compounds in a more sustainable way. The first step of the selective degradation of the P_4 tetrahedron is the formation of the tetraphospha-*bicyclo*[1.1.0]butane moiety (often entitled P_4 butterfly due to its geometry). This moiety can be used as a ligand in coordination chemistry, typically displaying small bite angles, like usual chelating diphosphine ligands.[3] This was demonstrated by the synthesis of the transition-metal stabilized bridging P_4 butterfly complex [{Cp'''Fe(CO)$_2$}$_2$(μ,η$^{1:1}$-P$_4$)] (**A**, Cp''' = η^5-C$_5$H$_2$^{t}Bu$_3$).[4]

The continuative degradation of white phosphorus via the P_4 butterfly structure is widely investigated and a plethora of polyphosphorus compounds could be isolated.[2] However, only very few examples are reported for a controlled fragmentation of the intact P_4 butterfly moiety affording a P_1 and a P_3 fragment. One of the reported examples originates from the butterfly anion Li[Mes*P$_4$·BR$_3$].[5] *Lammertsma et al.* studied its reactivity towards imidazolium salts and phenylisocyanate yielding the stabilized phosphinidene adducts and [Mes*P$_3$] fragments. They could isolate the P_3 fragment as the respective dimer [Mes*P$_3$]$_2$ or as the Diels-Alder adduct [Mes*P$_3$(C$_6$H$_8$)] after employing the trapping agent 1,3-cyclohexadiene. Starting from elemental phosphorus, *Zhang et al.* used intricate rare-earth-metal complexes to obtain *bicyclo*[4.1.0]triphospha-heptanide ligands alongside with phospholyl lithium.[6] Both of these fragmentation routes require additional reactants like non-innocent ligands in order to induce the P_1/P_3 fragmentation. A first step towards a more untouched P_1/P_3 fragmentation route was reported by reacting [Cp*Ni(μ-CO)]$_2$ with P_4 in the presence of stabilizing [Cr(CO)$_5$] fragments.[7] Various steps of irridiation and thermolysis induce the fragmentation process affording a bend *cyclo*-P$_4$ structure. Subsequently, the formation of [Cp*Ni(η^3-P$_3$){Cr(CO)$_5$}$_3$] and an [Cp*Ni≡P-Cr(CO)$_5$] intermediate that could be isolated as its corresponding dimer [{Cp*Ni}$_2$(μ,η$^{2:2}$-P$_2$){Cr(CO)$_5$}$_2$] was observed.

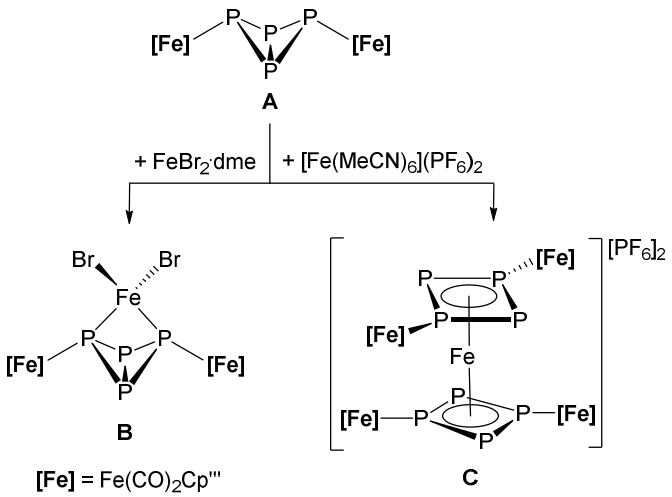

Scheme 1. Coordination and isomerization obtained from the reaction of **A** with different Fe(II) Lewis acids.

DFT calculations predicted that a chelating coordination mode via the lone pairs of the two wing tip P atoms of **A** is energetically most favorable.[8] Therefore, we studied the coordination behavior of **A** towards monovalent coinage metal salts and different Fe(II) compounds.[8,9] As anticipated, chelating coordination products, e.g. [{Cp'''Fe(CO)$_2$}$_2$(μ_3,$\eta^{1:1:1:1}$-P$_4$){FeBr$_2$}][8] (**B**, Scheme 1), in which **A** acts as a bidentate ligand could be obtained. With 70.27(3)° the bite angle of **B** compares well to the bite angle reported for dppm (72(2)°, 1,2-bis(diphenylphosphino)methane).[3] In contrast, [Fe(MeCN)$_6$]$^{2+}$, a Lewis acid containing labile acetonitrile ligands, reacts with **A** by inducing an isomerization of the P$_4$ butterfly unit forming the 6π-aromatic *cyclo*-P$_4$ sandwiched dication [{(Cp‴Fe(CO)$_2$)$_2$(μ_3,$\eta^{1:1:4}$-P$_4$)}$_2$Fe]$^{2+}$ (**C**, Scheme 1).[9]

While the reactivity of **A** under photolytic[10] and thermolytic[4] reaction conditions, its reactivity towards alkynes[11] and its coordination chemistry[8,9] have been intensively studied, the reactivity of the isostructural chromium containing complex [{Cp*Cr(CO)$_3$}$_2$(μ,$\eta^{1:1}$-P$_4$)] (**1,** Cp* = η^5-C$_5$(CH$_3$)$_5$) has only been scarcely investigated.[12] Consequently, this encouraged us to further study the reactivity of **1** and the question arose, whether simple coordination chemistry expected for a chelating polyphosphine would occur or a much more diverse reaction pathway would be unraveled.

3.3 Results and Discussion

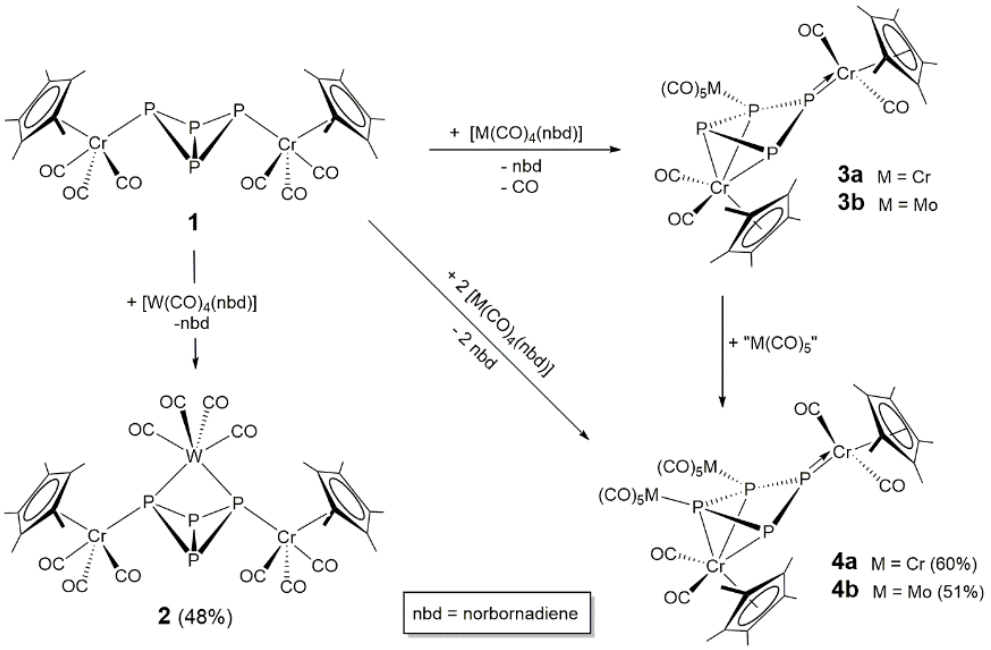

Scheme 2. Reactions of **1** with Lewis acidic [M(CO)$_4$(nbd)] (M = Cr, Mo, W).

Herein we report on the reaction of **1** with Lewis acidic group six carbonyl complexes [M(CO)$_4$(nbd)] (M = Cr, Mo, W; nbd = norbornadiene). The weakly coordinating norbornadiene ligand is expected to be replaced by the more strongly donating P$_4$ butterfly ligand affording new organometallic P$_4$ coordination compounds. The reaction of **1** with 1.0 eq. [W(CO)$_4$(nbd)] selectively yields the chelating adduct [{Cp*Cr(CO)$_3$}$_2$(μ_3,$\eta^{1:1:1:1}$-

P$_4$){W(CO)$_4$}] (**2**, Scheme 2). The formation of the tetraphosphatungsten-*tricyclo*[1.1.1.0^{2,4}]pentane compound could be verified by single crystal X-ray diffraction analysis.[13] Hereby, only little influence of the bidentate coordination on the overall structure of the P$_4$ scaffold could be detected in comparison to **1** (Fig. 1). While for **2** bond lengths and angles similar to those for **1** are given, the central P$_4$ unit in **2** is slightly distorted, whereas this moiety in **1** is more symmetrical. Due to the distortion, which probably perseveres in solution, **2** displays an AA'BB' spin system with a relatively large $\delta_{AA'}$ / $\delta_{BB'}$ separation affording two multiplets at δ = −168.8 ppm (bridgehead P atoms) and δ = −153.8 ppm (wing tip P atoms) in the ^{31}P{^{1}H} NMR spectrum. The outstanding feature of **2** is the exceedingly small P1–W–P2 bite angle of 64.21(11)° again highlighting the structural familiarity to the dppm ligand.[3]

Surprisingly, the reactions of **1** with [M(CO)$_4$(nbd)] (M = Cr (**a**), Mo (**b**)) do not afford P$_4$ butterfly–Lewis acid adducts, but the monosubstituted [{Cp*Cr(CO)$_2$}$_2$(μ$_3$,η$^{3:1:1}$-P$_4$){M(CO)$_5$}] (**3**) and the disubstituted derivative [{Cp*Cr(CO)$_2$}$_2$(μ$_4$,η$^{3:1:1:1}$-P$_4$){M(CO)$_5$}$_2$] (**4**) (Scheme 2). During the formation of **3** and **4** a cleavage of the P–P bond between the former bridgehead P atoms of **1** is observed affording a folded deltoid *cyclo*-P$_4$ unit as the central structural moiety. This is a direct result from an initial CO shift from the [Cp*Cr(CO)$_3$] substituents of **1** to the [M(CO)$_4$] fragments yielding [Cp*Cr(CO)$_2$] substituents and [M(CO)$_5$] units. The consequential electron deficit on Cr2 is balanced by an additional coordination of the two former bridgehead phosphorus atoms towards Cr2, leading to the cleavage of the P–P bond (labeling according to Fig. 1). The electron deficit of the Cr1 fragment is balanced by the formation of a formal double bond between Cr1 and the adjacent P1 atom and the former wing tip atom P1 reaches a planar coordination environment. The formal P=Cr double bond can be viewed as an additional coordination of the P lone pair to the Cr1 atom since the [Cp*Cr(CO)$_2$] fragment requires 3 additional electrons according to the 18 VE rule. Various terminal or bridging, square planar or distorted *cyclo*-P$_4$ ligands have been reported either as bare polyphosphorus units or stabilized by different Lewis acids.[2] However, the folded deltoid *cyclo*-P$_4$ unit of **3** and **4** represents a novel structural motif due to the adjacent P=Cr double bond that can be interpreted as the tail of the *cyclo*-P$_4$ kite. The structurally most related compound to **3** and **4** is [{(CH$_3$CN)$_2$(CO)$_2$WCl}(η^3-P$_3${W(CO)$_5$}$_2$-P{(X)W(CO)$_5$})] (X = Cl, OH) for which no phosphorus metal double bond but an additional stabilization with a chloride or hydroxy group on the P1 atom is observed.[14]

According to DFT calculations, the reaction of **1** with [Cr(CO)$_4$(nbd)] is slightly endothermic (1.34 kJ·mol^{-1}) while the reaction of **1** with [W(CO)$_4$(nbd)] yielding **2** is exothermic (−6.49 kJ·mol^{-1}). This reinforces that a stable complex, such as [{Cp*Cr(CO)$_3$}$_2$(μ$_3$,η$^{1:1:1:1}$-P$_4$){Cr(CO)$_4$}] ("**2a**") is not formed, but rather a CO shift from a [Cp*Cr(CO)$_3$] unit to the [Cr(CO)$_4$] moiety occurs.

When the reaction of **1** with [M(CO)$_4$(nbd)] (M = Cr (**a**), Mo (**b**)) is performed in a 1:1 stoichiometry, the mono-substituted compound **3** is the main product in the reaction solution alongside with traces of **4**. However, the conversion of **1** is limited to 50% due to the mismatched CO count. Two CO ligands are abstracted from each molecule of **1**, but only one CO ligand is needed to obtain a [M(CO)$_5$] fragment from [M(CO)$_4$(nbd)] (M = Cr, Mo). In contrast, **4** is formed almost quantitively (besides some impurities of **3**), when the reaction of **1** with [M(CO)$_4$(nbd)] (M = Cr, Mo) is performed in a 1:2 ratio. Attempts to isolate **3** by crystallization lead to rearrangement to **4**, which exclusively crystallizes from the solution. This process was monitored by ^{31}P{^{1}H} NMR spectroscopy (*vide infra*). Therefore, reasonable amounts of pure **3** could not be isolated although different isolation methods and alternative synthetic pathways have been examined. Yet, a few single crystals of **3a** could be obtained from the reaction mixture after storage at -78 °C, whereas **4a** already crystallizes

at -28 °C (Fig. 1). Unfortunately, no single crystals could be obtained for **3b** but a similar structure to **3a** can be proposed based on NMR spectroscopic data.[15] Compounds **3a**, **4a** and **4b** all crystallize readily in the form of stacked plates from saturated solutions in CH_2Cl_2 at -28 °C (**3a**: $P2_1/c$; **4a** and **4b**: $P\bar{1}$).The central deltoid *cyclo*-P_4 structural motif of **3a**, **4a** and **4b**, respectively, is very similar. The distances for the P1–P2 bond (**3a**: 2.2181(7) Å, **4a**: 2.2265(13) Å, **4b**: 2.2259(13) Å) and the P1–P3 bond (**3a**: 2.1973(7) Å, **4a**: 2.2013(14) Å, **4b**: 2.1938(13) Å) comply well with the value for an usual P–P single bond (2.209(5) Å).[16] In contrast, the P2–P4 bond (**3a**: 2.1606(7) Å, **4a**: 2.1390(15) Å, **4b**: 2.1427 (13) Å) and P3–P4 bond (**3a**: 2.1705(7) Å, **4a**: 2.1583(12) Å, **4b**: 2.1560(13) Å) are noticeably shortened indicating a delocalized electron system between P2, P3 and P4 (labeling according to Fig. 1). The Cr1–P1 bond attached to the rearranged *cyclo*-P_4 unit (**3a**: 2.1258(6) Å, **4a**: 2.1129(11) Å, **4b**: 2.1169 (11) Å) is significantly shortened in comparison to the corresponding P–Cr bond length in **1** (2.529(2) Å), revealing a Cr1–P1 multiple bond character. Moreover, the degree of folding of the *cyclo*-P_4 unit is independent of the nature of the substituent pattern as **3a**, **4a** and **4b** display nearly identical folding angles (**3a**: 135.50(8)°, **4a**: 135.92(6)°, **4b**: 136.18(8)°).

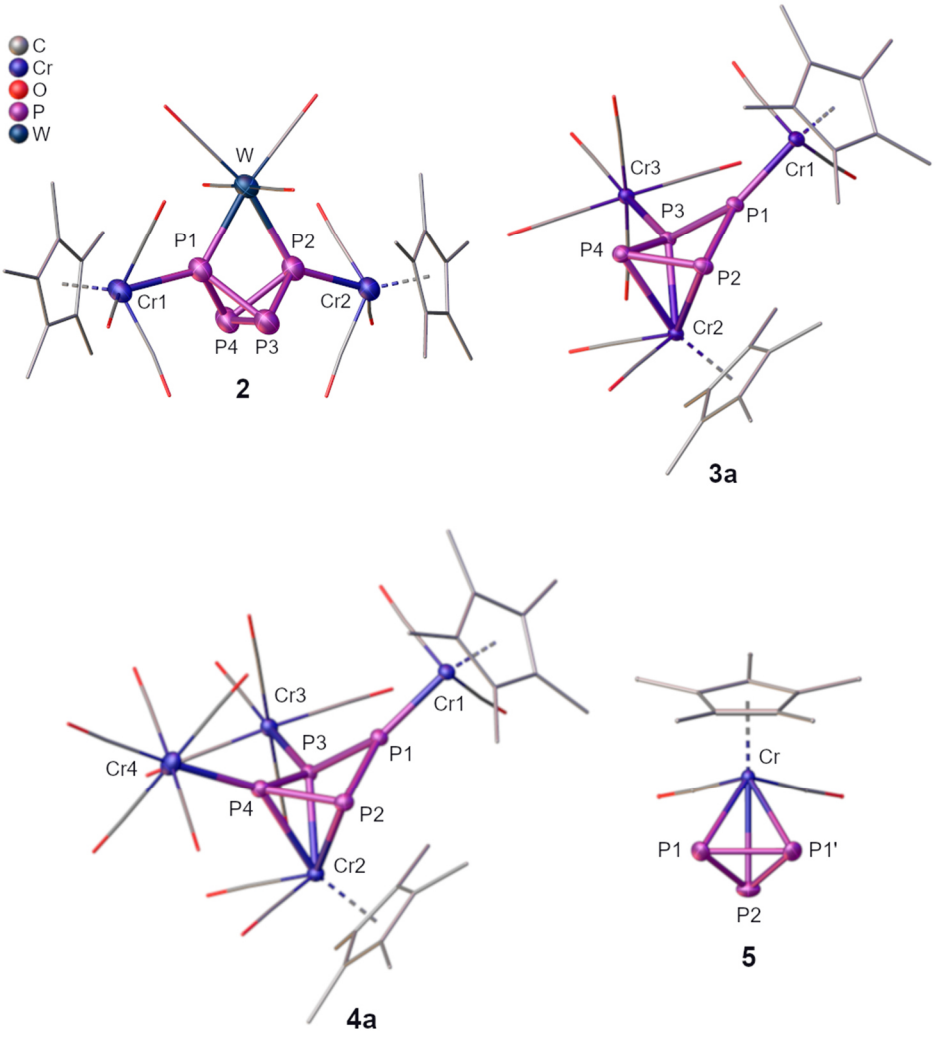

Figure 1. Molecular structures of **2**, **3a, 4a** and **5** in the solid state; H atoms and solvent molecules are omitted for clarity and CO as well as Cp* ligands are drawn in the wire frame model; thermal ellipsoids are drawn at 50% probability level.

The ^{31}P{^{1}H} NMR spectra of **3** and **4** are very similar displaying an AMNX spin system.[15] The chemical shift of the signal attributed to P$_A$ (δ = 515.4 ppm (**3a**), 515.4 ppm (**3b**), 489.1 ppm (**4a**), 487.8 ppm (**4b**); P1 in Fig. 1) is in the typical range for a phosphorus atom in planar environment that is part of a formal phosphorus metal multiple bond. In comparison to the formal [Cr=P(P)$_2$] structural motif in **3** and **4**, the ^{31}P NMR chemical shift of the trigonal planar [Mn=P(Fe)$_2$] moiety of [{(CpMn(CO)$_2$)-(μ$_3$,η$^{1:1:1}$-P)}$_2${Fe$_2$(CO)$_6$}] is even more downfield shifted (δ(^{31}P) = 977 ppm).[17] The ^{31}P{^{1}H} NMR spectrum of the reaction mixture after stirring **1** with 1.0 eq. of [Cr(CO)$_4$(nbd)] in thf for 3 days shows the signal set characteristic for **3a** (Fig. S6a in SI) as the main product as well as traces of **4a**. In contrast, the ^{31}P{^{1}H} NMR spectrum of the crystals obtained from storing the concentrated reaction mixture at -28 °C displays exclusively the signals of **4a** (Fig. S6b in SI). Obviously, **3a** coordinates to an excess of [Cr(CO)$_5$] units present in the solution during the crystallization process. Consequently, **4a** is formed, which crystallizes due to its lower solubility. The ^{31}P{^{1}H} NMR spectrum of the supernatant of the obtained crystals exhibits signals for both major compounds **3a** and **4a**. However, the intensity of the signals corresponding to **3a** decreased significantly in comparison to the signals corresponding to **4a**, now promoting **4a** to the primary component in solution after crystallization (Fig. S6c in SI). In summary, storing the concentrated reaction solution at low temperatures leads to the formation of **4a** from **3a** and excess [Cr(CO)$_5$] in the form of crystalline **4a** as well as in solution. The same observations can be reported for **3b** and **4b** but in the ^{31}P{^{1}H} NMR spectrum of crystalline **4b** minor amounts of **3b** can be detected indicating partial degradation after re-dissolving.

In order to elucidate the electronic structure of **4a**, DFT calculations at the B3LYP/def2-TZVP level were performed.[18] The DFT optimized geometry of **4a** compares well with the experimental geometry. According to NBO analysis, the Cr1–P1 bond is a double bond built from a σ-type and a π-type bond (Fig. 2). The σ-bond is realized over a sp$^{0.9}$ hybrid orbital on phosphorus and a sd$^{2.2}$ hybrid orbital on chromium, while the π-orbital is realized over a pure p-orbital on P and pure d-orbital on Cr. The partial double bond character is also reflected in the Wiberg Bond Index (WBI) of 1.16, while the WBI of the Cr3–P3 bond is 0.39.[15] The WBIs of the P1–P2 and P1–P3 bonds are slightly lower (0.91 and 0.93) then the WBIs of the P2–P4 and P3–P4 bonds (1.06 and 0.99).

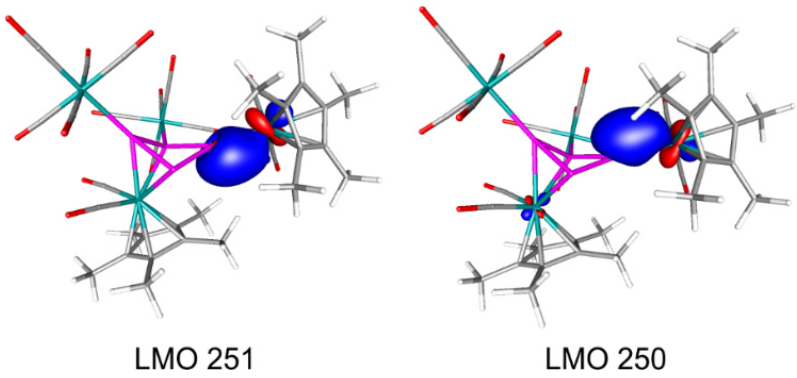

Figure 2. Localized molecular orbitals of **4a** representing the Cr1–P1 multiple bond.

A common observation for all experiments performed with **1** is the sensitivity of **1** towards temperature and light causing slow decomposition even at mild reaction conditions. In nearly all manipulations starting from **1**

one characteristic singlet at approx. -270 ppm can be detected in the $^{31}P\{^{1}H\}$ NMR spectrum. By comparison with literature data for similar compounds *Scherer et al.* attributed this chemical shift to [Cp*Cr(CO)$_2$(η^3-P$_3$)] (**5**)[19] and within this work we were able to confirm this proposal by single crystal X-ray diffraction of the isolated compound **5** (Fig. 1).[20] Alongside **5**, an insoluble solid (probably a mixture of various polyphosphides) is obtained after the quantitative decomposition of **1.**

Remarkably, after stirring a solution of **4a** in thf for three days at 50 °C a distinct second degradation product can be detected. In the $^{31}P\{^{1}H\}$ NMR spectrum, an additional singlet at δ = 1123.7 ppm is recorded next to the characteristic singlet at δ = -273.3 ppm corresponding to **5**. The drastic low field shift of this novel signal indicates a planar coordination sphere of the corresponding P atom, as it is typical for planar phosphinidene complexes like the μ$_3$-bridging complex [{CpW(CO)$_2$}(μ$_3$-P){Cr(CO)$_5$}$_2$] (**B**, δ(^{31}P NMR) = 945 ppm).[21] Hence, we propose the structurally analog [{Cp*Cr(CO)$_2$}(μ$_3$-P){Cr(CO)$_5$}$_2$] (**6**) as the second compound obtained from the degradation of **4a** attributable to the second signal at δ = 1123.7 ppm) observed in the $^{31}P\{^{1}H\}$ NMR spectrum. Although **6** could not be characterised by single crystal X-ray diffraction analysis, the mutual extreme low field ^{31}P NMR chemical shifts of **6** and **B** validate the proposed structure of **6**. Consequently, an unprecedented type of selective P$_1$/P$_3$-fragmentation of **4a** yielding **5** and **6** can be proposed (Scheme 3). A closer look on the molecular structure of **4a** in the solid state further supports the proposed P$_1$/P$_3$-fragmentation. As discussed above, two different P–P bond lenghts can be found in **4a**. The two longest and therefore comparatively weakest P–P bonds (P1–P2 and P1–P3) appear to be the predetermined breaking points of **4a** finally affording **5** and **6**.

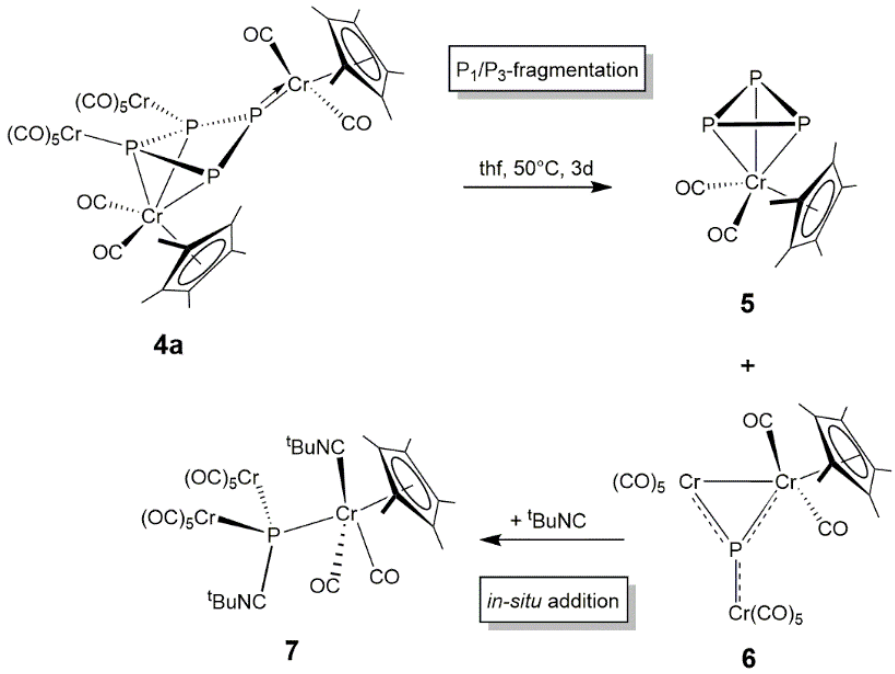

Scheme 3. P$_1$/P$_3$-fragmentation of **4a** and subsequent phosphinidene adduct formation of the obtained P$_1$-fragment **6** yielding **7**.

Since it was not possible to isolate **6** as a pure compound from the reaction mixture, we attempted to trap **6**

with ^{t}BuNC as this type of reaction is widely known for phosphinidene complexes. For instance, ^{t}BuNC reacts with [Cp*P{W(CO)$_5$}$_2$] affording the Lewis acid/base (LA/LB) adduct [Cp*P{W(CO)$_5$}$_2$(^{t}BuNC)].[22] Diagnostic is the extreme change in the ^{31}P NMR chemical shift from δ = 1076.5 ppm[22a] for the phosphinidene complex to δ = −73.1 ppm[22b] for the LA/LB adduct. Following this strategy, an excess of ^{t}BuNC was added to a solution of **6**. The reaction was monitored by ^{31}P{^{1}H} NMR spectroscopy, which shows that the characteristic signal for **6** at δ = 1124 ppm disappears while a new signal at δ = −166 ppm appears indicating the full conversion of **6** into the proposed LA/LB adduct [{Cp*Cr(^{t}BuNC)(CO)$_2$}-(μ$_3$-P){Cr(CO)$_5$}$_2$] (**7**, Scheme 3). In **7** the planar coordination geometry of the P atom is abolished by the additional coordination of one ^{t}BuNC ligand yielding a pseudo-tetrahedral phosphinidene adduct. Consequently, the deshielding of the P atom is strongly reduced leading to the drastic change in the chemical shift. A second ^{t}BuNC ligand additionally coordinates to the Cp*Cr(CO)$_2$ fragment, compensating the arisen electron deficit at the Cr atom accordingly. According to DFT calculations, the coordination of one ^{t}BuNC to the P atom in the center of **6** is exothermic with −48.5 kJ·mol^{-1}. The addition of the second ^{t}BuNC molecule to the Cp*Cr(CO)$_2$ fragment is even more exothermic with −53.2 kJ·mol^{-1}, indicating that the coordination of two ^{t}BuNC ligands to **6** is to be expected. In order to prove the identity of **6** and **7**, the ^{31}P NMR chemical shifts of **5**, **B**, **6** and **7** have been calculated by DFT methods. For this, the geometry of the compounds has been optimized in the gas phase at the BP86/Def2TZVP level of theory. For the calculation of the ^{31}P NMR chemical shifts using the GIAO method the aug-pcSseg-2 basis set for phosphorus has been used. The values of the calculated chemical shifts are in good agreement with the experimental values (Table 1), validating the proposed identity of **6** and **7**.

Table 1. Experimental (δ_{exp}) and calculated (δ_{cal}) ^{31}P NMR chemical shifts of compounds **5**, **B**, **6** and **7**.

	5	**B**	**6**	**7**
δ_{exp} / ppm	-273[a]	945[b]	1124[a]	−166[a]
δ_{cal} / ppm	-242	1046	1221	−111

[a] recorded in thf with C_6D_6 capillary at room temperature

[b] recorded in CD_2Cl_2 at -20°C[21]

It has to be noted, that the ^{31}P chemical shifts are very sensitive to geometry changes. In order to evaluate the accuracy of the calculated chemical shifts, we also included the known phosphinidene complex [CpW(CO)$_2$(Cr(CO)$_5$)$_2$(μ$_3$-P)] (**B**)[21] in our calculations. The calculated ^{31}P chemical shift of δ = 1046 ppm is in good agrement with the experimental value of δ = 954 ppm. This shows, that the electronic structure of **B** and **6** are well described by the applied DFT methods and confirms the identity of **6**.

3.4 Conclusion

In conclusion, we were able to illustrate the diverse coordination behavior of the P$_4$ butterfly complex **1** towards Lewis acidic carbonyl compounds of Cr, Mo and W. On the one hand a chelating coordination yielding **2**, a complex with a P$_4$ butterfly ligand that displays an exceedingly small bite angle, was achieved by implying [W(CO)$_4$] fragments. On the other hand, **1** manifested to be a promising starting material for rearrangement

processes yielding new compounds with folded *cyclo*-P_4 units (**3** and **4**), when reacted with [$M(CO)_4$] moieties (M = Cr (**a**), Mo (**b**)). Most importantly, an unprecedented P_1/P_3-fragmentation route was observed starting from **4a** yielding the *cyclo*-P_3 complex **5** and the novel μ_3-bridging phosphinidene compound **6**. The proposed structure of **6** could be verified by $^{31}P\{^1H\}$ NMR spectroscopy, DFT calculations and the *in-situ* reaction with ^{t}BuNC yielding the phosphinidene adduct **7**. These results promote the ongoing implementation of P_4 butterfly complexes as starting materials in the formation of unprecedented polyphosphorus compounds which represent further steps is the P_4 activation sequence.

3.5 References

[1] a) N. Hazari, Chem. *Soc. Rev.* **2010**, *39*, 4044-4056; b) I. Mellone, F. Bertini, L. Gonsalvi, A. Guerriero, M. Peruzzini, *Chimia* **2015**, *69*, 331-338; c) Z. Turner, *Inorganics* **2015**, *3*, 597; d) R. A. Henderson, *Trans. Met. Chem.* **1990**, *15*, 330-336; e) V. P. Indrakanti, J. D. Kubicki, H. H. Schobert, *Energy Environ. Sci.* **2009**, *2*, 745-758; f) X. Yin, J. R. Moss, *Coord. Chem. Rev.* **1999**, *181*, 27-59.

[2] a) B. M. Cossairt, N. A. Piro, C. C. Cummins, *Chem. Rev.* **2010**, *110*, 4164-4177; b) M. Caporali, L. Gonsalvi, A. Rossin, M. Peruzzini, *Chem. Rev.* **2010**, *110*, 4178-4235; c) M. Scheer, G. Balázs, A. Seitz, *Chem. Rev.* **2010**, *110*, 4236-4256; d) N. A. Giffin, J. D. Masuda, *Coord. Chem. Rev.* **2011**, *255*, 1342-1359.

[3] P. W. N. M. van Leeuwen, P. C. J. Kamer, J. N. H. Reek, P. Dierkes, *Chem. Rev.* **2000**, *100*, 2741-2770.

[4] O. J. Scherer, T. Hilt, G. Wolmershäuser, *Organometallics* **1998**, *17*, 4110-4112.

[5] J. E. Boger, A. W. Ehlers, M. Lutz, J. C. Slootweg, K. Lammertsma, *Angew. Chem. Int. Ed.,* **2017**, *56*, 285-290.

[6] S. Du, J. Yin, Y. Chi, L. Xu, W.-X. Zang, *Angew. Chem. Int. Ed.,* **2017**, *56*, 15886-15890.

[7] M. Scheer, U. Becker, *Chem. Ber.* **1996**, *129*, 1307-1310.

[8] C. Schwarzmaier, S. Heinl, G. Balázs, M. Scheer, *Angew. Chem.* **2015**, *127*, 13309-13314; *Angew. Chem. Int. Ed. Engl.* **2015**, *54*, 13116-13121.

[9] J. Müller, S. Heinl, C. Schwarzmaier, G. Balázs, M. Keilwerth, K. Meyer, M. Scheer, *Angew. Chem.* **2017**, *129*, 7418-7423; *Angew. Chem. Int. Ed.* **2017**, *56*, 7312-7317.

[10] O. J. Scherer, G. Schwarz, G. Wolmershäuser, *Z. Anorg. Allg. Chem.* **1996**, *622*, 951-957.

[11] O. J. Scherer, T. Hilt, G. Wolmershäuser, *Angew. Chem. Int. Ed. Engl.* **2000**, *39*, 1425-1427.

[12] C. Schwarzmaier, A. Y. Timoshkin, G. Balázs, M. Scheer, *Angew. Chem. Int. Ed.* **2014**, *53*, 9077-9081.

[13] O. V. Dolomanov, L. J. Bourhis, R. J. Gildea, J. A. K. Howard, H. Puschmann, *J. Appl. Cryst.* **2009**, *42*, 339-341.

[14] M. Scheer, M. Dargatz, P. G. Jones, *J. Organomet. Chem.* **1993**, 447, 259-264.

[15] Cf. SI for further detail

[16] a) A. Simon, H. Borrmann, H. Craubner, *Phosphorus Sulfur Silicon Relat. Elem.* **1987**, *30*, 507-710; b) H. Okudera, E. Dinnebier Robert, A. Simon, *Z. Kristallogr.* **2005**, *220*, 259.

[17] H. Lang, L. Zsolnai, G. Huttner, *Angew. Chem. Int. Ed.* **1983**, *22*, 976-976.

[18] The electronic structure of **3a**, **3b**, **4a** and **4b** are very similar, therefore only **4a** will be discussed. For details on the electronic structure of **4a** see SI.

[19] O. J. Scherer, J. Schwalb, G. Wolmershäuser, W. Kaim, R. Groß, *Angew. Chem.* **1986**, *98*, 349-350.

[20] The structure of **5** in the solid state complies well with the known Cp analog [$CpCr(CO)_2(\eta^3\text{-}P_3)$]; L. Y. Goh, C. K. Chu, R. C. S. Wong*, J. Chem. Soc, Dalton Trans.* **1989**, *1*, 1951-1956.

[21] G. Huttner, U. Weber, B. Sigwarth, O. Scheidsteger, H. Lang, L. Zsolnai, *J. Organomet. Chem.* **1985**, *282*, 331-348.

[22] a) M. Scheer, E. Leiner, P. Kramkowski, M. Schiffer, G. Baum, *Chem. Eur. J.* **1998**, *4*, 1917-1923; b) M. Seidl, M. Schiffer, M. Bodensteiner, A. Y. Timoshkin, M. Scheer, *Chem. Eur. J.* **2013**, *19*, 13783-13791.

3.6 Supplementary Information

3.6.1 General remarks

All experiments were carried out under an atmosphere of dry argon or nitrogen using glovebox and schlenk techniques. Residues of oxygen and water were removed from the inert gas by passing it over a BASF R 3-11 (CuO/MgSiO$_3$) catalyst, concentrated H_2SO_4 and finally granulated silica gel. Dry solvents were collected from a Braun SPS Apparatus and degassed prior to use. The deuterated solvents C_6D_6 and CD_2Cl_2 were degassed and dried by stirring with Na/K alloy and CaH_2, respectively, followed by distillation. After the distillation, CD_2Cl_2 was additionally stored over molecular sieve (3 Å) which had previously been dried for four hours under high vacuum at 100 °C. [{Cp*Cr(CO)$_3$}$_2$(μ,η$^{1:1}$-P$_4$)] (**1**)[1] and [M(CO)$_4$(nbd)] (M = Cr, Mo, W)[2] were prepared according to literature procedures.

NMR spectra were recorded at the NMR department of the University Regensburg using a Bruker Advance 300 or 400 spectrometer. Samples are referenced against TMS (^{1}H, ^{13}C) or 85% H_3PO_4 (^{31}P) as external standards. Chemical shifts (δ) are reported in ppm and coupling constants (*J*) in Hz. The spectra were processed using the TopSpin 3.5 software (Bruker) and the WIN-DAISY module of this software was used to perform simulations.[3]

Mass spectrometry experiments were performed by the MS department of the University Regensburg. The LIFDI-, FD-, and EI-MS spectra were recorded on an AccuToF GCX (Jeol) spectrometer. The observed fragments were assigned according to the mass/charge (m/z) ratio and the isotope pattern.

IR spectra were recorded on an ALPHA platinum ATR spectrometer (Bruker Optik GmbH) which was placed inside a glove box. Therefore, the air-sensitive solid samples could be placed directly on the spectrometer without any additional preparative measures.

Elemental analyses were performed by the department of central analyses of the University Regensburg on a Vario micro cube instrument (Elementar Analysensysteme GmbH).

3.6.2 Syntheses

Synthesis of [{Cp*Cr(CO)$_3$}$_2$(μ$_3$,η$^{1:1:1:1}$-P$_4$){W(CO)$_4$}] (2)

A dark orange solution of **1** (100 mg, 0.15 mmol, 1.0 eq.) in thf (5 mL) is added to a slightly yellow solution of [W(CO)$_4$(nbd)] (59 mg, 0.15 mmol, 1.0 eq.) in thf (5 mL). The resulting mixture is stirred at room temperature for 3 days. Hereby, the color of the solution changes from dark orange to red. The solvent is subsequently removed under reduced pressure. The resulting red solid is washed with *n*-hexane and dried in vacuo. To obtain pure **2**, *n*-pentane (15 mL) is slowly added to a concentrated solution of the crude product in dichloromethane (2 mL). Hereby, **2** precipitates as a dark red powder. Crystals suitable for single crystal X-ray analysis were obtained from a saturated solution in *n*-hexane (5 mL) and dichloromethane (1 mL) after storage at -28 °C.

Analytical data for 2

Yield	70 mg (0.8 mmol, 48%).
^{1}H NMR (C_6D_6, 300 K)	δ[ppm] = 1.42 (s, 30H, $C_5(C\underline{H}_3)_3$).
^{31}P NMR (C_6D_6, 300 K)	δ[ppm] = -153.8 (m, 2P, P_A), -168.8 (m, 2P, P_B).
^{31}P{^{1}H} NMR (C_6D_6, 300 K)	δ[ppm] = -153.8 (m, 2P, P_A), -168.8 (m, 2P, P_B).
IR (solid)	$\tilde{\nu}_{CO}$ [cm^{-1}] = 2069 (s), 2019 (s, br), 2006 (s, br), 1992 (s, br), 1988 (s, br).
ES-MS (toluene)	No reasonable peaks detectable.
LIFDI-MS (toluene)	No reasonable peaks detectable.

Synthesis of [{Cp*Cr(CO)$_2$}$_2$(μ$_3$,η$^{3:1:1}$-P$_4$){Cr(CO)$_5$}] (3a)

A dark orange solution of **1** (100 mg, 0.15 mmol, 1.0 eq.) in thf (5 mL) is added to a yellow solution of $[Cr(CO)_4(nbd)]$ (39 mg, 0.15 mmol, 1.0 eq.) in thf (5 mL). The resulting mixture displays a color change from orange to red while it is stirred at room temperature for 3 d. Subsequently, the solvent is removed under reduced pressure. The resulting solid is dried in vacuo and dissolved in CH_2Cl_2 (10 mL). Upon storage at -78°C for two weeks and subsequent storage at -28°C for three months, a few single crystals of **3a** can be obtained.

Analytical data for 3a

^{31}P{^{1}H} NMR (CD_2Cl_2, 300 K)	δ[ppm] = 22.3 (dd, $^{1}J_{MX}$ = 306 Hz, $^{1}J_{NX}$ = 290 Hz, 1P, P_X), 166.3 (dd, $^{1}J_{AN}$ = 257 Hz, $^{1}J_{NX}$ = 290 Hz, 1P, P_N), 226.3 (dd, $^{1}J_{AM}$ = 251 Hz, $^{1}J_{MX}$ = 306 Hz, 1P, P_M), 515.4 (m, 1P, P_A).

Synthesis of [{Cp*Cr(CO)$_2$}$_2$(μ$_3$,η$^{3:1:1}$-P$_4$){Mo(CO)$_5$}] (3b)

A dark orange solution of **1** (100 mg, 0.15 mmol, 1.0 eq.) in thf (5 mL) is added to a yellow solution of $[Mo(CO)_4(nbd)]$ (45 mg, 0.15 mmol, 1.0 eq.) in thf (5 mL). The resulting mixture displays a color change from orange to red while it is stirred at room temperature for 3 d. Subsequently, the solvent is removed under reduced pressure. The resulting solid is dried *in vacuo* and dissolved in CH_2Cl_2 (10 mL). Upon storage **3b** rearranges to **4b** obtainable in the form of dark black crystalline plates.

Analytical data for (3b)

^{31}P{^{1}H} NMR (CD_2Cl_2, 300 K)	δ[ppm] = 29.2 (dd, $^{1}J_{MX}$ = 285 Hz, $^{1}J_{NX}$ = 303 Hz, 1P, P_X), 174.1 (dd, $^{1}J_{AN}$ = 248 Hz, $^{1}J_{NX}$ = 303 Hz, 1P, P_N), 197.1 (dd, $^{1}J_{AM}$ = 251 Hz, $^{1}J_{MX}$ = 285 Hz, 1P, P_M), 515.4 (m, 1P, P_A).

Synthesis of [{Cp*Cr(CO)$_2$}$_2$(μ$_4$,η$^{3:1:1:1}$-P$_4$){Cr(CO)$_5$}$_2$] (4a)

A dark orange solution of **1** (200 mg, 0.3 mmol, 1.0 eq.) in thf (5 mL) is added to a yellow solution of [Cr(CO)$_4$(nbd)] (154 mg, 0.6 mmol, 2.0 eq.) in thf (5 mL). The resulting mixture is stirred at room temperature for 20 h. Hereby, the color of the solution darkens. The solvent is removed under reduced pressure yielding a brown-purple solid that is washed with *n*-pentane. The solid is taken up in dichloromethane (2 mL) and upon storage at -28°C pure **4a** is obtained in the form of purple crystals that are suitable for single crystal X-ray analysis.

Analytical data for 4a

Yield	184 mg (0.18 mmol, 60%).
^{1}H NMR (CD_2Cl_2, 300 K)	δ[ppm] = 1.84 (s, 15H, $C_5(C\underline{H}_3)_3$), 2.15 (s, 15H, $C_5(C\underline{H}_3)_3$).
^{13}C{^{1}H} NMR (CD_2Cl_2, 300 K)	δ[ppm] = 11.4 (s, $C_5(\underline{C}H_3)_3$), 12.0 (s, $C_5(\underline{C}H_3)_3$), 103.3 (s, $\underline{C}_5(CH_3)_3$), 105.8 (s, $\underline{C}_5(CH_3)_3$), 212.2 (s, CO), 214.7 (s, CO), 215.9 -216.1 (m, CO), 221.2 (s, CO), 221.9 (s, CO).
^{31}P{^{1}H} NMR (CD_2Cl_2, 300 K)	δ[ppm] = 107.9 (ddd, $^2J_{AX}$ = 28 Hz, $^1J_{MX}$ = 300 Hz, $^1J_{NX}$ = 330 Hz, 1P, P_X), 150.5 (ddd, $^2J_{MN}$ = 19.5 Hz, $^1J_{AN}$ = 252 Hz, $^1J_{NX}$ = 330 Hz, 1P, P_N), 219.5 (ddd, $^2J_{MN}$ = 19.5 Hz, $^1J_{AM}$ = 254 Hz, $^1J_{MX}$ = 300 Hz, 1P, P_M), 489.1 (dt, $^2J_{AX}$ = 28 Hz, $^1J_{AM}$ resp. $^1J_{AN}$ = 254 Hz, 1P, P_A).
IR (solid)	$\tilde{\nu}_{CO}$ [cm^{-1}] = 2069 (s), 2055 (s), 1995 (s), 1977 (m), 1921 (s, br), 1909 (s,br), 1867 (s, br).
LIFDI-MS (toluene)	m/z = 993.85 $[M]^+$ (100%), 801.92 $[M\text{-}Cr(CO)_5]^+$ (10%).
Elemental Analysis	calcd. for $C_{34}H_{30}Cr_4O_{14}P_4\cdot(CH_2Cl_2)$ (1079.42 g mol^{-1}) C 38.95, H 2.99; found C 39.09, H 3.07.

Synthesis of [{Cp*Cr(CO)$_2$}$_2$(μ$_4$,η$^{3:1:1:1}$-P$_4$){Mo(CO)$_5$}$_2$] (4b)

A dark orange solution of **1** (100 mg, 0.15 mmol, 1.0 eq.) in thf (5 mL) is added to a yellow solution of [Mo(CO)$_4$(nbd)] (90 mg, 0.30 mmol, 2.0 eq.) in thf (5 mL). The resulting mixture is stirred at room temperature for 20 h while the color of the solution turns from orange to dark brown. The solvent is removed under reduced pressure yielding a brown solid that is washed with *n*-pentane. The solid is subsequently taken up in a mixture of dichloromethane (2 mL) and *n*-pentane (5 mL). Upon storage at -28°C pure **4b** is obtained in the form of black crystals that are suitable for single crystal X-ray analysis.

Analytical data for 4b

Yield	83 mg (0.76 mmol, 51 %).
^{1}H NMR (CD_2Cl_2, 300 K)	δ[ppm] = 1.84 (s, 15H, $C_5(C\underline{H}_3)_3$), 2.14 (s, 15H, $C_5(C\underline{H}_3)_3$).
^{13}C{^{1}H} NMR (CD_2Cl_2, 300 K)	δ[ppm] = 11.4 (s, $C_5(\underline{C}H_3)_3$), 12.0 (s, $C_5(\underline{C}H_3)_3$), 103.2 (s, $\underline{C}_5(CH_3)_3$), 105.4 (s, $\underline{C}_5(CH_3)_3$) (no signals for CO ligands detectable).

$^{31}P\{^1H\}$ NMR (CD_2Cl_2, 300 K)	δ[ppm] = 75.2 (m, 1P, P_X), 152.9 (m, 1P, P_N), 192.2 (m, 1P, P_M), 487.8 (td, $^2J_{AX}$ = 24 Hz, $^1J_{AM}$ resp. $^1J_{AN}$ = 248 Hz, 1P, P_A).
IR (solid)	$\tilde{\nu}_{CO}$ [cm^{-1}] = 2078 (m), 2067 (m), 1997 (m, br), 1979 (m, br), 1924 (s, br), 1909 (s,br), 1865 (s, br).
LIFDI-MS (toluene)	m/z = 1081.77 $[M]^+$ (100%), 847.85 $[M\text{-}Mo(CO)_5]^+$ (24%).

Fragmentation of [{Cp*Cr(CO)$_2$}$_2$(μ$_4$,η$^{3:1:1:1}$-P$_4$){Cr(CO)$_5$}$_2$] (4a) and in situ reactivity of [{Cp*Cr(CO)$_2$}(μ$_3$-P){Cr(CO)$_5$}$_2$] (6) affording [{Cp*Cr(CO)$_2$(^{t}BuNC)}P{Cr(CO)$_5$}$_2$(^{t}BuNC)] (7)

A brown solution of **4a** (20 mg, 0.02 mmol, 1.0 eq.) in thf (50 mL) is stirred at 50 °C for 3 d. Using $^{31}P\{^1H\}$ NMR spectroscopy, the consumption of the starting material can be monitored and two new signals are obtained. ^{t}Bu-NC (1 mL, 8.8 mmol, 440 eq.) is added to the reaction solution and no color change can be observed. Again, with the help of $^{31}P\{^1H\}$ NMR spectroscopy the immediate quantitative reaction of **6** to **7** is observed, while the signal for **5** stays unchanged.

Analytical data

$^{31}P\{^1H\}$ NMR (**5**,thf with C_6D_6-capillary, 300 K)	δ[ppm] = -273.3 (s, 3P, [Cp*Cr(CO)$_2$(η^3-P$_3$)]).
$^{31}P\{^1H\}$ NMR (**6**,thf with C_6D_6-capillary, 300 K)	δ[ppm] = 1123.7 (s, 1P, [{Cp*Cr(CO)$_2$}(μ$_3$-P){Cr(CO)$_5$}$_2$]).
$^{31}P\{^1H\}$ NMR (7,thf with C_6D_6-capillary, 300 K)	δ[ppm] = -166.4 (s, 1P, [{Cp*Cr(CO)$_2$(^{t}BuNC)}P-{Cr(CO)$_5$}$_2$(^{t}BuNC)]).

3.6.3 NMR spectroscopic experiments

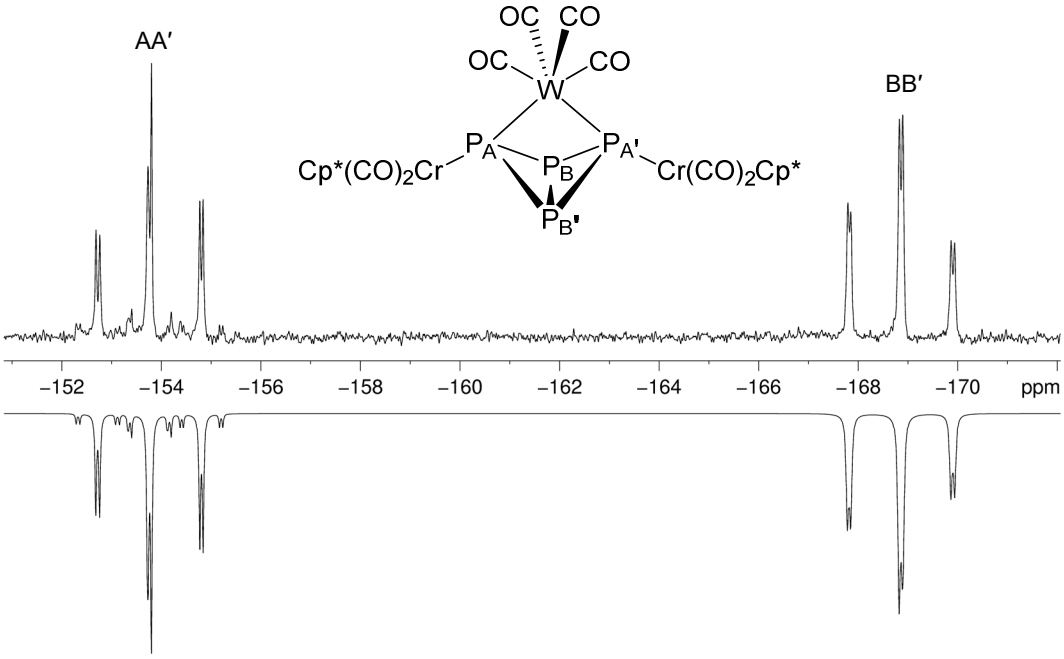

Figure S1. Experimental (top) and simulated (bottom) $^{31}P\{^1H\}$ NMR spectra of **2** (recorded in C_6D_6 at 300 K).

Table S1. Experimental and simulated values for the chemical shifts and coupling constants in the $^{31}P\{^1H\}$ NMR spectrum of **2** (recorded in C_6D_6 at 300 K).

	Exp.	F1 (85.69%)	F2 (14.28%)		Exp.	F1 (85.69%)	F2 (14.28%)
δ_A	-153.8 ppm	-153.8 ppm	-153.8 ppm	$^1J_{AB}$	168 Hz	169.2 Hz	169.4 Hz
				$^1J_{AB`}$	168 Hz	169.2 Hz	168.7 Hz
$\delta_{A`}$	-153.8 ppm	-153.8 ppm	-153.8 ppm	$^1J_{A`B}$	168 Hz	169.2 Hz	169.4 Hz
				$^1J_{A`B`}$	168 Hz	169.2 Hz	168.7 Hz
δ_B	-168.8 ppm	-168.8 ppm	-168.8 ppm	$^2J_{AA`}$	11 Hz	35.0 Hz	35.0 Hz
				$^2J_{BB`}$	11 Hz	15.4 Hz	18.7 Hz
$\delta_{B`}$	-168.8 ppm	-168.8 ppm	-168.8 ppm	$^1J_{AW}$	-	-	128.3 Hz
				$^1J_{A`W}$	-	-	129.0 Hz
				$^2J_{BW}$	-	-	9.8 Hz
				$^2J_{B`W}$	-	-	9.8 Hz

The simulation of the $^{31}P\{^1H\}$ NMR spectrum of **2** was carried out on the basis of an AA′BB′ spin system with a C_1 symmetry. According to the natural abundancy of the NMR active ^{138}W isotope, the simulation was performed using two fragments. The main fragment (F1, 85.69%) was simulated with an NMR inactive tungsten atom, whereas the second fragment (F2, 14.28%) considered the ^{138}W atom.

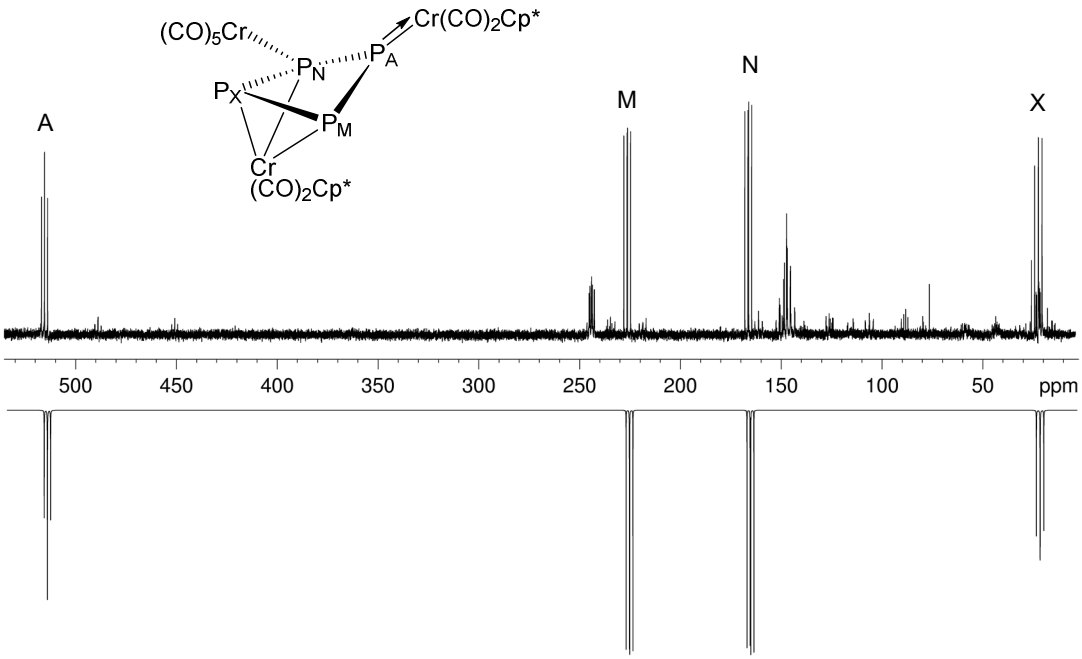

Figure S2. Experimental $^{31}P\{^{1}H\}$ NMR spectrum of the reaction of **1** with 1.0 eq. $[Cr(CO)_4(nbd)]$ (top, recorded in CD_2Cl_2 at 300 K) and simulated $^{31}P\{^{1}H\}$ NMR spectrum of **3a** (bottom).

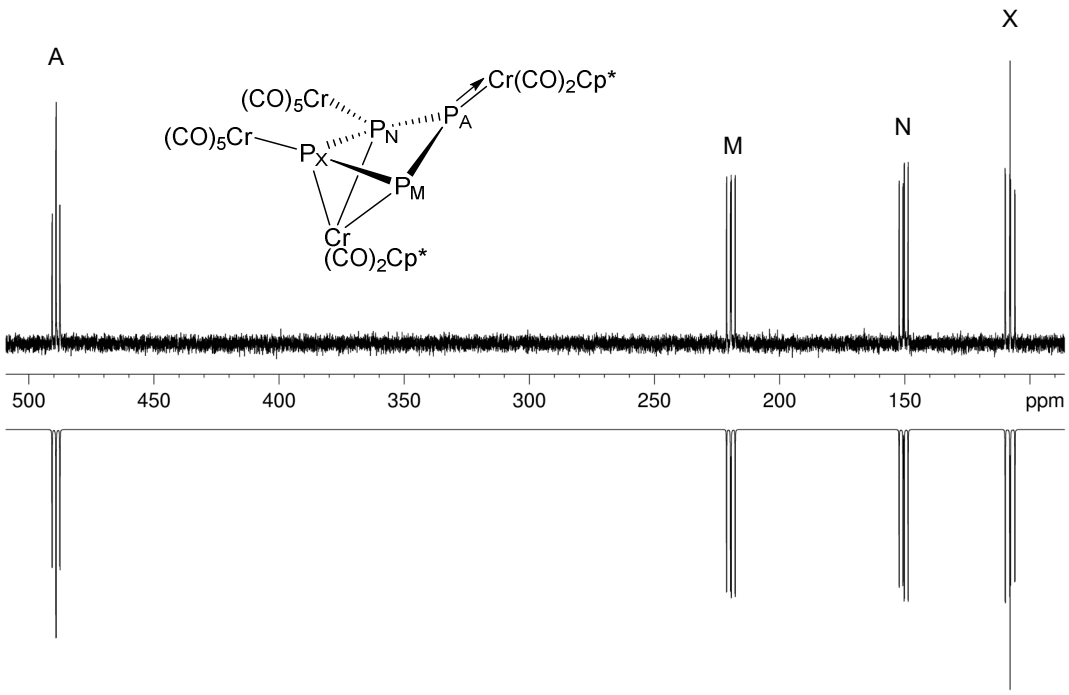

Figure S3. Experimental (top, recorded in CD_2Cl_2 at 300 K) and simulated (bottom) $^{31}P\{^{1}H\}$ NMR spectra of **4a**.

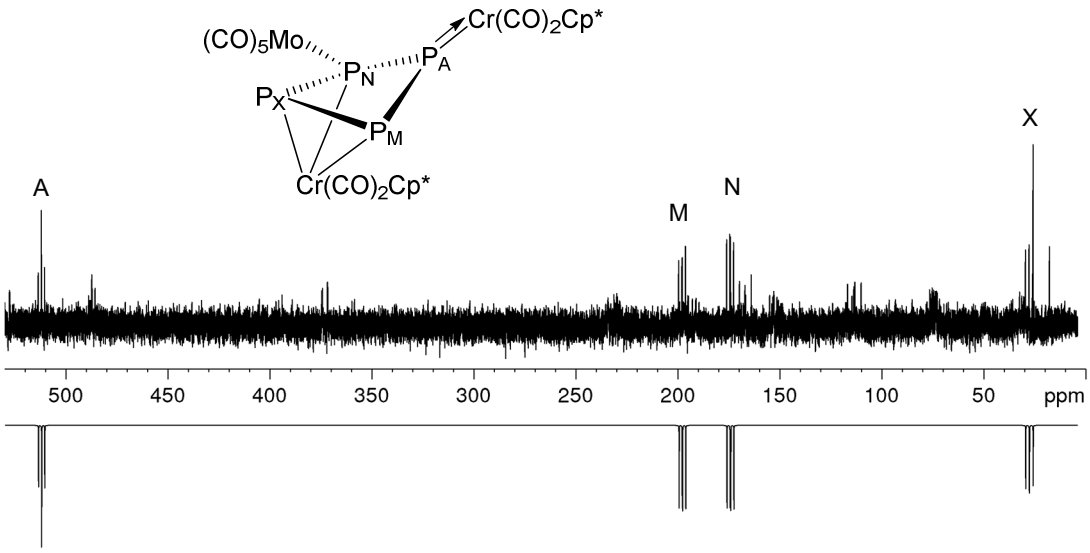

Figure S4. Experimental $^{31}P\{^1H\}$ NMR spectrum of the reaction of **1** with 1.0 eq. [Mo(CO)$_4$(nbd)] (top, recorded in CD_2Cl_2 at 300 K) and simulated $^{31}P\{^1H\}$ NMR spectrum of **3b** (bottom).

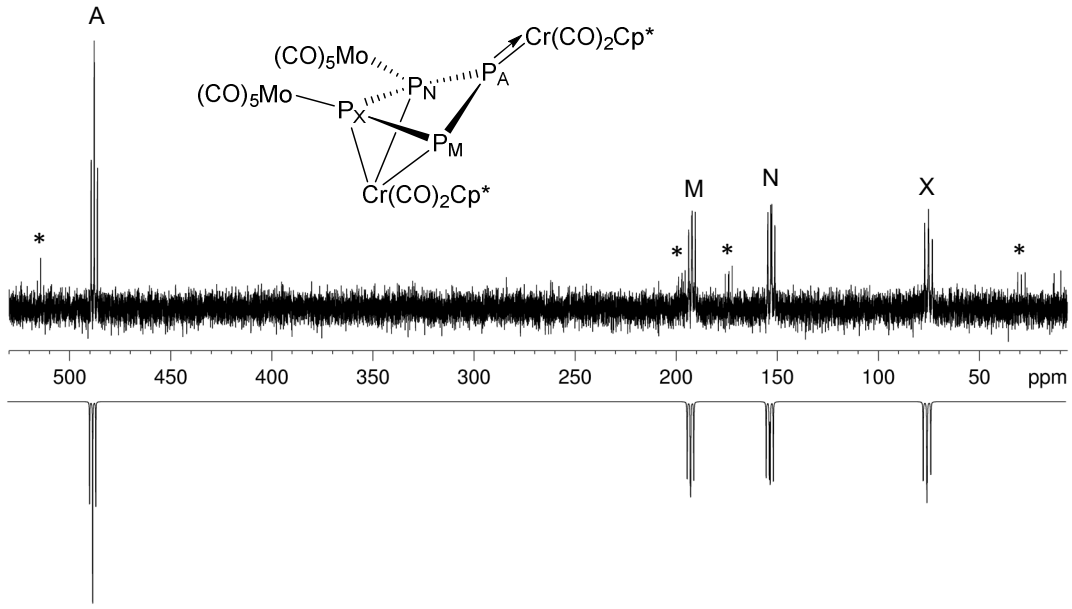

Figure S5. Experimental (top, recorded in CD_2Cl_2 at 300 K) and simulated (bottom) $^{31}P\{^1H\}$ NMR spectrum of **4b** (Signals marked with * can be attributed to **3b** as a result of decomposition).

Table S2. Experimental and simulated values for the chemical shifts and coupling constants in the $^{31}P\{^{1}H\}$ NMR spectra of **3a**, **4a** and **4b** (recorded in CD_2Cl_2 at 300 K).

	experimental values				simulated values[1]			
3a	δ_A	515.4 ppm	$^1J_{AM}$	251 Hz	δ_A	515.4 ppm	$^1J_{AM}$	249.3 Hz
	δ_M	226.3 ppm	$^1J_{AN}$	257 Hz	δ_M	226.3 ppm	$^1J_{AN}$	258.5 Hz
	δ_N	166.3 ppm	$^2J_{AX}$	-	δ_N	166.2 ppm	$^2J_{AX}$	6.8 Hz
	δ_X	22.3 ppm	$^2J_{MN}$	-	δ_X	22.3 ppm	$^2J_{MN}$	1.1 Hz
			$^1J_{MX}$	306 Hz			$^1J_{MX}$	306.2 Hz
			$^1J_{NX}$	290 Hz			$^1J_{NX}$	291.0 Hz
3b	δ_A	515.4 ppm	$^1J_{AM}$	252 Hz	δ_A	515.4 ppm	$^1J_{AM}$	250.5 Hz
	δ_M	197.1 ppm	$^1J_{AN}$	247 Hz	δ_M	197.1 ppm	$^1J_{AN}$	248.2 Hz
	δ_N	174.1 ppm	$^2J_{AX}$	-	δ_N	174.1 ppm	$^2J_{AX}$	5.7 Hz
	δ_X	29.2 ppm	$^2J_{MN}$	-	δ_X	29.2 ppm	$^2J_{MN}$	2.6 Hz
			$^1J_{MX}$	284 Hz			$^1J_{MX}$	284.6 Hz
			$^1J_{NX}$	303 Hz			$^1J_{NX}$	302.5 Hz
4a	δ_A	489.1 ppm	$^1J_{AM}$	254 Hz	δ_A	489.1 ppm	$^1J_{AM}$	256.0 Hz
	δ_M	219.5 ppm	$^1J_{AN}$	252 Hz	δ_M	219.6 ppm	$^1J_{AN}$	251.3 Hz
	δ_N	150.5 ppm	$^2J_{AX}$	28 Hz	δ_N	150.4 ppm	$^2J_{AX}$	26.9 Hz
	δ_X	107.9 ppm	$^2J_{MN}$	20 Hz	δ_X	108.0 ppm	$^2J_{MN}$	19.2 Hz
			$^1J_{MX}$	300 Hz			$^1J_{MX}$	230.0 Hz
			$^1J_{NX}$	330 Hz			$^1J_{NX}$	330.3 Hz
4b	δ_A	487.8 ppm	$^1J_{AM}$	-	δ_A	487.8 ppm	$^1J_{AM}$	247.3 Hz
	δ_M	192.2 ppm	$^1J_{AN}$	248 Hz	δ_M	192.1 ppm	$^1J_{AN}$	249.6 Hz
	δ_N	152.9 ppm	$^2J_{AX}$	24 Hz	δ_N	152.9 ppm	$^2J_{AX}$	22.6 Hz
	δ_X	75.2 ppm	$^2J_{MN}$	-	δ_X	75.2 ppm	$^2J_{MN}$	20.8 Hz
			$^1J_{MX}$	-			$^1J_{MX}$	286.9 Hz
			$^1J_{NX}$	-			$^1J_{NX}$	324.0 Hz

[1] based on an AMNX spin system with a C_1 symmetry.

The simulation of the $^{31}P\{^{1}H\}$ NMR spectrum of **3a**, **4a** and **4b** was carried out on the basis of an AMNX spin system with a C_1 symmetry.

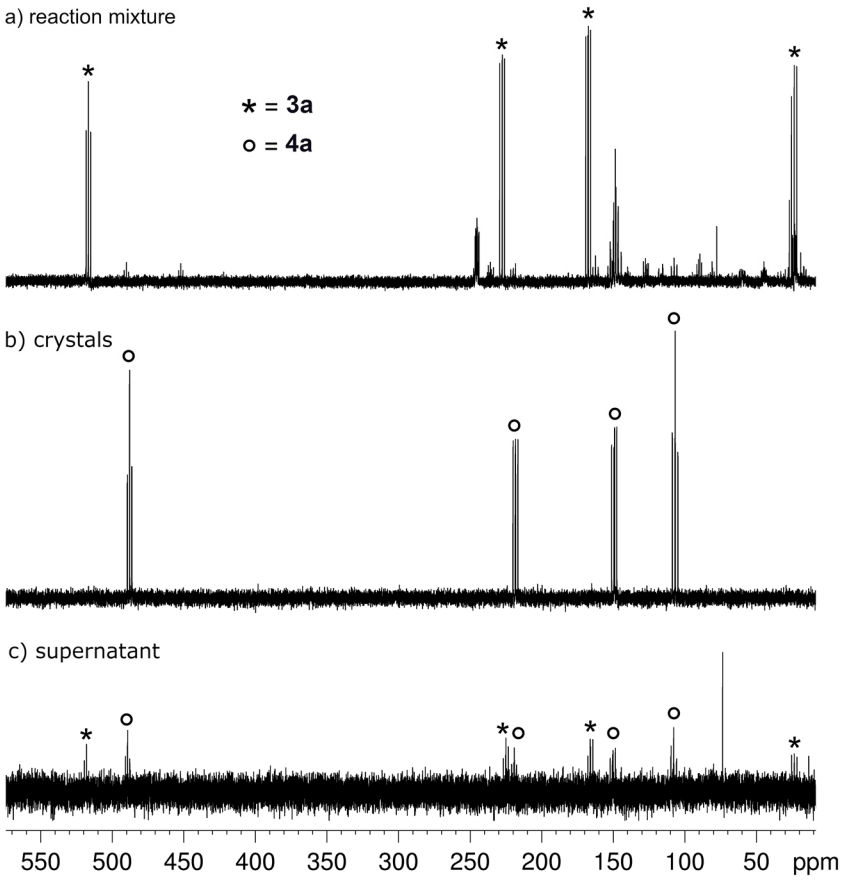

Figure S6: $^{31}P\{^1H\}$ NMR spectra (recorded in CD_2Cl_2 at 300 K) of the reaction of **1** with 1.0 eq. [Cr(CO)$_4$(nbd)]: (a) reactions solution (b) dissolved crystals obtained from the reaction solution (c) supernatant of the obtained crystals.

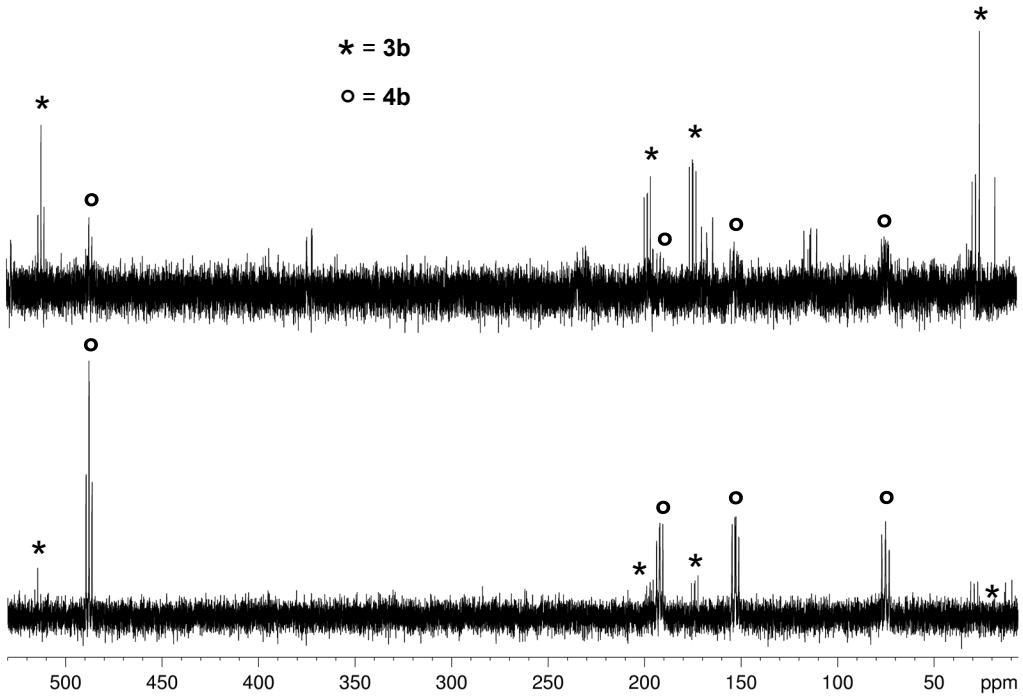

Figure S7. $^{31}P\{^1H\}$ NMR spectrum (recorded in CD_2Cl_2 at 300 K) of the reaction solution (top) and the isolated crystals (bottom) from the reaction of **1** with 1.0 eq. [Mo(CO)$_4$(nbd)].

As discussed for **3a**, the monosubstituted **3b** is the main species in the reaction solution when reacting **1** with 1.0 eq. [Mo(CO)$_4$(nbd)]. When storing the solution at -28 °C during the crystallization process, a second substitution occurs giving **4b** as the exclusive crystallization product. However, if the crystals are dissolved in CD_2Cl_2 a small amount of **4b** decomposes to give **3b** as a side product.

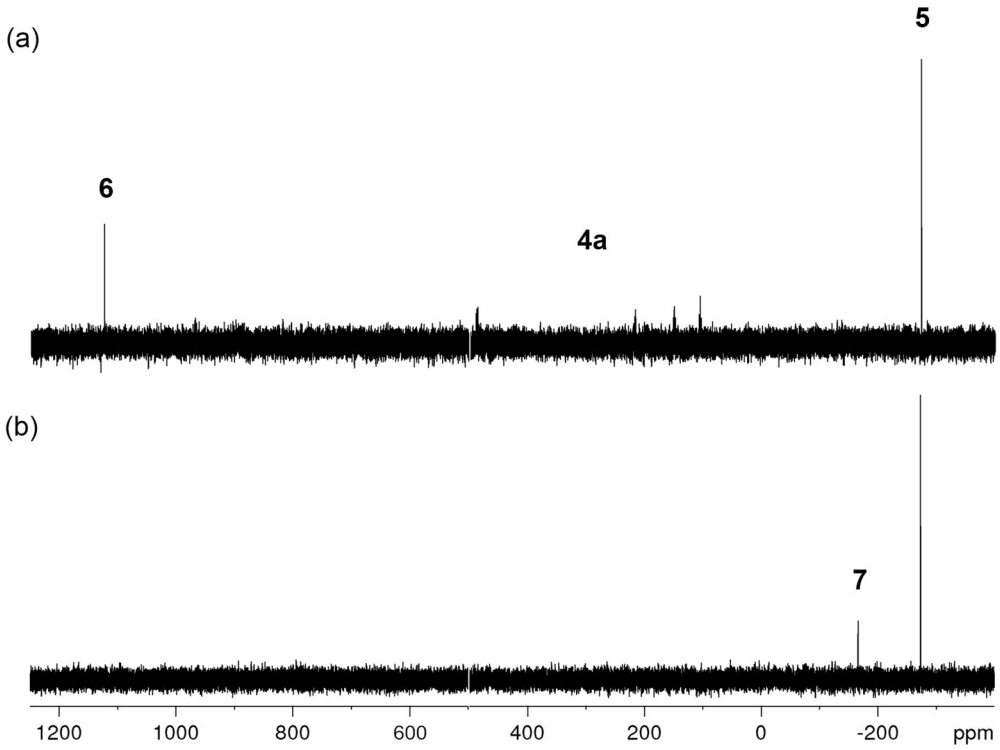

Figure S8: $^{31}P\{^1H\}$ NMR spectra (recorded in thf with C_6D_6 capillary at 300 K) of the fragmentation of **4a** yielding **5** and **6** (a) and the *in-situ* reaction with ^{t}BuNC affording **7** (b).

3.6.4 DFT calculations

For the calculation of the reaction energies the geometry of the compounds has been optimized in the gas phase at the RI-[4]B3LYP[5]/def2-TZVP[6] level of theory using the TURBOMOLE[7] program package. The Multipole Accelerated Resolution of Identity (MARI-J)[8] approach has been used in the geometry optimization steps to speed up the calculations. The final energy has been determined by single point calculations on the optimized geometries without the RI approximation. The SCF energies has been used without corrections for zero-point vibration energies.

The ^{31}P NMR chemical shifts have been calculated using the Gauge-Independent Atomic Orbital (GIAO) method[9] as implemented in Gaussian09.[10] For this, the geometries have been optimized using the BP86[11] functional together with the def2-TZVP basis set and a fine integration grid. The magnetic shielding has been computed by a single point calculation in which for the phosphorus atom the def2-TZVP basis set has been replaced by the aug-pcSseg-2 basis set,[12] obtained from the basis set exchange library.[13] The values of the ^{31}P NMR chemical shifts have been calculated using the formula $\delta_{mol} = \sigma_{ref} - \sigma_{mol} + \delta_{ref}$, where PH_3 was used as reference with $\delta(^{31}P) = -266$ ppm.

The natural bond orbital analysis (NBO) has been performed with NBO 6.0[14] on the wave function obtained at the B3LYP/def2-TZVP level of theory.

Table S3. Section of the NBO-output for compound **4a**.

(Occupancy) Bond orbital / Coefficients / Hybrids

140. (1.85698) BD (1) Cr1–P6					
(57.67%)	0.7594*Cr1	s (1.83%)	p 0.03 (0.05%)	d 53.74 (98.12%)	f 0.00 (0.00%)
(42.33%)	0.6506*P6	s (21.10%)	p 3.72 (78.51%)	d 0.02 (0.37%)	f 0.00 (0.02%)
141. (1.83957) BD (1) Cr1–P8					
(64.52%)	0.8032*Cr1	s (0.55%)	p 0.18 (0.10%)	d 99.99 (99.34%)	f 0.00 (0.00%)
(35.48%)	0.5957* P8	s (6.95%)	p 13.28 (92.25%)	d 0.11 (0.79%)	f 0.00 (0.01%)
144. (1.76395) BD (1) Cr2–P5					
(35.03%)	0.5918*Cr2	s (30.60%)	p 0.04 (1.10%)	d 2.23 (68.28%)	f 0.00 (0.01%)
(64.97%)	0.8061*P5	s (46.42%)	p 0.93 (43.33%)	d 0.22 (10.06%)	f 0.00 (0.19%)
145. (1.86275) BD (2) Cr2–P5					
(47.05%)	0.6860*Cr2	s (0.04%)	p 0.72 (0.03%)	d 99.99 (99.93%)	f 0.06 (0.00%)
(52.95%)	0.7276*P5	s (0.02%)	p 99.99 (99.83%)	d 4.90 (0.11%)	f 1.97 (0.04%)
148. (1.85150) BD (1) Cr3–P6					
(24.66%)	0.4966*Cr3	s (35.21%)	p 0.00 (0.07%)	d 1.84 (64.72%)	f 0.00 (0.00%)
(75.34%)	0.8680*P6	s (44.08%)	p 1.27 (55.83%)	d 0.00 (0.06%)	f 0.00 (0.03%)
155. (1.79766) BD (1) P5–P8					
(47.00%)	0.6855*P5	s (25.13%)	p 2.24 (56.34%)	d 0.73 (18.42%)	f 0.00 (0.10%)
(53.00%)	0.7280*P8	s (11.87%)	p 7.31 (86.74%)	d 0.12 (1.37%)	f 0.00 (0.03%)
156. (1.93333) BD (1) P6–P7					
(45.31%)	0.6731*P6	s (15.06%)	p 5.57 (83.90%)	d 0.07 (1.00%)	f 0.00 (0.04%)
(54.69%)	0.7396*P7	s (36.73%)	p 1.70 (62.44%)	d 0.02 (0.79%)	f 0.00 (0.04%)
157. (1.92869) BD (1) P7–P8					
(53.78%)	0.7333*P7	s (31.80%)	p 2.12 (67.29%)	d 0.03 (0.87%)	f 0.00 (0.04%)
(46.22%)	0.6799*P8	s (12.05%)	p 7.17 (86.42%)	d 0.12 (1.50%)	f 0.00 (0.03%)

Table S4. Wiberg bond index matrix in the NAO basis.

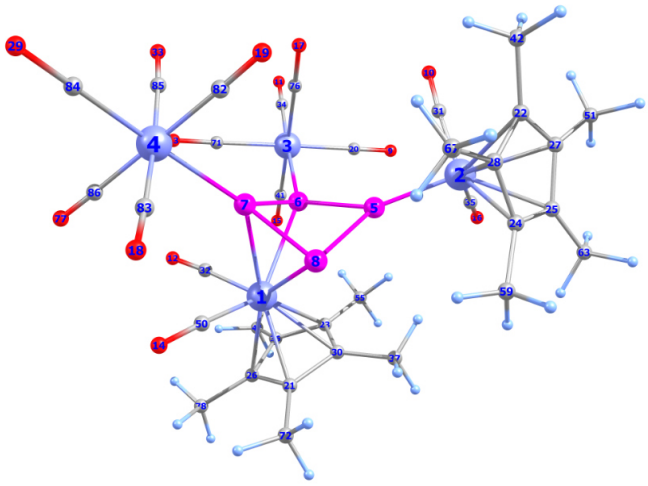

Atom	1	2	3	4	5	6	7	8	9
Cr1	0.0000	0.0359	0.0248	0.0266	0.0306	0.4698	0.4212	0.5083	0.0009
Cr2	0.0359	0.0000	0.0037	0.0090	1.1572	0.0414	0.0509	0.0494	0.0029
Cr3	0.0248	0.0037	0.0000	0.0015	0.0205	0.3892	0.0212	0.0258	0.0796
Cr4	0.0266	0.0090	0.0015	0.0000	0.0103	0.0271	0.3951	0.0245	0.0001
P5	0.0306	1.1572	0.0205	0.0103	0.0000	0.9126	0.0364	0.9301	0.0013
P6	0.4698	0.0414	0.3892	0.0271	0.9126	0.0000	0.9942	0.0637	0.0101
P7	0.4212	0.0509	0.0212	0.3951	0.0364	0.9942	0.0000	1.0579	0.0004
P8	0.5083	0.0494	0.0258	0.0245	0.9301	0.0637	1.0579	0.0000	0.0010

Table S5. Total SCF energies at the B3LYP/def2-TZVP level.

Compound	Total energy (a. u.)	Compound	Total energy (a. u.)
norbornadiene	-271.3943365	**3b**	-5322.473081
$[Cr(CO)_4(nbd)]$	-1769.183676	**4a**	-7909.770896
$[Mo(CO)_4(nbd)]$	-793.0132628	**4b**	-5957.430388
$[W(CO)_4(nbd)]$	-791.8932707	**5**	-2685.1003
1	-4914.174548	**6a**	-5224.64971
2a	-6411.963378	$[\{Cp^*Cr(CO)_2\}(\mu_3\text{-}PCN^tBu)\{Cr(CO)_5\}_2]$	-5475.264526
2b	-5435.795267	^{t}BuNC	-250.5963615
2c	-5434.675954	**7**	-5725.88115
3a	-6298.643788		

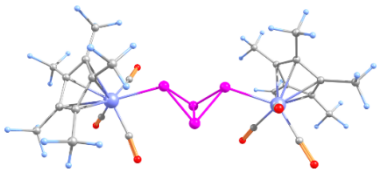

Table S6. Cartesian coordinates of the optimized geometry of **1** at the B3LYP/def2-TZVP level (E = -4914.17454760153 a.u.).

Atom	x	y	z
Cr	1.5889583	-2.3470836	-2.7678121
Cr	-1.8231907	3.0758139	1.6631681
P	0.6476663	-1.0392644	-0.7148162
P	-0.6773190	0.8723584	0.8659234
P	-1.1607257	0.1550313	-1.2097715
P	0.7244201	1.2042144	-0.8259995
C	-0.0469361	-3.0968091	-2.2769762
C	0.8897325	-2.6769089	-4.4451335
C	1.4861891	-0.5915402	-3.3943381
C	0.0000153	3.1805668	2.0391232
C	-1.5197922	4.8438142	1.2211263
C	-2.2512835	3.0013660	-0.1530500
O	-1.0216022	-3.6395687	-2.0021866
O	0.4732437	-2.9015663	-5.4927589
O	1.5025304	0.4520871	-3.8727627
O	1.1007064	3.2964054	2.3479483
O	-1.3428231	5.9508458	0.9670634
O	-2.6053283	3.0402395	-1.2446301
C	3.8447915	-2.1449923	-2.6126888
C	3.5036823	-3.1472897	-3.5681976
C	2.8022171	-4.1919639	-2.8836627
C	2.7181388	-3.8293087	-1.5035319
C	3.3832337	-2.5785178	-1.3363212
C	-3.6266087	3.8274155	2.7366720
C	-2.5661202	3.6188251	3.6754763
C	-2.2689525	2.2202323	3.6938454
C	-3.1562477	1.5705096	2.7839136
C	-3.9768777	2.5639107	2.1765241
C	4.6939690	-0.9367118	-2.8696081
H	5.7507591	-1.1718517	-2.7067677
H	4.4364512	-0.1115522	-2.2061145
H	4.5927852	-0.5796368	-3.8939177
C	3.9591487	-3.1773920	-4.9964817
H	4.9611347	-3.6131859	-5.0637391
H	4.0081231	-2.1779126	-5.4285453
H	3.3006352	-3.7760114	-5.6246240
C	2.3881157	-5.5072951	-3.4721810
H	3.1984839	-6.2381408	-3.3820977
H	2.1433830	-5.4217656	-4.5306515
H	1.5169392	-5.9223082	-2.9656628
C	2.1870556	-4.6833645	-0.3919271
H	2.9959931	-5.2614884	0.0663502
H	1.4395307	-5.3916404	-0.7474015
H	1.7279335	-4.0825011	0.3933759
C	3.7112416	-1.9346293	-0.0262172
H	4.6425168	-2.3573642	0.3661137
H	2.9350200	-2.0997617	0.7198895
H	3.8535879	-0.8589818	-0.1220692
C	-4.3660887	5.1122609	2.5105869
H	-5.2291984	5.1726795	3.1812906
H	-4.7397682	5.1926364	1.4898327
H	-3.7422447	5.9842097	2.7027777
C	-1.9904736	4.6526521	4.5962408
H	-2.5711239	4.7059504	5.5230401
H	-1.9993852	5.6463565	4.1488473
H	-0.9604695	4.4242117	4.8691492
C	-1.3227951	1.5234255	4.6242241
H	-1.8571562	1.1496727	5.5036158
H	-0.5370053	2.1899892	4.9782807
H	-0.8428190	0.6699901	4.1446177
C	-3.3289038	0.0911081	2.6389348
H	-4.0307262	-0.2724794	3.3972587
H	-2.3919727	-0.4479810	2.7729572
H	-3.7301072	-0.1802334	1.6631732
C	-5.1236230	2.3028353	1.2472261
H	-6.0334224	2.0863535	1.8164576
H	-4.9340172	1.4492435	0.5969717
H	-5.3332247	3.1617918	0.6106472

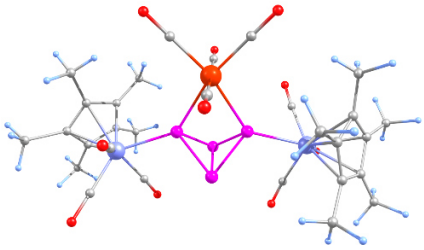

Table S7. Cartesian coordinates of the optimized geometry of **2** at the B3LYP/def2-TZVP level (E = -5434.675953999 a.u.).

Atom	x	y	z
W	-1.4251134	0.5377818	-1.6599126
Cr	-1.2269073	2.4012107	2.8876573
Cr	2.2214589	-2.7619606	-1.7332537
P	-0.6338125	0.8773018	0.8787759
P	0.6878544	-0.8819059	-0.8233026
P	0.2176627	-1.1427409	1.3400326
P	1.5568468	0.4976674	0.7128166
O	-3.9356220	2.4148833	-1.9194751
O	-3.4443720	-1.8477446	-0.9365663
O	-0.5768963	4.2306825	0.5668129
O	-0.6213455	-3.7786953	-1.9334208
O	0.3644551	3.0078563	-2.6537766
O	0.8065088	0.5817672	4.1656777
C	-2.9110270	3.5021918	3.8107273
C	-0.8028102	3.5039532	1.4202936
C	-1.6365018	0.0201099	-3.5647260
C	2.9995393	-2.3668753	-0.0771151
C	0.0624189	1.2539895	3.6118571
C	2.7370290	-1.2930545	-3.4314607
C	-2.5203733	2.4300073	4.6746933
C	-3.9568958	0.5322912	1.7744073
H	-3.9168442	0.8732586	0.7425247
H	-5.0119820	0.3893449	2.0313058
H	-3.4760883	-0.4429758	1.8242488
C	-4.0808301	3.6899858	1.4920439
H	-3.6618076	4.6883658	1.3703180

O	-1.7439284	-0. 2851418	-4.6787685
O	3.5782008	-2.1771667	0.8931464
C	3.0637215	-3.5709842	-3.6133057
C	-3.3468126	1.5152712	2.7196281
C	2.2029768	-2.4918377	-3.9855775
O	0.5560747	4.3976207	4.2412313
C	-3.0076141	1.7240721	-1.8345800
C	-2.7763222	1.2007157	3.9888395
C	2.9705901	-4.9730433	-4.1357275
H	3.4531405	-5.6913292	-3.4740842
H	3.4632712	-5.0430225	-5.1105493
H	1.9362046	-5.2883173	-4.2710169
C	-3.4135479	2.9330347	2.5993883
C	4.1244078	-3.0357205	-2.8150555
O	2.5460791	-5.5322109	-0.6304714
C	-0.1126646	3.6314903	3.7094890
C	-2.0892716	2.5599968	6.1045303
H	-1.4204678	1.7533031	6.4037789
H	-2.9610021	2.5240848	6.7655378
H	-1.5766655	3.5026704	6.2932439
C	0.4377396	-3.3603924	-1.8287949
C	-2.6912316	-1.0103093	-1.1670564
C	1.0639247	-2.5789806	-4.9548765
H	0.5664021	-3.5474205	-4.9137369
H	1.4367749	-2.4481069	-5.9759417
H	0.3128574	-1.8110142	-4.7834324
H	-5.1459382	3.8095137	1.7155928
H	-4.0063383	3.1789644	0.5345794
C	-2.6625534	-0.1754045	4.5714626
H	-2.4087555	-0.9167826	3.8143503
H	-3.6163298	-0.4755620	5.0165820
H	-1.9061552	-0.2264872	5.3535499
C	-0.2513531	2.1197517	-2.2617957
C	-2.9721218	4.9550186	4.1753102
H	-2.2356070	5.2201592	4.9328232
H	-3.9598226	5.1988783	4.5791062
H	-2.8066979	5.5981357	3.3112375
C	3.9097468	-1.6266827	-2.6909745
C	2.2713864	0.0920193	-3.7427608
H	1.1966965	0.1395306	-3.9026519
H	2.7547124	0.4386932	-4.6623975
H	2.5249583	0.8003089	-2.9561414
C	2.4074581	-4.4690986	-1.0398322
C	4.8550081	-0.6412462	-2.0732196
H	4.3297400	0.2144500	-1.6500239
H	5.5467167	-0.2587471	-2.8303297
H	5.4532515	-1.0893542	-1.2808638
C	5.3377709	-3.7793645	-2.3441076
H	5.7383528	-3.3619925	-1.4205264
H	6.1294148	-3.7245331	-3.0980125
H	5.1290771	-4.8341262	-2.1679785

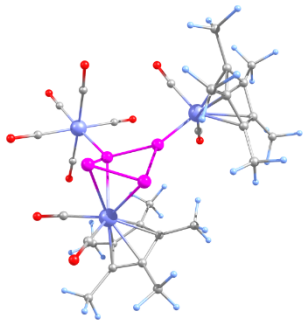

Table S8. Cartesian coordinates of the optimized geometry of **3a** at the B3LYP/def2-TZVP level (E = -5434.675953999 a.u.).

Atom	x	y	z
Cr	0.4303934	-2.3822836	-1.6320987
Cr	-0.1403160	2.4883773	0.9335014
Cr	3.9616669	-1.0386640	1.0940488
P	0.4354068	0.7976792	-0.2379036
P	1.9301053	-0.8555476	-0.2645331
P	2.0012663	-0.6160621	-2.4209554
P	-0.0589930	0.0150163	-2.2634172
O	2.5074143	-0.0613282	3.6012581
O	2.5306719	3.0051907	2.1840937
O	6.5174047	-1.0406758	2.7066085
O	2.9023668	-4.1063081	-1.7938558
O	5.5416938	-2.1231574	-1.2841095
O	0.3372179	-2.7637800	-4.6210110
O	3.4525540	-3.8879811	2.0425373
O	-0.7926395	0.9498461	3.4305654
O	4.6754951	1.7701916	0.1047031
C	3.0255661	-0.3970522	2.6403126
C	-1.6768380	-3.1088737	-1.7688018
C	-0.1893627	4.6502197	0.4101974
C	-0.7162647	-2.8622434	0.3171600
C	-1.9322861	3.2772768	-0.2279584
C	-2.0822636	3.5614224	1.1623271
C	-0.8052501	-4.2220308	-1.5537466
C	-1.0098803	4.4217591	1.5586663
C	-0.7632123	3.9457972	-0.6906389
C	-1.6311481	-2.2811399	-0.6039684
C	1.5193452	2.7646957	1.6889807
H	0.6186172	6.5970036	0.0267050
H	1.7066794	5.2794899	-0.4040862
C	0.5971080	-5.1022656	0.4517567
H	1.1777504	-5.7210588	-0.2306306
H	-0.0806102	-5.7668708	0.9973559
H	1.2843575	-4.6708222	1.1751200
C	0.3892702	-2.5872041	-3.4908261
C	-0.8587294	5.0854895	2.8946479
H	-1.2639018	4.4727897	3.6999466
H	-1.3896175	6.0433954	2.9131171
H	0.1859125	5.2871980	3.1309896
C	-0.5145712	-2.4374982	1.7374572
H	0.4668196	-2.7208442	2.1130499
H	-1.2598799	-2.9250892	2.3752186
H	-0.6308363	-1.3640508	1.8675806
C	-2.9310452	2.5630986	-1.0866012
H	-2.4615801	2.0641976	-1.9342378
H	-3.6601899	3.2736892	-1.4915563
H	-3.4888103	1.8156277	-0.5234035
C	-3.2598676	3.1804665	2.0090445
H	-3.6747974	2.2151186	1.7181793
H	-4.0583236	3.9233202	1.9105903
H	-2.9991356	3.1201959	3.0651558
C	-0.2970156	4.0283424	-2.1126682
H	0.7863222	4.1255746	-2.1782684
H	-0.7347791	4.9036384	-2.6052019
H	-0.5859757	3.1508241	-2.6903287

C	1.9923953	-3.4187104	-1.7194439
C	5.5479009	-1.0394245	2.0947037
C	-0.5221728	1.5311906	2.4731844
C	-0.2069578	-4.0623898	-0.2659686
C	-2.5919925	-1.1773924	-0.2987809
H	-2.1571694	-0.4228159	0.3535601
H	-3.4679488	-1.5936884	0.2110313
H	-2.9428507	-0.6836128	-1.2032488
C	3.6165302	-2.8170980	1.6654962
C	0.9656632	5.6027946	0.3269055
H	1.4749907	5.7095158	1.2838940
C	4.9267928	-1.7207844	-0.4079710
C	-2.6439661	-2.9435151	-2.9008941
H	-2.7631677	-1.8971650	-3.1813796
H	-3.6282547	-3.3220685	-2.6079782
H	-2.3344465	-3.4927441	-3.7886415
C	4.3770990	0.7381825	0.4899265
C	-0.6857290	-5.4350981	-2.4255693
H	-0.8745277	-5.2077866	-3.4740126
H	-1.4165642	-6.1896279	-2.1179636
H	0.3010910	-5.8918619	-2.3569176

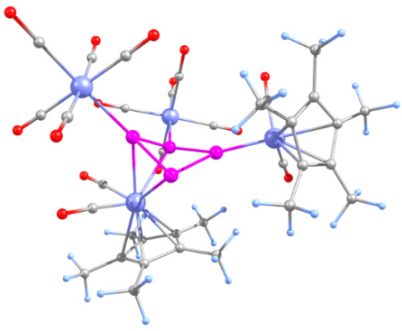

Table S9. Cartesian coordinates of the optimized geometry of **4a** at the B3LYP/def2-TZVP level (E = -7909.77089551509 a.u.).

Atom	x	y	z
Cr	-0.0225995	-2.3667261	-1.0927354
Cr	-0.6100679	2.4789618	1.5359972
Cr	3.4567587	-1.0660854	1.7435176
Cr	2.9768158	-0.0444645	-3.7020401
P	-0.0414960	0.7903497	0.3565335
P	1.4891152	-0.8435748	0.2997310
P	1.4831808	-0.5325938	-1.8518293
P	-0.5765277	0.0373830	-1.6717116
O	2.0150549	0.1215817	4.1617488
O	2.1151186	3.0496674	2.6391338
O	5.9350688	-1.0861171	3.4740838
O	2.4546205	-4.0826699	-1.2429675
O	5.1113721	-2.5418686	-0.3575216
O	-0.1547071	-2.7920049	-4.0691084
O	2.7312037	-3.7864751	2.8975154
O	-1.1617905	0.9870414	4.0876550
O	4.3404912	1.6641294	0.6627441
O	0.6087732	0.0324259	-5.6320701
O	2.5064235	2.9195005	-3.1164983
C	2.5195349	-0.2825139	3.2204151
C	-2.1288980	-3.1097097	-1.2235926
C	-0.6968507	4.6321825	0.9883681
C	-1.1601212	-2.8788094	0.8609874
C	-2.4571527	3.2425834	0.4422401
C	-2.5483006	3.5409340	1.8347960
C	-1.2472186	-4.2179633	-1.0252023
C	-1.4651890	4.4126291	2.1739960
C	-1.3145080	3.9124034	-0.0791598
O	4.6962566	0.7455282	-6.0609298
C	-2.0838911	-2.2955368	-0.0489494
C	1.0808717	2.7878050	2.2079748
C	1.5447578	-3.3953798	-1.1777552
O	5.5462086	0.0896614	-2.0465166
C	4.9959264	-1.0789298	2.8183571
C	-0.9257941	1.5506996	3.1123353
C	-0.6429992	-4.0680471	0.2613343
C	-3.0560147	-1.2080086	0.2774574
H	-2.6253710	-0.4557038	0.9351567
H	-3.9208250	-1.6429784	0.7906156
H	-3.4237659	-0.7089733	-0.6172427
C	2.9748999	-2.7647051	2.4358325
C	0.4445075	5.5930905	0.8400427
H	0.9902512	5.7253729	1.7733967
H	0.0744991	6.5769871	0.5337486
H	1.1581586	5.2621804	0.0857965
C	0.1638580	-5.1171038	0.9622145
H	0.7488394	-5.7205412	0.2699176
H	-0.5139500	-5.7949599	1.4911163
H	0.8446318	-4.6978253	1.6981569
C	-0.0863047	-2.5885695	-2.9450835
C	-1.2609852	5.0932439	3.4942162
H	-1.6225516	4.4861286	4.3240850
H	-1.8013492	6.0453680	3.5251589
H	-0.2091205	5.3092549	3.6802892
C	-0.9635682	-2.4676400	2.2859571
H	0.0041860	-2.7797121	2.6722396
H	-1.7296926	-2.9392901	2.9108404
H	-1.0545128	-1.3918593	2.4208803
C	-3.4879095	2.5126139	-0.3633612
H	-3.0538488	2.0178840	-1.2318836
H	-4.2440962	3.2132911	-0.7341502
H	-4.0088353	1.7606661	0.2284166
C	-3.6873027	3.1653284	2.7350034
H	-4.1083259	2.1936655	2.4755796
H	-4.4933911	3.9024088	2.6585409
H	-3.3833914	3.1223820	3.7803362
C	-0.9149809	3.9898824	-1.5213256
H	0.1635591	4.0844082	-1.6413000
H	-1.3744814	4.8653353	-1.9931345
H	-1.2347878	3.1131406	-2.0837289
C	4.4658928	-1.9674324	0.3897585
C	-3.1065840	-2.9413141	-2.3459621
H	-3.2374234	-1.8934767	-2.6154241
H	-4.0847577	-3.3308864	-2.0472866
H	-2.8009402	-3.4795990	-3.2415092
C	3.9921811	0.6550298	1.0629028
O	3.4849458	-2.9948963	-4.3516598
C	-1.1262693	-5.4234184	-1.9071417
H	-1.3329895	-5.1921894	-2.9511146
H	-1.8447819	-6.1869236	-1.5929382
H	-0.1340433	-5.8705283	-1.8556105
C	2.6756269	1.8075066	-3.3173850
C	1.4719326	-0.0196834	-4.8856582
C	4.0482880	0.4465382	-5.1657283
C	4.5626535	0.0119184	-2.6181583
C	3.2887997	-1.9014044	-4.0917464

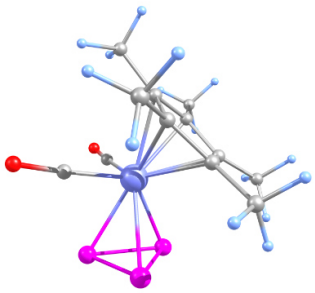

Table S10. Cartesian coordinates of the optimized geometry of **5** at the B3LYP/def2-TZVP level (E = -2685.10029983595 a.u.).

Atom	x	y	z
Cr	0.6127740	-1.1776482	-0.0000023
P	-0.5694597	-3.0416221	-1.0814615
P	1.1700975	-3.6448836	-0.0000474
P	-0.5694033	-3.0416470	1.0814897
O	2.7421218	-1.3191173	2.1205726
C	0.7822576	1.0210189	-0.0000033
C	-1.1883370	0.0418380	-0.7136502
C	0.0242679	0.6447452	-1.1552794
C	1.9279437	-1.3067894	1.3103546
C	0.3421050	1.0032359	-2.5755590
C	2.0403402	1.8357166	-0.0000096
C	-2.3611815	-0.3033629	-1.5779691
H	1.4108900	1.1341676	-2.7365630
H	-0.1480255	1.9454586	-2.8407598
H	-2.9304267	-1.1438827	-1.1813191
H	-2.0589699	-0.5576594	-2.5925777
H	-3.0420692	0.5528911	-1.6390513
H	1.8036129	2.9048716	-0.0000173
H	2.6534845	1.6375390	-0.8788286
C	-1.1883330	0.0418328	0.7136516
C	0.0242771	0.6447403	1.1552758
C	0.3421225	1.0032423	2.5755519
C	-2.3611775	-0.3033694	1.5779679
H	1.4109092	1.1341634	2.7365505
H	-0.1479956	1.9454719	2.8407491
H	-2.9304058	-1.1439062	1.1813308
H	-2.0589692	-0.5576424	2.5925831
H	-0.0070176	0.2429742	3.2739884
H	-3.0420823	0.5528736	1.6390320
H	2.6534893	1.6375512	0.8788090
O	2.7422040	-1.3190197	-2.1205005
C	1.9279876	-1.3067412	-1.3103197

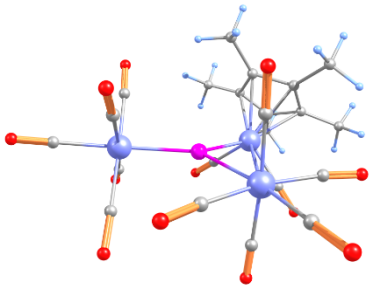

Table S11. Cartesian coordinates of the optimized geometry of **6** at the B3LYP/def2-TZVP level (E = -5224.64971048614 a.u.).

Atom	x	y	z
P	-1.3683383	0.5575896	0.4143550
Cr	0.6489845	-0.2140411	0.6084532
Cr	-0.3800432	2.8591053	0.2803675
Cr	-3.6658722	-0.0521682	0.3329558
C	-0.2184564	-1.2003816	1.8755864
O	-0.6918399	-1.8828614	2.6723890
C	1.5407108	0.5360719	2.0855488
O	2.1126283	0.8997327	3.0068234
C	2.0582912	-0.3006315	-1.2428015
C	2.7721999	-0.7378404	-0.0970117
C	2.0997238	-1.8857999	0.4315529
C	0.9706119	-2.1576986	-0.4066454
C	0.9338230	-1.1629438	-1.4323967
C	-0.4041935	2.6567451	-1.6180111
O	-0.4464748	2.5663677	-2.7573099
C	1.5305142	2.7670400	0.3187147
O	2.6644317	2.9428724	0.3250289
C	-0.0349243	4.7006656	0.1498413
O	0.1865867	5.8198381	0.0672697
C	-2.1870157	3.4687883	0.1898570
O	-3.2167733	3.9547783	0.1160861
C	-0.4700298	2.9446847	2.2037298
C	-5.5131390	-0.4400449	0.1810111
O	-6.6288328	-0.6672261	0.0788117
C	-3.6142689	-1.2849785	1.8115575
O	-3.7036150	-2.0341695	2.6657862
C	-3.3036221	-1.5188390	-0.8227225
O	-3.1438329	-2.4231698	-1.5067203
C	0.0638005	-1.1800879	-2.6527797
H	-0.8625004	-1.7238535	-2.4869560
H	-0.1887658	-0.1773454	-2.9942941
H	0.5914451	-1.6777100	-3.4737207
C	0.1330627	-3.3988441	-0.3523515
H	-0.0254346	-3.7466343	0.6677286
H	-0.8414518	-3.2572754	-0.8132486
H	0.6384026	-4.2042169	-0.8951979
C	2.6110877	-2.7687160	1.5296515
H	3.3054631	-3.5113200	1.1236937
H	3.1481403	-2.2040558	2.2916682
H	1.8069346	-3.3111503	2.0250001
C	4.1004674	-0.2158439	0.3590672
H	4.9021402	-0.7120799	-0.1972319
H	4.1991811	0.8554354	0.1933384
H	4.2734023	-0.4082117	1.4170849

O	-0.5452648	3.0149577	3.3387598
C	-3.8755473	1.0953589	-1.1882666
O	-4.0384506	1.7334119	-2.1205987
C	-4.0981636	1.3299465	1.6052003
O	-4.3874499	2.0969364	2.3970210
C	2.5360598	0.7250908	-2.2227023
H	1.7203721	1.1819509	-2.7778993
H	3.1164955	1.5139245	-1.7493350
H	3.1893401	0.2388466	-2.9557385

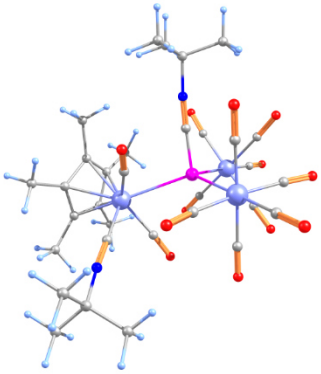

Table S12. Cartesian coordinates of the optimized geometry of **7** at the B3LYP/def2-TZVP level (E = -5725.88114970216 a.u.).

Atom	x	y	z
P	-1.4984880	0.6076991	-0.5628551
Cr	1.0065009	-0.6773792	-0.4313522
Cr	-3.5743486	-0.1861720	-2.1050077
Cr	-1.2834010	3.3231860	-0.2482467
C	0.7847412	0.2825573	1.1634354
O	0.7134896	0.7544183	2.2074536
C	2.5417089	0.4875777	-0.5801127
N	3.4876319	1.1630741	-0.6864869
C	1.2514369	-2.7215332	-1.4414296
C	2.4744443	-2.3171512	-0.8255715
C	2.2474689	-2.1994951	0.5769290
C	0.8741576	-2.5303914	0.8242271
C	0.2714410	-2.8635457	-0.4222912
C	-3.9962630	-1.6815248	-1.0220703
O	-4.3349727	-2.5731307	-0.3808397
C	-2.4948321	-1.2553621	-3.2494664
O	-1.9218877	-1.9192547	-3.9885007
C	-5.0317304	-0.5958408	-3.1799373
O	-5.9347279	-0.8554801	-3.8421764
C	-4.7402521	0.8177105	-0.9711192
O	-5.4961181	1.3385101	-0.2871876
C	-3.2189091	1.3217744	-3.2461264
O	-3.0577187	2.1789809	-3.9821199
C	-1.9473247	3.2013436	1.5260463
O	-2.3342161	3.1600943	2.6058090
C	-3.0548670	3.6426374	-0.9152413
O	-4.0806279	3.9772385	-1.2909034
C	-1.1710812	5.1677111	-0.1098653
O	-1.0966277	6.3116714	-0.0161693
C	-0.5667245	3.4096270	-2.0281398
O	-0.1030413	3.5412184	-3.0641472
C	0.4863516	3.3246756	0.4287705
O	1.5485961	3.4813019	0.8373364
C	-1.0859689	-3.4628979	-0.5948058
H	-1.7897183	-3.1129139	0.1560653
H	-1.5075220	-3.2526662	-1.5744037
H	-1.0225452	-4.5523354	-0.4963552
C	0.2556759	-2.7340859	2.1736452
H	0.6742827	-2.0635401	2.9237131
H	3.7361979	-2.9091276	1.9445350
H	4.0996878	-1.3299452	1.2569527
H	2.8772048	-1.4808514	2.5118111
C	3.7991777	-2.2410552	-1.5212669
H	4.2207058	-3.2448081	-1.6367489
H	3.7138971	-1.8084642	-2.5183548
H	4.5195363	-1.6478258	-0.9610476
C	1.1086694	-3.1318300	-2.8749240
H	0.0842193	-3.0513557	-3.2290266
H	1.7350340	-2.5324845	-3.5354894
H	1.4192119	-4.1755216	-2.9924750
C	-2.2034734	0.1515826	0.9615895
N	-2.7098270	-0.1268298	1.9736540
C	-3.4215556	-0.3775747	3.2130532
C	-2.4835115	-0.0287568	4.3774077
C	-3.8172270	-1.8608281	3.2471042
H	-4.4420228	-2.1206460	2.3931308
H	-2.9358287	-2.5026880	3.2428606
H	-4.3777148	-2.0583873	4.1616548
H	-1.5834605	-0.6435067	4.3515571
H	-3.0015907	-0.2140877	5.3193884
H	-2.1918601	1.0197450	4.3389326
C	-4.6703557	0.5173279	3.2277598
H	-5.3229054	0.2945455	2.3841427
H	-5.2219961	0.3351005	4.1511602
H	-4.3946735	1.5699286	3.1888589
C	0.7314064	0.0383527	-2.1564040
O	0.6208104	0.4176745	-3.2309025
C	4.5909627	2.0861500	-0.8443804
C	5.0132288	2.5735390	0.5490268
H	5.3418025	1.7380177	1.1688972
H	5.8424316	3.2758747	0.4516586
H	4.1862896	3.0762889	1.0483052
C	4.1118789	3.2594851	-1.7121154
H	3.2912515	3.7871721	-1.2288125
H	4.9357069	3.9595308	-1.8591420
H	3.7764224	2.9099053	-2.6890158
C	5.7441114	1.3422373	-1.5331821
H	5.4379881	0.9690538	-2.5109965

H	-0.8214810	-2.5776188	2.1477194
H	0.4281049	-3.7590168	2.5180729
C	3.2912743	-1.9609767	1.6253476
H	6.5841888	2.0238749	-1.6724119
H	6.0840691	0.5004928	-0.9283869

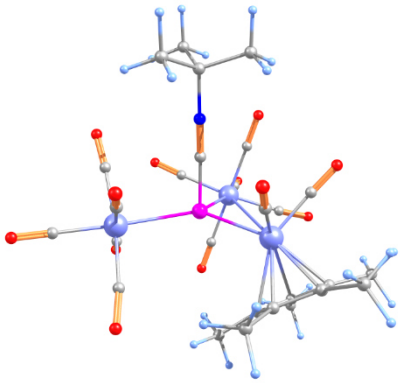

Table S13. Cartesian coordinates of the optimized geometry of [{Cp*Cr(CO)$_2$}(μ$_3$-PCN^{t}Bu){Cr(CO)$_5$}$_2$] at the B3LYP/def2-TZVP level (E = -5475.26452574106 a.u.).

Atom	x	y	z
P	0.8017548	0.2022314	-0.6376475
Cr	-1.3831028	0.3233973	0.3262144
Cr	-0.2898718	-1.1482626	-2.6028246
Cr	3.0458803	1.5783896	-0.7480021
C	-0.4625073	-0.0425670	1.8678953
O	0.0676579	-0.2609052	2.8690840
C	-2.0108281	-1.3897486	0.6617508
O	-2.4283746	-2.4199319	0.9569302
C	-2.9811764	1.7055660	-0.6880187
C	-3.5438568	1.0192245	0.4236053
C	-2.8229635	1.4109572	1.5906983
C	-1.7919037	2.3224428	1.1847759
C	-1.8914474	2.4959182	-0.2320755
C	-0.4568054	0.5392919	-3.4914195
O	-0.5686218	1.5168081	-4.0725627
C	-2.1760082	-1.2608899	-2.2971709
O	-3.3004853	-1.4909227	-2.3131839
C	-0.7205515	-2.0138360	-4.1990019
O	-0.9835422	-2.5425689	-5.1809714
C	1.5211817	-1.3175536	-3.2021429
O	2.5713295	-1.4778721	-3.6194627
C	-0.1280610	-2.8244380	-1.7093378
O	-0.0331367	-3.8530892	-1.2164887
C	2.7995949	1.8521963	-2.6320994
O	2.6892393	2.0446237	-3.7522997
C	4.0392938	-0.0225552	-1.0539149
O	4.7062926	-0.9435078	-1.1920820
C	4.6780198	2.4721890	-0.8181599
O	5.6866844	3.0190857	-0.8597202
C	3.2342467	1.3300389	1.1337555
O	3.3782904	1.2037389	2.2627493
C	2.2776173	3.2825583	-0.3825255
O	1.9503404	4.3530282	-0.1365888
C	-1.2038182	3.5426390	-1.0558862
H	-0.4169336	4.0420872	-0.5001365
H	-0.7695133	3.1468096	-1.9734549
H	-1.9270404	4.3090773	-1.3530876
C	-0.9221278	3.1208766	2.1079686
H	-0.7032118	2.5836346	3.0301380
H	0.0262604	3.3901062	1.6473009
H	-1.4267494	4.0520693	2.3857414
C	-3.2094361	1.0840771	3.0023354
H	-3.9697370	1.7869406	3.3579493
H	-3.6281652	0.0812870	3.0881616
H	-2.3630554	1.1481009	3.6850756
C	-4.7974036	0.1971983	0.4007339
H	-5.6738805	0.8477514	0.4864557
H	-4.8974649	-0.3700178	-0.5233445
H	-4.8353065	-0.5093416	1.2290470
C	-3.5777901	1.7809692	-2.0585219
H	-2.8300577	1.9467347	-2.8311729
H	-4.1493167	0.8918286	-2.3136155
H	-4.2679145	2.6316211	-2.0962030
C	1.5035430	-1.1841650	0.2014405
N	1.9898913	-2.0686118	0.7706363
C	2.5969801	-3.1611596	1.5111838
C	3.6510976	-2.5551278	2.4483933
H	4.1060209	-3.3566594	3.0315209
H	4.4354551	-2.0535630	1.8818314
H	3.1998532	-1.8380003	3.1336397
C	3.2410967	-4.1137928	0.4940020
H	3.7194391	-4.9326674	1.0327625
H	2.4916090	-4.5323220	-0.1769584
H	3.9981921	-3.5983530	-0.0968127
C	1.4834366	-3.8594543	2.3039126
H	0.7200352	-4.2578905	1.6361479
H	1.9175081	-4.6861167	2.8676163
H	1.0143247	-3.1696030	3.0054417

3.6.5 Crystallographic details

Table 14: Overview of selected crystallographic parameters of the single crystal X-ray diffraction experiments performed for **2**, **3a**, **4a**, **4b** and **5**.

	2	**3a**	**4a**	**4b**	**5**
Formula	$C_{30}H_{30}Cr_2O_{10}P_4W$	$C_{30}H_{32}Cl_2Cr_3O_9P_4$	$C_{35}H_{32}Cl_2Cr_4O_{14}P_4$	$C_{35}H_{32}Cl_2Cr_2Mo_2O_{14}P_4$	$C_{12}H_{15}CrO_2P_3$
$D_{calc.}$/ g cm^{-3}	1.790	1.583	1.639	1.721	1.582
m/mm^{-1}	12.906	10.458	11.028	11.297	9.816
Formula Weight	962.27	887.33	1079.38	1167.26	336.15
Colour	dark brown	dark orange	dark orange	dark green	light orange
Shape	block	plate	plate	plate	block
Size/mm^3	0.10×0.10×0.07	0.15×0.12×0.04	0.11×0.09×0.02	0.36×0.20×0.04	0.08×0.06×0.05
T/K	123.01(13)	123.01(10)	123.00(10)	123.0	123.01(10)
Crystal System	tetragonal	monoclinic	triclinic	triclinic	orthorhombic
Flack Parameter	-0.007(8)	-	-	-	-
Hooft Parameter	-0.008(6)	-	-	-	-
Space Group	$I\bar{4}$	$P2_1/c$	$P\bar{1}$	$P\bar{1}$	$Pnma$
a/Å	19.1084(4)	8.61978(12)	11.0293(5)	11.1540(3)	8.3549(2)
b/Å	19.1084(4)	21.5601(3)	11.2147(5)	11.2534(3)	12.7888(3)
c/Å	19.5531(6)	20.3044(2)	19.6309(7)	19.9843(5)	13.2096(2)
α/°	90	90	83.486(4)	83.065(2)	90
β/°	90	99.3350(13)	89.878(3)	89.507(2)	90
γ/°	90	90	65.220(5)	64.897(2)	90
V/Å^3	7139.4(4)	3723.47(9)	2187.57(18)	2252.35(10)	1411.44(6)
Z	8	4	2	2	4
Z'	1	1	1	1	0.5
Wavelength/Å	1.54184	1.54184	1.54184	1.54184	1.54184
Radiation type	Cu K$_\alpha$	Cu K$_\alpha$	Cu K$_\alpha$	Cu K$_\alpha$	Cu K$_\alpha$
Q_{min}/°	3.234	4.101	4.376	4.375	4.813
Q_{max}/°	74.141	74.213	74.174	66.404	79.927
Measured Refl's.	18647	21477	18305	23984	7393
Ind't Refl's	6396	7429	8439	7857	1448
Refl's with I > 2(I)	5883	6622	6231	7480	1397
R_{int}	0.0577	0.0315	0.0584	0.0375	0.0245
Parameters	434	633	561	569	119
Restraints	0	520	18	66	0
Largest Peak	2.722	0.700	0.725	1.271	0.324
Deepest Hole	-1.883	-0.599	-0.627	-1.371	-0.370
GooF	1.082	1.026	1.018	1.036	1.083
wR_2 **(all data)**	0.1235	0.0760	0.1252	0.1235	0.0618
wR_2	0.1192	0.0728	0.1103	0.1215	0.0600
R_1 **(all data)**	0.0542	0.0353	0.0750	0.0449	0.0243
R_1	0.0483	0.0298	0.0484	0.0433	0.0230

[{Cp*Cr(CO)$_3$}$_2$(μ$_3$,η$^{1:1:1:1}$-P$_4$){W(CO)$_4$}] (**2**)

Compound **2** crystalizes in the form of dark brown blocks from a saturated solution in hexane/CH_2Cl_2 upon storage at -28°C. A suitable crystal with dimensions 0.10 × 0.10 × 0.07 mm^3 was selected and mounted on a GV50, TitanS2 diffractometer. The crystal was kept at a steady T = 123.01(13) K during data collection. The structure was solved with the ShelXT 2018/2 (Sheldrick, 2018) solution program using Olex2 (Dolomanov et al., 2009) as the graphical interface. The model was refined with ShelXL 2018/3 (Sheldrick, 2015) using full matrix least squares minimisation on F^2. The asymmetric unit contains one molecule of **2**.

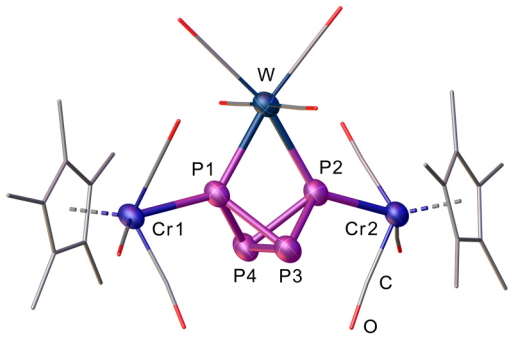

Figure S9. Molecular structure of **2** in the solid state; for clarity H atoms are omitted and the Cp* as well as CO ligands are drawn in the wire frame model; thermal ellipsoids drawn at 50% probability level.

Table S15: Selected bond lengths [Å] and angles [°] of **2** in the solid state.

d / Å		α / °	
Cr1–P1	2.449(4)	**P1–W–P2**	64.21(11)
Cr2–P2	2.445(4)	**P1–P3–P2**	76.21(17)
W–P1	2.583(4)	**P1–P4–P2**	76.51(17)
W–P2	2.582(3)	**P3–P1–P4**	59.49(17)
P1–P3	2.214(5)	**P3–P2–P4**	59.38(17)
P1–P4	2.224(5)	**P2-P4-P3**	60.86(17)
P2–P3	2.235(5)	**P1-P4-P3**	60.03(16)
P2–P4	2.210(5)	**P2-P3-P4**	59.75(16)
P1··P2	2.74(5)	**P1-P3-P4**	60.48(16)
P3–P4	2.202(6)		

[{Cp*Cr(CO)$_2$}$_2$(μ$_3$,η$^{3:1:1}$-P$_4$){Cr(CO)$_5$}] (**3a**)

Compound **3a** crystalizes in the form of dark orange plates from a reaction solution of **1** with 1.0 eq. [Cr(CO)$_4$(nbd)]. The reaction solution is stored at -78°C for one week and subsequently held at -28°C for three months. A suitable crystal with dimensions 0.15 × 0.12 × 0.04 mm^3 was selected and mounted on a GV50, TitanS2 diffractometer. The crystal was kept at a steady T = 123.01(10) K during data collection. The structure was solved with the ShelXT 2018/2 (Sheldrick, 2018) solution program using Olex2 (Dolomanov et al., 2009) as the graphical interface. The model was refined with ShelXL 2018/3 (Sheldrick, 2015) using full matrix least squares minimization on F^2.The asymmetric unit contains one molecule of Compound **3a** (displaying a highly disordered Cp* ligand) and one CH_2Cl_2 molecule.

[{Cp*Cr(CO)$_2$}$_2$(μ$_4$,η$^{3:1:1:1}$-P$_4$){Cr(CO)$_5$}$_2$] (**4a**)

Compound **4a** crystalizes in the form of dark orange plates from a saturated solution in CH_2Cl_2 upon storage at -28°C. A suitable crystal with dimensions 0.11 × 0.09 × 0.02 mm^3 was selected and mounted on a SuperNova, Single source at offset/far, Atlas diffractometer. The crystal was kept at a steady T = 123.00(10) K during data collection. The structure was solved with the ShelXT 2018/2 (Sheldrick, 2018) solution program using Olex2 (Dolomanov et al., 2009) as the graphical interface. The model was refined with ShelXL 2018/3 (Sheldrick, 2015) using full matrix least squares minimisation on F^2. The asymmetric unit contains one molecule of **4a** as well as one disordered solvent molecule.

[{Cp*Cr(CO)$_2$}$_2$(μ$_4$,η$^{3:1:1:1}$-P$_4$){Mo(CO)$_5$}$_2$] (**4b**)

Compound **4b** crystalizes in the form of dark green plates from a saturated solution in CH_2Cl_2/*n*-pentane upon storage at -28°C. A suitable crystal with dimensions 0.36 × 0.20 × 0.04 mm^3 was selected and mounted on a Xcalibur, AtlasS2, Gemini ultra diffractometer. The crystal was kept at a steady T = 123.0 K during data collection. The structure was solved with the ShelXT 2018/2 (Sheldrick, 2018) solution program using Olex2

(Dolomanov et al., 2009) as the graphical interface. The model was refined with ShelXL 2018/3 (Sheldrick, 2015) using full matrix least squares minimisation on F^2.The asymmetric unit contains one molecule of **4b** as well as one disordered solvent molecule.

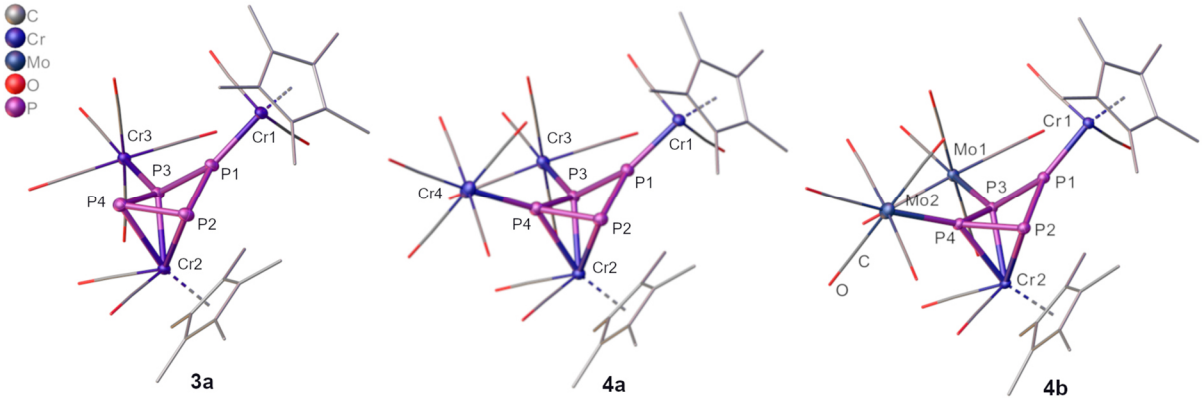

Figure S10. Molecular structure of Compound **3a, 4a** and **4b** in the solid state; for clarity H atoms and solvent molecules are omitted, Cp* and CO ligands are drawn in the wire frame model and only position of disordered Cp* ligand is displayed; thermal ellipsoids drawn at 50% probability level.

Table S16: Selected bond lengths [Å] and angles [°] of **3a**, **4a** and **4b** in the solid state.

		3a	**4a**	**4b**
d / Å	**Cr1–P1**	2.1258(6)	2.1129(11)	2.1169(11)
	Cr2–P2	2.4774(6)	2.4926(12)	2.4970(11)
	Cr2–P3	2.4451(5)	2.4778(11)	2.4726(11)
	Cr2–P4	2.4512(6)	2.4428(11)	2.4354(11)
	Cr3–P3 / Mo1-P3	2.3664(5)	2.3564(12)	2.5002(9)
	Cr4–P4 / Mo2-P4	-	2.3517(11)	2.4896(10)
	P1–P2	2.2181(7)	2.2265(13)	2.2259(13)
	P1–P3	2.1973(7)	2.2013(14)	2.1938(13)
	P3–P4	2.1705(7)	2.1583(12)	2.1560(13)
	P2–P4	2.1606(7)	2.1390(15)	2.1427(13)
α / °	**Cr1–P1–P2**	137.83(3)	138.98(6)	139.54(5)
	Cr1–P1–P3	139.04(3)	137.30(6)	136.42(5)
	P2–P1–P3	82.99(2)	83.72(5)	84.02(5)
	P1–P2–P4	86.79(2)	85.88(5)	85.66(5)
	P1–P3–P4	87.07(2)	86.04(5)	86.14(5)
	P2–P4–P3	84.98(3)	86.88(5)	86.96(5)
	Plane$_{P1–P2–P3}$ vs. Plane$_{P2–P3–P4}$	135.50(8)	135.92(6)	136.18(8)

[Cp*Cr(CO)$_2$(η^3-P$_3$)] (**5**)

Compound **5** crystalizes as light orange blocks from a saturated solution in *n*-hexane upon storage at -28°C. A suitable crystal with dimensions 0.08 × 0.06 × 0.05 mm^3 was selected and mounted on a GV50, TitanS2 diffractometer. The crystal was kept at a steady T = 123.01(10) K during data collection. The structure was solved with the ShelXT 2018/2 (Sheldrick, 2018) solution program using Olex2 (Dolomanov et al., 2009) as the graphical interface. The model was refined with ShelXL 2018/3 (Sheldrick, 2015) using full matrix least squares minimisation on F^2.The asymmetric unit contains half a molecule of **5.**

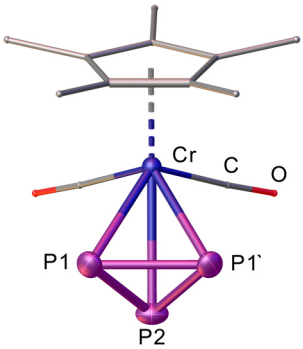

Figure S11. Molecular structure of **5** in the solid state; for clarity H atoms are omitted and the Cp* as well as CO ligands are drawn in the wire frame model; thermal ellipsoids drawn at 50% probability level.

Table S17: Selected bond lengths [Å] and angles [°] of **5** in the solid state.

d / Å		α / °	
Cr–P1	2.4773(5)	**P1–P1′–P2**	60.646(15)
Cr–P1′	2.4773(5)	**P1–P2–P1′**	58.71(3)
Cr–P2	2.5406(7)		
P1–P2	2.1205(7)		
P1–P1′	2.0790(8)		

3.6.6 References

[1] a) R. B. King, *J. Organomet. Chem.* **1967**, *8*, 139-148; b) P. Leoni, A. Landi, M. Pasquali, *J. Organomet. Chem.* **1987**, *321*, 365-369; c) T. J. Jaeger, M. C. Baird, *Organometallics* **1988**, *7*, 2074-2076; d) C. Schwarzmaier, A. Y. Timoshkin, G. Balázs, M. Scheer, *Angew. Chem. Int. Ed.* **2014**, *53*, 9077-9081.

[2] R. B. King, A. Frozalia, *Inorg. Chem.* **1966**, *5*, 1837.

[3] TopSpin 3.0, Bruker BioSpin GmbH

[4] a) K. Eichkorn, O. Treutler, H. Oehm, M. Häser, R. Ahlrichs, *Chem. Phys. Lett.* **1995**, *242*, 652–660; b) K. Eichkorn, F. Weigend, O. Treutler, R. Ahlrichs, *Theor. Chem. Acc.* **1997**, *97*, 119.

[5] a) A. D. Becke, *J. Chem. Phys.* **1993**, *98*, 5648-5652; b) C. Lee, W. Yang, R. G. Parr, *Phys. Rev. B* **1988**, *37*, 785-789; c) A. D. Becke, *Phys. Rev. A* **1988**, *38*, 3098-3100; d) S. H. Vosko, L. Wilk, M. Nusair, *Can. J. Phys.* **1980**, *58*, 1200-1211; e) J. C. Slater, *Phys. Rev.* **1951**, *81*, 385-390.

[6] a) A. Schäfer, C. Huber, R. Ahlrichs, *J. Chem. Phys.* **1994**, *100*, 5829; b) K. Eichkorn, F. Weigend, O. Treutler, R. Ahlrichs, *Theor. Chem. Acc.* **1997**, *97*, 119; c) F. Weigend, R. Ahlrichs, *Phys. Chem. Chem. Phys.* **2005**, *7*, 3297; d) F. Weigend, *Phys. Chem. Chem. Phys.* **2006**, *8*, 1057.

[7] a) F. Furche, R. Ahlrichs, C. Hättig, W. Klopper, M. Sierka, F. Weigend, *WIREs Comput. Mol. Sci.* **2014**, *4*, 91-100; b) R. Ahlrichs, M. Bär, M. Häser, H. Horn, C. Kölmel, *Chem. Phys. Lett.* **1989**, *162*, 165–169; c) O. Treutler, R. Ahlrichs, *J. Chem. Phys.* **1995**, *102*, 346–354.

[8] M. Sierka, A. Hogekamp, R. Ahlrichs, *J. Chem. Phys.* **2003**, *118*, 9136.

[9] a) J. R. Cheeseman, G. W. Trucks, T. A. Keith, M. J. Frisch, *J. Chem. Phys.* **1996**, *104*, 5497-5509; b) K. Wolinski, J. F. Hinton, P. Pulay, *J. Am. Chem. Soc.* **1990**, *112*, 8251-8260; c) R. Ditchfield, *Mol.*

Phys. **1974**, *27*, 789-807; d) R. McWeeny, *Phys. Rev.* **1962**, *126*, 1028-1034; e) F. London, *J. Phys. Radium* **1937**, *8*, 397-409.

[10] Gaussian 09, Revision E.01, M. J. Frisch, G. W. Trucks, H. B. Schlegel, G. E. Scuseria, M. A. Robb, J. R. Cheeseman, G. Scalmani, V. Barone, B. Mennucci, G. A. Petersson, H. Nakatsuji, M. Caricato, X. Li, H. P. Hratchian, A. F. Izmaylov, J. Bloino, G. Zheng, J. L. Sonnenberg, M. Hada, M. Ehara, K. Toyota, R. Fukuda, J. Hasegawa, M. Ishida, T. Nakajima, Y. Honda, O. Kitao, H. Nakai, T. Vreven, J. A. Montgomery, Jr., J. E. Peralta, F. Ogliaro, M. Bearpark, J. J. Heyd, E. Brothers, K. N. Kudin, V. N. Staroverov, T. Keith, R. Kobayashi, J. Normand, K. Raghavachari, A. Rendell, J. C. Burant, S. S. Iyengar, J. Tomasi, M. Cossi, N. Rega, J. M. Millam, M. Klene, J. E. Knox, J. B. Cross, V. Bakken, C. Adamo, J. Jaramillo, R. Gomperts, R. E. Stratmann, O. Yazyev, A. J. Austin, R. Cammi, C. Pomelli, J. W. Ochterski, R. L. Martin, K. Morokuma, V. G. Zakrzewski, G. A. Voth, P. Salvador, J. J. Dannenberg, S. Dapprich, A. D. Daniels, O. Farkas, J. B. Foresman, J. V. Ortiz, J. Cioslowski, and D. J. Fox, Gaussian, Inc., Wallingford CT, **2013**.

[11] a) P. A. M. Dirac *Proc. Royal Soc. A*, **1929**, *123*, 714–733; b) J. C. Slater *Phys. Rev.*, **1951**, *81*, 385–390; c) S. Vosko; L. Wilk; M. Nusair, *Can. J. Phys.*, **1980**, *58*, 1200–1211; d) A. D. Becke *Phys. Rev. A*, **1988**, *38*, 3098–3100; e) J. P. Perdew. *Phys. Rev. B*, **1986**, *33*, 8822–8824; f) J. P. Perdew, *Phys.l Rev. B* **1986**, *34*, 7406-7406.

[12] F. Jensen, *J. Chem. Theory Comput.* **2015**, *11*, 132-138.

[13] B. P. Pritchard, D. Altarawy, B. Didier, T. D. Gibson, T. L. Windus, *J. Chem. Inf. Model.* **2019**, *59*, 4814-4820. www.basissetexchange.org/

[14] NBO 6.0. E. D. Glendening, J. K. Badenhoop, A. E. Reed, J. E. Carpenter, J. A. Bohmann, C. M. Morales, C. R. Landis, F. Weinhold (Theoretical Chemistry Institute, University of Wisconsin, Madison, WI, **2013**); http://nbo6.chem.wisc.edu/

3.7 Author Contributions

Rebecca Grünbauer

- Synthesis and characterization of all reported compounds.

  The synthesis and characterization of compounds **2**, **3a** and **4a** was already performed in the scope of the Master thesis of Rebecca Grünbauer *(University of Regensburg,* **2016**) and the results are also included therein.

- Preparation of manuscript (including figures, schemes, tables and supplementary information) except for paragraphs on the topic of DFT calculations.

Gábor Balázs

- Execution of DFT calculations.
- Preparation of manuscript (including figures, schemes and tables and supplementary information) for paragraphs on the topic of DFT calculations.

Manfred Scheer

- Supervision of project.

4. The reactivity of the P_4 butterfly ligand [{Cp'''Fe(CO)$_2$}$_2$(μ,η$^{1:1}$-P_4)] towards Lewis acids: Coordination vs. rearrangement

Rebecca Grünbauer, Christoph Schwarzmaier, Miriam Eberl, Gábor Balázs and Manfred Scheer

4.1 Abstract

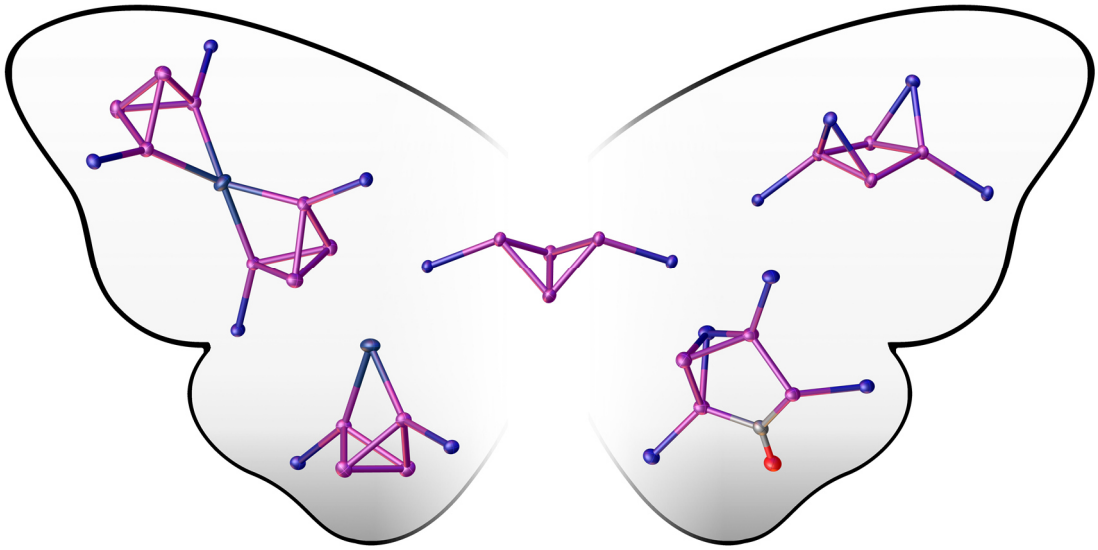

*The following report focuses on the reaction of the P_4 butterfly compound [{Cp'''Fe(CO)$_2$}$_2$(μ,η$^{1:1}$-P_4)] (**1**, Cp''' = $C_5H_2{}^tBu_3$) with various Lewis acids. On the one hand, the reaction of **1** with [(PPh$_3$)Au(tht)][PF$_6$] (tht = tetrahydrothiophene) or [M(CO)$_4$(nbd)] (M = Cr, Mo, W; nbd = norbornadiene) yields chelating complexes of the type [{Cp'''Fe(CO)$_2$}$_2$(μ$_3$,η$^{1:1:1:1}$-P_4){ML$_n$}] (**2**, {ML$_n$} = M(CO)$_4$ or AuPPh$_3$) bearing intact P_4 butterfly ligands with exceedingly small bite angles (ca. 65°). The reaction of **1** with [AgPF$_6$] even afforded the spiro complex [{(Cp'''Fe(CO)$_2$)$_2$(μ$_3$,η$^{1:1:1:1}$-P_4)}$_2$Ag][PF$_6$] (**3**), in which the silver cation is coordinated in a tetrahedrally distorted fashion by two P_4 butterfly motifs. On the other hand, the reaction of **1** with more reactive carbonyl Lewis Acids like [Fe$_2$(CO)$_9$] or [Co$_2$(CO)$_8$] leads to rearrangement yielding [{Cp'''(CO)$_2$Fe}$_2${Co(CO)$_3$}$_2$(μ$_4$,η$^{2:2:1:1}$-P_4)] (**4**), incorporating a folded cyclo-P_4 scaffold, and [{Cp'''Fe(CO)$_2$}$_2$(μ$_4$,η$^{1:1:1:3}$-P_4CO){Fe(CO)$_4$}{Fe(CO)$_3$}] (**5**), displaying a tetraphosphol motif obtained after carbonyl insertion, respectively. The obtained compounds are comprehensively characterized by different spectroscopic methods as well as single crystal X-ray diffraction analysis and theoretical calculations.*

4.2 Introduction

Over the last decades the interest in the activation of small molecules gained great popularity, as these investigations are presumed to improve fundamental chemical processes towards an increased economical sustainability.[1] In this crucial area of research, the selective degradation of the extremely reactive P_4 tetrahedron found in white phosphorus (called P_4 activation) is a promising approach towards the selective generation of phosphorus containing compounds.[2] In this field, the tetraphospha-*bicyclo*[1.1.0]butane structural motif is of immense importance, since it represents the first step in the P_4 activation process. With one P–P bond cleaved in comparison to the intact P_4 tetrahedron, the so called P_4 butterfly motif was part of major milestones in the development of the polyphosphorus ligand chemistry. *Ginsberg* and *Lindsell* were the first to report on the P_4 butterfly motif within the Type **A** chelating complex [(PPh$_3$)$_2$RhCl(η$^{1:1}$-P_4)] (Scheme 1), although it was thought to be an intact P_4 tetrahedron at first.[3] Later on, the group of *Scherer* intensively studied the reactivity of the Type **B** bridging complexes [{Cp^{R}Fe(CO)$_2$}$_2$(μ,η$^{1:1}$-P_4)] (Cp^R: Cp″ = $C_5H_3{}^tBu_2$; Cp‴ = $C_5H_2{}^tBu_3$ (**1**); Scheme 1) under photolytic and thermolytic conditions.[4] Due to decarbonylation processes induced by the reaction conditions, several products incorporating P_n ligands (n ≤ 4) could be obtained in each case, delineating the consecutive P_4 activation steps. Another major scope of application for P_4 butterfly compounds was introduced by *Scherer* et al. with the complex [Cp″$_2$Zr(η$^{1:1}$-P_4)], which has proven to be an excellent source for the transfer of P_4 units.[5] Thus, our group was able to obtain a vast variety of products like phosphorus-carbon cage compounds[6], inorganic benzene analoga[7] and different P_4 ligand complexes[8] from several reactions with the P_4 butterfly transfer reagent.

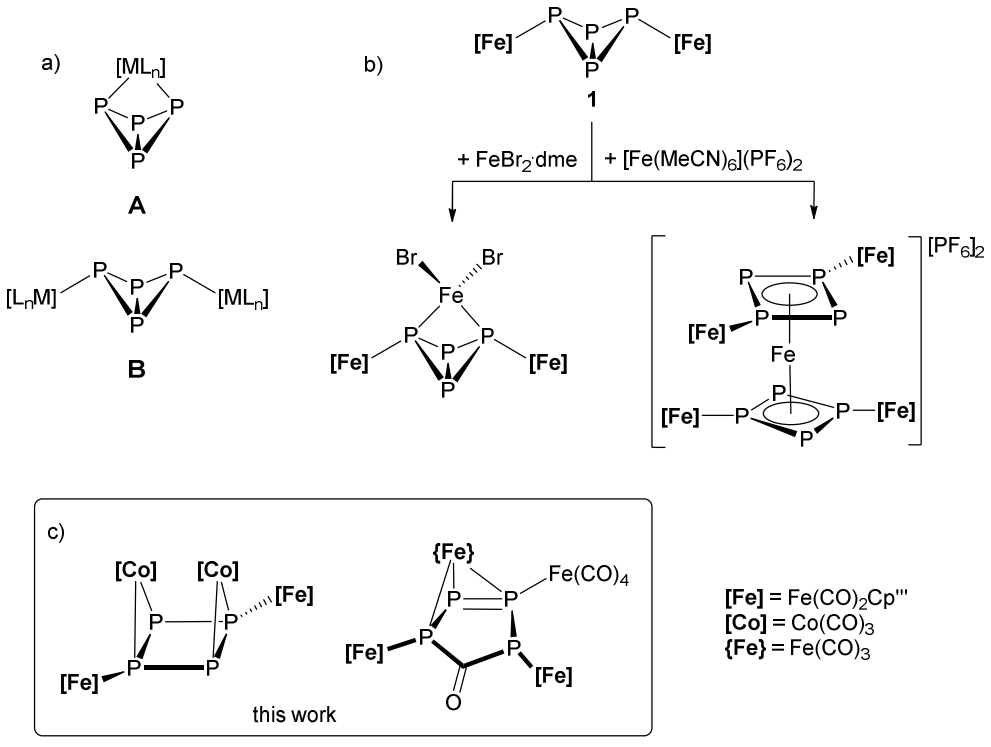

Scheme 1. a) chelating (**A**) and bridging (**B**) coordination mode for the P_4 butterfly motif; b) reactivity of **1** towards different Fe(II) salts; c) novel compounds obtained in this work.

Next to these commonly observed rearrangement processes, our group takes major interest in the coordination properties of intact P_n ligand complexes. Characteristically, every P atom of the P_n scaffold displays coordinatively available lone pairs. Therefore, we were able to obtain various coordination compounds, polymers and even spherical aggregates originating from compounds like $[Cp^RFe(\eta_5\text{-}P_5)]$ (Cp^R: Cp* = $C_5(CH_3)_5$, Cp^{BIG} = $C_5(4\text{-}^n Bu\text{-}C_6H_4)_5$)[9] or $[\{CpM(CO)_2\}_2(\mu,\eta^{2:2}\text{-}E_2)]$ (M = Cr, Mo; E = P, As)[10]. In contrast, the coordination chemistry of **1** has been neglected, as previously mainly its degradation affording novel P_n ligand complexes was examined.[4] However, DFT calculations predicted that a chelating coordination via the two wing tip P atoms is thermodynamically favored and reactions of **1** with monovalent Cu salt supported these calculations.[11] Depending on the stoichiometry, the monoadduct $[\{Cp'''Fe(CO)_2\}_2(\mu_3,\eta^{1:1:1:1}\text{-}P_4)\{Cu(CH_3CN)\}][BF_4]$ and the spiro compound $[\{(Cp'''Fe(CO)_2)_2(\mu_3,\eta^{1:1:1:1}\text{-}P_4)\}_2Cu][BF_4]$ can be isolated from the reactions of **1** with $[Cu(CH_3CN)_4][BF_4]$. Reactions of **1** with $[FeBr_2\cdot dme]$ (dme = dimethoxyethane) again lead to the formation of the P_4 butterfly adduct $[\{Cp'''Fe(CO)_2\}_2(\mu_3,\eta^{1:1:1:1}\text{-}P_4)\{FeBr_2\}]$, while reactions with $[Fe(CH_3CN)_6][PF_6]_2$ afforded $[\{(Cp'''Fe(CO)_2)_2(\mu_3,\eta^{1:1:4}\text{-}P_4)\}_2Fe][PF_6]_2$ (Scheme 1).[12] In this first ever reported "carbon-free" sandwich complex the former P_4 butterfly motif rearranged to a six valence electron donating aromatic *cyclo*-P_4 ligand delineating the reaction potential originating from the P_4 butterfly motif. Intrigued by these results, we were prompted to investigate the reactivity of **1** towards Lewis Acids of different reactivity and report herein on the various obtained products (Scheme 2).

4.3 Results and Discussion

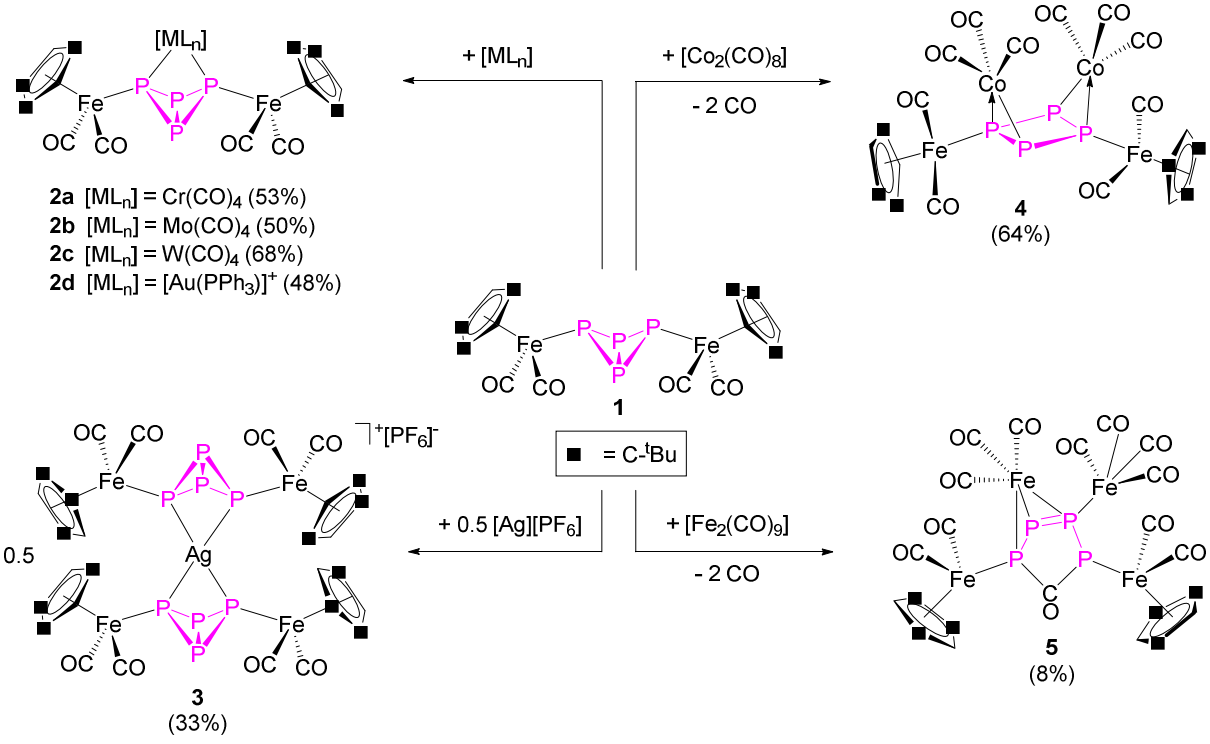

Scheme 2. Reactivity of the P_4 butterfly compound **1** towards different Lewis acids and their precursors.

The reactions of **1** with one equivalent of [M(CO)$_4$(nbd)] (M = Cr, Mo, W; nbd = norbornadiene) or [(PPh$_3$)Au(tht)][PF$_6$] (tht = tetrahydrothiophene) selectively afford the coordination products [{Cp'''Fe(CO)$_2$}$_2$(μ$_3$,η$^{1:1:1:1}$-P_4){M(CO)$_4$}] (M = Cr (**2a**), Mo (**2b**), W (**2c**)) and [{Cp'''Fe(CO)$_2$}$_2$(μ$_3$,η$^{1:1:1:1}$-P_4){AuPPh$_3$}][PF$_6$] (**2d**), respectively (Scheme 2 and Fig. 1). By means of a straightforward ligand exchange, both the nbd and tht ligand are replaced by the more strongly donating P_4 butterfly ligand. Consequently, **1** serves as a bidentate ligand coordinating towards the Lewis acidic [M(CO)$_4$] and [AuPPh$_3$] fragment, respectively, via the two wing tip P atoms. Moreover, the reaction of **1** with 0.5 eq. [AgPF$_6$] yields the spiro compound [{(Cp'''Fe(CO)$_2$)$_2$(μ$_3$,η$^{1:1:1:1}$-P_4)}$_2$Ag][PF$_6$] (**3**), in which the Ag^+ ion is coordinated by two chelating molecules of **1** in a distorted tetrahedral fashion (Scheme 2 and Fig. 1). The red **2a-c** as well as the orange **2d** and **3** are not soluble in pentanes, moderately soluble in toluene and very well soluble in CH_2Cl_2. Single crystal X-ray diffraction analysis confirms, that the coordination towards the Lewis acidic fragments [M(CO)$_4$] and [AuPPh$_3$] has only little influence on the geometric parameters of the P_4 butterfly scaffold. Whereas **2a-c** crystalize with an almost identical monoclinic-sphenoidal unit cell (spacegroup *C2/c*), **2d** crystalizes in the monoclinic *P*2$_1$/*n* and **3** crystalizes in the C*c* space group. Moreover, the asymmetric units of **2a-c** contain two stereoisomeric molecules each, as the *tert*-butyl groups of the Cp''' ligand can be arranged in a cis- or trans-like fashion respectively (Fig. 1). Analogously to the uncoordinated **1**, all the P–P bonds of the coordination adducts are in the range of an usual P–P single bond.[13] However, the central P_4 butterfly structural motif in the adducts **2** and **3** is slightly distorted compared to the symmetrical P_4 butterfly scaffold in **1**, resulting in marginally different bond lengths between the wing tip P atoms and the coordinated metal atom (d_{PM}, Table 1).

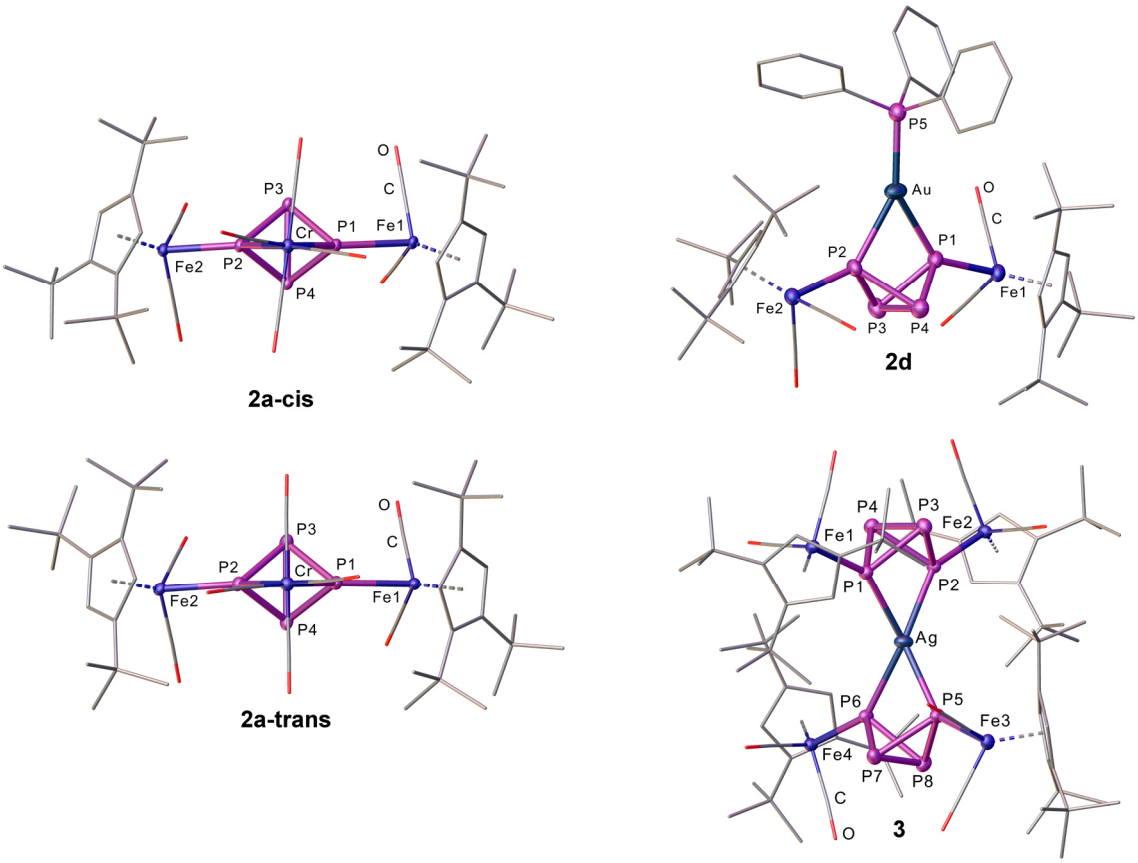

Figure 1. Molecular structures of the two isomers of **2a** and the cationic entities of **2d** and **3** in the solid state; for clarity H Atoms as well as solvent molecules are omitted and CO as well as Cp''' ligands are drawn in the wire frame model; thermal ellipsoids are drawn at 50% probability.

Table 1. P–M–P bite angles, P–M bond lengths and selected ^{31}P NMR chemical shifts of compounds **2a-d** and **3** ($^{31}P\{^{1}H\}$ NMR spectra are recorded in CD_2Cl_2 at 300 K).

	P–M–P [°]	d_{PM} [Å]	$\delta_{P\text{-wing tip}}$ [ppm]	$\delta_{P\text{-bridgehead}}$ [ppm]
2a (M = Cr)	66.78(3) 67.25(3)	2.3043(9) - 2.3162(9)	-98.8 (t, $^{1}J_{PP}$ = 162 Hz)	-152.1 (t, $^{1}J_{PP}$ = 162 Hz)
2b (M = Mo)	64.63(4) 65.62(4)	2.2944(12) - 2.3055(14)	-121.8 (t, $^{1}J_{PP}$ = 162 Hz)	-178.4 (t, $^{1}J_{PP}$ = 162 Hz)
2c (M = W)	64.56(5) 65.07(5)	2.2927(16) - 2.3051(17)	-161.6 (m)	-168.3 (m)
2d (M = Au)	68.16(7)	2.480(2) 2.557(2)	-22.9 (dt, $^{1}J_{PP}$ = 196 Hz, $^{2}J_{PP}$ = 111 Hz)	-299.2 (t, $^{1}J_{PP}$ = 196 Hz)
3 (M = Ag)	67.07(2) 66.08(3)	2.5882(8) 2.6342(8)	-63.8 (dt, $^{1}J_{PP}$ = 191 Hz $^{1}J_{P107Ag}$ = 138 Hz)	-63.8 (dt, $^{1}J_{PP}$ = 191 Hz $^{1}J_{P109Ag}$ = 158 Hz)	-305.0 (t,$^{1}J_{PP}$ = 191 Hz)

Surprisingly, **2a-c** display very similar P–M bond lengths (approx. 2.30 Å) independent of the nature of the coordinated metal atom. This observation suggests that the steric properties of **1** determinate the structural composition of the adducts **2a-c** while the [M(CO)$_4$] fragment has only very little impact on the structural motif. In the classical complexes [M(CO)$_4$(dppm)] (M = Cr[14], Mo[15], W[16], dppm = bis(diphenylphosphino)methane) the corresponding P–M bonds are elongated about 0.2 Å in comparison to **2a-c**, respectively. Similarly, [{Cp*Cr(CO)$_3$}$_2$(μ_3,$\eta^{1:1:2}$-P$_4$){W(CO)$_4$}], the chromium analog to **2c**, incorporates P–W bond lengths of 2.582(3) Å and 2.583(4) Å, respectively.[17] Consequently, **2a-c** display a exceptionally strong interaction between the P$_4$ butterfly ligand **1** and the coordinated [M(CO)$_4$] fragment when compared to analog compounds. In contrast to the shortened P–M bond lengths of **2a-c**, the P–Au bonds in **2d** (2.480(2) Å and 2.557(2) Å, respectively) are elongated in comparison to the corresponding bonds in similar compounds. For the trigonal planar gold complex [{o-B$_{10}$H$_{10}$C$_2$(PPh$_2$)$_2$}Au(PPh$_3$)][ClO$_4$] two Au–P bond lengths of 2.405(1) Å and 2.417(1) Å are reported involving the chelating ligand and the Au–PPh$_3$ bond is given at 2.318(1) Å.[18] Consequently, **1** displays a comparably weaker interaction with the Lewis acidic fragment [AuPPh$_3$]$^+$ than the [o-B$_{10}$H$_{10}$C$_2$(PPh$_2$)$_2$] ligand most likely due to steric repulsion of the Cp‴ and Ph ligands. The remarkably long P–Ag bonds in **3** are given at 2.5882(8) Å and 2.6342(8) Å, respectively, and can be interpreted as a result of the steric repulsion of the four Cp‴ ligands in **3** resulting in a strained coordination sphere. The previously reported Cu analog of **3** incorporates P–Cu bonds of 2.3630(8) Å and 2.4268(8) Å, causing an even more distorted coordination sphere in comparison to **3** due to an increased steric repulsion.[11]

The most prominent shared feature of **2a-d** and **3** are the exceedingly small P–M–P bite angles of 64.07(5)° - 68.16(7)°, which are smaller than the corresponding angles of most established bisphosphane ligands applied in catalytic processes.[19] This suggest that the P$_4$ butterfly ligand **1** could be an all-phosphorus inorganic alternative for established ligands like dppm (bite angle = 72(2)°), as reports showed that the activity of a catalyst mainly depends on the direct environment of the active metal site making the bite angle an important parameter in terms of catalyst improvement.[20]

IR spectroscopic and mass spectrometric analysis of **2** and **3** gave the expected results (cf. Si). The ^{1}H NMR spectra of **2a, 2b**, **2d** and **3** each display the expected three sharp singlets for the freely rotating Cp‴ ligands.

In the $^{31}P\{^1H\}$ NMR spectrum of **2a** and **2b** identical A_2M_2 spin systems yielding two triplets with $^1J_{PP}$ coupling constants of 162 Hz can be detected (Table 1).[21] In contrast, an additional $^2J_{PP}$ coupling (111 Hz) of the wing tip P atoms and the PPh_3 ligand coordinated to the central Au ion is observed in the $^{31}P\{^1H\}$ NMR spectrum of **2d**. In the $^{31}P\{^1H\}$ NMR spectrum of **3** a sharp triplet ($^1J_{PP}$ = 191Hz) at δ = -305.0 ppm corresponding to the bridgehead P atoms and two overlapping doublets of triplets at δ = -63.8 ppm corresponding to the wing tip P atoms can be observed. The overlapping doublet of triplet splitting of the signal attributed to the wing tip P atoms is due to the coupling with the two NMR active nuclei of silver: ^{107}Ag and ^{109}Ag ($^1J_{P107Ag}$ = 138 Hz and $^1J_{P109Ag}$ = 158 Hz, respectively). Analogous observations are reported for similar compounds like [Ag(dppe)$_2$][NO] (dppe = bis-(diphenylphosphino)ethane) which incorporates coupling constants of $^1J_{P107Ag}$ = 231 Hz and $^1J_{P109Ag}$ = 266 Hz.[22]

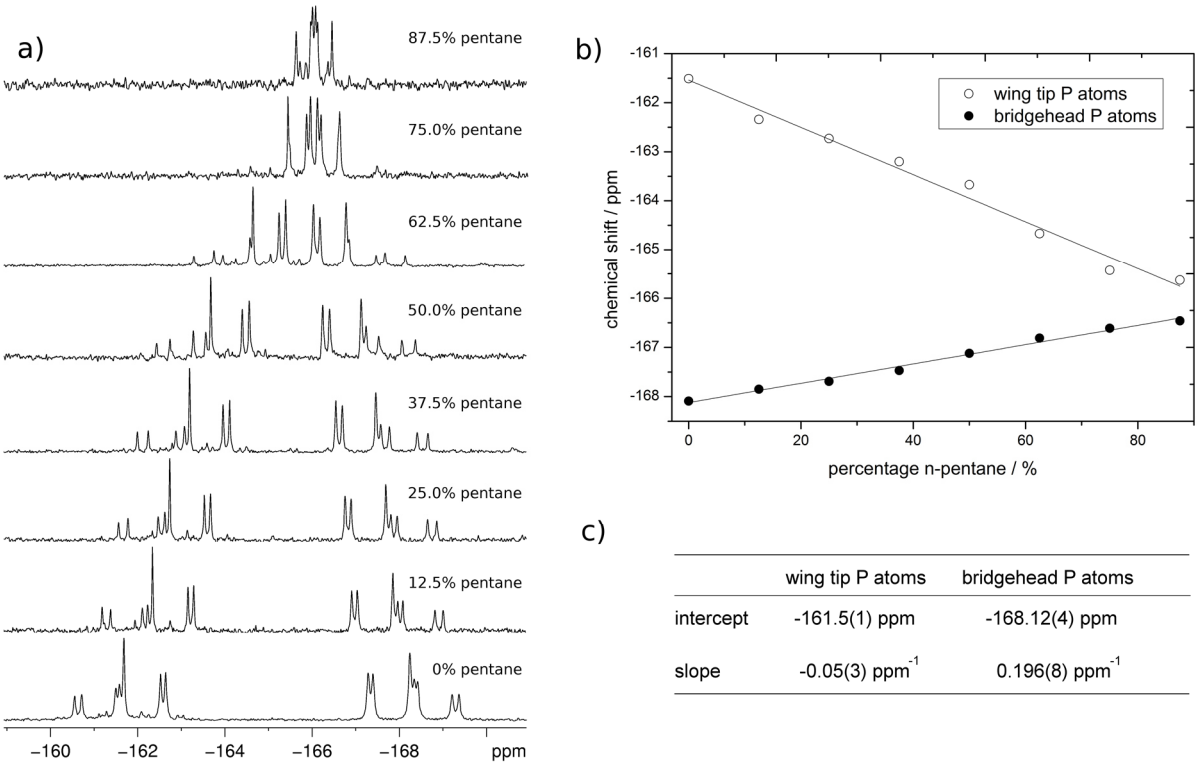

	wing tip P atoms	bridgehead P atoms
intercept	-161.5(1) ppm	-168.12(4) ppm
slope	-0.05(3) ppm^{-1}	0.196(8) ppm^{-1}

Figure 2. (a) $^{31}P\{^1H\}$ NMR spectra of **2c** in CH_2Cl_2/*n*-pentane mixtures with increasing *n*-pentane percentage (recorded with C_6D_6-capillary at 300 K); (b) chemical shifts of the signals in the recorded $^{31}P\{^1H\}$ NMR spectra compared with the *n*-pentane percentage of the corresponding solutions; (c) parameters of the linear fits displayed in (b)

Unlike **2a** and **2b**, all NMR spectra of the higher homologue complex **2c** are highly solvent dependent. Similar observations are established for biomolecules bearing phosphate groups (like ribonucleic acids or proteins) as protic solvents are able to change the environment of the phosphate groups via hydrogen bonding in contrast to non-polar solvents.[23] The ^1H NMR spectrum of **2c** displays three sharp singlets in non-polar solvents like benzene (δ = 1.19 ppm (36H), 1.34 ppm (18H) and 4.70 ppm (4H)) and toluene (δ = 1.27 ppm (36H), 1.39 ppm (18H) and 4.73 ppm (4H)), whereas two broad signals are recorded in polar solvents like thf (δ = 1.43 ppm (54H) and 4.89 ppm (4H)) and CH_2Cl_2 (δ = 1.41 ppm (54H) and 4.71 ppm (4H)). This indicates that the three *tert*-butyl groups of the Cp‴ ligand are magnetically very similar in a polar environment, while magnetically different *tert*-butyl substituents are observed in a non-polar environment. However, the polarity of the solvent effects the $^{31}P\{^1H\}$ NMR spectrum of **2c** even more distinctly. Whereas polar solvents

like CH_2Cl_2 afford two distinct multiplets for the AA′BB′ spin system, a decrease in solvent polarity causes a convergence of the two multiplets resulting in a high order spin system in non-polar solvents like benzene or toluene.[24] However, control experiment showed that concentration variations have no influence on the $^{31}P\{^1H\}$ NMR spectra. Moreover, protonated and deuterated solvents gave the same $^{31}P\{^1H\}$ NMR spectra excluding isotope effects. A simulation of the $^{31}P\{^1H\}$ NMR spectrum of **2c** in CD_2Cl_2 based on an AA′BB′ spin system results in chemical shifts of δ = -161.6 ppm (wing tip P atoms) and δ = -168.2 ppm (bridgehead P atoms) and these values comply well with the chemical shifts obtained for the highest peak found in the experimentally recorded spectrum.

To further investigate the uncommon degree of solvent dependency, a series of $^{31}P\{^1H\}$ NMR spectra was recorded in CH_2Cl_2/*n*-pentane mixtures with increasing *n*-pentane percentage delineating a linear convergence of the two multiplets with decreasing polarity (Fig. 2). Moreover, it is obvious that the polarity of the solvent has more influence on the environment of the wing tip P atoms as the corresponding signal in the $^{31}P\{^1H\}$ NMR spectra is more noticeably shifted (steeper slope; Fig. 2) than the signal attributed to the bridgehead P atoms. In summary, these observations suggest, that in solution the structural composition of **2c** is not rigid and highly solvent dependent. The underlying process of the observed dynamic behavior could be the wobbling of the $[W(CO)_4]$ fragment between the two wing tip P atoms of **1** due to steric repulsion of the $[W(CO)_4]$ fragment and the bulky Cp‴ ligands of **1**. Hence, the environment of the wing tip P atoms is directly susceptible to solvent changes due to the weak coordination of the Lewis acid. Another possibility is the complete or partial dissociation of the $[W(CO)_4]$ fragment from the P_4 butterfly ligand yielding ionogenic Lewis structures with separated (formal) charges. Naturally, only polar solvents endorse this (partial) fragmentation by stabilizing the afforded polar fragmentation products, which explains the solvent dependent observation of this phenomenon. The fact, that an analog observation cannot be made for the lighter homologues **2a** and **2b**, suggests that the tungsten atom of **2c** is essential to the observed dynamic process.

Intrigued by the for P_4 butterfly compounds unprecedented relation between solvent polarity and chemical shift in the $^{31}P\{^1H\}$ NMR spectrum, the influence of temperature on the NMR spectra of **2c** was investigated. Here, a common variation of the chemical shifts as well as line broadening could be detected in the ^1H and ^{31}P NMR spectra of **2c**.[24] Moreover, these effects are observed in polar as well as non-polar solvents. In contrast to the previously discussed dependency on solvent polarity, the change in temperature has only little influence on the chemical shift of the signal corresponding to the wing tip P atoms in the $^{31}P\{^1H\}$ NMR spectrum but influences the chemical shift attributed to the bridgehead P atoms more distinctly.[24] However, none of these effects are out of the ordinary and therefore no additional information about the composition of **2c** can be deducted.

Besides the formation of P_4 butterfly adducts, **1** can also be the starting point for the generation of novel P_n ligand systems by converting it with highly reactive Lewis acidic fragments. Depending on the electronic requirement of the metal fragment, different rearrangements of the tetraphospha-*bicyclo*[1.1.0]butane unit can occur. One example for such a rearrangement is the formation of the afore mentioned *cyclo*-P_4 sandwich complex $[\{(Cp'''Fe(CO)_2)_2(\mu_3,\eta^{1:1:4}\text{-}P_4)\}_2Fe][PF_6]_2$ obtained from the reaction of **1** with $[Fe(CH_3CN)_6][PF_6]$ (Fig. 1).[12] Additionally, the chromium P_4 butterfly complex $[\{Cp^*Cr(CO)_3\}_2(\mu,\eta^{1:1}\text{-}P_4)]$ undergoes rearrangement processes affording a bend deltoid *cyclo*-P_4 motif with a unique substitution pattern when reacted with $[M(CO)_4(nbd)]$ (M = Cr, Mo).[17]

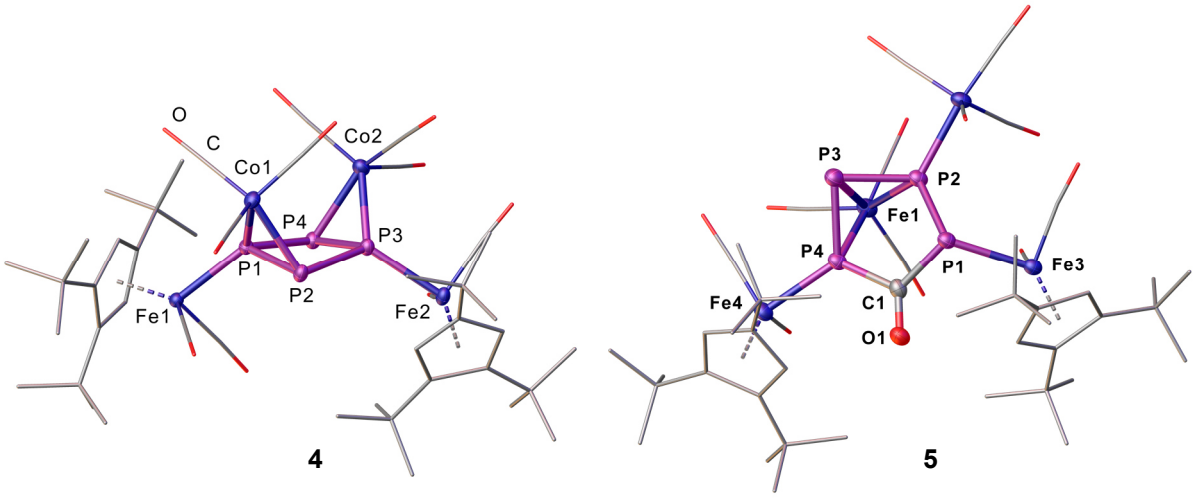

Figure 3. Molecular structures of **4** and **5** in the solid state. For clarity H Atoms as well as solvent molecules are omitted and CO as well as Cp‴ ligands are drawn in the wire frame model; thermal ellipsoids are drawn at 50% probability.

However, in this report we focus on the reactions of **1** with the two transition metal carbonyls [$Co_2(CO)_8$] and [$Fe_2(CO)_9$]. By reacting **1** with [$Co_2(CO)_8$], the P–P bond between the former bridgehead P atoms of **1** is cleaved yielding the *cyclo*-P_4 incorporating [{Cp‴(CO)$_2$Fe}$_2$(μ$_4$,η$^{1:1:2:2}$-P_4){Co(CO)$_3$}$_2$] (**4**). Stabilized by the chelating coordination towards two [$Co(CO)_3$] fragments, **4** is left with a central [P_4Co_2] structural motif which strongly resembles the "boot conformation" known for organic six membered rings (Fig. 3). Formally, each [$Co(CO)_3$] fragment is covalently bound to one of the former bridgehead P atoms via a 2-center-2-electron-bond and additionally datively coordinated by one former wing tip P atom. Thus, the *cyclo*-P_4 ligand in **4** represents a six-valence electron donor. Compound **4** can be isolated in the form of dark brown needles, which are very well soluble in CH_2Cl_2. The single crystal X-ray diffraction analysis of **4** displays a slightly folded *cyclo*-P_4 moiety incorporating two different P–P bond lengths (Fig. 3). With 2.1351(14) Å and 2.1361(14) Å, respectively, the two P–P bonds which are asymmetrically canopied by [$Co(CO)_3$] fragments are noticeable shortened compared to an ordinary P–P single bond (2.21 Å).[13] In contrast, the two remaining P–P bonds are slightly elongated (2.2804(15) Å and 2.2923(15) Å, respectively). Moreover, the four Co–P bond lengths in **4** vary from 2.2438(10) Å (Co2–P3) to 2.2872(13) Å (Co2–P4) with Co1–P1 and Co2–P3 being shorter than Co1–P2 and Co2–P4 (labeling according to Fig. 3). The different P–P and Co–P bond lengths in **4** are nicely reflected in the corresponding Wiberg Bond Indices (WBI). WBIs of 1.03 and 0.87 are given for the canopied and non-canopied P–P bonds, respectively, while WBIS of 0.63 and 0.51 are determined for the Co1–P1/Co2–P3 and Co1–P2/Co2–P4 bonds, respectively. The P–Fe bonds in **4** (2.2954(11) Å and 2.2872(13) Å) are shortened compared to the corresponding bonds in the starting material **1** (2.355(2) Å and 2.348(2) Å), due to the electron withdrawing properties of the [$Co(CO)_3$] fragments. Finally, with a torsion angle of 13.4° the central *cyclo*-P_4 unit in **4** displays only a slight deviation from planarity.

In the ^{1}H NMR spectrum of **4** two associated sets of three signals each are detected for the two Cp‴ ligands indicating, that **4** is not symmetrical in solution, probably due to the hindered rotation of the [Cp‴Fe(CO)$_2$] fragments. The ^{31}P{^{1}H} NMR spectrum of **4** in CD_2Cl_2 displays two distinct signals at δ_X = -12.6 ppm (attributed to the former bridgehead P atoms; P2 and P4 in Fig. 3) and δ_A = 24.4 ppm (attributed to the former wing tip P atoms; P1 and P3 in Fig. 3) indicating an AA′XX′ spin system. The simulation of this ^{31}P{^{1}H} NMR

spectrum affords two different types of $^1J_{PP}$ coupling constants ($^1J_{AX'}$ = 237.5 Hz/$^1J_{A'X}$ = 250.5 Hz and $^1J_{AX}$ = 361.1 Hz/ $^1J_{A'X'}$ = 369.1 Hz) corresponding to the non-canopied and canopied P–P bonds, respectively. This complies well with the values obtained from the WBI analysis as higher WBIs are given for the canopied P–P bonds (WBI = 1.03) in comparison to the non-canopied P–P bonds (WBI = 0.87). The IR spectrum of solid **4** exclusively displays carbonyl stretching bands for terminal CO ligands, while an additional bridging CO band at $\tilde{\nu}_{CO}$ = 1712 cm^{-1} is detected for a solution of **4** in CH_2Cl_2. Therefore, dynamic processes like the opening and rearrangement of carbonyl bridges as those that have been observed for $[Fe_3(CO)_{12}]$[25] are to be expected for **4** in solution.[26] Consequently, $^{31}P\{^1H\}$ NMR spectra of **4** at different temperatures were recorded to further investigate the proposed dynamic processes. Hereby, a broadening of the two multiplets with decreasing temperature can be observed, with the effect being more pronounced for the signal corresponding to the two former bridgehead P atoms (P_X; P2 and P4 in Fig. 3). However, as this is a quite common observation in variable temperature $^{31}P\{^1H\}$ NMR spectroscopy, no further conclusions can be drawn regarding the nature of the proposed dynamic processes occurring in solution.

In contrast to the straight forward P–P bond cleavage accompanied by stabilization trough Lewis acidic fragments that affords **4**, the reaction of **1** with $[Fe_2(CO)_9]$ yields $[\{Cp'''Fe(CO)_2\}_2(\mu_4,\eta^{1:1:1:3}\text{-}P_4CO)\{Fe(CO)_4\}\{Fe(CO)_3\}]$ (**5**) after chromatographic workup and crystallization. The central moiety of **5** is a tetraphosphol scaffold obtained by the insertion of a carbonyl ligand into the P_4 butterfly unit alongside bond cleavage of the P–P bond between the two former bridgehead P atoms (Fig. 3). Additionally, the distorted five membered $[P_4C]$ ring is stabilized by the two $[Cp'''Fe(CO)_2]$ substituents of the starting material **1** as well as a canopying $[Fe(CO)_3]$ and a terminal $[Fe(CO)_4]$ fragment. However, $^{31}P\{^1H\}$ NMR spectroscopy suggest the initial formation of a different product (**5***) with a subsequent CO insertion affording **5** during the chromatographic workup or the crystallization process. Since no single crystals suitable for X-ray diffraction analysis could be obtained for the dark brown **5***, the structural composition of **5*** is yet to be determined. In the ^{31}P NMR spectrum of **5*** only one triplet (δ = -257.5 ppm, $^1J_{PP}$ = 217 Hz; recorded in toluene-d_8) can be detected at room temperature. After cooling the sample below -20 °C, two additional multiplets centered at δ = 16.0 ppm and δ = -19.9 ppm emerge. The intensity ratio of the three signals in the ^{31}P NMR spectrum at -50 °C is given at 1:1:2 indicating an ABX_2 spin system. IR spectroscopic investigations of **5*** reveal the exclusive presence of terminal carbonyl ligands, while EI-MS spectrometric investigations give m/z = 1053 as the peak with highest mass to charge ratio. However, this type of ionization is prone to cause decarbonylation. Hence, it is not obvious, whether this peak is assignable to the molecular ion peak of **5***. With these experimental parameters, two possible compositions for **5*** can be deducted. If the recorded peak from the EI-MS spectrum is considered to be the molecular ion peak $[M^+]$, the molecular composition of **5*** would be $C_{34}H_{58}Fe_4O_9P_4$. This composition corresponds to $[\{Cp'''Fe(CO)_2\}_2(\mu_4,\eta^{1:1:1:2}\text{-}P_4)\{Fe(CO)_4\}\{Fe(CO)_3\}]$ (**5*-1**) representing an intact molecule of **1** coordinating to one $[Fe(CO)_4]$ fragment in a η^1-coordination mode accompanied by the additional coordination towards a $[Fe(CO)_3]$ fragment in a chelating η^2-fashion. However, if the peak observed in the EI-MS spectrum of **5*** is attributed to $[M^+\text{-}CO]$, the composition of **5*** amounts to $C_{35}H_{58}Fe_4O_{10}P_4$ suggesting $[\{Cp'''Fe(CO)_2\}_2(\mu_4,\eta^{1:1:1:1}\text{-}P_4)\{Fe(CO)_4\}_2]$ (**5-2***), an intact molecule of **1** coordinating towards two $[Fe(CO)_4]$ fragments, as the second structural proposal for **5***. For both **5*-1** and **5*-2** the coordination of the (second) $[Fe(CO)_4]$ fragment could be alternating between the two (former) bridgehead atoms explaining the dynamic behavior obtained in solution.

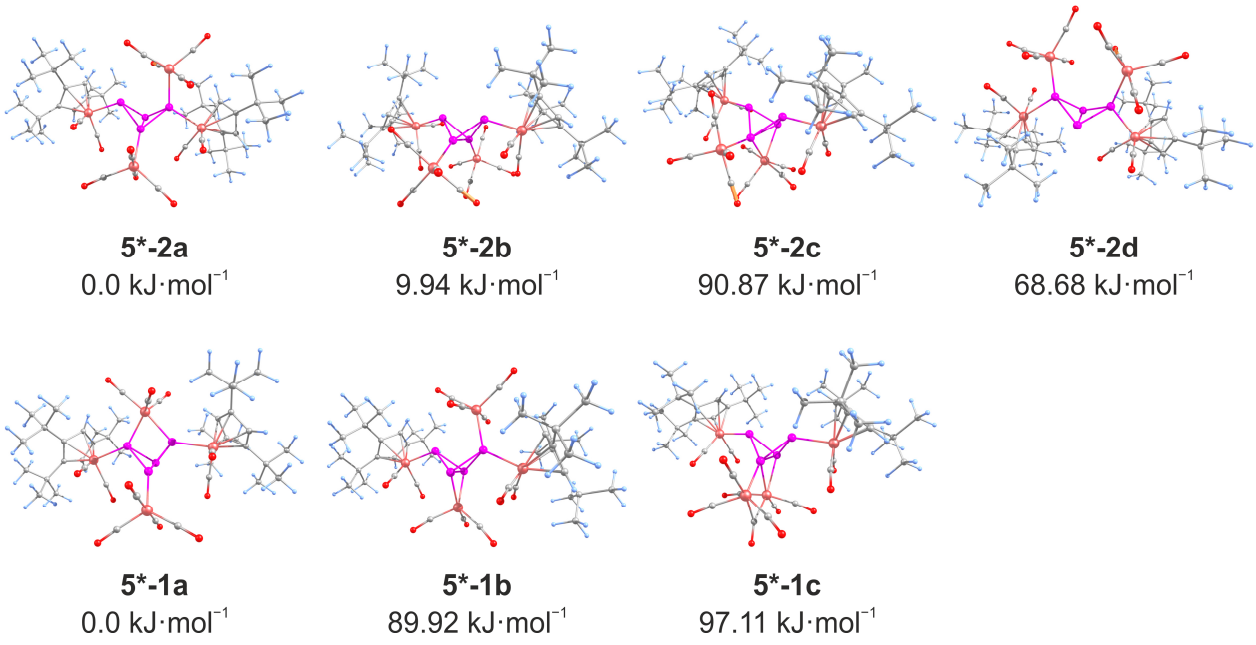

Figure 4. Structure and relative energies of suggested isomers for **5*-1** and **5*-2** (calculated on the B3LYP/def2TZVP level of theory).

In order to elucidate the nature of **5*** we calculated the relative energy of different feasible isomers of **5*-1** and **5*-2** at the B3LYP/def2TZVP level of theory (Fig. 4).[27] The results show that the coordination of both wing tip P atoms to two [Fe(CO)$_4$] fragments is rather unlikely due to steric reasons. Additionally, the binding of one [Fe(CO)$_4$] fragment to only one wing tip P atom is preferred instead of a symmetrical [Fe(CO)$_4$] bridge. All attempts to localize an intermediate of the latter type failed (geometries converge to the η^1-coordination) indicating that such a geometry might be a transition state but not a stable minimum. The energetically most stable compound from the analyzed series is **5*-2a** in which one of the wing tip P atoms and one of the bridgehead P atoms coordinate in a η^1-fashion to a [Fe(CO)$_4$] fragment each. The isomer **5*-2b**, in which both bridgehead P atoms coordinate to two [Fe(CO)$_4$] fragments, lies energetically higher than **5*-2a** (9.94 kJ·mol^{-1}, Fig. 4). Additionally, we were able to locate the isomer **5*-2c** in which one [Fe(CO)$_4$] fragment is bound in a η^2-mode to the bridgehead P atoms and a second [Fe(CO)$_4$] fragment is bound to one bridgehead P atom a η^1-fashion. However, with 90.87 kJ·mol^{-1} **5*-2c** lies much higher in energy than **5*-2a** and **5*-2b** (Fig. 4). Furthermore, a η^1:η^1-coordination of **1** via the wing tip P atoms towards a [Fe(CO)$_3$] fragment (**5*-1a**) is clearly preferred with -89.92 kJ·mol^{-1} over a η^2-coordination promoted by the two bridgehead P atoms (**5*-1b**). With 97.11 kJ·mol^{-1} the isomer **5*-1c**, displaying a η^2:η^1-coordination mode of the two bridgehead P atoms, lies only slightly higher in energy compared to **5*-2b** (Fig. 4).

By comparing the ^{31}P NMR spectrum of **5*** and **1**, it is obvious that in **5*** both the wing tip P atoms and the bridgehead P atoms interact with an Fe fragment as both signals attributed to the respective P atoms are distinctly altered in the ^{31}P NMR spectra. For complex **5***, both bridgehead P atoms are equivalent on the NMR time scale at low temperatures as well as at room temperature. Meanwhile the ^{31}P NMR spectra depict that the wing tip P atoms of **5*** are inequivalent at low temperatures and at room temperature an accentuated dynamic process can be observed by the dissolving of the corresponding signals. This indicates that the wing tip P atoms are involved in the underlying dynamic process. Since the coordination of a [Fe(CO)$_3$] fragment by the wing tip P atoms would result in a stable core, no dynamic behavior could be observed. The

coordination of a $[Fe(CO)_3]$ fragment to the P–P bond of the bridgehead P atoms and the wobbling of the $[Fe(CO)_4]$ fragment between both wing tip P atoms in **5*-1b** could explain the observations in the ^{31}P NMR spectra. Although **5*-1b** is energetically less stable than **5*-1a**, the formation of **5*-1b** might be endorsed due to kinetic reasons. A similar process has been reported for the protonated **1**, i.e. $[\{Cp'''Fe(CO)_2\}_2(\mu,\eta^{1:1}\text{-}P_4)H]^+$.[28]

Compound **5** crystallizes in the triclinic space group $P\bar{1}$ and single crystal X-ray diffraction analysis depicts the central tetraphosphol moiety, which adopts a distorted envelope conformation in the solid state (Fig. 3). The strained five membered ring consists of two different type of P–P bonds: the $[Fe(CO)_3]$ bridged bonds P2–P3 (2.1625(15) Å) and P3–P4 (2.1876(15) Å) which are slightly shortened compared to the P1–P2 bond (2.2114(51) Å). Consequently, a partial double bond character can be proclaimed for P2–P3 and P3–P4. A similar P–P distance with double bond character has been reported for the diphosphene complex $[\{Fe(CO)_4\}_2(\mu,\eta^{2:1}\text{-}P_2Ph_2)]$ (2.139(2) Å).[29] In contrast, the P1–P2 bond length compares well with an usual P–P single bond.[13] Additionally, the P1–C–P4 angle of 115.2(2)° in **5** matches well with the corresponding angle in $[Li(thf)_3\textit{cyclo}\text{-}(P_4{}^tBu_4CH)]$ (116.9°).[30]

Due to the asymmetric substitution pattern of the five membered ring, two sets of five singlets are recorded in the ^1H NMR spectrum of **5**. Moreover, **5** displays an ABMX spin system yielding four distinct signals in the $^{31}P\{^1H\}$ NMR spectrum (δ = 69.0 ppm, 40.3 ppm, 6.5 ppm and -133.9 ppm; recorded in C_6D_6). In contrast to **5***, **5** displays a broad band at $\tilde{\nu}_{CO}$ = 1638 cm^{-1} in the IR spectrum typical for the bridging CO group of the teraphosphol motif.

4.4 Conclusion

In conclusion, we were able to illustrate the diverse coordination behavior of the P_4 butterfly compound **1** towards different carbonyl Lewis acids. On the one hand, a chelating coordination via the two wing tip P atoms of **1** towards $[M(CO)_4]$ (M = Cr, Mo, W) as well as $[(Ph_3P)Au]^+$ fragments was reported. Hereby, complexes **2a-d** incorporating intact P_4 butterfly ligands that display exceedingly small bite angles (approx. 65°) were obtained. These compounds might represent an all-phosphorus alternative to dppm and could give new impulses in catalytic applications. Additionally, the reaction of **1** with $[AgPF_6]$ afforded **3**, a spiro complex with two intact P_4 butterfly ligands. Moreover, the interesting solvent depended $^{31}P\{^1H\}$ NMR spectra of **2c** were intensively discussed to highlight this for P_n ligands unprecedented behavior.

On the other hand, **1** verified to be a promising starting material for P_4 rearrangement processes, as the reactions of **1** with $[Co_2(CO)_8]$ and $[Fe_2(CO)_9]$ afforded the *cyclo*-P_4 compound **4** and the tetraphosphol **5**, respectively. In **4** a slightly bend P_4 ring (obtained after a selective P–P bond cleavage) is stabilized by two canopying $[Co(CO)_3]$ fragments. In contrast, **5** is the result of a CO insertion into the P_4 motif found in **5*** which is originally obtained from the reaction of **1** with $[Fe_2(CO)_9]$. DFT calculations suggest that **5*** can be described as an intact molecule of **1** coordinated towards a $[Fe(CO)_3]$ fragment in a chelating fashion accompanied by an additional coordination towards a terminal $[Fe(CO)_4]$ fragment. In summary, we were able to demonstrate the diverse potential of the P_4 butterfly compound **1** as a starting material in the formation of unprecedented P_n ligands, which are an incentive for the examination of P_4 activation processes

4.5 References

[1] (a) N. Hazari, Chem. *Soc. Rev.* **2010**, *39*, 4044-4056.
(b) I. Mellone ,F. Bertini, L. Gonsalvi, A. Guerriero, M. Peruzzini, *CHIMIA Int. J. Chem.* **2015**, *69*, 331-338.
(c) Z. Turner, *Inorganics* **2015**, *3*, 597.
(d) R. A. Henderson, *Trans. Met. Chem.* **1990**, *15*, 330- 336;
(e) V. P. Indrakanti, J. D. Kubicki, H. H. Schobert, *Energy Environ. Sci.* **2009**, *2*, 745-758.
(f) X. Yin, J. R. Moss, *Coord. Chem. Rev.* **1999**, *181*, 27-59.

[2] (a) B. M. Cossairt, N. A. Piro, C. C. Cummins, *Chem. Rev.* **2010**, *110*, 4164-4177.
(b) M. Caporali, L. Gonsalvi, A. Rossin, M. Peruzzini, *Chem. Rev.* **2010**, *110*, 4178-4235.
(c) M. Scheer, G. Balázs, A. Seitz, *Chem. Rev.* **2010**, *110*, 4236-4256.
(d) N. A. Giffin, J. D. Masuda, *Coord. Chem. Rev.* **2011**, *255*, 1342-1359.

[3] (a) A. P. Ginsberg, W. E. Lindsell, *J. Am. Chem. Soc.* **1971**, *93*, 2082-2084.
(b) W. E. Lindsell, *J. Chem. Soc., Chem. Commun.* **1982**, 1422-1424.

[4] (a) O. J. Scherer, G. Schwarz, G. Wolmershäuser, *Z. Anorg. Allg. Chem* **1996**, *622*, 951-957.
(b) O. J. Scherer, T. Hilt, G. Wolmershäuser, *Organometallics* **1998**, *17*, 4110-4112.

[5] O. J. Scherer, M. Swarowsky, H. Swarowsky, G. Wolmershäuser, *Angew. Chem.* **1998**, *5*, 738-739.

[6] U. Vogel, M. Eberl, M. Eckhardt, A. Seitz, E.-M. Rummel, A. Y. Timoshkin, E. V. Peresypkina, M. Scheer, *Angew. Chem. Int. Ed.* **2011**, *50*, 8982-8985.

[7] A. E. Seitz, M. Eckhardt, A. Erlebach, E. V. Peresypkina, M. Sierka, M. Scheer, *J. Am. Chem. Soc.* **2016**, *33*, 10433-10436.

[8] A. E. Seitz, U. Vogel, M. Eberl, M. Eckhardt, G. Balázs, E. V. Peresypkina, M. Bodensteiner, M. Zabel, M. Scheer, *Chem. Eur. J.* **2017**, *23*, 10319-10327.

[9] (a) J. Bai, A. V. Virovets, M. Scheer, *Angew. Chem. Int. Ed.*, **2002**, *41*, 1737-1740.
(b) J. Bai, A. V. Virovets, M. Scheer, *Science*, **2003**, *300*, 781-783.
(c) M. Scheer, J. Bai, B. P. Johnson, R. Merkle, A. V. Virovets, C. E. Anson, *Eur. J. Inorg. Chem.* **2005**, *20*, 4023-4026.
(d) M. Scheer, L. J. Gregoriades, A. V. Virovets, W. Kunz, R. Neueder. I. Krossing, *Angew. Chem. Int. Ed.* **2006**, *45*, 5689-5693.
(e) M. Scheer, A. Schindler, R. Merkle, B. P. Johnson, M. Linseis, R. Winter, C. E. Anson, A. V. Virovets, *J. Am. Chem. Soc.* **2007**, *129*, 13386-13387.
(f) S. Welsch, L. J. Gregoriades, M. Sierka, M. Zabel, A. V. Virovets, M. Scheer, *Angew. Chem. Int. Ed.* **2007**, *46*, 9323-9326.
(g) M. Scheer, L. J. Gregoriades, R. Merkle, B. P. Johnson, F. Dielmann, *Phosphorus, Sulfur, Silicon and the Related Elements* **2008**, *183*, 504-508.
(h) M. Scheer, A. Schindler, C. Gröger, A. V. Virovets, E. V. Peresypkina, *Angew. Chem. Int. Ed.* **2009**, *48*, 5046-5049.
(i) M. Scheer, A. Schindler, J. Bai, B. P. Johnson, R. Merkle, R. Winter, A. V. Virovets, E. V. Peresypkina, V. A. Blatov, M. Sierka, H. Eckert, *Chem. Eur. J.*, **2010**, *16*, 2092-2107.
(j) A. Schindler, G. Balázs, M. Zabel, C. Gröger, R. Kalbitzer, M. Scheer, *C. R. Chimie* **2010**, *13*, 1241-1248.
(k) A. Schindler, C. Heindl, G. Balázs, C. Gröger, A. V. Virovets, E. V. Peresypkina, M. Scheer, *Chem. Eur. J.* **2012**, *18*, 829-835.
(l) F. Dielmann, A. Schindler, S. Scheuermayer, J. Bai, R. Merkle, M. Zabel, A. V. Virovets, E. V. Peresypkina, G. Brunklaus, H. Eckert, M. Scheer, *Chem. Eur. J.* **2012,** *18,* 1168-1179.
(m) C. Heindl, S. Heinl, D. Lüdeker, G. Brunklaus, W. Kremer, M. Scheer**,** *Inorg Chim. Acta* **2014**,*422*, 218-223.
(n) E. V. Peresypkina, C.Heindl, A. Schindler, M. Bo, W. Kremer, M. Scheer**,** *Z. Krist.* **2014**,*229*, 735-740.
(o) F. Dielmann, C. Heindl, F. Hastreiter, E. V. Peresypkina, A. V. Virovets, R. M. Gschwind, M. Scheer**,** *Angew. Chem. Int. Ed.* **2014**, *53*, 13605-13608.
(p) M. Fleischmann, J. S. Jones,F.P. Gabbai, M. Scheer**,** *Chem. Sci.* **2015**, *6,* 132-139.
(q) M. Fleischmann, L. Dütsch, M. Elsayed Moussa, A. Schindler, G. Balázs, C. Lescop, M. Scheer**,** *Chem. Comm.* **2015**, *51*, 2893-2895.

(r) F. Dielmann, M. Fleischmann, C. Heindl, E. V. Peresypkina, A. V. Virovets, R. M. Gschwind, M. Scheer**,** *Chem. Eur. J.* **2015**, *21*, 6208-6214.
(s) S. Heinl, E. Peresypkina, M. Scheer**,** *Angew. Chem. Int. Ed.* **2015**, *54*, 13431-13435.
(t) C. Heindl, E. V. Peresypkina, A. V. Virovets, W. Kremer, M. Scheer, *J. Am. Chem. Soc.* **2015**, *137*, 10938-10941.
(u) C. Heindl, E. V. Peresypkina, A. V. Virovets, I. S. Bushmarinov, M. G. Medvedev, B. Krämer, B. Dittrich, M. Scheer**,** *Angew. Chem. Int. Ed.* **2017**, *56*, 13237-13243.
(v) M. Elsayed Moussa, B. Attenberger, E. V. Peresypkina, M. Scheer**,** *Dalton Trans*. **2018**, *47,* 1014-1017.
(w) E. V. Peresypkina, C. Heindl, A. V. Virovets, H. Brake, E. Mädl, M. Scheer**,** *Chem. Eur. J.* **2018***, 24,* 2503-2508.
(x) M. Elsayed Moussa, M. Piesch, M. Fleischmann, A. Schreiner, M. Seidl, M. Scheer**,** *Dalton Trans.* **2018***, 47,* 16031-16035.

[10] (a) J. Bai, E. Leiner, M. Scheer, *Angew. Chem. Int. Ed.* **2002**, *41*, 783-786.
(b) M. Scheer, L. Gregoriades, J. Bai, M. Sierka, G. Brunklaus, H. Eckert, *Chem. Eur. J.* **2005**, *11*, 2163-2169.
(c) M. Pronold, M. Scheer, J. Wachter, M. Zabel, *Inorg. Chem.* **2007**, *46*, 1396-1400.
(d) M. Scheer, L. J. Gregoriades, M. Zabel, M. Sierka, L. Zhang, H. Eckert, *Eur. J. Inorg. Chem.* **2007**, 2775-2782.
(e) M. Scheer, L. J. Gregoriades, M. Zabel, J. Bai, I. Krossing, G. Brunklaus, H. Eckert, *Chem. Eur. J.* **2008**, *14*, 282-295.
(f) S. Welsch, C. Lescop, G. Balázs, R. Réau, M. Scheer, *Chem. Eur. J.* **2011**, *17*, 9130-9141.
(g) B. Attenberger, S. Welsch, M. Zabel, E. Peresypkina, M. Scheer, *Angew. Chem. Int. Ed.* **2011**, *50*, 11516-11519.
(h) B. Attenberger, E. V. Peresypkina, M. Scheer**,** *Inorg. Chem.* **2015***, 54,* 7021-7029.
(i) M. Fleischmann, L. Dütsch, M. Elsayed Moussa, G. Balázs, W. Kremer, Ch. Lescop, M. Scheer**,** *Inorg. Chem.* **2016***, 55,* 2840-1854.
(j) M. Fleischmann, J. S. Jones, G. Balázs, F. P. Gabbaï, M. Scheer**,** *Dalton Trans.* ***2016****, 45,* 13742-13749.
(k) M. Elsayed Moussa, B. Attenberger, E. V. Peresypkina, M. Fleischmann, G. Balázs, M. Scheer**,** *Chem. Commun.* ***2016****, 52,* 10004-10007.
(l) M. Elsyaed Moussa, B. Attenberger, M. Fleischmann, A. Schreiner, M. Scheer, *Eur. J. Inorg. Chem.* **2016**, 4538-4541.
(m) M. Elsayed Moussa, M. Fleischmann, E. V. Peresypkina, L. Dütsch, M. Seidl, G. Balázs, M. Scheer, *Eur. J. Inorg. Chem.* **2017**, 3222-3226.
(n) M. Elsayed Moussa, B. Attenberger, M. Seidl, A. Schreiner, M. Scheer**,** *Eur. J. Inorg. Chem.* **2017**, 5616-5620.
(o) M. Elsayed Moussa, M. Seidl, G. Balázs, A. V. Virovets, B. Attenberger, A. Schreiner, M. Scheer**,** *Chem. Eur. J.* **2017**, 23, 16199-16203.
(p) M. Elsayed Moussa, S. Welsch, M. Lochner, E. V. Peresypkina, A. V. Virovets, M. Scheer**,** *Eur. J. Inorg. Chem.* **2018**, 2689-2694.
(q) M. Elsayed Moussa, S. Welsch,L. J. Gregoriades, G. Balázs, M. Seidl, M. Scheer**,** *Eur. J. Inorg. Chem.* **2018**, 1683-1687.
(r) M. Elsayed Moussa, E. Peresypkina, A. V. Virovets, G. Balázs, M. Scheer**,** *CrystEngComm* **2018**, 20, 7417-7422.

[11] C. Schwarzmaier, S. Heinl, G. Balázs, M. Scheer, *Angew. Chem. Int. Ed. Engl.* **2015**, *54*, 13116-13121.

[12] J. Müller, S. Heinl, C. Schwarzmaier, G. Balázs, M. Keilwerth, K. Meyer, M. Scheer, *Angew. Chem. Int. Ed.* **2007**, *56*, 7312-7317.

[13] (a) A. Simon, H. Borrmann, H. Craubner, *Phosphorus Sulfur Silicon Relat. Elem.* **1987**, *30*, 507-510.
(b) H. Okudera, E. Dinnebier Robert, A. Simon, *Z. Kristallogr.,* **2005**, *220*, 259.

[14] Chambridge Crystallographic Database, 1032637

[15] K. K. Cheung, T. F. Lai, K. S. Mok, J. Chem. Soc. A. 1971, 0, 1644-1647.

[16] G. W. Wong, J. L. Harkreader, C. A. Mebi, B. J. Frost, Inorg. Chem. 2006, 45, 6748-6755.

[17] Cf. chapter 3 of this thesis.

[18] O. Crespo, M. C. Gimeno, A. Laguna, P. G. Jones, Dalton Trans. 1992, 1601-1605.

[19] P. W. N. M. van Leeuwen, P. C. J. Kamer, J. N. H. Reek, P. Dierkes, *Chem. Rev.* **2000**, *100*, 2741-2770.

[20] (a) C. A. Tolman, *Chem. Rev.* **1977**, *77*, 313-348.
(b) W.-J. van Zeist, F. M. Bickelhaupt, *Dalton Trans.* **2011**, *40*, 3028-3038.

[21] In the NMR spectra of the reaction mixtures and crystals obtained from the reaction of **1** with [Mo$(CO)_4$(nbd)] a second species next to **2b** was observed. (^{1}H NMR (C_6D_6): δ[ppm] = 1.18 (s, 36H, $C_5H_2(C_4\underline{H}_9)_3$), 1.36 (s, 18H, $C_5H_2(C_4\underline{H}_9)_3$), 4.67 (s, 4H, $C_5\underline{H}_2(C_4H_9)_3$); ^{31}P NMR ($C_6D_6$): δ[ppm] = -99.9 (t, $^1J_{AB}$ = 162 Hz, 2P, P_A), -149.5 (t, $^1J_{AB}$ = 162 Hz, 2P, P_B)). Throughout various workup and crystallization steps the ratio of **2b** and the unidentified side product stayed constant (5:1). The side product could not be identified and characterized so far, however, one feasible suggestion is the spiro compound [{(Cp‴Fe$(CO)_2)_2(\mu_3,\eta^{1:1:1:1}$-$P_4$)}$_2${Mo$(CO)_2$}]). [Mo$(CO)_2(nbd)_2$] is a known side product in the synthesis of [Mo$(CO)_4$(nbd)] and a peak corresponding to [**2b**-2CO]$^+$ (967.86 m/z) could be identified in the mass spectrum of **2b**.

[22] S. J. B. Price, C. Brevard, A. Pagelot, P. J. Sadler, *Inorg. Chem.* **1985**, *24*, 4278-4281.

[23] (a) D. B. Lerner, W. J. Becktel, R. Everett, M. Goodman, D. R. Kearns, *Biopolymers* **1984**, *23*, 2157-2172.
(b) R. Streck, A. J. Barnes, *Spectrochimica Acta Part A* **1999**, *55*, 1059-1076.

[24] See SI for further detail.

[25] B. E. Mann, *J. Chem. Soc., Dalton Trans.* **1997**, 1457-1472.

[26] A structural suggestion for an according intermediate with bridging CO ligands is given in the SI alongside corresponding DFT calculations.

[27] Extensive DFT calculations for **5*-1**, **5*-2** and additional structural suggestion for **5*** are given in the SI.

[28] C. Schwarzmaier, S. Heinl, G. Balázs, M. Scheer, *Angew. Chem.* **2015**, *127*, 13309-13314; *Angew. Chem. Int. Ed.* **2015**, *54*, 13116-13121.

[29] R. Mathieu, A.-M. Caminade, J.-P. Majoral, S. Attali, M. Sanchelz, *Organometallics* **1986**, *5*, 1914-1916.

[30] R. Wolf, E. Hey-Hawkins, *Chem. Commun.* **2004**, 2626-2627.

4.6 Supplementary Information

4.6.1 General Remarks

All experiments were carried out under an atmosphere of dry argon or nitrogen using glovebox and schlenk techniques. Residues of oxygen and water were removed from the inert gas by passing it over a BASF R 3-11 ($CuO/MgSiO_3$) catalyst, concentrated H_2SO_4 and finally granulated silica gel. Dry solvents were collected from a Braun SPS Apparatus and degassed prior to use. The deuterated solvents C_6D_6 and CD_2Cl_2 were degassed and dried by stirring with Na/K alloy and CaH_2, respectively, followed by distillation. After the distillation, CD_2Cl_2 was additionally stored over molecular sieve (3 Å) which had previously been dried for four hours under high vacuum at 100 °C.

[{Cp‴Fe(CO)$_2$}$_2$(μ,η$^{1:1}$-P$_4$)] (**1**)[1], [M(CO)$_4$(nbd)] (M = Cr, Mo, W)[2], [Au(PPh$_3$)(tht)][PF$_6$][3], [Fe$_2$(CO)$_9$][4] and [Co$_2$(CO)$_8$][5] were prepared according to literature procedure. [AgPF$_6$] is commercially available and was used without any further modification.

NMR spectra were recorded at the NMR department of the University Regensburg using a Bruker Advance 300 or 400 spectrometer. Samples are referenced against TMS (^{1}H, ^{13}C) or 85% H_3PO_4 (^{31}P) as external standards. Chemical shifts (δ) are reported in ppm and coupling constants (*J*) in Hz. The spectra were processed using the TopSpin 3.5 software (Bruker) and the WIN-DAISY module of this software was used to perform simulations.[6]

Mass spectrometry experiments were performed by the MS department of the University Regensburg. The LIFDI-, FD-, and EI-MS spectra were recorded on an AccuToF GCX (Jeol) spectrometer and the ESI-MS spectra were recorded on a Q-TOF 6540 UHD (Agilent) spectrometer, respectively. The observed fragments were assigned according to the mass/charge (m/z) ratio and the isotope pattern.

For compounds **2a**, **2b** and **2c** the IR spectra were recorded on an ALPHA platinum ATR spectrometer (Bruker Optik GmbH) which was placed inside a glove box. Therefore, the air-sensitive solid samples could be placed directly on the spectrometer without any additional preparative measures. For compounds **2d**, **3**, **4**, **5*** and **5** the IR spectra were recorded on a VARIAN FTS-800 FT-IR spectrometer as KBr discs.

Elemental analyses were performed by the department of central analyses of the University Regensburg on a Vario micro cube instrument (Elementar Analysensysteme GmbH).

4.6.2 Syntheses

Synthesis of [{Cp‴Fe(CO)$_2$}$_2$(μ$_3$,η$^{1:1:1:1}$-P$_4$){Cr(CO)$_4$}] (2a)

A red-orange solution of **1** (100 mg, 0.13 mmol, 1.0 eq.) in thf (5 mL) is added to a yellow solution of [Cr(CO)$_4$(nbd)] (31 mg, 0.13 mmol, 1.0 eq.) in thf (5 mL). The resulting mixture is stirred at room temperature for 19 h while the color of the solution changes to brown. The solvent is subsequently removed under reduced pressure. To obtain pure **2a**, a saturated solution in *n*-pentane (5 mL) and dichloromethane (1 mL) was stored at -28 °C yielding crystals suitable for single crystal X-ray diffraction analysis.

Analytical data for 2a

Yield	68 mg (0.07 mmol, 53%).
^{1}H NMR (CD_2Cl_2, 300 K)	δ[ppm] = 1.39 (s, 36H, $C_5H_2(C_4\underline{H}_9)_3$), 1.43 (s, 18H, $C_5H_2(C_4\underline{H}_9)_3$), 4.68 (s, 4H, $C_5\underline{H}_2(C_4H_9)_3$).
^{31}P NMR (CD_2Cl_2, 300 K)	δ[ppm] = -98.8 (t, $^1J_{AB}$ = 162 Hz, 2P, P_A), -152.1 (t, $^1J_{AB}$ = 162 Hz, 2P, P_B).
^{31}P{^{1}H} NMR (CD_2Cl_2, 300 K)	δ[ppm] = -98.8 (t, $^1J_{AB}$ = 162 Hz, 2P, P_A), -152.1 (t, $^1J_{AB}$ = 162 Hz, 2P, P_B).
IR (solid)	$\tilde{\nu}_{CO}$ [cm^{-1}] = 2011 (m), 1989 (s), 1967 (s), 1923 (m, br), 1889 (s), 1871 (s,br), 1827 (s, br).
LIFDI-MS (toluene)	m/z = 978.19 [M]$^+$ (13.6%), 950.18 [M-CO]$^+$ (100.0%), 922.15 [M-2CO]$^+$ (2.5%), 894.11 [M-3CO]$^+$ (1.9%).
Elemental Analysis	calcd. for $[C_{42}H_{58}CrFe_2O_8P_4]_2(CH_2Cl_2)$ (2041.94 g mol^{-1}) C 50.00, H 5.82; found C 49.86, H 5.72.

Synthesis of [{Cp‴Fe(CO)$_2$}$_2$(μ$_3$,η$^{1:1:1:1}$-P_4){Mo(CO)$_4$}] (2b)

A red-orange solution of **1** (100 mg, 0.13 mmol, 1.0 eq.) in thf (5 mL) is added to an orange solution of $[Mo(CO)_4(nbd)]$ (37 mg, 0.13 mmol, 1.0 eq.) in thf (5 mL). The resulting mixture is stirred at 60 °C for 17 h while a color change yielding a red-brown solution is observed. The solvent is subsequently removed under reduced pressure affording a red solid. To obtain crystalline **2b**, the solid was taken up in a mixture of *n*-pentane (5 mL) and dichloromethane (5 mL) and the saturated solution was stored at -28 °C yielding crystals suitable for single crystal X-ray diffraction analysis. A constant amount of side product could be observed in every step of the workup and could not be separated by differences in solubility, crystallization or extraction. NMR spectroscopy suggest [{(Cp‴Fe(CO)$_2$)$_2$(μ$_3$,η$^{1:1:1:1}$-P_4)}$_2${Mo(CO)$_2$}] as the side product.

Crystalline Yield of mixture 92 mg

For product ratio of 5:1 (as found in by NMR spectroscopic studies):

2b: 68 mg (0.065 mmol, 50%).

[{(Cp‴Fe(CO)$_2$)$_2$(μ$_3$,η$^{1:1:1:1}$-P_4)}$_2${Mo(CO)$_2$}] (assumed side product): 24 mg (0.013 mmol, 10%).

Analytical data for 2b

^{1}H NMR (C_6D_6, 300 K)	δ[ppm] = 1.20 (s, 36H, $C_5H_2(C_4\underline{H}_9)_3$), 1.34 (s, 18H, $C_5H_2(C_4\underline{H}_9)_3$), 4.65 (s, 4H, $C_5\underline{H}_2(C_4H_9)_3$).
^{31}P NMR (C_6D_6, 300 K)	δ[ppm] = -121.8 (t, $^1J_{AB}$ = 162 Hz, 2P, P_A), -178.5 (t, $^1J_{AB}$ = 162 Hz, 2P, P_B).
^{31}P{^{1}H} NMR (C_6D_6, 300 K)	δ[ppm] = -121.8 (t, $^1J_{AB}$ = 162 Hz, 2P, P_A), -178.5 (t, $^1J_{AB}$ = 162 Hz, 2P, P_B).
FD$^+$-MS (toluene)	m/z [%] = 345.06 [Cp‴Fe(CO)$_2$]$^+$ (88.4), 967.86 [M-2CO]$^+$ (100.0).

Analytical data for side product (presumably [{(Cp‴Fe(CO)$_2$)$_2$(μ_3,$\eta^{1:1:1:1}$-P$_4$)}$_2${Mo(CO)$_2$}]

^{1}H NMR (C_6D_6, 300 K)	δ[ppm] = 1.18 (s, 36H, $C_5H_2(C_4\underline{H}_9)_3$), 1.36 (s, 18H, $C_5H_2(C_4\underline{H}_9)_3$), 4.67 (s, 4H, $C_5\underline{H}_2(C_4H_9)_3$).
^{31}P NMR (C_6D_6, 300 K)	δ[ppm] = -99.9 (t, $^1J_{AB}$ = 162 Hz, 2P, P_A), -149.5 (t, $^1J_{AB}$ = 162 Hz, 2P, P_B).
^{31}P{^{1}H} NMR (C_6D_6, 300 K)	δ[ppm] = -99.9 (t, $^1J_{AB}$ = 162 Hz, 2P, P_A), -149.5 (t, $^1J_{AB}$ = 162 Hz, 2P, P_B).

Synthesis of [{Cp‴Fe(CO)$_2$}$_2$(μ_3,$\eta^{1:1:1:1}$-P$_4$){W(CO)$_4$}] (2c)

A red-orange solution of **1** (100 mg, 0.13 mmol, 1.0 eq.) in thf (5 mL) is added to a slightly yellow solution of [W(CO)$_4$(nbd)] (47 mg, 0.13 mmol, 1.0 eq.) in thf (5 mL). The resulting mixture is stirred at 55°C for 17h while the color of the solution changes to red. The solvent is subsequently removed under reduced pressure. To obtain pure **2c**, a saturated solution in *n*-pentane (5 mL) and dichloromethane (1 mL) was stored at -28 °C yielding crystals suitable for single crystal X-ray diffraction analysis.

Analytical data for 2c

Yield	100 mg (0.09 mmol, 68%).
^{1}H NMR (C_6D_6, 300 K)	δ[ppm] = 1.19 (s, 36H, $C_5H_2(C_4\underline{H}_9)_3$), 1.34 (s, 18H, $C_5H_2(C_4\underline{H}_9)_3$), 4.70 (s, 4H, $C_5\underline{H}_2(C_4H_9)_3$).
^{1}H NMR (toluene-d_8, 300 K)	δ[ppm] = 1.27 (s, 36H, $C_5H_2(C_4\underline{H}_9)_3$), 1.39 (s, 18H, $C_5H_2(C_4\underline{H}_9)_3$), 4.73 (s, 4H, $C_5\underline{H}_2(C_4H_9)_3$).
^{1}H NMR ($CDCl_3$, 300 K)	δ[ppm] = 1.39 (s, 18H, $C_5H_2(C_4\underline{H}_9)_3$), 1.41 (s, 36H, $C_5H_2(C_4\underline{H}_9)_3$), 4.83 (s, 4H, $C_5\underline{H}_2(C_4H_9)_3$).
^{1}H NMR (THF-d_8, 300 K)	δ[ppm] = 1.43 (s, 54H, $C_5H_2(C_4\underline{H}_9)_3$), 4.89 (s, 4H, $C_5\underline{H}_2(C_4H_9)_3$).
^{1}H NMR (CD_2Cl_2, 300 K)	δ[ppm] = 1.41 (s, 54H, $C_5H_2(C_4\underline{H}_9)_3$), 4.71 (s, 4H, $C_5\underline{H}_2(C_4H_9)_3$).
^{31}P NMR (C_6D_6, 300 K)	δ[ppm] = -164.3 (m, 4P).
^{31}P{^{1}H} NMR (C_6D_6, 300 K)	δ[ppm] = -164.3 (m, 4P).
^{31}P NMR (toluene-d_8, 300 K)	δ[ppm] = -164.9 (m, 4P).
^{31}P{^{1}H} NMR (toluene-d_8, 300 K)	δ[ppm] = -164.9 (m, 4P).
^{31}P NMR (THF-d_8, 300 K)	δ[ppm] = -161.6 (m, 2P, P_A), -164.3 (m, 2P, P_B).
^{31}P{^{1}H} NMR (THF-d_8, 300 K)	δ[ppm] = -161.6 (m, 2P, P_A), -164.3 (m, 2P, P_B).
^{31}P NMR (CD_2Cl_2, 300 K)	δ[ppm] = -161.6 (m, 2P, P_A), -168.3 (m, 2P, P_B).
^{31}P{^{1}H} NMR (CD_2Cl_2, 300 K)	δ[ppm] = -161.6 (m, 2P, P_A), -168.3 (m, 2P, P_B).
IR (solid)	$\tilde{\nu}_{CO}$ [cm^{-1}] = 2017 (m), 2002 (m), 1994 (m), 1977 (w), 1969 (s), 1957 (m), 1898 (s, br), 1882 (s, br), 1863 (s, br), 1832 (s, br), 1813 (s, br).
LIFDI-MS (toluene)	no reasonable peaks detectable .
Elemental Analysis	calcd. for $[C_{42}H_{58}WFe_2O_8P_4]_2(CH_2Cl_2)$ (2305.64 g mol^{-1}) C 44.28, H 5.16; found C 44.49, H 5.11.

Synthesis of [{Cp'''Fe(CO)$_2$}$_2$(μ$_3$,η$^{1:1:1:1}$-P_4){Au(PPh$_3$)}]$^+$[PF$_6$]$^-$ (2d)

To a solution of [(Ph$_3$P)Au(tht)][PF$_6$] (43 mg, 0.061 mmol, 1.0 eq.) in thf (5 ml) is given a solution of **1** (50 mg, 0.061 mmol, 1.0 eq.) in thf (5 ml) affording a bright red colored solution. The reaction mixture is stirred for one hour at room temperature and the solution is reduced to about 3 ml *in vacuo*. Filtration via canula and layering with hexane (4 ml) yields **2d** as orange crystals, suitable for single crystal X-ray diffraction analysis.

Analytical data for 2d

Yield	42 mg (0.029 mmol, 48 %).
^{1}H NMR (CD_2Cl_2, 300 K)	δ [ppm] = 1.21 (s, 18H, $C_5H_2(C_4\underline{H}_9)_3$), 1.31 (s, 36H, $C_5H_2(C_4\underline{H}_9)_3$), 4.67 (s, 4H, $C_5\underline{H}_2(C_4H_9)_3$), 7.55-7.65 (m, 15H, P$\underline{Ph}_3$).
^{13}C{^{1}H} NMR (CD_2Cl_2, 300 K)	δ [ppm] = 31.7 (s, -(C($\underline{C}$(CH$_3$)$_3$)), 31.9 (s, -(C($\underline{C}$(CH$_3$)$_3$)$_2$), 33.2 (s, -(C($\underline{C}$H$_3$)$_3$)), 33.7 (s, -(C($\underline{C}$H$_3$)$_3$)$_2$), 91.0 (s, $\underline{C}_2H_2C^tBuC_2^tBu_2$), 109.9 (s, $C_2H_2\underline{C}^tBuC_2^tBu_2$), 111.9 (s, $C_2H_2C^tBu\underline{C}_2^tBu_2$), 130.1 (br, P$\underline{Ph}_3$), 134.4 (br, P$\underline{Ph}_3$).
^{31}P{^{1}H} NMR (CD_2Cl_2, 300 K)	δ [ppm] = 42.5 (t, 1P, $^2J_{AM}$ = 111 Hz, Au-P$_A$Ph$_3$), -22.9 (dt, 2P, $^1J_{MX}$ = 196 Hz, $^2J_{AM}$ = 111 Hz, P$_M$), -143.5 (sept, 1P, $^1J_{PF}$ = 710 Hz, PF$_6$), -299.2 (t, 2P, $^1J_{MX}$ = 196 Hz, P$_X$).
ES-MS (CH_2Cl_2)	*m*/*z* = 1245.8 [M_2^{2+}] (5%), 721.2 [$(PPh_3)_2Au^+$] (100%).
IR (KBr)	$\tilde{\nu}_{CO}$ [cm^{-1}] = 2030 (s, sh), 2008 (vs), 1966 (vs), 1944 (s, sh).
Elemental analysis	calcd. for $C_{55}H_{73}AuF_6Fe_2O_4P_6$ (1418.67 g mol^{-1}) C 47.41, H 5.19; found C 45.62, H 4.93.

Synthesis of [{(Cp'''Fe(CO)$_2$)$_2$(μ$_3$,η$^{1:1:1:1}$-P_4)}$_2$Ag]$^+$[PF$_6$]$^-$ (3)

To a solution of [AgPF$_6$] (16 mg, 0.061 mmol, 1.0 eq.) in dichloromethane (5 ml) is given a solution of **1** (100 mg, 0.123 mmol, 2.0 eq.) in dichloromethane (5 ml). The reaction mixture is stirred for 16 hours at room temperature and the solvent is removed under reduced pressure. The resulting solid is washed with *n*-hexane (5 ml) and dried *in vacuo*. The crude product is taken up in thf (4 ml) and layered with *n*-hexane (4 ml) to yield **3** as orange crystals, suitable for single crystal X-ray diffraction analysis.

Analytical data for 3

Yield	38 mg (0.020 mmol, 33 %).
^{1}H NMR (CD_2Cl_2, 300 K)	δ ppm] = 1.41 (s, 36H, $C_5H_2(C_4\underline{H}_9)_3$), 1.44 (s, 72H, $C_5H_2(C_4\underline{H}_9)_3$), 4.81 (s, 8H, $C_5\underline{H}_2(C_4H_9)_3$).
^{13}C{^{1}H} NMR (CD_2Cl_2, 300 K)	δ [ppm] = 32.0 (s, -(C($\underline{C}$(CH$_3$)$_3$)), 32.6 (s, -(C($\underline{C}$(CH$_3$)$_3$)$_2$), 33.4 (s, -(C($\underline{C}$H$_3$)$_3$)), 34.1 (s, -(C($\underline{C}$H$_3$)$_3$)$_2$), 88.7 (s, $\underline{C}_2H_2C^tBuC_2^tBu_2$), 109.6 (s, $C_2H_2\underline{C}^tBuC_2^tBu_2$), 111.7 (s, $C_2H_2C^tBu\underline{C}_2^tBu_2$), 213.9 (s, CO).
^{31}P{^{1}H} NMR (CD_2Cl_2, 300 K)	δ [ppm] = -63.8 (dt, 2P, $^1J_{AM}$ = 191 Hz, $^1J_{P^{109}Ag}$ = 158 Hz, P$_A$), -63.8 (dt, 2P, $^1J_{AM}$ = 191 Hz, $^1J_{P^{107}Ag}$ = 138 Hz, P$_A$), -143.9 (sept, 1P, $^1J_{PF}$ = 710 Hz, PF$_6$), -305.0 (t, 4P, $^1J_{AM}$ = 191 Hz, P$_M$).
ES-MS (CH_2Cl_2)	*m*/*z* = 1736.2 [M^+] (100%), 1709.0 [M^+-CO] (10%), 1679.0 [M^+-2CO] (5%), 1651.2 [M^+ - 3CO] (1%).
IR (KBr)	$\tilde{\nu}_{CO}$ [cm^{-1}] = 2006 (vs), 1961 (vs).

Elemental analysis	calcd. for $C_{76}H_{116}AgF_6Fe_4O_8P_9$ (1881.73 g mol^{-1}) C 48.51, H 6.21; found C 48.91, H 6.54.

Synthesis of [{Cp‴(CO)$_2$Fe}$_2$(μ_4,$\eta^{1:1:2:2}$-P$_4$){Co(CO)$_3$}$_2$] (4)

At -20°C, 20 ml CH_2Cl_2 were added to a mixture of **1** (700 mg, 0.86 mmol, 1.0 eq.) and [$Co_2(CO)_8$] (323.5 mg, 0.95 mmol, 1.1 eq.). Subsequently, the mixture was stirred two hours at this temperature and another 12 hours without further cooling. By then, some dark brown crystals of **4** suitable for single crystal X-ray diffraction formed and the crystalline yield could be increased by concentrating and storing of the solution at -28°C.

Analytical data for 4

Yield	602 mg (0.55 mmol, 64%).
^{1}H NMR (C_6D_6, 300 K)	δ[ppm] = 1.1 (s, 9H, $C_5H_2(C_4\underline{H}_9)_3$), 1.51 (s, 9H, $C_5H_2(C_4\underline{H}_9)_3$), 1.41 (s, 18H, $C_5H_2(C_4\underline{H}_9)_3$), 1.26 (s, 18H, $C_5H_2(C_4\underline{H}_9)_3$), 5.16 (s, 2H, $C_5\underline{H}_2(C_4H_9)_3$), 5.26 (s, 2H, $C_5\underline{H}_2(C_4H_9)_3$).
^{13}C{^{1}H} NMR (C_6D_6, 300 K)	δ[ppm] = 31.35 (s, $\underline{C}_5H_2(C(C_3H_9)_3)$, 31.78 (s, $C_5H_2(C(\underline{C}_3H_9)_3)$, 32.76 (s, $\underline{C}_5H_2(C(C_3H_9)_3)$, 32.82 (s, $\underline{C}_5H_2(C(C_3H_9)_3)$, 33.25 (s, $C_5H_2(C(\underline{C}_3H_9)_3)$, 33.68 (s, $C_5H_2(C(\underline{C}_3H_9)_3)$, 88.82 (s, $C_3\underline{C}_2H_2(C(C_3H_9)_3)$, 89.95 (s, $C_3\underline{C}_2H_2(C(C_3H_9)_3)$, 109.94 (s, $C_5H_2(\underline{C}(C_3H_9)_3)$, 111.22 (s, $C_5H_2(\underline{C}(C_3H_9)_3)$, 112.99 (s, $C_5H_2(\underline{C}(C_3H_9)_3)$, 207.76 (s, $\underline{C}O$), 213.80 (s, $\underline{C}O$), 214.51 (s, $\underline{C}O$).
^{31}P{^{1}H} NMR (C_6D_6, 300 K)	δ[ppm] = 24.4 (m, 1P, P_A), 24.4 (m, 1P, $P_{A'}$), –12.6 (m, 1P, P_X), –12.6 (m, 1P, $P_{X'}$).
^{31}P{^{1}H} NMR (CD_2Cl_2, 300 K)	δ[ppm] = 24.3 ppm (m, 2P, P_A), –12.6 (m, 2P, P_X).
IR (KBr)	$\tilde{\nu}_{CO}$ [cm^{-1}] = 2041 (s), 2019 (s), 1977 (s), 1955 (sh).
IR (CH_2Cl_2)	$\tilde{\nu}_{CO}$ [cm^{-1}] = 2042 (s), 2019 (s), 1982 (s), 1950 (sh), 1712 (s).
FD-MS (toluene)	m/z = 1072 [M-CO]$^+$ (100%), 1044 [M-2CO]$^+$ (27%).
Elemental Analysis	calcd. for $C_{44}H_{58}Co_2Fe_2O_{10}P_4$ (1100.39 g mol^{-1}) C 45.60 , H 5.10; found C 45.79, H 5.36.

Synthesis of [Cp‴Fe(CO)$_2$}$_2$(μ_4,$\eta^{1:1:1:3}$-P$_4$CO){Fe(CO)$_4$}{Fe(CO)$_3$}] (5)

A solution of **1** (200 mg, 0.25 mmol, 1.0 eq.) and [$Fe_2(CO)_9$] (91 mg, 0.25 mmol, 1.0 eq.) in toluene (50 mL) is stirred for 12 h at r.t. Hereby, a color change from red-brown to dark brown is observed. The reaction solution is filtered over celite and the initial product **5*** is obtained as a dark brown solid after removing the solvent under reduced pressure. Chromatographic workup of **5*** yields two fractions upon elution with a n-hexane:toluene (1:1) mixture. The first fraction yields a dark brown solid after removing the solvent under reduced pressure, which could not be characterized so far. The second brown-greenish fraction was concentrated and crystals of **5** suitable for single crystal X-ray diffraction could be obtained after storage for 3-4 weeks at -12°C.

Analytical data for 5*:

Yield	167 mg (0.15 mmol, 60%, for **5-2***: [{Cp‴Fe(CO)$_2$}$_2$(μ$_4$,η$^{1:1:1:1}$-P_4){Fe(CO)$_4$}$_2$]).
^{1}H NMR (toluene-d$_8$, 300 K)	δ[ppm] = 1.24 (s, 36H, $C_5H_2(C_4\underline{H}_9)_3$), 1.28 (s, 18H, $C_5H_2(C_4\underline{H}_9)_3$), 4.79 (s, 4H, $C_5\underline{H}_2(C_4H_9)_3$).
^{1}H NMR (toluene-d$_8$, 123 K)	δ[ppm] = 1.16 (s, 18H, $C_5H_2(C_4\underline{H}_9)_3$), 1.22 (s, 18H, $C_5H_2(C_4\underline{H}_9)_3$), 1.24 (s, 9H, $C_5H_2(C_4\underline{H}_9)_3$), 1.30 (s, 9H, $C_5H_2(C_4\underline{H}_9)_3$), 4.79 (s, 4H, $C_5\underline{H}_2(C_4H_9)_3$), 4.83 (s, 2H, $C_5\underline{H}_2(C_4H_9)_3$).
^{31}P NMR (toluene-d$_8$, 300 K)	δ[ppm] = -257.5 (2PX, dd, $^1J_{PP}$ = 217 Hz).
^{31}P NMR (toluene-d$_8$, 123 K)	δ[ppm]= 16.0 (m, P_A, 1P), -19.9 (m, P_B, 1P), -257.8 (P_X, m, 2P).
IR (toluene)	$\tilde{\nu}_{CO}$ [cm^{-1}] = 2052 (w), 2036 (s), 2011(m), 1993 (m), 1977 (m), 1951 (s), 1930 (m).
EI-MS	m/z = 1086 [M$^+$-3CO] (0.5%), 1053 [M$^+$-3CO-CH$_3$] (7.2%), 997 [M$^+$-5CO-CH$_3$] (0.8%), 702 [M$^+$-2Fe-12CO] (100%).
	(M$^+$ = molecular peak of **5*-2**: [{Cp‴Fe(CO)$_2$}$_2$(μ$_4$,η$^{1:1:1:1}$-P_4){Fe(CO)$_4$}$_2$])

Analytical data for 5:

Yield	25 mg (0.02 mmol, 8%).
^{1}H NMR (C_6D_6, 300 K)	δ[ppm] = 1.02 (s, 9H, $C_5H_2(C_4\underline{H}_9)_3$), 1.06 (s, 9H, $C_5H_2(C_4\underline{H}_9)_3$), 1.11 (s, 9H, $C_5H_2(C_4\underline{H}_9)_3$), 1.15 (s, 9H, $C_5H_2(C_4\underline{H}_9)_3$), 1.17 (s, 9H, $C_5H_2(C_4\underline{H}_9)_3$), 1.25 (s, 9H, $C_5H_2(C_4\underline{H}_9)_3$), 4.05 (s, 1H, $C_5\underline{H}_2(C_4H_9)_3$), 5.09 (s, 1H, $C_5\underline{H}_2(C_4H_9)_3$), 5.17 (s, 1H, $C_5\underline{H}_2(C_4H_9)_3$), 5.41 (s, 1H, $C_5\underline{H}_2(C_4H_9)_3$).
^{31}P NMR (C_6D_6, 300 K)	δ[ppm]= 69.0 (P_A, ddd, $^1J_{AX}$ = 384 Hz, $^2J_{AN}$ = 37 Hz, $^2J_{AM}$ = 29 Hz, 1P), 40.3 (P_M, ddd, $^1J_{MN}$ = 378 Hz, $^1J_{MX}$ = 358 Hz, $^2J_{AM}$ = 29 Hz, 1P), 6.5 (P_N, dd, $^1J_{MN}$ = 378 Hz, $^2J_{AN}$ = 37 Hz, 1P), -133.9 (P_X, dd, $^1J_{AX}$ = 384 Hz, $^1J_{MX}$ = 358 Hz, 1P).
IR (KBr)	$\tilde{\nu}_{CO}$ [cm^{-1}] = 2030 (br), 1986 (br), 1638 (br).

4.6.3 NMR spectroscopic experiments

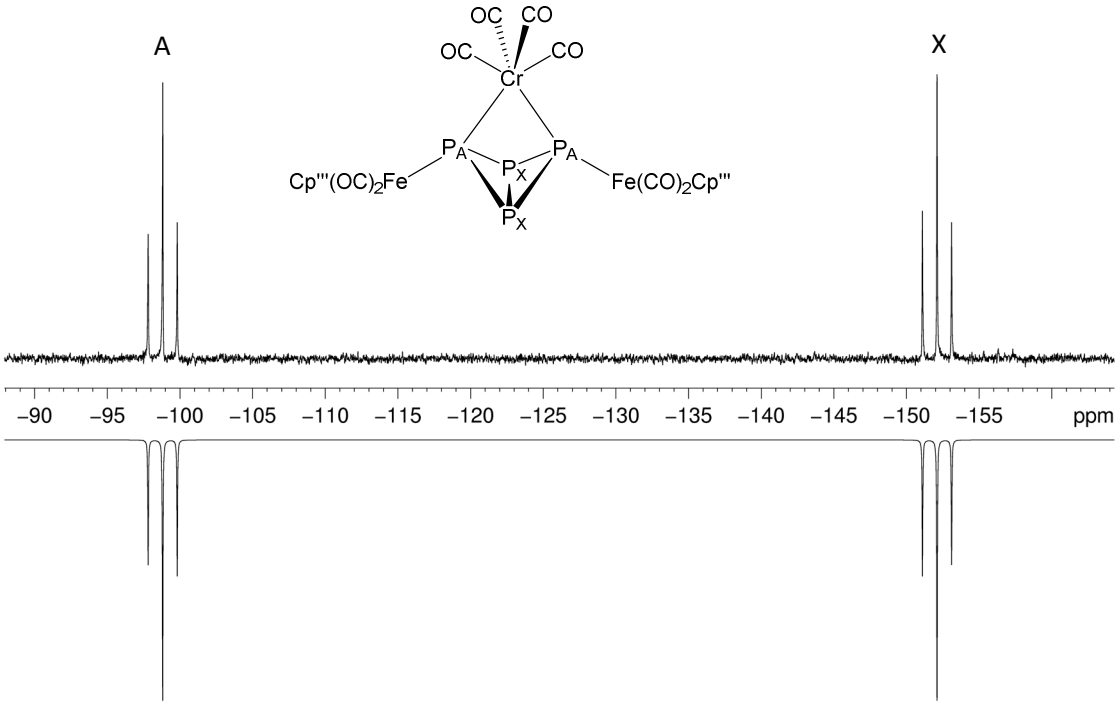

Figure S1. Experimental (top, recorded in CD_2Cl_2 at 300 K)) and simulated (bottom) $^{31}P\{^1H\}$ NMR spectra of **2a**.

Table S1. Experimental and simulated values for the chemical shifts and coupling constants in the $^{31}P\{^1H\}$ NMR spectrum of **2a**.

experimental values				simulated values			
δ_A	-98.8 ppm	$^1J_{AX}$	162 Hz	δ_A	-98.8 ppm	$^1J_{AX}$	162.3 Hz
δ_X	-152.1 ppm			δ_X	-152.1 ppm		

The simulation of the $^{31}P\{^1H\}$ NMR spectrum of **2a** was carried out on the basis of an A_2X_2 spin system with a C_{2h} symmetry.

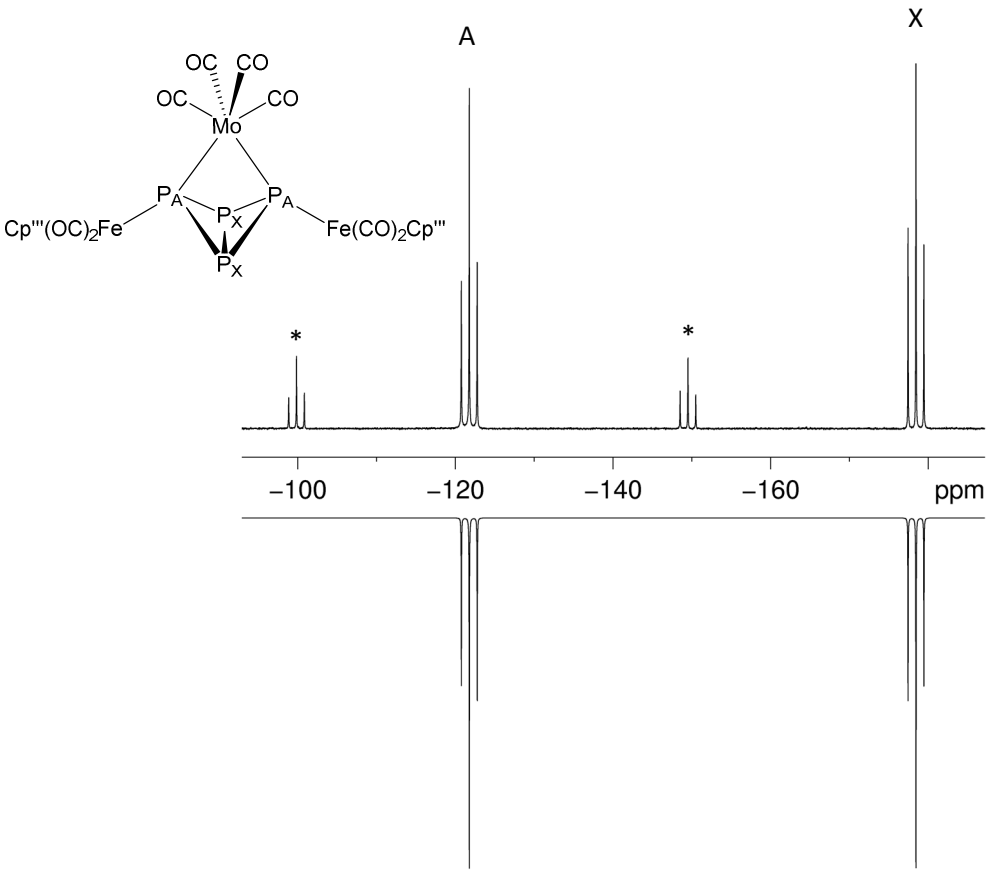

Figure S2. Experimental (top, recorded in C_6D_6 at 300 K) and simulated (bottom) $^{31}P\{^1H\}$ NMR spectra of **2b** (signals marked with asterisk are attributed to the proposed side product [{(Cp‴Fe(CO)$_2$)$_2$(μ$_3$,η$^{1:1:2}$-P_4)}$_2${Mo(CO)$_2$}]).

Table S2. Experimental and simulated values for the chemical shifts and coupling constants in the $^{31}P\{^1H\}$ NMR spectrum of **2b**.

experimental values				**simulated values**			
δ_A	-121.8 ppm	$^1J_{AX}$	162 Hz	δ_A	-121.8 ppm	$^1J_{AX}$	163.3 Hz
δ_X	-178.4 ppm			δ_X	-178.5 ppm		

The simulation of the $^{31}P\{^1H\}$ NMR spectrum of **2b** was carried out on the basis of an A_2X_2 spin system with a C_{2h} symmetry.

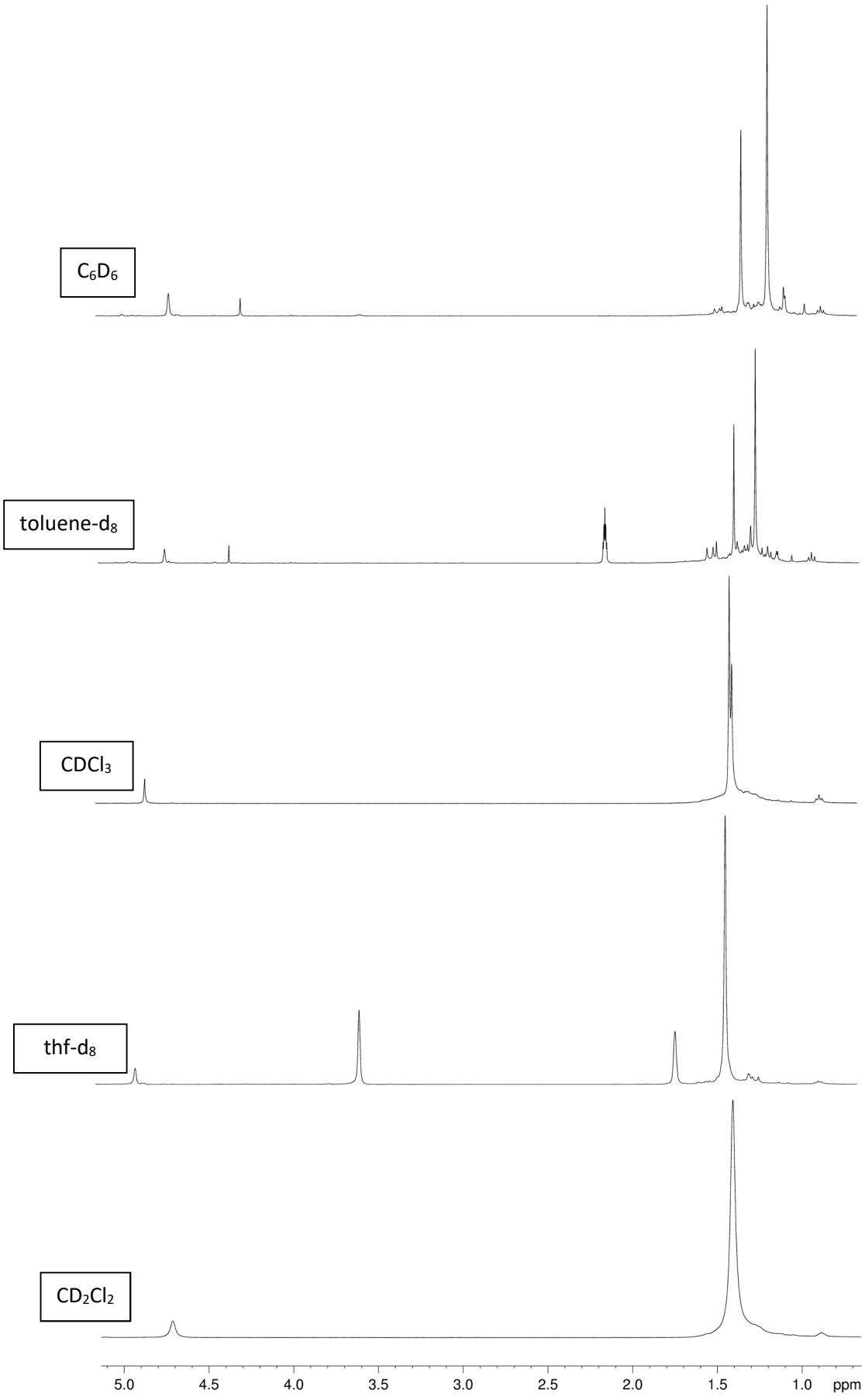

Figure S3. ^{1}H NMR spectra of **2c** in different deuterated solvents (recorded at 300 K).

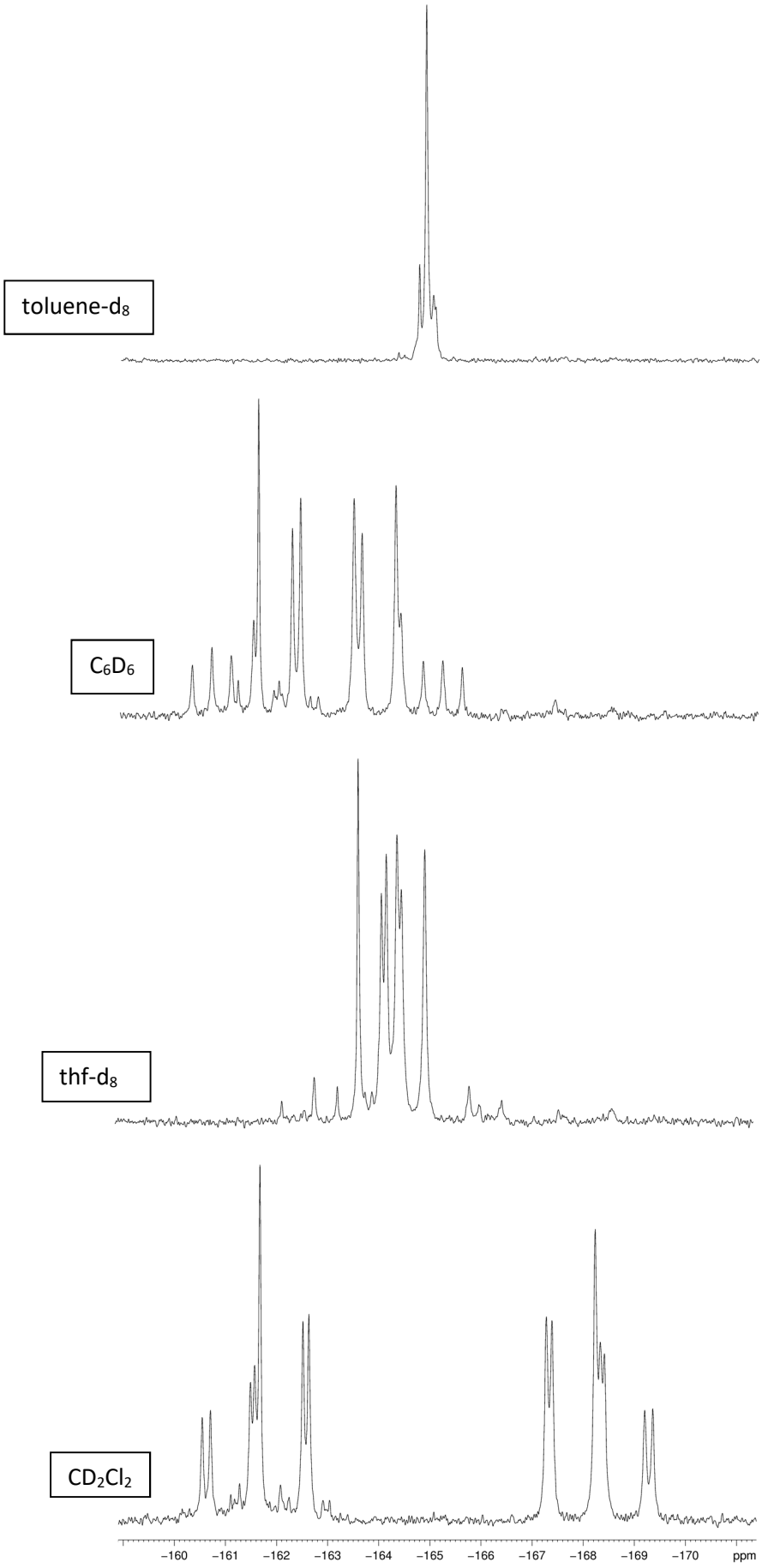

Figure S4. $^{31}P\{^1H\}$ NMR spectra of **2c** in different deuterated solvents (recorded at 300 K).

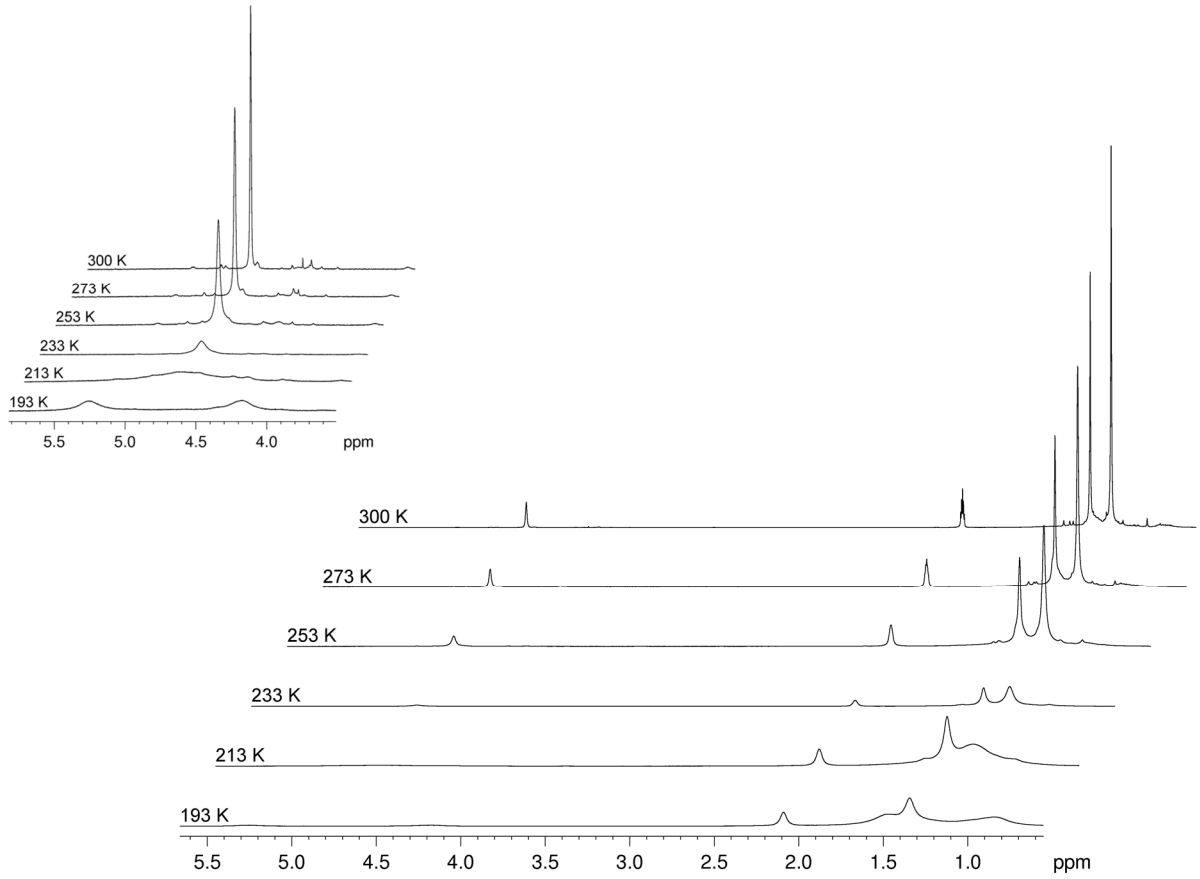

Figure. S5. ^{1}H NMR spectra of **2c** at different temperatures (recorded in toluene-d_8).

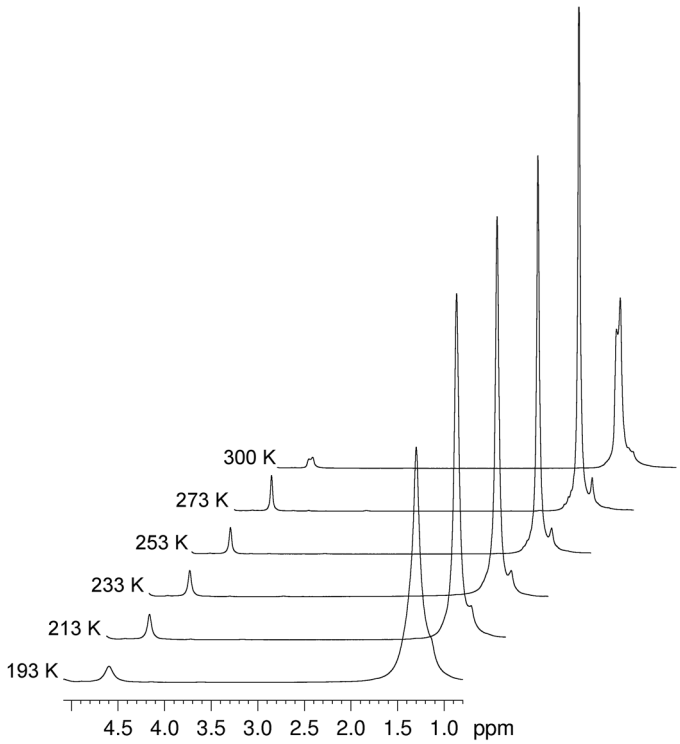

Figure. S6. ^{1}H NMR spectra of **2c** at different temperatures (recorded in CD_2Cl_2).

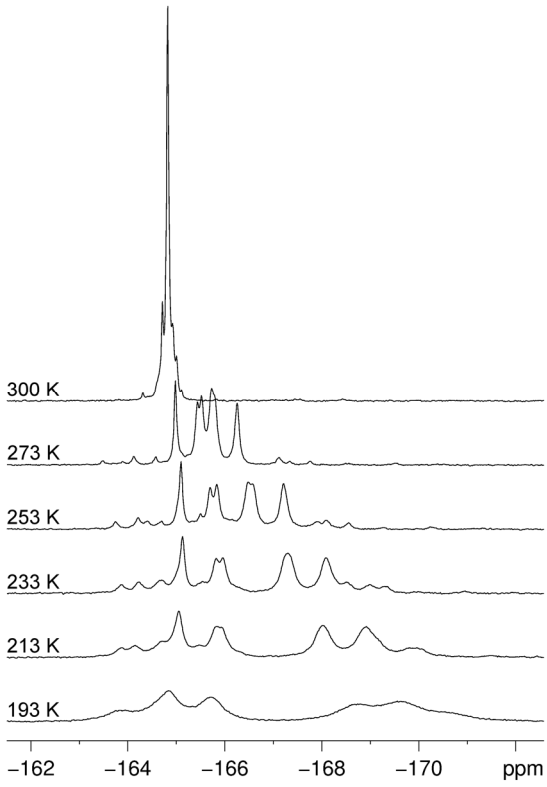

Figure. S7. $^{31}P\{^1H\}$ NMR spectra of **2c** at different temperatures (recorded in toluene-d_8).

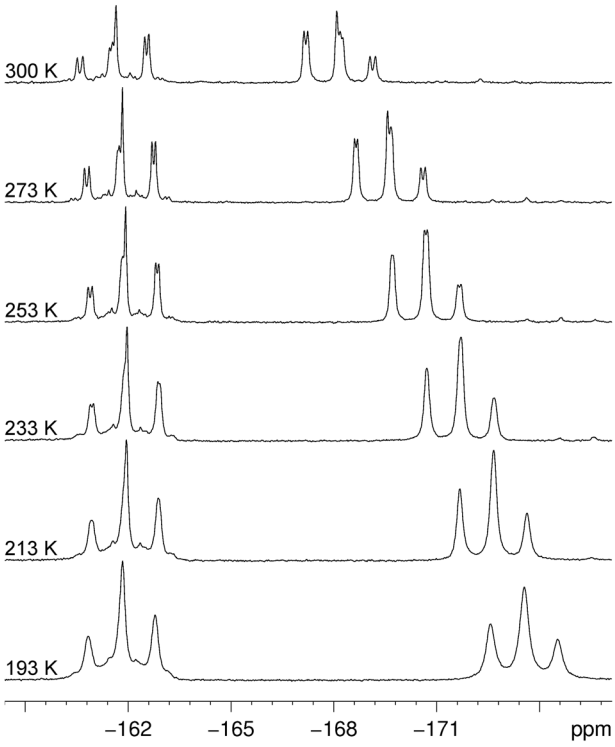

Figure. S8. $^{31}P\{^1H\}$ NMR spectra of **2c** at different temperatures (recorded in CD_2Cl_2).

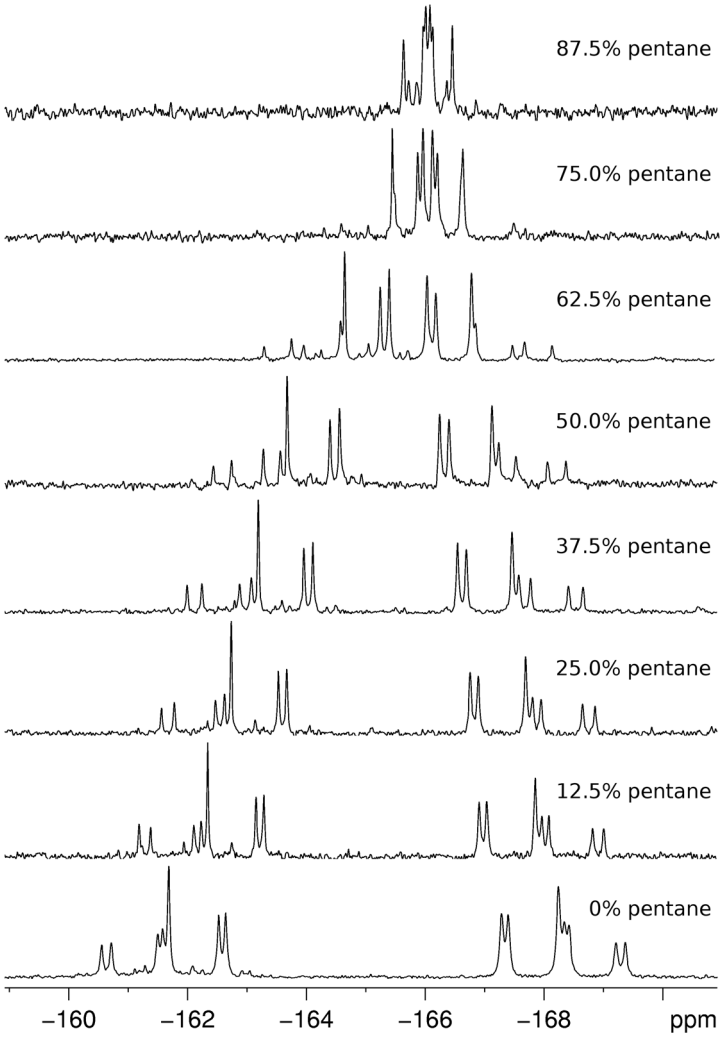

Figure S9. $^{31}P\{^{1}H\}$ NMR spectra of **2c** in different CH_2Cl_2 / *n*-pentane mixtures with increasing *n*-pentane percentage (recorded at 300 K).

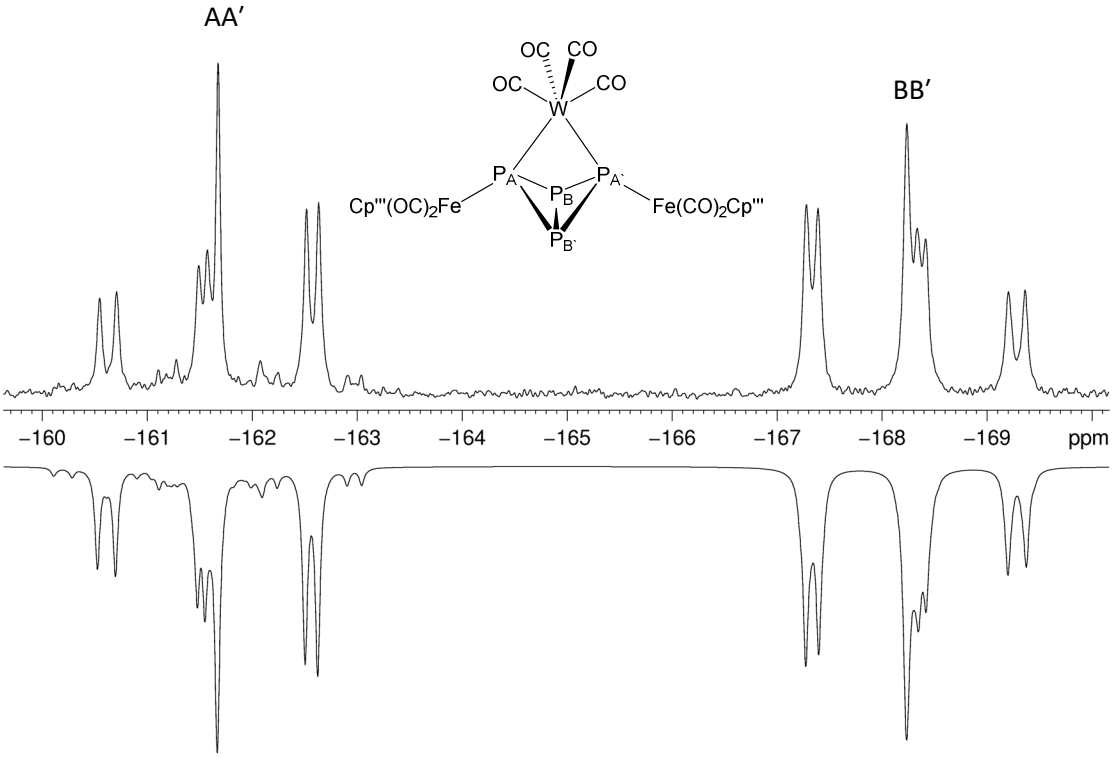

Figure S10. Experimental (top, recorded in CD_2Cl_2 at 300 K) and simulated (bottom) $^{31}P\{^1H\}$ NMR spectrum of **2c.**

Table S3. Experimental and simulated values for the chemical shifts and coupling constants in the $^{31}P\{^1H\}$ NMR spectrum of **2c**.

chemical shift δ [ppm]				**coupling constant *J* [Hz]**			
	Exp.	**F1 (85.69%)**	**F2 (14.28%)**		**Exp.**	**F1 (85.69%)**	**F2 (14.28%)**
δ_A	-161.6	-161.66	-161.66	$^1J_{AB}$	-	155.9	155.0
				$^1J_{AB`}$	-	169.5	165.6
$\delta_{A`}$	-161.6	-161.66	-161.66	$^1J_{A`B}$	-	155.2	165.6
				$^1J_{A`B`}$	-	159.0	164.3
δ_B	-168.3	-168.23	-168.23	$^2J_{AA`}$	-	10.8	6.2
				$^2J_{BB`}$	-	2.4	16.3
$\delta_{B`}$	-168.3	-168.24	-168.24	$^1J_{AW}$	-	-	145.9
				$^1J_{A`W}$	-	-	118.6
				$^2J_{BW}$	-	-	11.0
				$^2J_{B`W}$	-	-	18.4

The simulation of the $^{31}P\{^1H\}$ NMR spectrum of **2c** was carried out on the basis of an AA′BB′ spin system with a C_1 symmetry. According to the natural abundancy of the NMR active ^{138}W isotope, the simulation was performed using two fragments. The main fragment (F1, 85.69%) was simulated with an NMR inactive tungsten atom, whereas the second fragment (F2, 14.28%) considered the ^{138}W atom.

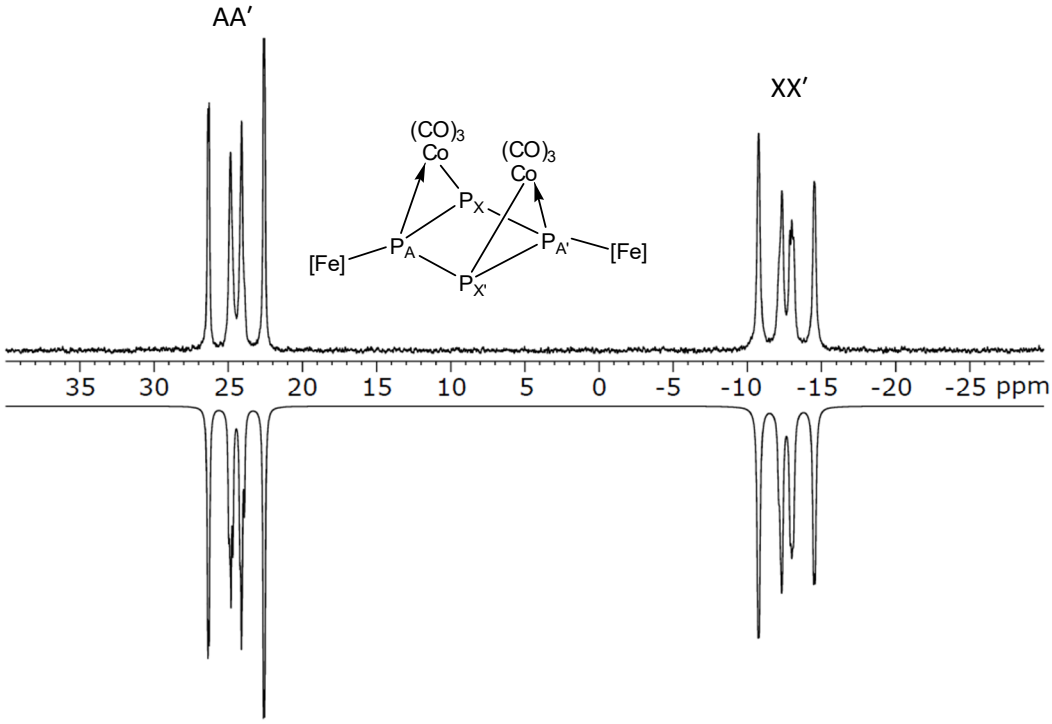

Figure S11. Experimental (top) and simulated (bottom) $^{31}P\{^{1}H\}$ NMR spectrum of **4** in CD_2Cl_2.

Table S4. Experimental and simulated values for the chemical shifts and coupling constants in the $^{31}P\{^{1}H\}$ NMR spectrum of **4**

experimental values				**simulated values**			
δ_A	24.4 ppm	$^1J_{AM}$	-	δ_A	24.39 ppm	$^1J_{AX}$	369.1 Hz
$\delta_{A`}$	24.4 ppm	$^1J_{AN}$	-	$\delta_{A`}$	24.40 ppm	$^1J_{AX`}$	237.5 Hz
δ_B	-12.6 ppm	$^2J_{AX}$	-	δ_X	-12.60 ppm	$^1J_{A`X}$	250.5 Hz
$\delta_{B`}$	-12.6 ppm	$^2J_{MN}$	-	$\delta_{X`}$	-12.59 ppm	$^1J_{A`X`}$	361.1 Hz
		$^1J_{MX}$	-			$^2J_{AA`}$	27.7 Hz
		$^1J_{NX}$	-			$^2J_{XX`}$	-5.5 Hz

The simulation of the $^{31}P\{^{1}H\}$ NMR spectrum of **4** was carried out on the basis of an AA′XX′ spin system.

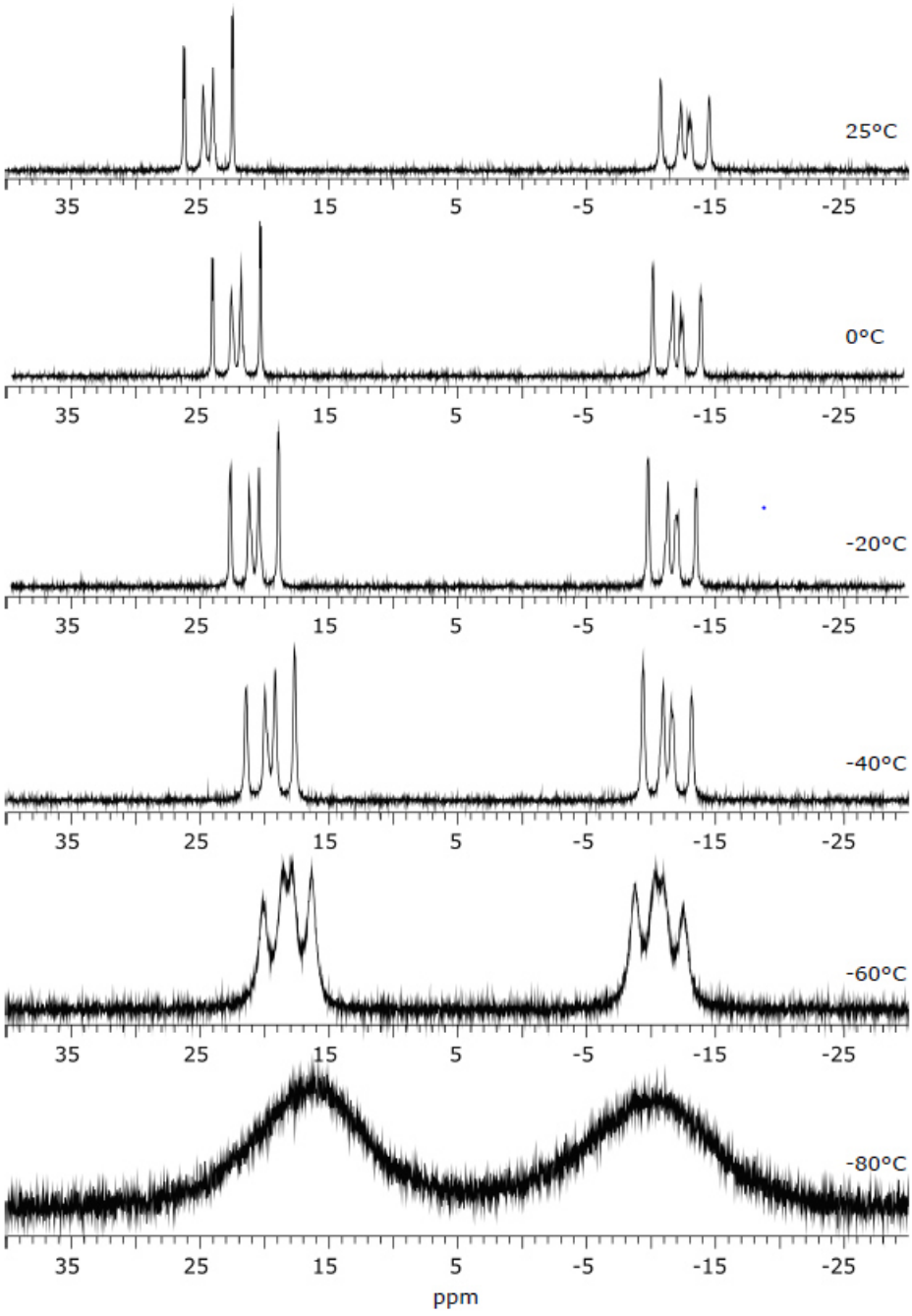

Figure. S12. $^{31}P\{^1H\}$ NMR spectra of **4** at different temperatures (recorded in CD_2Cl_2).

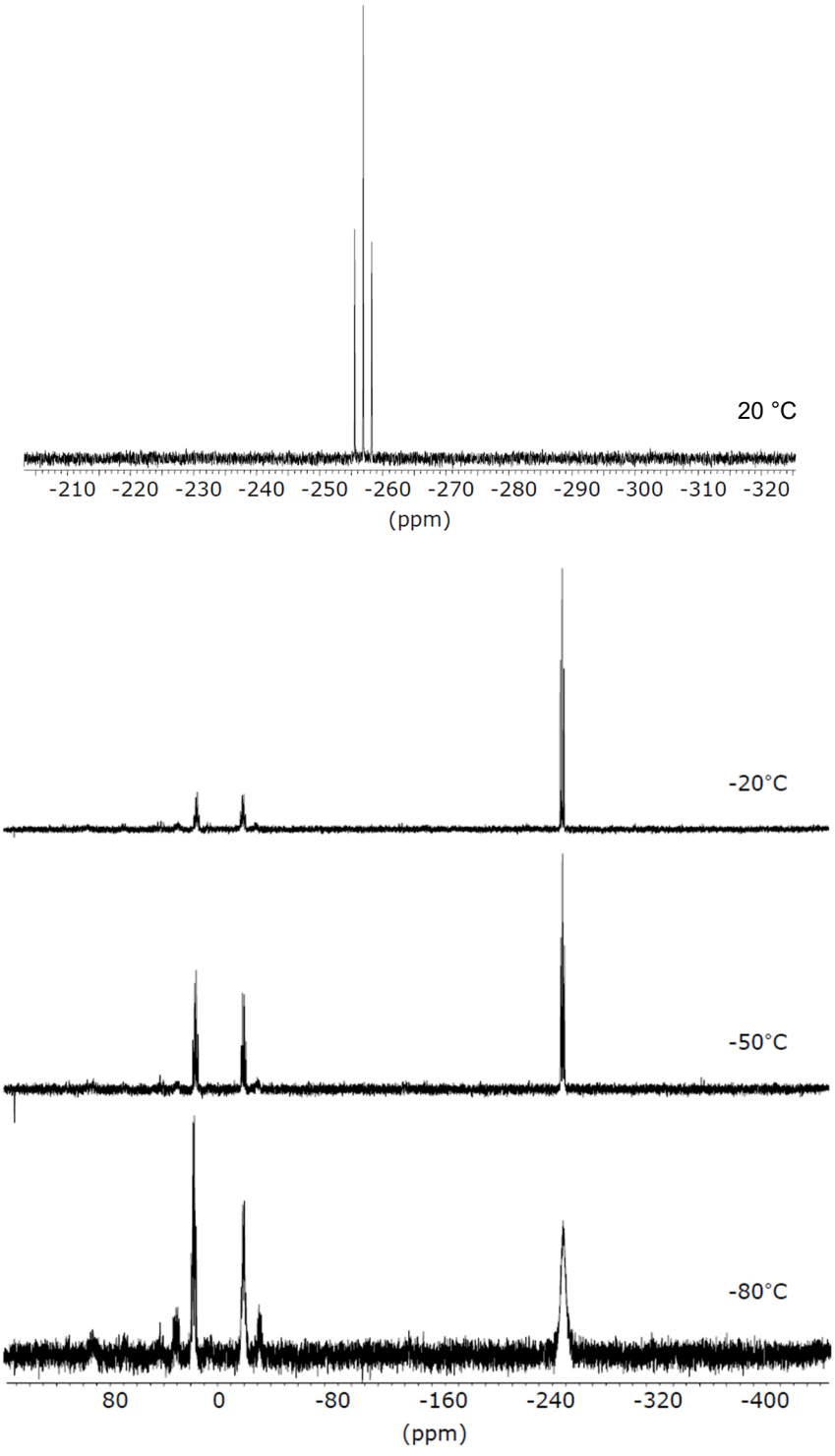

Figure. S13. ^{31}P NMR spectrum of **5*** at room temperature at variable temperatures (recorded in toluene-d_8).

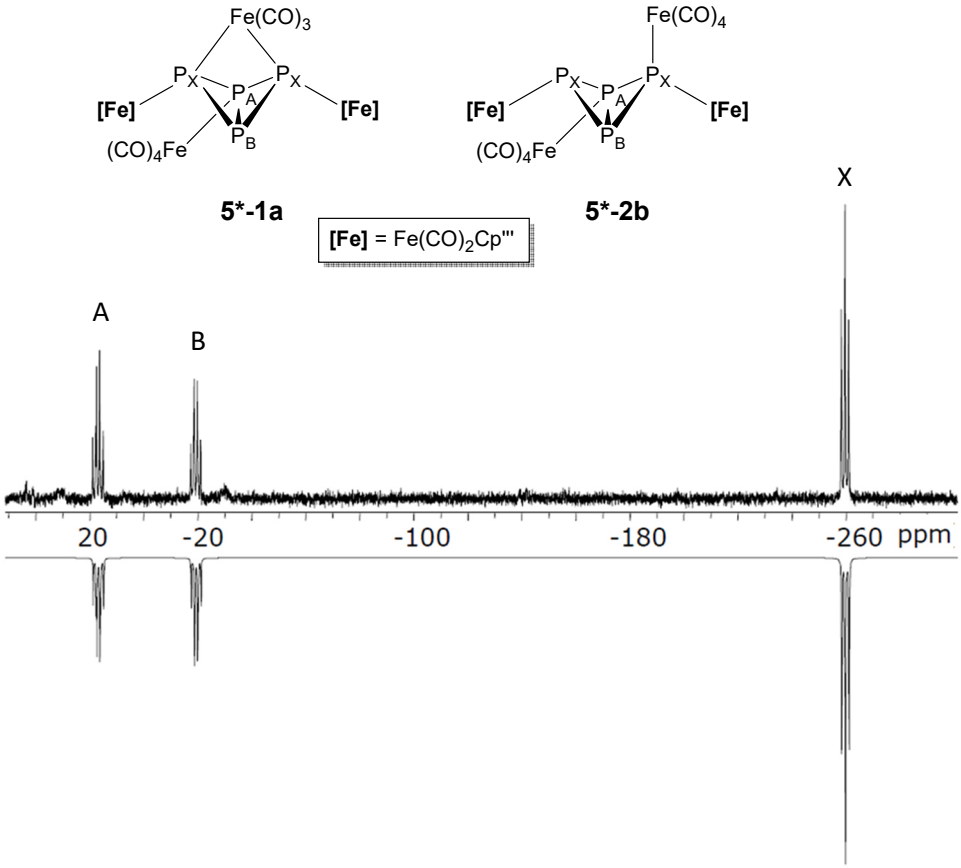

Figure. S14. Experimental (top) and simulated (bottom) ^{31}P NMR spectrum of **5*** (recorded in toluene-d_8 at -50 °C)

Table S5. Experimental and simulated values for the chemical shifts and coupling constants in the ^{31}P NMR spectrum of **5***

experimental values				simulated values			
δ_A	16.0 ppm	$^1J_{AX}$	-	δ_A	16.0 ppm	$^1J_{AX}$	208.1 Hz
δ_B	-19.9 ppm	$^1J_{BX}$	-	δ_B	-19.9 ppm	$^1J_{BX}$	225.6 Hz
δ_X	-257.8 ppm	$^1J_{AB}$	-	δ_X	-257.8 ppm	$^1J_{AB}$	170.3 Hz

The simulation of the ^{31}P NMR spectrum of **5*** was carried out on the basis of an ABX_2 spin system.

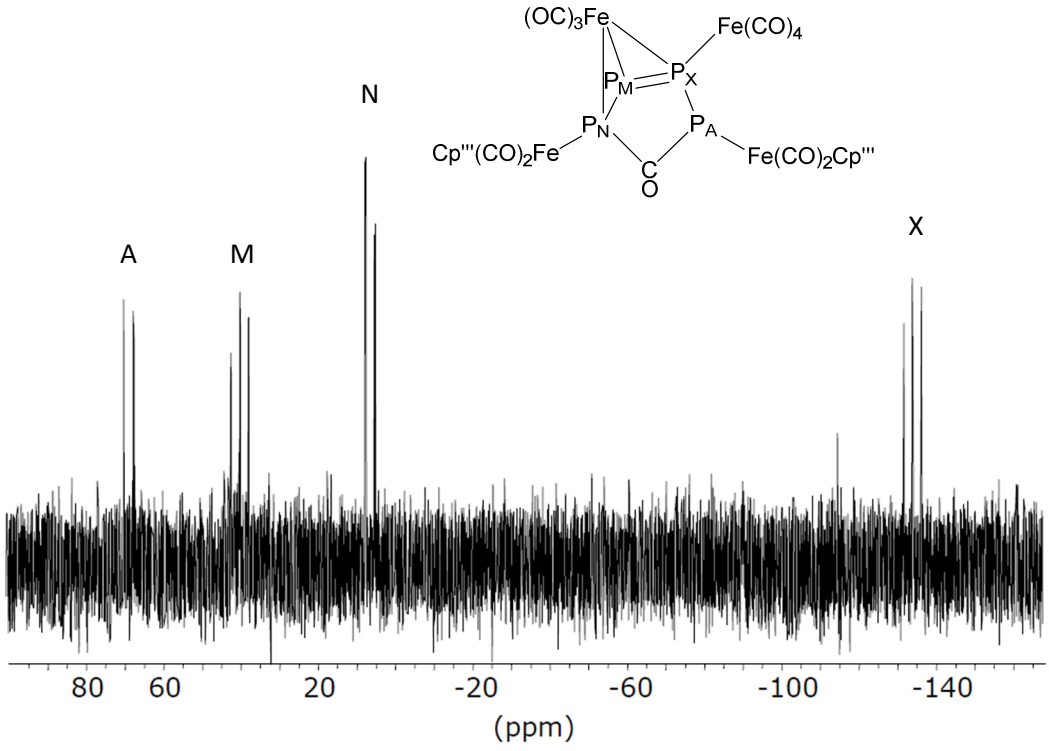

Figure. S15. ^{31}P NMR spectrum of **5** (recorded in C_6D_6 at 300 K).

4.6.4 DFT calculations

The geometry of the molecules has been optimized using the TURBOMLE program package[7] at the RI-[8]B3LYP[9] level together with the def2-TZVP basis set for all atoms.[10] To speed up the calculations, the Coulomb part was evaluated by using the Multipole Accelerated Resolution of Identity method (MARI-*J*)[11] along with optimized auxiliary basis sets on all atoms.[12] The natural bond orbital analysis (NBO) has been performed with NBO 6.0[13] on the wave function obtained at the B3LYP/def2-TZVP level of theory. The topological analysis of the electron density obtained from the DFT calculations, according to the Atoms in Molecules theory[14] has been performed with the MultiWFN program (version 3.6).[15]

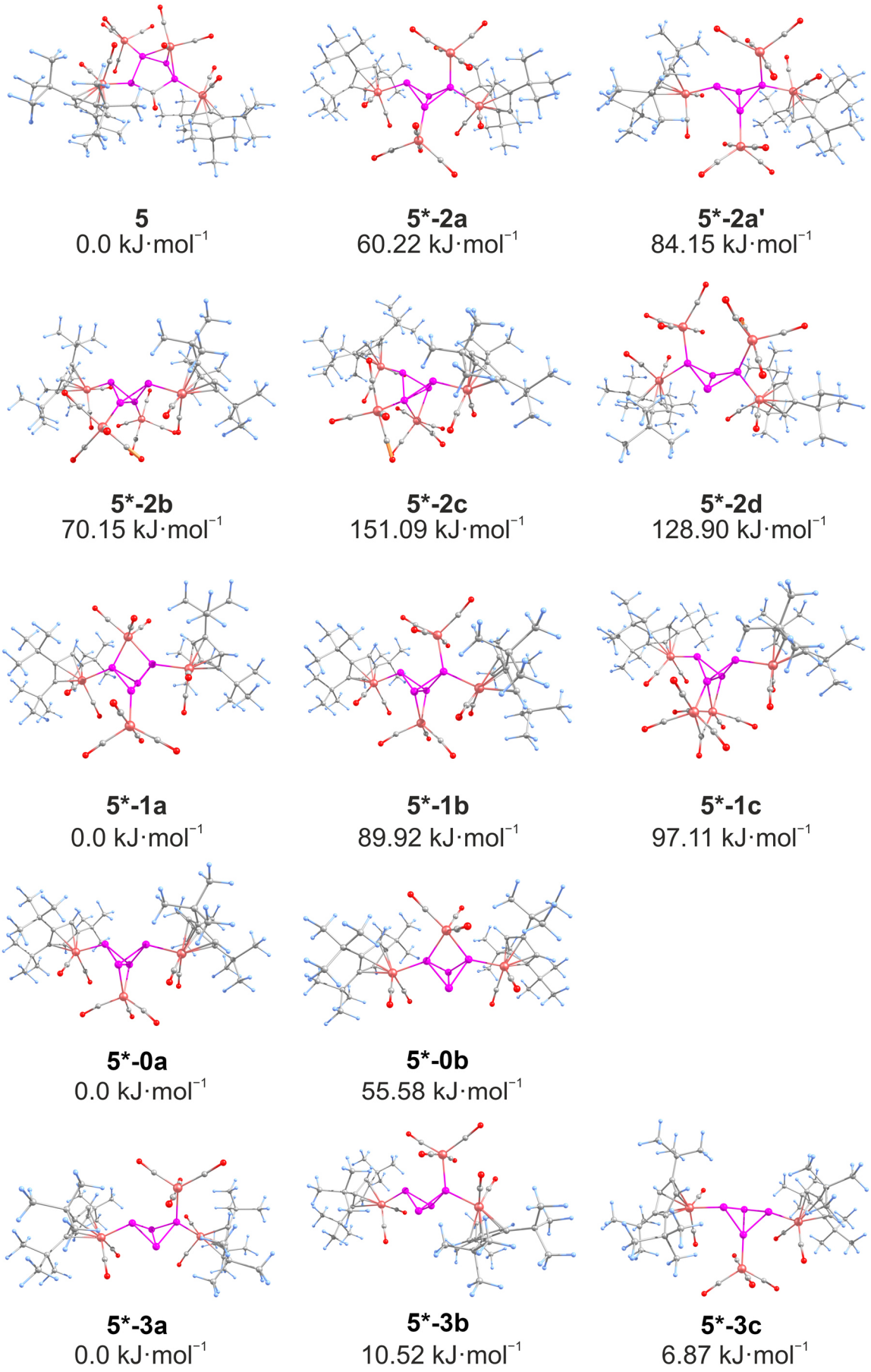

Figure S16. Structure and relative energies of suggested isomers for **5**, **5*-0**, **5*-1**, **5*-2** and **5*-3** (calculated on the B3LYP/def2TZVP level of theory).

Table S6. Total SCF energies at the B3LYP/def2-TZVP level.

	Total energy (a.u.)		Total energy (a.u.)
1	-5676.125867	**5*-2a**	-9110.174705
4	-9121.666449	**5*-2a'**	-9110.165589
4-i	-9121.63229561	**5*-2b**	-9110.170921
5	-9110.197641	**5*-2c**	-9110.140095
5*-0a	-7279.79448	**5*-2d**	-9110.148545
5*-0b	-7279.815651	**5*-3a**	-7393.155018
5*-1a	-8996.846448	**5*-3b**	-7393.151012
5*-1b	-8996.812202	**5*-3c**	-7393.152401
5*-1c	-8996.80946		

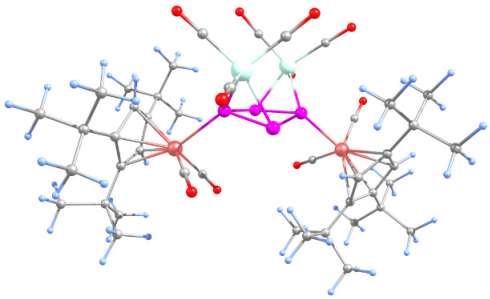

Table S7. Cartesian coordinates of the optimized geometry of **4** at the B3LYP/def2-TZVP level.

Atom	x	y	z
Fe	-0.3219001	-0.5409696	-2.8822998
Fe	0.4066561	-0.1826637	3.8258906
Co	2.8771712	1.5802570	-1.1967576
Co	3.4947446	-1.5856472	1.4173238
P	1.3684567	-0.1633766	-1.2665565
P	1.0875681	1.3516851	0.2410061
P	1.6711983	-0.2322503	1.8082135
P	1.4597960	-1.8086957	0.3560778
O	-1.1904797	2.2017398	-2.3954414
O	-2.0973330	-1.6086014	-0.8291593
O	-0.8834036	-2.6688997	2.9981630
O	2.5267674	-1.6387872	5.2021819
O	4.4773690	0.6263660	-3.4463099
O	1.9263143	4.1742419	-2.1849999
O	4.9818978	2.1145213	0.7741751
O	5.2763145	-1.7159897	-0.9093349
O	5.2725776	-0.2593563	3.3192479
O	3.2868954	-4.2618405	2.6048857
C	-1.2808290	-0.9638441	-4.7752075
C	-0.0599820	-0.1941325	-5.0382285
C	1.0204553	-0.9677880	-4.5208089
H	2.0515831	-0.6647394	-4.5514745
C	0.5633251	-2.2069087	-4.0005556
C	-0.8436631	-2.1722262	-4.1498680
H	-1.5004089	-2.9644321	-3.8381786
C	-2.7610969	-0.7918473	-5.1879935
C	-3.5957077	-2.0011426	-4.7103753
H	-4.6364431	-1.8454424	-4.9986341
H	-3.5737303	-2.1164344	-3.6256181
H	-3.2673431	-2.9359328	-5.1677871
C	-2.8743457	-0.7776080	-6.7287514
H	-2.4210150	0.1012050	-7.1794561
H	-3.9274550	-0.7878048	-7.0182434
H	-2.4003532	-1.6609944	-7.1618963
C	-3.4427856	0.4534248	-4.5881276
H	-3.5170958	0.3637927	-3.5035132
C	1.5170979	-4.2511107	-4.9759031
H	2.0045809	-3.6669304	-5.7589986
H	0.5376651	-4.5626967	-5.3448546
H	2.1148517	-5.1485962	-4.8021911
C	-0.8332123	1.1330703	-2.5807147
C	-1.3710767	-1.1893015	-1.6046302
C	-1.4062019	1.0860019	3.8998399
C	-1.1183296	0.4800803	5.2087089
C	0.1657092	0.9698954	5.5867441
H	0.6566673	0.7266382	6.5129262
C	0.7160086	1.8247152	4.5941236
C	-0.2598808	1.8607751	3.5651322
H	-0.1509348	2.4068841	2.6456063
C	-2.6933354	1.1818822	3.0478023
C	-2.4800246	2.1444840	1.8602359
H	-2.2499952	3.1587465	2.1918485
H	-3.4015740	2.1918857	1.2776653
H	-1.6849155	1.8119350	1.1932354
C	-3.1594294	-0.1537007	2.4401818
H	-4.1058661	-0.0013402	1.9161532
H	-3.3148771	-0.9343369	3.1771309
H	-2.4371375	-0.5179010	1.7101575
C	-3.8194375	1.8061219	3.9025244
H	-4.6855692	2.0051704	3.2678553
H	-3.4988587	2.7557979	4.3361675
H	-4.1507924	1.1611777	4.7119049
C	-1.9431882	-0.3087151	6.2512613
C	-3.0360412	-1.2340187	5.6942160
H	-3.5119997	-1.7536942	6.5282138
H	-2.6241466	-1.9944242	5.0311700
H	-3.8195514	-0.7012828	5.1642547
C	-2.5940527	0.7267018	7.2006317
H	-1.8346076	1.3382054	7.6915203
H	-3.1657009	0.2124831	7.9767006
H	-3.2710499	1.3967191	6.6723301
C	-1.0236004	-1.2097096	7.1068466

H	-4.4582334	0.5372373	-4.9827526
H	-2.9254045	1.3797578	-4.8112359
C	0.2606472	1.0402330	-5.9094101
C	0.5394318	0.5056612	-7.3371633
H	1.3653016	-0.2076090	-7.3327052
H	0.8141085	1.3354245	-7.9923119
H	-0.3297456	0.0101425	-7.7682265
C	-0.8208143	2.1287212	-5.9924365
H	-0.4511817	2.9360610	-6.6275460
H	-1.0400855	2.5617414	-5.0172451
H	-1.7485804	1.7782707	-6.4346812
C	1.5440443	1.7416727	-5.4184851
H	2.4269217	1.1089521	-5.4917933
H	1.4499089	2.0790936	-4.3871024
H	1.7288997	2.6189085	-6.0403283
C	1.3931868	-3.4376379	-3.6640536
C	2.8028494	-3.0647442	-3.1876793
H	2.7757179	-2.4797783	-2.2698112
H	3.3504202	-2.4912874	-3.9373418
H	3.3782112	-3.9699209	-2.9857498
C	0.7068610	-4.3157594	-2.6054235
H	-0.2786986	-4.6534716	-2.9327476
H	0.5931000	-3.7905380	-1.6566355
H	1.3089918	-5.2076657	-2.4212129
H	-0.5050958	-1.9496799	6.4962859
H	-1.6322459	-1.7479168	7.8353695
H	-0.2798636	-0.6480692	7.6710007
C	1.9222997	2.7390627	4.7577843
C	1.4237512	3.9950940	5.5127206
H	1.0295627	3.7364767	6.4978384
H	0.6346957	4.5037900	4.9552612
H	2.2472938	4.6989479	5.6520315
C	3.0369025	2.0781236	5.5844303
H	3.4568506	1.2103838	5.0760028
H	2.6870310	1.7649234	6.5702400
H	3.8489501	2.7906051	5.7415518
C	2.4960563	3.1743641	3.4025874
H	1.7557262	3.6934828	2.7917940
H	2.8727366	2.3230928	2.8364970
H	3.3304916	3.8608181	3.5574247
C	-0.3896712	-1.6816996	3.2875687
C	1.7185106	-1.0749910	4.6278899
C	3.8652166	1.0042057	-2.5565865
C	2.2486886	3.1402285	-1.8138720
C	4.1567289	1.8405852	0.0315994
C	4.5565339	-1.6115124	-0.0262305
C	4.5842751	-0.7760915	2.5672663
C	3.3278036	-3.2081795	2.1602376

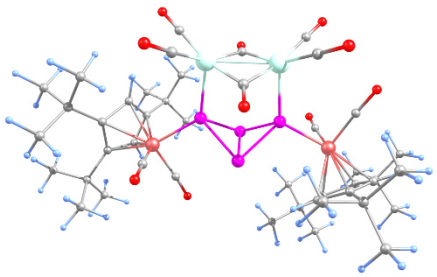

Table S8. Cartesian coordinates of the optimized geometry of **4-i** at the B3LYP/def2-TZVP level.

Atom	x	y	z
Fe	-0.3021240	0.0143336	-3.1710132
Fe	0.6197793	-0.0517770	3.9793532
Co	3.6030271	0.0962510	-1.3009651
Co	3.8610658	0.0015228	1.2848576
P	1.2081827	-0.0387982	-1.3052143
P	0.1929751	1.0770476	0.3519566
P	1.5497870	0.0153999	1.7751868
P	0.2117572	-1.1269441	0.3880841
O	0.1544920	2.8976289	-3.1012387
O	-2.7180374	0.1453164	-1.5426473
O	0.4786522	-2.9494712	3.6456418
O	3.3086876	-0.2140752	5.0940681
O	4.5990042	-1.8211072	-3.2698268
O	4.6464405	2.2859876	-2.9343319
O	3.2745328	2.6284295	0.1389203
O	3.5094054	-2.5699074	-0.0747776
O	5.3247635	1.9945403	2.8532680
O	5.0228568	-2.1373099	2.9114221
C	-1.1003911	-0.2916375	-5.1595537
C	0.3560569	-0.1677787	-5.2571656
C	0.9030998	-1.2212892	-4.4632329
H	1.9551815	-1.3975141	-4.3310911
C	-0.1214607	-2.0407912	-3.9209188
C	-1.3319490	-1.4412636	-4.3418725
H	-2.3074925	-1.8144690	-4.0863803
C	-2.2816794	0.4130350	-5.8656289
C	-3.6228819	-0.2224043	-5.4355750
H	-4.4368605	0.3038914	-5.9365510
H	-3.7961242	-0.1388933	-4.3618104
H	-3.6916452	-1.2736994	-5.7203251
C	-0.1361640	-4.4288262	-4.4928203
H	0.6362529	-4.2652735	-5.2469070
H	-1.1100341	-4.3336829	-4.9776705
H	-0.0383567	-5.4530627	-4.1262699
C	-0.0118897	1.7679078	-3.1260088
C	-1.7346694	0.1015068	-2.1239358
C	-1.5396103	0.3506633	4.2603381
C	-0.8649608	0.1203187	5.5459584
C	0.1193112	1.1440850	5.6545608
H	0.7727591	1.2664179	6.5007793
C	0.1236779	1.9946033	4.5143073
C	-0.8894052	1.4730309	3.6710910
H	-1.1474990	1.8824855	2.7116928
C	-2.8400198	-0.2162469	3.6446041
C	-3.2146002	0.5624401	2.3654683
H	-3.3930406	1.6201302	2.5681071
H	-4.1377149	0.1461577	1.9591538
H	-2.4531173	0.4789250	1.5907396
C	-2.7641130	-1.7000126	3.2378745
H	-3.7460287	-2.0289994	2.8895450
H	-2.4658628	-2.3567211	4.0479319
H	-2.0625491	-1.8364165	2.4142775
C	-4.0059412	0.0113656	4.6339299
H	-4.9471408	-0.2595144	4.1509527
H	-4.0706357	1.0621168	4.9244871
H	-3.9214786	-0.5834680	5.5391607
C	-1.1342224	-0.7772428	6.7750993
C	-1.7872964	-2.1392129	6.4931236
H	-1.8901844	-2.6788852	7.4366857
H	-1.1751206	-2.7538785	5.8337392

C	-2.1795567	0.1950577	-7.3919522
H	-1.3221252	0.6931620	-7.8359722
H	-3.0752077	0.5873687	-7.8785849
H	-2.1098059	-0.8689103	-7.6281082
C	-2.4037776	1.9149947	-5.5419363
H	-2.6466244	2.0614441	-4.4885423
H	-3.2153191	2.3489333	-6.1309195
H	-1.5030159	2.4782116	-5.7574945
C	1.3005080	0.6417348	-6.1720854
C	1.5096445	-0.2144986	-7.4467015
H	1.9373138	-1.1871350	-7.1981882
H	2.2007128	0.2950636	-8.1218891
H	0.5775805	-0.3849313	-7.9846592
C	0.8295655	2.0435708	-6.5904366
H	1.6028870	2.4948781	-7.2149522
H	0.6868148	2.6996832	-5.7323902
H	-0.0839169	2.0332939	-7.1771612
C	2.6776012	0.8343107	-5.5070384
H	3.1903838	-0.1058563	-5.3117266
H	2.5941514	1.3834022	-4.5709685
H	3.3187816	1.4134169	-6.1731746
C	0.0106574	-3.4317877	-3.3164514
C	1.3803130	-3.6530893	-2.6627722
H	1.5506361	-2.9790341	-1.8257463
H	2.1961122	-3.5247962	-3.3757053
H	1.4440641	-4.6729652	-2.2788600
C	-1.1006885	-3.7156647	-2.2929886
H	-2.0960460	-3.6236264	-2.7327348
H	-1.0397952	-3.0417015	-1.4384582
H	-1.0044866	-4.7372428	-1.9198429
H	-2.7811017	-2.0571759	6.0643874
C	-2.0403586	0.0260013	7.7404074
H	-1.5620984	0.9608675	8.0384758
H	-2.2305269	-0.5578954	8.6438531
H	-3.0013651	0.2719549	7.2905975
C	0.1816725	-1.0873814	7.5248156
H	0.8874991	-1.6265912	6.8921979
H	-0.0418368	-1.7186661	8.3863648
H	0.6758782	-0.1950686	7.9075399
C	0.8238136	3.3430757	4.4021509
C	-0.0805111	4.3649301	5.1336495
H	-0.2091018	4.1018154	6.1858296
H	-1.0697693	4.4157869	4.6743081
H	0.3662913	5.3604416	5.0861463
C	2.2031047	3.3334176	5.0806337
H	2.8953318	2.6586229	4.5775512
H	2.1442565	3.0454713	6.1321843
H	2.6366566	4.3344525	5.0432837
C	0.9905629	3.7902816	2.9433438
H	0.0333102	3.8523707	2.4228138
H	1.6413804	3.1201360	2.3831059
H	1.4409286	4.7843224	2.9144672
C	0.5129619	-1.8127048	3.7507262
C	2.2764469	-0.1500436	4.6123481
C	4.1985171	-1.0990207	-2.4759199
C	4.2095145	1.4469894	-2.2913399
C	3.4970137	1.4803080	0.0719537
C	3.6334086	-1.4071247	-0.0426103
C	4.7403180	1.2356477	2.2282435
C	4.5609941	-1.3174723	2.2642994

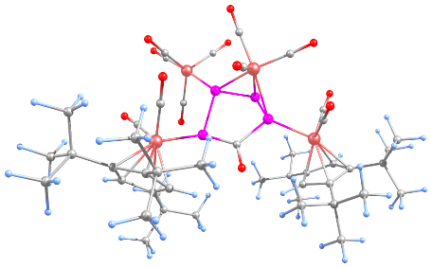

Table S9. Cartesian coordinates of the optimized geometry of **5** at the B3LYP/def2-TZVP level.

Atom	x	y	z
P	0.3683193	1.6046742	1.6940266
P	-0.4424949	1.3434961	3.6888322
P	0.1960638	-0.7228616	3.5620377
P	-0.5981517	-1.4167719	1.5926863
Fe	0.2081579	3.7021136	0.6345922
Fe	0.2325698	-3.4821020	0.7344043
Fe	1.8848469	0.9171247	3.3426752
Fe	-0.3901725	-2.0492912	5.4060428
O	-0.0378291	0.1575328	-0.5711655
C	-0.0496155	0.0574143	0.6384817
O	-0.1551972	0.2372458	7.2561521
O	3.0944090	3.5051157	0.2153675
O	0.3331431	5.0572034	3.2190818
O	-0.8496373	-5.0451180	2.9514974
O	2.8324020	-3.0121906	1.9704903
O	3.8981262	-0.1955606	1.5238240
O	3.0420834	0.0091861	5.8891786
O	3.1266480	3.5564762	3.7098544
O	-3.0577136	-2.4444837	4.2071483
O	1.9961861	-3.7274800	4.9649458
O	-1.1664412	-3.8186953	7.6088245
C	-0.1520201	4.0680547	-1.4963167
C	-0.3156167	5.3019413	-0.7215439
C	-1.3870765	5.0415717	0.1881833
H	-1.7674227	5.7586657	0.8936000
H	-3.3529916	4.7740193	2.1880413
C	-3.3420771	1.7068419	0.5548762
H	-2.6005688	1.2025934	1.1722602
H	-3.2443400	1.3422539	-0.4688938
H	-4.3271539	1.4060949	0.9164076
C	1.9681961	3.5786668	0.3807054
C	0.3139547	4.4868556	2.2322360
C	0.7083556	-5.0318840	-0.7016625
C	-0.7046391	-4.9474313	-0.4962456
H	-1.3061020	-5.7467795	-0.1007814
C	-1.2187687	-3.6897481	-0.8862114
C	-0.0888260	-2.9476914	-1.3239756
H	-0.1244027	-1.9271375	-1.6594403
C	1.1013998	-3.7352755	-1.2590014
C	1.4434829	-6.3781501	-0.5052106
C	2.6019734	-6.3207955	0.5093975
H	3.3475864	-5.5699610	0.2736314
H	3.1059647	-7.2897239	0.5402450
H	2.2248164	-6.1144999	1.5117977
C	0.4681541	-7.4517973	0.0276915
H	0.0407855	-7.1810038	0.9940610
H	1.0163816	-8.3846581	0.1672911
H	-0.3453612	-7.6536094	-0.6713604
C	1.9426728	-6.8995515	-1.8716376
H	1.1200175	-6.9603344	-2.5875757

C	-1.8968399	3.7304444	0.0415277
C	-1.1005317	3.1354770	-0.9747956
H	-1.2020007	2.1227001	-1.3192883
C	0.5915792	3.7235053	-2.8063647
C	0.9043002	2.2158056	-2.8920379
H	1.4157304	2.0186963	-3.8359656
H	0.0121323	1.5943824	-2.8698376
H	1.5532273	1.8874525	-2.0813963
C	1.9199470	4.4509899	-3.0658682
H	1.8140343	5.5284457	-3.1433159
H	2.3220368	4.1020847	-4.0189028
H	2.6644049	4.2275166	-2.3026665
C	-0.3928333	4.0619894	-3.9553107
H	-0.6568261	5.1189286	-3.9734881
H	-1.3152576	3.4867023	-3.8607678
H	0.0642360	3.8119344	-4.9153041
C	0.2717187	6.7275573	-0.8423215
C	-0.3595760	7.6617778	0.2144223
H	-0.1713682	7.3229028	1.2341232
H	-1.4361154	7.7751339	0.0757943
H	0.0863095	8.6525781	0.1167039
C	1.7941227	6.8034614	-0.6150402
H	2.1357991	7.8266457	-0.7872022
H	2.3633677	6.1524912	-1.2687531
H	2.0414164	6.5440759	0.4153078
C	-0.1032348	7.3267260	-2.2164620
H	-1.1833175	7.2905863	-2.3741471
H	0.3739426	6.8162635	-3.0484238
H	0.2043089	8.3738851	-2.2540988
C	-3.2099483	3.2327843	0.6315488
C	-4.3334703	3.8638063	-0.2278038
H	-5.3092759	3.5380493	0.1387860
H	-4.2476289	3.5626225	-1.2739706
H	-4.3035264	4.9544832	-0.1857766
C	-3.3893279	3.6872722	2.0894318
H	-2.6278765	3.2569212	2.7401425
H	-4.3638275	3.3618009	2.4583802
H	2.3554875	-7.9034856	-1.7511125
H	2.7197730	-6.2770170	-2.3066629
C	-2.6962773	-3.3523222	-1.0410806
C	-3.5027347	-3.7378101	0.2110305
H	-3.3893749	-4.7949735	0.4590515
H	-4.5658450	-3.5576744	0.0367578
H	-3.1992927	-3.1488315	1.0766755
C	-2.9093642	-1.8623486	-1.3413634
H	-2.5631671	-1.2359746	-0.5204419
H	-3.9742498	-1.6684807	-1.4870478
H	-2.3895212	-1.5564070	-2.2514012
C	-3.2175373	-4.1727594	-2.2451557
H	-2.6619066	-3.9356635	-3.1551109
H	-4.2715199	-3.9474027	-2.4231602
H	-3.1287684	-5.2459713	-2.0653985
C	2.3787516	-3.2126216	-1.9534401
C	3.7195046	-3.7781068	-1.4588184
H	4.5231308	-3.3114057	-2.0319245
H	3.8129696	-4.8505467	-1.5986810
H	3.8974085	-3.5458244	-0.4097631
C	2.2212965	-3.5490878	-3.4578284
H	1.3279724	-3.0779802	-3.8717313
H	2.1453812	-4.6220968	-3.6320079
H	3.0868869	-3.1780384	-4.0114302
C	2.4922109	-1.6791925	-1.8272694
H	2.5895036	-1.3676095	-0.7879260
H	1.6455459	-1.1508182	-2.2593099
H	3.3879547	-1.3487954	-2.3565296
C	-0.4256687	-4.3686036	2.1377431
C	1.8101662	-3.1733397	1.4908878
C	3.1048695	0.2000232	2.2445294
C	2.5656251	0.3582013	4.9152481
C	2.6210640	2.5435724	3.5536315
C	-2.0096842	-2.2862165	4.6500638
C	1.0718698	-3.0619249	5.1153033
C	-0.8625179	-3.1260689	6.7505966
C	-0.2318504	-0.6358319	6.5166720

Table S10. Cartesian coordinates of the optimized geometry of **5*-0a** at the B3LYP/def2-TZVP level.

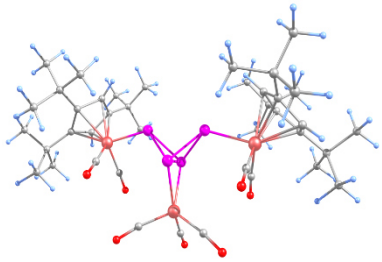

Atom	x	y	z
Fe	3.7708765	-0.0079220	-0.7787597
Fe	-3.6517825	-0.0161378	-0.8018104
P	1.4912400	-0.1542894	-0.2489219
P	0.0643945	-0.9022898	-1.8305672
P	0.0473775	1.2322779	-1.2803397
P	-1.3809646	-0.1785744	-0.2547386
O	3.3951193	2.3844762	-2.4027448
O	3.4699850	-1.9401708	-2.9402134
O	-3.3919068	2.3215660	-2.5256949
O	-3.2122285	-2.0803513	-2.8141837
C	5.6883127	0.6800211	-0.0161995
C	4.6542929	0.8975221	1.0072507
C	4.1367377	-0.3955194	1.3157938
C	4.7676987	-1.4056111	0.5596354
C	5.7094282	-0.7201879	-0.2639723
C	-4.9462182	-1.2954696	0.4054630
C	-5.7567398	-0.3362037	-0.3574794
C	-5.3332444	0.9528719	0.0766519
H	5.6484611	3.2426800	-1.4330318
H	7.5503274	0.0289619	-2.0595882
H	7.9352889	1.6851089	-2.4807423
H	6.2979832	1.0800158	-2.7294849
H	6.2504592	3.0251521	2.0404581
H	5.8836510	1.8080254	3.2607672
H	5.1449193	3.4092603	3.3512534
H	3.4211259	4.1206277	1.7015372
H	2.6897547	2.9729303	0.5823286
H	4.2811655	3.6418550	0.2464980
H	2.8818413	2.6079783	3.4580862
H	3.5367041	0.9805668	3.5965132
H	2.2658236	1.3331257	2.4116698
H	5.3377439	-4.2900813	2.3268445
H	4.8635125	-2.7097496	2.9602831
H	6.4008846	-2.8944035	2.1095212
H	2.6649336	-3.2213701	-0.0673129
H	2.6381266	-2.8151591	1.6473680

C	-4.3244121	0.8679307	1.0754698
C	-4.1001551	-0.5173389	1.2500663
C	6.7998801	1.5517354	-0.6441598
C	8.0538313	1.3813143	0.2489978
C	6.5059580	3.0529904	-0.7895012
C	7.1578011	1.0452797	-2.0599584
C	3.5552051	-1.1589479	-2.1111895
C	3.5058479	1.4366145	-1.7751766
C	-3.4289074	1.3829364	-1.8769876
C	-3.3716857	-1.2517449	-2.0435221
C	4.2421384	2.1240160	1.8524972
C	5.4590187	2.6192454	2.6654370
C	3.6326468	3.2798954	1.0364225
C	3.1673333	1.7229847	2.8868562
C	4.6531047	-2.9087603	0.7859363
C	5.3574181	-3.2159090	2.1288072
C	3.1869972	-3.3623236	0.8795653
C	5.3584933	-3.7058041	-0.3229494
C	-5.0063513	-2.8224954	0.6367861
C	-5.9400550	-3.0509315	1.8512184
C	-5.5093705	-3.6803149	-0.5343613
C	-3.6110805	-3.3751072	1.0039226
C	-6.9655736	-0.4820153	-1.3090231
C	-8.1321051	-1.1568888	-0.5533994
C	-7.4792683	0.9092566	-1.7403746
C	-6.6581272	-1.2388844	-2.6154050
C	-3.8216484	2.0170142	1.9408394
C	-4.9976094	2.4560246	2.8449200
C	-3.3760825	3.2187681	1.0906972
C	-2.6557480	1.5747461	2.8385747
H	3.3458540	-0.5770649	2.0212064
H	6.3626842	-1.2028004	-0.9687119
H	-5.7338900	1.8786502	-0.2970082
H	-3.3745218	-0.9313681	1.9269199
H	8.3558640	0.3341213	0.3061118
H	7.8796800	1.7349824	1.2651725
H	8.8870011	1.9516078	-0.1682174
H	7.3707962	3.5312524	-1.2538715
H	6.3437930	3.5497200	0.1624215
C	-0.0113083	2.3890742	-4.3346529
H	3.1429330	-4.4238116	1.1336442
H	5.2732357	-4.7744193	-0.1161704
H	6.4232656	-3.4693771	-0.3753179
H	4.9176802	-3.5242351	-1.3032570
H	-6.9520870	-2.6952188	1.6577546
H	-5.5664436	-2.5326915	2.7361441
H	-5.9960633	-4.1172849	2.0821338
H	-6.5332627	-3.4563417	-0.8184055
H	-5.4859393	-4.7290248	-0.2309340
H	-4.8742525	-3.5841159	-1.4138119
H	-3.6846456	-4.4536014	1.1548054
H	-3.2146750	-2.9515878	1.9257389
H	-2.8855826	-3.1980591	0.2093662
H	-9.0237262	-1.1640133	-1.1843053
H	-8.3725435	-0.6079667	0.3598149
H	-7.9185115	-2.1865370	-0.2776853
H	-8.3238875	0.7780130	-2.4184989
H	-6.7187521	1.4792271	-2.2763809
H	-7.8298186	1.5014283	-0.8932179
H	-6.2536561	-2.2317990	-2.4556087
H	-5.9452551	-0.6807473	-3.2232736
H	-7.5768420	-1.3451752	-3.1970975
H	-5.3552234	1.6254638	3.4570876
H	-5.8378136	2.8266925	2.2545165
H	-4.6774641	3.2574945	3.5146603
H	-3.1052230	4.0541019	1.7402108
H	-4.1695294	3.5649407	0.4260962
H	-2.5075544	2.9707821	0.4801520
H	-2.9566923	0.7808690	3.5255747
H	-2.3165849	2.4188443	3.4426871
H	-1.8069749	1.2150213	2.2550586
Fe	0.0407362	0.7870439	-3.5954066
O	-2.3812683	0.0247351	-5.0520613
O	2.5102696	0.1934782	-5.0512915
O	-0.0462692	3.4566552	-4.7552508
C	-1.4872002	0.3383090	-4.3962743
C	1.5970906	0.4399136	-4.3937107

Table S11. Cartesian coordinates of the optimized geometry of **5*-0b** at the B3LYP/def2-TZVP level.

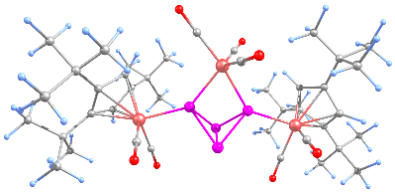

Atom	x	y	z
Fe	3.6298909	-1.0087573	-0.6833781
Fe	-3.5853834	-0.4206427	-0.7120818
P	1.3754621	-0.6862889	-0.1061906
P	-0.0762820	-1.7349714	-1.4217270
P	0.1085507	0.4703761	-1.5279709
P	-1.3062384	-0.4663384	-0.0509656
O	2.9042708	-1.0889839	-3.5061795
O	3.2278874	-3.8941585	-0.4585445
O	-2.8837732	0.1614133	-3.4822849
O	-3.3546129	-3.3108903	-1.0431739
C	5.5885919	-0.1740196	-1.0909485
C	4.6909962	0.8982380	-0.6369103
C	4.2831286	0.5335356	0.6847698
C	4.8702371	-0.6849679	1.0916246
C	5.6407242	-1.1167764	-0.0271432
C	-5.1937353	-0.5981130	0.7536829
C	-5.7278593	-0.1596648	-0.5402894
C	-5.0870094	1.0859471	-0.8160174
H	5.2715712	0.0105100	-3.9999535
H	7.1329898	-2.4426365	-1.7988263
H	7.4343472	-1.9504615	-3.4525669
H	5.7865513	-2.2988527	-2.9336152
H	6.3615314	2.7309670	-2.0307442
H	6.1783094	3.1471773	-0.3274317
H	5.4305893	4.1497393	-1.5724977
H	3.4988885	3.3195865	-2.8986242
H	2.6416072	1.8477217	-2.4590155
H	4.1667784	1.7542896	-3.3318256
H	3.2103821	4.0413962	-0.6537328
H	3.9051768	3.2328654	0.7450996
H	2.4900866	2.5497846	-0.0643041
H	6.4969078	-1.2966833	4.0372296
H	6.5840469	0.1247343	2.9911187
H	7.1472533	-1.4443731	2.4018243
H	2.9192936	-0.7498848	3.1190185
H	4.1223104	0.4735126	3.5373884

C	-4.1938495	1.4595974	0.2184143
C	-4.2558184	0.3997402	1.1600679
C	6.5702143	-0.3568571	-2.2721846
C	7.9450369	0.1648785	-1.7846343
C	6.2204542	0.3525190	-3.5892896
C	6.7322933	-1.8535444	-2.6227349
C	3.3636312	-2.7629560	-0.5174263
C	3.1690302	-1.0364726	-2.3959032
C	-3.1204902	-0.0746621	-2.3891608
C	-3.4347243	-2.1791467	-0.9048386
C	4.3601538	2.2991664	-1.1981646
C	5.6659719	3.1208832	-1.2916447
C	3.6330696	2.2908892	-2.5559533
C	3.4372447	3.0636056	-0.2254786
C	4.9567765	-1.2621997	2.5000076
C	6.3857085	-0.9489639	3.0079134
C	3.9476635	-0.6002583	3.4468329
C	4.7497955	-2.7853697	2.5224166
C	-5.5960370	-1.6933326	1.7662445
C	-6.6483530	-1.0521484	2.7060718
C	-6.1820992	-2.9911665	1.1887373
C	-4.3897697	-2.1131098	2.6329571
C	-6.8672436	-0.6674575	-1.4528951
C	-8.2031939	-0.6337237	-0.6771156
C	-7.0508909	0.2786366	-2.6605310
C	-6.6230502	-2.0670371	-2.0499894
C	-3.5646609	2.8373299	0.3813427
C	-4.7093981	3.8041269	0.7702933
C	-2.9292640	3.3287295	-0.9301182
C	-2.5112120	2.8569073	1.4965157
H	3.6168809	1.1154044	1.2959561
H	6.2261568	-2.0197000	-0.0437940
H	-5.2659613	1.6768068	-1.6966924
H	-3.6892951	0.3614536	2.0733575
H	8.2827434	-0.3814065	-0.9023801
H	7.9092950	1.2236674	-1.5287335
H	8.6916852	0.0327261	-2.5709603
H	6.9937352	0.1179935	-4.3237520
H	6.1902773	1.4339133	-3.4960184
H	4.0452501	-1.0336672	4.4442231
H	4.9578326	-3.1689843	3.5234071
H	5.4185286	-3.3014393	1.8301609
H	3.7228043	-3.0539598	2.2769961
H	-7.5433453	-0.7412968	2.1669609
H	-6.2386619	-0.1764242	3.2118949
H	-6.9474488	-1.7732834	3.4699260
H	-7.1093446	-2.8401447	0.6442794
H	-6.4068837	-3.6654095	2.0174370
H	-5.4752980	-3.5058838	0.5390924
H	-4.7067008	-2.8967020	3.3233054
H	-3.9952592	-1.2998139	3.2372938
H	-3.5752176	-2.5143939	2.0287564
H	-9.0255598	-0.8861296	-1.3501717
H	-8.3932821	0.3642809	-0.2762266
H	-8.2300441	-1.3366296	0.1510622
H	-7.8504334	-0.1098548	-3.2931828
H	-6.1521020	0.3414243	-3.2760820
H	-7.3373822	1.2864000	-2.3553223
H	-6.4463954	-2.8316562	-1.3022572
H	-5.7646224	-2.0508747	-2.7228864
H	-7.4953208	-2.3699312	-2.6341779
H	-5.1985186	3.4850114	1.6929654
H	-5.4681201	3.8613423	-0.0129291
H	-4.3114396	4.8088979	0.9292834
H	-2.5579310	4.3477795	-0.8021222
H	-3.6479289	3.3445964	-1.7519643
H	-2.0887978	2.6997180	-1.2245991
H	-2.9397606	2.5815021	2.4620920
H	-2.1015449	3.8639730	1.5973457
H	-1.6834818	2.1794911	1.2896242
Fe	0.0755568	-0.5135064	1.8769271
O	0.8746083	-3.1796304	2.8140914
O	-1.8247749	-0.1648972	4.0656097
O	1.4288386	1.9651981	2.6578936
C	0.5147121	-2.1596273	2.4082810
C	-1.0727746	-0.3174249	3.2046496
C	0.8542695	1.0181584	2.3168153

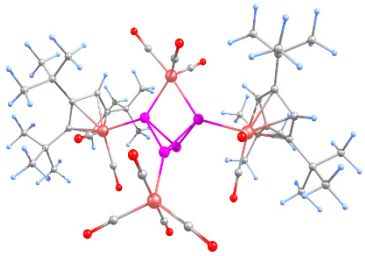

Table S12. Cartesian coordinates of the optimized geometry of **5*-1a** at the B3LYP/def2-TZVP level.

Atom	x	y	z
Fe	3.6787376	-0.7293401	-0.4723085
Fe	-3.5885011	-0.2518268	-0.3997372
P	1.4188740	-0.4989116	0.1037994
P	-0.0565364	-1.5316331	-1.2032237
P	0.1001931	0.6646339	-1.2911592
P	-1.3034320	-0.3058034	0.2006212
O	3.0125278	-0.6773865	-3.3101817
O	3.3777300	-3.6340970	-0.3341443
O	-2.9536406	0.1067152	-3.2238635
O	-3.4420344	-3.1671253	-0.4375408
C	5.6228927	0.1557708	-0.8459074
C	4.7022710	1.1972339	-0.3655712
C	4.2952374	0.7862475	0.9425652
C	4.9053820	-0.4311438	1.3184009
C	5.6874418	-0.8161463	0.1907790
C	-5.2343134	-0.2962715	1.0424750
H	6.3548118	3.0999488	-1.6783371
H	6.1431303	3.4612059	0.0341852
H	5.3936117	4.4882374	-1.1896256
H	3.4921145	3.6693163	-2.5620988
H	2.6535219	2.1711653	-2.1797611
H	4.1893274	2.1297920	-3.0378309
H	3.1648317	4.3124635	-0.2991542
H	3.8566764	3.4714416	1.0814932
H	2.4640024	2.7903497	0.2324707
H	6.5480167	-1.0962059	4.2431972
H	6.6163371	0.3507976	3.2314390
H	7.1956686	-1.1974349	2.6035459
H	2.9632063	-0.5661836	3.3482159
H	4.1557102	0.6573210	3.7953443
H	4.0946346	-0.8735459	4.6630943
H	5.0261758	-2.9743269	3.6872866

C	-5.7192209	0.1009028	-0.2817279
C	-5.0235572	1.3096241	-0.5968637
C	-4.1400149	1.6937629	0.4395183
C	-4.2582937	0.6761560	1.4230580
C	6.6175190	0.0262366	-2.0236889
C	7.9797491	0.5478988	-1.5010818
C	6.2749557	0.7792066	-3.3184955
C	6.8021832	-1.4547339	-2.4257742
C	3.4717834	-2.4986113	-0.3677729
C	3.2481039	-0.6887189	-2.1931251
C	-3.1642255	-0.0516098	-2.1124170
C	-3.4865339	-2.0262727	-0.4263072
C	4.3509851	2.6092532	-0.8855693
C	5.6435661	3.4555488	-0.9370377
C	3.6390030	2.6324634	-2.2510112
C	3.4038303	3.3254247	0.1001340
C	5.0034896	-1.0428463	2.7114447
C	6.4301914	-0.7251837	3.2228588
C	3.9905830	-0.4153785	3.6776443
C	4.8149075	-2.5683707	2.6959135
C	-5.7116821	-1.3188287	2.0982226
C	-6.7515645	-0.5747442	2.9742371
C	-6.3512824	-2.6150860	1.5767034
C	-4.5487092	-1.7495519	3.0168862
C	-6.8546817	-0.4061127	-1.1996031
C	-8.2082521	-0.2690560	-0.4672803
C	-6.9618709	0.4781144	-2.4621743
C	-6.6563817	-1.8462524	-1.7114809
C	-3.4733998	3.0575799	0.5639800
C	-4.5916934	4.0585831	0.9449372
C	-2.8452502	3.5054954	-0.7660871
C	-2.4067650	3.0781378	1.6663283
H	3.6167628	1.3385970	1.5673269
H	6.2904317	-1.7067346	0.1504864
H	-5.1628253	1.8678094	-1.5055019
H	-3.7150684	0.6568992	2.3509875
H	8.3153393	-0.0247019	-0.6348328
H	7.9273151	1.5966278	-1.2087367
H	8.7365132	0.4532652	-2.2829437
H	7.0630388	0.5845774	-4.0486740
H	6.2256923	1.8556726	-3.1853641
H	5.3389169	0.4376089	-3.7574708
H	7.1966255	-2.0698919	-1.6180355
H	7.5189287	-1.5125350	-3.2465035
H	5.8679764	-1.8996162	-2.7699750
H	5.4908576	-3.0586852	1.9922109
H	3.7917528	-2.8433391	2.4421087
H	-7.6161375	-0.2498066	2.3953553
H	-6.3098349	0.3057158	3.4434716
H	-7.1059489	-1.2372885	3.7670049
H	-7.2570010	-2.4477080	1.0019771
H	-6.6292633	-3.2291888	2.4354064
H	-5.6582560	-3.2012044	0.9748793
H	-4.9195592	-2.4815606	3.7361229
H	-4.1295682	-0.9262247	3.5899063
H	-3.7398828	-2.2192536	2.4560241
H	-9.0220519	-0.5243451	-1.1494350
H	-8.3640389	0.7583145	-0.1308211
H	-8.2908713	-0.9197944	0.3989542
H	-7.7591962	0.0882758	-3.0966127
H	-6.0449157	0.4680414	-3.0533208
H	-7.2132829	1.5127192	-2.2226155
H	-6.5266306	-2.5740327	-0.9188363
H	-5.7857023	-1.9048691	-2.3659526
H	-7.5284955	-2.1464761	-2.2970326
H	-5.0749397	3.7728347	1.8814753
H	-5.3594690	4.1135277	0.1705221
H	-4.1693298	5.0576122	1.0740190
H	-2.4372372	4.5129631	-0.6610764
H	-3.5775978	3.5342312	-1.5752858
H	-2.0322803	2.8438595	-1.0656390
H	-2.8294494	2.8331850	2.6426331
H	-1.9744867	4.0779360	1.7408521
H	-1.5966984	2.3783888	1.4649383
Fe	0.1112284	-0.3516342	2.0640996
O	1.0003542	-2.9702105	3.0557604
O	-1.8204906	-0.0337440	4.2321529
O	1.4263805	2.1301729	2.8912337
C	0.6149285	-1.9675356	2.6348661
C	-1.0616003	-0.1788576	3.3777103
C	0.8757336	1.1792792	2.5252051
Fe	-0.1684977	-3.1110123	-2.8243533
O	2.2815095	-4.3291654	-3.9027849
O	-0.3160657	-5.1991848	-0.7267052
O	-0.0277516	-0.9657269	-4.8569448
O	-2.7583921	-3.9841642	-3.9099208
C	-0.2590277	-4.3879150	-1.5249343
C	-0.0803794	-1.7883255	-4.0697543
C	-1.7666147	-3.6238901	-3.4624302
C	1.3464745	-3.8377806	-3.4580324

Table S13. Cartesian coordinates of the optimized geometry of **5*-1b** at the B3LYP/def2-TZVP level.

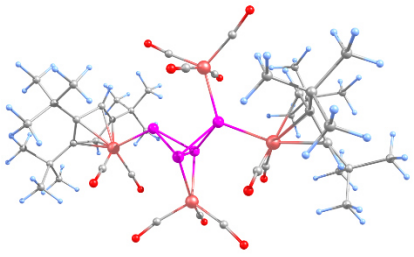

Atom	x	y	z
Fe	2.4638743	-2.4680168	-1.2068246
Fe	-2.5422231	3.0511570	-0.2333124
P	0.7360096	-1.1757066	-0.0658605
P	-0.7197799	-0.1924117	-1.5294554
P	0.8083844	1.0627309	-0.5686383
P	-1.3005507	1.1258876	0.2139587
O	3.9091373	-0.0088234	-1.8364386
O	0.6649300	-2.8096309	-3.4791660
O	-0.4989394	4.5850280	-1.6398460
H	6.8249364	-3.3624707	0.7054452
H	5.9059549	-4.5593793	1.6155122
H	6.6237911	-3.1748696	2.4396089
H	5.7261380	-0.8650998	2.0922825
H	4.1997857	-0.5961813	1.2581603
H	5.6651714	-0.9142284	0.3358619
H	4.6042294	-2.4590539	3.4833131
H	3.8617089	-3.9368316	2.8784924
H	3.0672016	-2.3774503	2.6394086

O	-3.7064007	1.6342153	-2.5032048
C	4.3912495	-3.4914540	-1.2504753
C	4.0220012	-3.2518957	0.1524778
C	2.7805649	-3.9287909	0.3517090
C	2.3702071	-4.6153888	-0.8143549
C	3.3589817	-4.3026242	-1.7921944
C	-4.4195886	3.0697161	0.8891470
C	-4.2090850	4.3714765	0.2367000
C	-2.9914874	4.8756769	0.7721422
C	-2.4292343	3.9885745	1.7328917
C	-3.3197067	2.8905770	1.7793816
C	5.6623467	-3.2758464	-2.1101870
C	6.4875533	-4.5831810	-1.9967046
C	6.5751370	-2.0927621	-1.7460062
C	5.2921605	-3.0866823	-3.5998803
C	1.3598447	-2.5981445	-2.6002507
C	3.2840794	-0.9360425	-1.6141083
C	-1.2650124	3.9141431	-1.1244758
C	-3.2288849	2.1971424	-1.6314637
C	4.8171892	-2.6830109	1.3475115
C	6.1224389	-3.4929478	1.5230218
C	5.1222305	-1.1778205	1.2375005
C	4.0298148	-2.8816672	2.6576718
C	1.3124869	-5.7100646	-0.9230035
C	1.8002601	-6.8850511	-0.0420094
C	-0.0594814	-5.2486255	-0.4174354
C	1.1709250	-6.2178650	-2.3676863
C	-5.6088036	2.0876185	0.9838901
C	-6.4533241	2.5322808	2.2040386
C	-6.5298021	1.9982708	-0.2422761
C	-5.1116272	0.6504077	1.2535444
C	-5.0801697	5.2594173	-0.6814895
C	-6.3865875	5.6227109	0.0593854
C	-4.3630423	6.5960811	-0.9730942
C	-5.3948931	4.6449231	-2.0588746
C	-1.2932015	4.3171094	2.6931175
C	-1.8615188	5.3102703	3.7348609
C	-0.1071201	4.9799272	1.9732893
C	-0.7953098	3.0658394	3.4296160
H	2.2361013	-3.9308223	1.2778029
H	3.3424981	-4.6631260	-2.8049705
H	-2.5528116	5.8175357	0.4946091
H	-3.1817464	2.0244704	2.4024816
H	5.9136699	-5.4431326	-2.3462701
H	6.7990380	-4.7828319	-0.9718094
H	7.3860804	-4.5045897	-2.6125641
H	7.4226425	-2.0922393	-2.4342749
H	6.9840511	-2.1564714	-0.7427608
H	6.0724640	-1.1346605	-1.8559238
H	4.7815353	-3.9500906	-4.0245546
H	6.2087616	-2.9478926	-4.1753123
H	4.6661873	-2.2086407	-3.7588883
H	1.1047418	-7.7234523	-0.1211759
H	1.8608244	-6.5957647	1.0082646
H	2.7864223	-7.2329614	-0.3571452
H	-0.4676868	-4.4540392	-1.0419314
H	-0.0069169	-4.8850523	0.6075291
H	-0.7640000	-6.0827541	-0.4367515
H	0.4222734	-7.0114507	-2.3997198
H	2.1057600	-6.6383964	-2.7440485
H	0.8450892	-5.4336960	-3.0516432
H	-6.8482734	3.5407574	2.0797591
H	-5.8593281	2.5143708	3.1192679
H	-7.2985465	1.8532315	2.3369813
H	-7.0324323	2.9339633	-0.4684023
H	-7.3079482	1.2604736	-0.0368868
H	-5.9959816	1.6646126	-1.1313362
H	-5.9732514	-0.0159902	1.3220845
H	-4.5611592	0.5559761	2.1878020
H	-4.4757057	0.2871042	0.4453399
H	-6.9555647	6.3435154	-0.5318317
H	-6.1704427	6.0802009	1.0273218
H	-7.0278234	4.7621134	0.2321013
H	-4.9927475	7.1963304	-1.6313976
H	-3.4097383	6.4476666	-1.4828078
H	-4.1896928	7.1792576	-0.0670738
H	-5.8755242	3.6750559	-2.0016319
H	-4.4839240	4.5345971	-2.6480754
H	-6.0629608	5.3130667	-2.6073331
H	-2.7116824	4.8786413	4.2669169
H	-2.1930764	6.2368973	3.2620351
H	-1.0944173	5.5622629	4.4705361
H	0.6470374	5.2793577	2.7039218
H	-0.4051243	5.8762158	1.4262709
H	0.3644768	4.2940986	1.2687694
H	-1.5849186	2.5963935	4.0180503
H	0.0090548	3.3375772	4.1159542
H	-0.4027255	2.3213675	2.7363549
Fe	0.6388616	1.1835595	-2.9487145
O	-1.4079279	2.6696018	-4.4121592
O	2.0682920	-0.4287158	-4.9283347
O	2.5550531	3.3441004	-3.3191525
C	-0.6491961	2.1165401	-3.7456424
C	1.5396251	0.1276164	-4.0684907
C	1.7947759	2.4928255	-3.2068605
Fe	-0.2048006	-1.7385126	2.0581200
O	1.8611505	0.0456337	3.1795204
O	-2.2281684	-0.3225872	3.6344617
O	-2.4005498	-3.0050751	0.5462617
O	0.5840543	-4.1595123	3.5090250
C	-1.4344022	-0.8418028	2.9846329
C	-1.5343579	-2.5382155	1.1302097
C	0.3248991	-3.2263155	2.8872512
C	1.0751830	-0.6693602	2.7510136

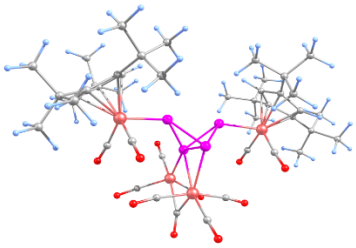

Table S14. Cartesian coordinates of the optimized geometry of **5*-1c** at the B3LYP/def2-TZVP level.

Atom	x	y	z
Fe	3.7938028	0.1495953	-0.6581817
Fe	-3.6498083	0.1142027	-0.6502824
P	1.4464398	-0.0676892	-0.5172731
H	5.6126480	3.4524139	2.3478209
H	5.0985333	2.2895823	3.5683669
H	4.2890592	3.8524298	3.4325449

P	0.0794881	-1.1144098	-1.9571807
P	0.0471545	1.2050140	-1.7643516
P	-1.3071950	-0.1070475	-0.5035589
O	3.4797861	2.4364178	-2.4371942
O	4.2183891	-1.8202138	-2.7586311
O	-3.4944812	2.2579465	-2.6178158
O	-3.7840987	-2.1525677	-2.4754992
C	5.5073087	0.9649695	0.3951647
C	4.3001122	1.1888651	1.2077886
C	3.7834878	-0.1065595	1.4990898
C	4.5743408	-1.1272279	0.9307133
C	5.6248817	-0.4445330	0.2481449
C	-4.7405163	-0.9602326	0.9118898
C	-5.6425730	-0.0328732	0.2137140
C	-5.0903916	1.2634950	0.4167185
C	-3.9158128	1.2164308	1.2194033
C	-3.7203134	-0.1543243	1.4989724
C	6.6760885	1.8541722	-0.0860154
C	7.7577457	1.8110237	1.0216508
C	6.3440922	3.3229269	-0.3913101
C	7.3035006	1.2795549	-1.3763095
C	3.9898745	-1.0387224	-1.9583498
C	3.5849562	1.5341496	-1.7412742
C	-3.5206553	1.3928083	-1.8701388
C	-3.7065063	-1.2486094	-1.7815555
C	3.7031848	2.4394304	1.8925482
C	4.7460835	3.0422972	2.8598359
C	3.1914380	3.5148913	0.9148208
C	2.4885588	2.0433502	2.7603526
C	4.4738459	-2.6182713	1.2297544
C	4.9408484	-2.8144695	2.6917610
C	3.0303908	-3.1299765	1.0962501
C	5.3890591	-3.4468780	0.3143991
C	-4.8177684	-2.4504207	1.3152170
C	-5.4969676	-2.4979938	2.7066039
C	-5.5830515	-3.3860791	0.3667521
C	-3.4019303	-3.0512892	1.4609515
C	-7.0215517	-0.1952654	-0.4647101
C	-8.0408036	-0.7117985	0.5755425
C	-7.5496710	1.1759876	-0.9411682
C	-7.0189783	-1.0991309	-1.7121397
C	-3.2177022	2.4133325	1.8531290
C	-4.1883819	3.0024494	2.9039699
C	-2.8921651	3.5012238	0.8158241
C	-1.9237244	1.9937521	2.5668333
H	2.8838293	-0.2859318	2.0594587
H	6.4117390	-0.9348650	-0.2967424
H	-5.5169819	2.1707882	0.0270846
H	-2.8964194	-0.5443727	2.0689447
H	8.0902481	0.7877442	1.2046560
H	7.3920289	2.2170370	1.9645373
H	8.6262167	2.3991584	0.7161167
H	7.2535173	3.8208632	-0.7336329
H	5.9916547	3.8700216	0.4779398
H	5.6052281	3.4179176	-1.1858680
H	7.7342344	0.2890709	-1.2333269
H	8.1149210	1.9335599	-1.7002353
H	6.5759073	1.2231090	-2.1865795
H	2.8425057	4.3822144	1.4804455
H	2.3472106	3.1373744	0.3364390
H	3.9464629	3.8599889	0.2174322
H	2.0776036	2.9432467	3.2211715
H	2.7642086	1.3600590	3.5656717
H	1.6954775	1.5837921	2.1687029
H	4.9217880	-3.8749785	2.9527629
H	4.2920187	-2.2826645	3.3901475
H	5.9605098	-2.4495763	2.8331352
H	2.6787044	-3.0657181	0.0661641
H	2.3372316	-2.5664188	1.7227308
H	2.9769991	-4.1766652	1.4029790
H	5.3093443	-4.5032038	0.5778565
H	6.4375957	-3.1629061	0.4259651
H	5.1161127	-3.3499935	-0.7364000
H	-6.5107203	-2.0982377	2.6780429
H	-4.9302920	-1.9215784	3.4399737
H	-5.5519997	-3.5310028	3.0575318
H	-6.6327826	-3.1265115	0.2671476
H	-5.5432177	-4.3987887	0.7729524
H	-5.1359263	-3.4194573	-0.6255463
H	-3.4885745	-4.1007197	1.7476424
H	-2.8087011	-2.5594097	2.2306906
H	-2.8464778	-3.0084190	0.5236236
H	-9.0408801	-0.7224568	0.1365998
H	-8.0664538	-0.0598101	1.4514518
H	-7.8223105	-1.7206688	0.9161278
H	-8.5171412	1.0317939	-1.4243861
H	-6.8866195	1.6387236	-1.6740296
H	-7.6985236	1.8718798	-0.1137197
H	-6.6365229	-2.0960330	-1.5257419
H	-6.4198607	-0.6533545	-2.5069055
H	-8.0403137	-1.2014380	-2.0863517
H	-4.4569777	2.2556306	3.6539262
H	-5.1091160	3.3620625	2.4405608
H	-3.7191437	3.8448851	3.4174322
H	-2.4766888	4.3790867	1.3154966
H	-3.7814577	3.8256137	0.2721269
H	-2.1597757	3.1493929	0.0888186
H	-2.1229469	1.2894213	3.3774970
H	-1.4451381	2.8714988	3.0059767
H	-1.2154577	1.5290523	1.8794522
Fe	0.0411976	0.1044693	-4.1062700
O	-2.8778145	-0.0419721	-4.5819945
O	2.9555429	0.2733274	-4.5967695
O	-0.0836338	2.4884104	-5.7944744
C	-1.7742929	0.0133231	-4.3097670
C	1.8543408	0.1990930	-4.3202838
C	-0.0333145	1.5476049	-5.1469399
Fe	0.1232093	-2.5920512	-3.5884208
O	0.1390340	-1.6261112	-6.4529343
O	0.1437666	-4.7576790	-1.6219951
O	-2.3221688	-3.7575983	-4.7353506
O	2.6404623	-3.6509957	-4.6782632
C	0.1353977	-3.9004147	-2.3837939
C	-1.4187333	-3.2386115	-4.2576042
C	1.7072872	-3.1668082	-4.2211848
C	0.1137920	-1.4599220	-5.3014900

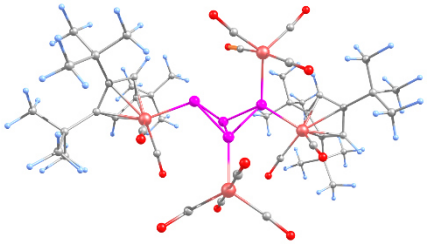

Table S15. Cartesian coordinates of the optimized geometry of **5*-2a** at the B3LYP/def2-TZVP level.

Atom	x	y	z
Fe	3.5872224	-0.8536293	-0.3062523
Fe	-3.7307673	-0.0045376	-0.7946267
P	1.3519824	-0.7661452	0.6211066
P	-0.1715214	-1.4767232	-0.8953609
P	0.0607705	0.6665615	-0.5654858
P	-1.6977499	-0.4144157	0.3396018
O	2.6684838	0.0514162	-2.9168996
O	3.1290935	-3.6858185	-0.8534592
O	-2.5605713	0.5329175	-3.4069915
O	-3.8600524	-2.9061102	-1.0628758
C	5.4089758	0.3214734	-0.6660967
C	4.6519265	0.9174643	0.4363385
C	4.5865240	-0.0911961	1.4558064
C	5.2739683	-1.2588990	1.0678073
C	5.7081588	-1.0110458	-0.2673488
C	-5.4345891	0.0826076	0.5723514
C	-5.8578570	0.4473783	-0.7884839
C	-5.0951758	1.5986811	-1.1322125
C	-4.2309707	1.9932644	-0.0748543
C	-4.4484492	1.0410901	0.9500426
C	6.1019135	0.8632911	-1.9407918
C	7.5418401	1.2449181	-1.5093264
C	5.4647136	2.0807646	-2.6287088
C	6.2251943	-0.2349648	-3.0224678
C	3.2813497	-2.5783504	-0.6307203
C	2.9784718	-0.3084328	-1.8786991
C	-2.9738426	0.2960924	-2.3679403
C	-3.7989111	-1.7680211	-0.9766069
C	4.2185446	2.3685100	0.7386759
C	5.4728749	3.2695820	0.8059825
C	3.1980163	2.9463999	-0.2581898
C	3.5589533	2.4511546	2.1306730
C	5.8007511	-2.3862684	1.9514451
C	7.2772626	-2.0178935	2.2471649
C	5.0535267	-2.4800071	3.2848938
C	5.7703998	-3.7589949	1.2601777
C	-5.9834644	-0.8759217	1.6527453
C	-7.0247405	-0.0724076	2.4711721
C	-6.6447359	-2.1701788	1.1545792
C	-4.8610792	-1.3120152	2.6184983
C	-6.9919879	-0.0400218	-1.7192240
C	-8.3530584	0.1842673	-1.0226924
C	-7.0262933	0.8053322	-3.0115600
C	-6.8575425	-1.5038324	-2.1803313
C	-3.4947474	3.3228686	0.0207471
C	-4.5706458	4.4111537	0.2530054
C	-2.7338541	3.6511124	-1.2744104
C	-2.5180873	3.3456126	1.2043356
H	4.0902777	0.0330983	2.4010774
H	6.2683208	-1.7114998	-0.8609023
H	-5.1684611	2.1145233	-2.0730487
H	-3.9374851	1.0404606	1.8965032
H	8.0734653	0.3816184	-1.1060278
H	7.5486353	2.0266886	-0.7508374
H	8.0985227	1.6102333	-2.3751471
H	6.0596457	2.3284463	-3.5100916
H	5.4505399	2.9650475	-1.9988444
H	4.4513185	1.8793281	-2.9711624
H	6.2030951	2.8687896	1.5123080
H	5.1867746	4.2655037	1.1511181
H	3.0037545	3.9932176	-0.0125542
H	2.2514449	2.4117933	-0.1912327
H	3.5294593	2.9066676	-1.2894968
H	3.2309997	3.4768546	2.3061881
H	4.2514447	2.1876715	2.9316834
H	2.6817281	1.8107447	2.2077443
H	7.7151321	-2.7617856	2.9161284
H	7.3516545	-1.0420402	2.7308886
H	7.8752349	-1.9917181	1.3342667
H	4.0049143	-2.7277163	3.1385837
H	5.1096465	-1.5514606	3.8537020
H	5.4966963	-3.2669130	3.8983704
H	6.3143002	-4.4838719	1.8691435
H	6.2440453	-3.7401989	0.2768926
H	4.7528106	-4.1274955	1.1424054
H	-7.8614774	0.2589929	1.8561968
H	-6.5698905	0.8109438	2.9227705
H	-7.4231399	-0.6950323	3.2755196
H	-7.5270777	-1.9936983	0.5467070
H	-6.9666450	-2.7497334	2.0220587
H	-5.9510263	-2.7928290	0.5910467
H	-5.2762230	-1.9905730	3.3652667
H	-4.4171690	-0.4793381	3.1618343
H	-4.0607099	-1.8405504	2.1013552
H	-9.1631120	-0.0486842	-1.7173021
H	-8.4650969	1.2262735	-0.7152372
H	-8.4862052	-0.4403319	-0.1433054
H	-7.8253749	0.4327596	-3.6541696
H	-6.0952672	0.7315871	-3.5761770
H	-7.2325511	1.8581979	-2.8114572
H	-6.7822095	-2.2112903	-1.3625822
H	-5.9784083	-1.6279414	-2.8136030
H	-7.7325889	-1.7771338	-2.7747137
H	-5.1433971	4.2107299	1.1607751
H	-5.2705547	4.4656229	-0.5832037
H	-4.0968756	5.3895522	0.3608701
H	-2.2961766	4.6492683	-1.2038859
H	-3.3897012	3.6440744	-2.1470534
H	-1.9244368	2.9427531	-1.4517941
H	-3.0322480	3.2020194	2.1565322
H	-2.0158144	4.3140363	1.2494258
H	-1.7509574	2.5776936	1.1147640
Fe	0.8518570	-1.1923145	2.8993202
O	1.7112160	-3.9593917	2.3281711
O	-1.7380150	-2.1763043	3.8695109
O	2.7018349	-0.7880934	5.1332750
C	1.3901005	-2.8851269	2.5584194
C	-0.7491051	-1.7921139	3.4326107
C	2.0271764	-0.9430176	4.2139549
Fe	-0.2095290	-2.8111219	-2.7678677
O	2.1939047	-4.0050042	-3.9627458
O	-0.5615186	-5.1518358	-0.9863687
O	0.1366462	-0.4758097	-4.5505795
O	-2.7325600	-3.4247650	-4.1389495
C	-0.4249664	-4.2467909	-1.6658412
C	0.0040763	-1.3609662	-3.8458333

H	6.8181297	-1.0879513	-2.6950189
H	6.7321662	0.1854244	-3.8924564
H	5.2537189	-0.5994403	-3.3533382
H	5.9642030	3.3868616	-0.1564087
C	-1.7763492	-3.1614329	-3.5637910
C	1.2877066	-3.5234566	-3.4511980
C	0.3064761	0.5218163	3.0320060
O	-0.0409739	1.6093951	3.1202991

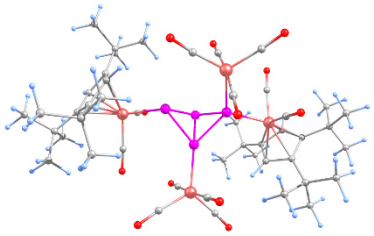

Table S16. Cartesian coordinates of the optimized geometry of **5*-2a'** at the B3LYP/def2-TZVP level.

Atom	x	y	z
Fe	3.8032744	-0.5061440	0.0926605
Fe	-3.7861269	-0.4907386	0.1222755
P	1.5751415	-0.1098206	0.8190616
P	0.0494431	-1.3562628	-0.2673540
P	0.0616193	0.8110089	-0.5481917
P	-1.4688481	-0.1200853	0.8349510
O	3.6916567	1.0513239	-2.3591931
O	3.0443312	-2.9243705	-1.3460212
O	-3.7135036	-2.8172531	1.8902643
O	-4.4794480	1.5253996	2.1179628
C	5.8702397	0.0698547	0.4481866
C	5.0010738	0.8165743	1.3700153
C	4.3445519	-0.1671465	2.1674186
C	4.7352055	-1.4759579	1.8095099
C	5.6604708	-1.3072478	0.7375168
C	-5.0685173	0.6073937	-1.2735112
C	-5.7683398	-0.5728747	-0.7538019
C	-4.9896515	-1.6922101	-1.1709593
C	-3.8658415	-1.2998450	-1.9344094
C	-3.9029443	0.1187499	-1.9444232
C	7.0265784	0.4484154	-0.5059430
C	8.3248618	0.3943609	0.3378230
C	6.9471326	1.8222396	-1.1897858
C	7.1625335	-0.5903069	-1.6425416
C	3.3062218	-1.9727183	-0.7676776
C	3.6855448	0.4697293	-1.3742384
C	-3.6947215	-1.8895460	1.2270425
C	-4.1656378	0.7291251	1.3647151
C	4.8608974	2.3179037	1.7052495
C	6.2166544	2.8616261	2.2093351
C	4.3331743	3.1733320	0.5380974
C	3.8602705	2.5157681	2.8637432
C	4.4563693	-2.7546469	2.5889618
C	5.3783209	-2.7250372	3.8317642
C	2.9957173	-2.8319206	3.0575540
C	4.7900427	-4.0101081	1.7674992
C	-5.4559976	2.0942463	-1.4490788
C	-6.0314704	2.2120304	-2.8839024
C	-6.4851002	2.6835602	-0.4715728
C	-4.2134901	3.0000368	-1.3535605
C	-7.1566645	-0.8011628	-0.1114155
C	-8.2449858	-0.4013296	-1.1343915
C	-7.3772220	-2.3028998	0.1811456
C	-7.3785936	-0.0812941	1.2318909
C	-3.0710606	-2.2453079	-2.8263454
C	-4.0370883	-2.6923825	-3.9523019
C	-2.6027597	-3.4941929	-2.0613006
C	-1.8745934	-1.5468964	-3.4797535
H	3.6260494	0.0594886	2.9352265
H	6.1566833	-2.1166093	0.2326202
H	-5.2420507	-2.7159125	-0.9594690
H	6.5839321	2.2677979	3.0491265
H	6.0903551	3.8890807	2.5572776
H	4.3095066	4.2234469	0.8380041
H	3.3138554	2.8808379	0.2837741
H	4.9349286	3.1026821	-0.3609828
H	3.7688134	3.5832397	3.0704886
C	-1.3740124	1.8843295	2.9531079
H	4.1889535	2.0309332	3.7839828
H	2.8655277	2.1444389	2.6162698
H	5.2424198	-3.6345896	4.4213592
H	5.1512368	-1.8707474	4.4718285
H	6.4299937	-2.6627363	3.5434674
H	2.3068523	-2.8865186	2.2140686
H	2.7172118	-1.9716486	3.6669289
H	2.8479556	-3.7259705	3.6667347
H	4.6079342	-4.9004205	2.3723403
H	5.8392088	-4.0329632	1.4658858
H	4.1734102	-4.0896319	0.8719212
H	-6.9139251	1.5848285	-3.0170358
H	-5.2931354	1.9209537	-3.6320012
H	-6.3202651	3.2466771	-3.0806188
H	-7.4518181	2.1910613	-0.5131207
H	-6.6495942	3.7277766	-0.7441682
H	-6.1295224	2.6753010	0.5570289
H	-4.5083541	4.0335215	-1.5430158
H	-3.4535585	2.7457728	-2.0857007
H	-3.7634523	2.9624003	-0.3618600
H	-9.2316741	-0.6469512	-0.7356789
H	-8.1158125	-0.9502968	-2.0696499
H	-8.2393278	0.6599343	-1.3687162
H	-8.3530692	-2.4270871	0.6526365
H	-6.6319893	-2.7041913	0.8695800
H	-7.3778935	-2.9077900	-0.7268964
H	-7.2308556	0.9904772	1.1826010
H	-6.7104856	-0.4790046	1.9968883
H	-8.4026363	-0.2579600	1.5684004
H	-4.4138765	-1.8344441	-4.5128403
H	-4.8929328	-3.2405459	-3.5538545
H	-3.5123349	-3.3477998	-4.6508355
H	-2.0981026	-4.1801771	-2.7448144
H	-3.4404171	-4.0352487	-1.6163620
H	-1.9017367	-3.2384405	-1.2675899
H	-2.1929499	-0.7073878	-4.1007888
H	-1.3418563	-2.2486354	-4.1240502
H	-1.1689099	-1.1802476	-2.7375451
Fe	0.0932075	2.2720244	-2.3417921
O	-1.0690594	4.3459271	-0.5773239
O	2.4323793	3.9983197	-2.7624839
O	1.1931892	0.0932233	-4.0100730
O	-1.9996395	2.6393123	-4.3611677
C	1.5549917	3.2921268	-2.5556011

H	-3.1800980	0.7434212	-2.4380246
H	8.4722072	-0.5973117	0.7691726
H	8.3077742	1.1152448	1.1547778
H	9.1871254	0.6204572	-0.2936193
H	7.8258223	1.9419811	-1.8268647
H	6.9511437	2.6492867	-0.4867103
H	6.0706402	1.9135872	-1.8290414
H	7.4004390	-1.5890250	-1.2780727
H	7.9792070	-0.2903234	-2.3011927
H	6.2552496	-0.6514306	-2.2442728
H	6.9862368	2.8693654	1.4416561
C	0.7812555	0.9352760	-3.3600606
C	-1.2179957	2.4656634	-3.5356361
C	-0.6269368	3.5402273	-1.2527295
Fe	-1.1632999	0.1015396	3.1884043
O	-1.4847737	3.0111684	2.7912104
O	-0.6536390	-2.8042922	3.1971838
O	1.3431405	0.5254756	4.6535014
O	-3.4908881	-0.1389143	4.9546220
C	-0.8656260	-1.6794802	3.2026226
C	0.3841150	0.3718055	4.0362026
C	-2.6131683	-0.0486515	4.2183895

Table S17. Cartesian coordinates of the optimized geometry of **5*-2b** at the B3LYP/def2-TZVP level.

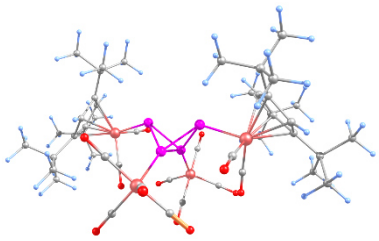

Atom	x	y	z
Fe	3.2765389	0.8334443	1.9634843
Fe	-2.7830147	-0.6224794	-2.1752201
P	1.1402378	0.2093486	1.1733144
P	0.9669138	-0.8199096	-0.8287904
P	0.2820168	1.2207231	-0.6648165
P	-1.2159006	-0.4409596	-0.4209153
O	3.8367636	2.4945861	-0.3634422
O	4.6238443	-1.4478950	0.7624763
O	-3.5383593	2.1188511	-1.5402204
O	-0.7730431	0.0715507	-4.1673783
C	4.3037292	2.1180829	3.3860712
C	2.8539760	2.3045543	3.5382941
C	2.3338035	1.0269451	3.9027913
C	3.3516344	0.0546437	3.9959783
C	4.5544245	0.7445550	3.6591080
C	-3.6090465	-2.2260715	-3.4311888
C	-4.6304624	-1.2398063	-3.1271807
C	-4.7666698	-1.2531114	-1.6929610
C	-3.9073032	-2.2018651	-1.1014657
C	-3.1545877	-2.7474689	-2.1725172
C	5.5139482	3.0658334	3.2235225
C	5.9989854	3.4191167	4.6514658
C	5.2703157	4.3711787	2.4509274
C	6.6763192	2.3485809	2.4994329
C	4.0503176	-0.5632873	1.2052143
C	3.5778839	1.8578411	0.5494835
C	-3.1997248	1.0571237	-1.7974516
C	-1.5425873	-0.2043100	-3.3682701
C	1.9479816	3.5539754	3.5767925
C	2.4170428	4.4924525	4.7105629
C	1.8745921	4.3153330	2.2417329
C	0.4963370	3.1532472	3.9202447
C	3.2202407	-1.3402788	4.5960192
C	3.0010119	-1.1545650	6.1164104
C	2.0213920	-2.1050587	4.0116562
C	4.4963978	-2.1717248	4.3895409
C	-3.1513624	-2.9229550	-4.7316046
C	-4.1186339	-4.1142846	-4.9500853
C	-3.1247541	-2.0598257	-6.0027746
C	-1.7343323	-3.5140940	-4.5803063
C	-5.6016355	-0.4070289	-3.9977034
C	-6.4834638	-1.3452648	-4.8515315
C	-6.5790229	0.3886948	-3.1031601
C	-4.9014119	0.6326960	-4.8959983
H	2.4562842	3.9616700	5.6643789
H	1.7116040	5.3194558	4.8165889
H	1.2428634	5.1986730	2.3588528
H	1.4265563	3.6872004	1.4722377
H	2.8395947	4.6484014	1.8775271
H	-0.1246982	4.0501866	3.9239077
H	0.4187112	2.6959737	4.9083176
H	0.0731120	2.4673810	3.1846562
H	2.9360074	-2.1276992	6.6084627
H	2.0768515	-0.6106697	6.3202731
H	3.8258805	-0.6005545	6.5695450
H	2.1610801	-2.3131006	2.9502664
H	1.0882278	-1.5510585	4.1220332
H	1.9036559	-3.0596865	4.5292431
H	4.3719756	-3.1526861	4.8521849
H	5.3655263	-1.7019454	4.8544841
H	4.7159756	-2.3326823	3.3338845
H	-5.1482158	-3.7894837	-5.0900627
H	-4.0940188	-4.7969611	-4.0988794
H	-3.8163214	-4.6729924	-5.8387379
H	-4.1044195	-1.6913402	-6.2905810
H	-2.7579685	-2.6703265	-6.8302551
H	-2.4486349	-1.2109465	-5.9038915
H	-1.4495785	-3.9942848	-5.5176861
H	-1.6752627	-4.2732232	-3.8025666
H	-0.9931943	-2.7446682	-4.3717079
H	-7.2566707	-0.7607769	-5.3547954
H	-6.9813933	-2.0890337	-4.2256514
H	-5.9235243	-1.8721615	-5.6190923
H	-7.2424640	0.9731083	-3.7425221
H	-6.0651005	1.0907996	-2.4460862
H	-7.2057282	-0.2659610	-2.4946870
H	-4.1382492	0.2041866	-5.5360220
H	-4.4312599	1.4109545	-4.2950569
H	-5.6417076	1.1158647	-5.5385148
H	-5.0570401	-4.5152771	-0.3416485
H	-6.1311944	-3.1831212	0.1003530
H	-5.3118180	-4.1134543	1.3609734
H	-4.3971750	-1.9966829	2.3343772
H	-5.1783918	-1.0307118	1.0893943
H	-3.4370317	-0.8733738	1.3694196
H	-2.5502452	-4.3390027	0.0928855
H	-2.8735516	-3.8817007	1.7616576
H	-1.8555382	-2.8528351	0.7559454

C	-3.9982473	-2.7144407	0.3308845
C	-5.2000981	-3.6907895	0.3597654
C	-4.2667137	-1.5793230	1.3335286
C	-2.7399558	-3.4896340	0.7511633
H	1.2910796	0.8247861	4.0700051
H	5.5276493	0.2881169	3.6345738
H	-5.4653336	-0.6458410	-1.1457654
H	-2.3997109	-3.5050416	-2.0644473
H	6.2744291	2.5202687	5.2059978
H	5.2339711	3.9435599	5.2234998
H	6.8785902	4.0644375	4.5948317
H	6.2120706	4.9205540	2.3924332
H	4.5526197	5.0257493	2.9363224
H	4.9394609	4.1880435	1.4295528
H	7.0508804	1.4863073	3.0499959
H	7.5110263	3.0432620	2.3923686
H	6.3871395	2.0191755	1.5009753
H	3.3981027	4.9220057	4.5251137
Fe	0.3211090	3.1944942	-1.8306982
O	-1.5442730	4.3393816	0.1609969
O	2.2101828	1.9923353	-3.7685861
O	2.2303277	5.3588812	-1.2779093
C	-0.8305067	3.8920573	-0.6092051
C	1.4852951	2.4475023	-3.0169782
C	1.5114861	4.4841355	-1.4556226
Fe	2.1914669	-2.2334692	-2.1529278
O	-1.6022902	3.6788737	-3.9968288
O	0.1510306	-4.3128214	-1.6660124
O	1.7759604	-2.2999617	-5.0620956
O	4.1871559	-4.1064426	-1.0853216
C	0.9318018	-3.5009363	-1.8640388
C	1.8962752	-2.2326841	-3.9251570
C	3.4098376	-3.3491358	-1.4519707
C	-0.8728081	3.4442050	-3.1440833
C	3.4738884	-0.9545037	-2.3465381
O	4.2922577	-0.1696754	-2.4607693

Table S18. Cartesian coordinates of the optimized geometry of **5*-2c** at the B3LYP/def2-TZVP level.

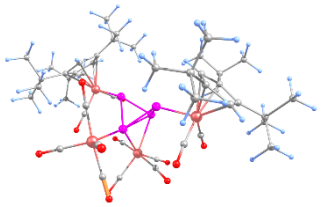

Atom	x	y	z
Fe	3.8020315	0.5788778	-0.6682115
Fe	-3.6001538	0.2273329	-0.4403859
P	1.4410956	0.2555523	-0.6348790
P	0.0609126	-0.4682359	-2.2826554
P	0.0514339	1.9526479	-1.1866787
P	-1.2245282	0.1908122	-0.5346019
O	3.5051392	3.0227265	-2.2196049
O	4.2024301	-1.2031554	-2.9397709
O	-3.5777459	3.1321976	-0.6513734
O	-3.7427254	-0.4757283	-3.2633339
C	5.4882549	1.3197582	0.4807495
C	4.2636093	1.4672763	1.2849445
C	3.7567014	0.1473830	1.4648661
C	4.5687952	-0.8167294	0.8337509
C	5.6211541	-0.0716816	0.2217994
C	-4.9151841	-1.4492937	0.0902882
C	-5.5747588	-0.1753654	0.3544559
C	-4.7582561	0.4820233	1.3309404
C	-3.6478698	-0.3128534	1.7056312
C	-3.7342121	-1.4740332	0.9039145
C	6.6580461	2.2534090	0.0961489
C	7.7246671	2.1176767	1.2108727
C	6.3229421	3.7420354	-0.0818354
C	7.3061620	1.7985195	-1.2311187
C	3.9988028	-0.4946040	-2.0661717
C	3.5985307	2.0541373	-1.6131516
C	-3.5521422	1.9881295	-0.6181395
C	-3.6627860	-0.1842317	-2.1584786
C	3.6463888	2.6512819	2.0637749
C	4.6671917	3.1618193	3.1053249
C	3.1536475	3.8128680	1.1798387
C	2.4133157	2.1783928	2.8646897
C	4.4969550	-2.3262434	1.0269455
C	5.0708459	-2.6203992	2.4339069
C	3.0503253	-2.8392896	0.9647041
C	5.3442941	-3.0810533	-0.0095198
C	-5.3515882	-2.7527644	-0.6148309
C	-6.1058172	-3.5883779	0.4508308
H	5.0095192	2.3462858	3.7460935
H	4.1955290	3.9129275	3.7430162
H	2.7967747	4.6254966	1.8172983
H	2.3169404	3.4940228	0.5569682
H	3.9203537	4.2187830	0.5297323
H	1.9848142	3.0345357	3.3884309
H	2.6727792	1.4304266	3.6161264
H	1.6370476	1.7670045	2.2178674
H	5.0667601	-3.6962618	2.6232329
H	4.4771318	-2.1372874	3.2122950
H	6.0996928	-2.2650260	2.5241725
H	2.6150376	-2.6808722	-0.0216791
H	2.4088020	-2.3460814	1.6962617
H	3.0275793	-3.9107586	1.1739380
H	5.3010084	-4.1525256	0.1943464
H	6.3947114	-2.7854293	0.0315502
H	4.9817875	-2.9286307	-1.0256604
H	-7.0034189	-3.0843324	0.8074282
H	-5.4678776	-3.7890814	1.3132332
H	-6.4047658	-4.5473118	0.0215004
H	-7.2066857	-2.1436437	-1.6370165
H	-6.4608697	-3.6053193	-2.2450109
H	-5.7612346	-2.0478110	-2.6493069
H	-4.4720626	-4.4858815	-1.5580766
H	-3.4935910	-3.8824391	-0.2348201
H	-3.5156500	-3.0283808	-1.7809988
H	-9.0416818	0.0369147	0.2102839
H	-8.0206433	-0.6320942	1.4852563
H	-8.1158806	-1.4265149	-0.0845466
H	-8.0915097	2.2211928	0.2690999
H	-6.3627415	2.5272016	0.3317630
H	-7.1783187	1.7283132	1.6889377
H	-6.8699080	-0.1955102	-2.1928898
H	-6.3217433	1.4494367	-1.9081138
H	-8.0407028	1.0642530	-1.8265352
H	-4.0292623	-1.2518728	4.2050427
H	-4.4210308	0.4711802	4.2089540
H	-2.9874910	-0.1101130	5.0631831

C	-6.2496786	-2.6083225	-1.8535152
C	-4.1269725	-3.5757569	-1.0650177
C	-6.9269038	0.4362522	-0.0771985
C	-8.0887866	-0.4587785	0.4090309
C	-7.1375687	1.8083218	0.6011323
C	-7.0401519	0.6916360	-1.5934623
C	-2.7370611	-0.0551552	2.8997869
C	-3.6006012	-0.2481919	4.1694431
C	-2.1836265	1.3803608	2.8959762
C	-1.5716494	-1.0550199	2.9499437
H	2.8483558	-0.0839363	1.9905693
H	6.4228076	-0.5103667	-0.3451980
H	-4.9792441	1.4463734	1.7536714
H	-3.0273422	-2.2839963	0.9252554
H	8.0608910	1.0838678	1.3076298
H	7.3425152	2.4368032	2.1803405
H	8.5936049	2.7350803	0.9714540
H	7.2347948	4.2719986	-0.3649084
H	5.9557101	4.2077000	0.8278086
H	5.5947295	3.9047055	-0.8750949
H	7.7363594	0.7993593	-1.1721894
H	8.1206921	2.4803753	-1.4817214
H	6.5905071	1.8149205	-2.0537476
H	5.5416794	3.6215045	2.6518558
H	-1.6023651	1.5566819	3.8038885
H	-2.9828623	2.1236538	2.8695555
H	-1.5312427	1.5508221	2.0393884
H	-1.9305276	-2.0832763	3.0310003
H	-0.9557002	-0.8536429	3.8294277
H	-0.9391948	-0.9795424	2.0655008
Fe	-0.0378864	1.5922455	-3.6935828
O	-2.8615983	2.4229659	-3.4727327
O	2.7670446	0.9661649	-4.3844583
O	0.5610629	4.4487615	-4.1715879
C	-1.7938822	2.0309174	-3.4713210
C	1.7105717	1.1858045	-4.0279084
C	0.3218597	3.3499461	-3.9981699
Fe	0.1669125	-2.6831421	-3.0432223
O	-0.8260198	0.5876299	-6.3675171
O	-0.6978443	-3.4556673	-0.3311613
O	-2.1863322	-3.8740901	-4.3390952
O	2.5090750	-4.4236328	-2.7353282
C	-0.3741426	-3.1541463	-1.3872892
C	-1.2944462	-3.3661299	-3.8261334
C	1.6150501	-3.7104288	-2.8416669
C	-0.4896333	0.9342526	-5.3385201
C	0.8250716	-2.0900809	-4.6165085
O	1.2488656	-1.7114145	-5.6093967

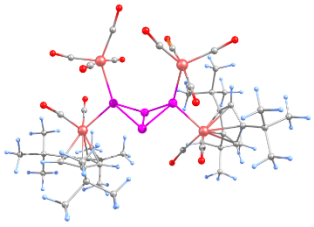

Table S19. Cartesian coordinates of the optimized geometry of **5*-2d** at the B3LYP/def2-TZVP level.

Atom	x	y	z
Fe	2.9917302	0.5392181	0.5684589
Fe	-3.6733045	-0.1032558	-1.4001738
P	1.7633704	-0.5087986	-1.3009905
P	-0.0556714	0.7787723	-1.4766863
P	-0.1822817	-1.0798639	-0.3031644
P	-1.4408735	-0.8667946	-2.1320755
O	0.6214575	1.2428013	2.1108606
O	2.7647934	3.0646528	-0.8693683
O	-4.5618038	-0.2584738	-4.1766815
O	-3.9416773	-2.9197688	-0.6763883
C	3.9693289	-0.1111980	2.4516034
C	4.0829308	-1.1814771	1.4708274
C	4.7983747	-0.6194736	0.3576993
C	5.1788558	0.7156088	0.6176036
C	4.5986672	1.0351980	1.8751857
C	-4.2752773	0.5644748	0.6061577
C	-5.4078835	0.6322239	-0.3256540
C	-5.0121383	1.5530481	-1.3368411
C	-3.7190368	2.0872339	-1.0972740
C	-3.2706278	1.4349747	0.0781903
C	3.5662989	-0.0504829	3.9437692
C	4.8268897	-0.4395887	4.7594968
C	2.3921121	-0.9479568	4.3642101
C	3.2059797	1.3900984	4.3793168
C	2.8546918	2.0541650	-0.3444018
C	1.5091807	0.9067663	1.4718749
C	-4.1549785	-0.2506868	-3.1111839
C	-3.8271988	-1.8245730	-0.9768669
C	3.8172536	-2.7045562	1.5477198
C	4.5888837	-3.3219412	2.7358083
C	2.3269106	-3.0790994	1.6429929
H	5.6400442	-3.0266036	2.7213608
H	4.5489209	-4.4102872	2.6581000
H	2.2311255	-4.1528051	1.8203929
H	1.8145359	-2.8563403	0.7091253
H	1.8040030	-2.5608515	2.4406161
H	4.1417201	-4.4665746	0.3428677
H	5.4529939	-3.2982171	0.2048892
H	3.9165734	-3.0191742	-0.6241453
H	8.4065265	1.5332341	-0.1334802
H	7.7004989	-0.0814094	-0.0041842
H	7.7198966	0.9902957	1.4024615
H	5.1975798	1.9014637	-2.0066311
H	6.1494507	0.4120253	-1.9842643
H	6.9527264	1.9700816	-2.1038233
H	6.9757480	3.5684241	-0.2218263
H	6.3700105	3.1496987	1.3737214
H	5.2404871	3.4978169	0.0565156
H	-5.6205514	1.4563868	2.8181113
H	-3.9660228	2.0653337	2.8429644
H	-4.4818112	0.8603610	4.0274356
H	-5.9899946	-1.1116649	2.3257321
H	-4.6941971	-1.5126389	3.4303053
H	-4.6231911	-2.0853725	1.7719778
H	-2.5875448	-0.6167027	3.4148801
H	-2.0022773	0.5885337	2.2857921
H	-2.2540548	-1.0705733	1.7459303
H	-8.6614233	0.4391415	0.8672442
H	-7.5257545	1.7888115	0.9259193
H	-7.2240439	0.3315799	1.8709636
H	-8.6468725	0.1753385	-1.5085425
H	-7.1801278	0.2349703	-2.4727932

C	4.3693892	-3.4012692	0.2874500
C	6.2296699	1.5438155	-0.1136603
C	7.5968129	0.9558950	0.3179725
C	6.1153233	1.4445515	-1.6400329
C	6.1900890	3.0233610	0.3044031
C	-4.1249941	0.0299074	2.0473766
C	-4.5815692	1.1756158	2.9862730
C	-4.9145175	-1.2411284	2.3959978
C	-2.6527157	-0.2785601	2.3788787
C	-6.8621590	0.1001285	-0.2964527
C	-7.6021555	0.6993852	0.9208262
C	-7.6355271	0.5826929	-1.5444702
C	-6.9892280	-1.4353803	-0.2978951
C	-3.1464263	3.3200628	-1.8025109
C	-4.2661985	4.3851797	-1.8685406
C	-2.6846883	3.0138891	-3.2383400
C	-1.9846359	3.9211752	-0.9956476
H	5.0530345	-1.1601649	-0.5352846
H	4.6904694	1.9885406	2.3620313
H	-5.6307009	1.8353369	-2.1696903
H	-2.3146085	1.6043643	0.5406739
H	5.6553875	0.2355067	4.5378143
H	5.1586036	-1.4546807	4.5579297
H	4.6067001	-0.3617243	5.8265959
H	2.1840885	-0.7834213	5.4233253
H	2.6023864	-2.0055646	4.2412399
H	1.4823644	-0.7127932	3.8122350
H	4.0482925	2.0750664	4.2875542
H	2.9281302	1.3733480	5.4343390
H	2.3641653	1.8015838	3.8264785
H	4.1710022	-3.0533883	3.7020320
H	-7.7244443	1.6696755	-1.5823052
H	-6.4462339	-1.9192880	0.5057295
H	-6.6337202	-1.8502474	-1.2416397
H	-8.0420898	-1.7084733	-0.1967149
H	-4.6560976	4.6136057	-0.8742705
H	-5.0993805	4.0646523	-2.4960068
H	-3.8702184	5.3087021	-2.2957280
H	-2.3302403	3.9285525	-3.7189537
H	-3.5008251	2.6174359	-3.8449247
H	-1.8708612	2.2901025	-3.2528490
H	-2.3077948	4.2066667	0.0082815
H	-1.6182232	4.8202100	-1.4949616
H	-1.1482652	3.2301583	-0.9049085
Fe	2.8564757	-1.2246654	-3.2629451
O	3.2740941	1.6424213	-3.8172558
O	1.7921115	-1.3736838	-5.9924028
O	5.7070866	-1.8917059	-3.2805977
C	3.1301341	0.5302159	-3.5887502
C	2.1274908	-1.3294492	-4.8980681
C	4.5907818	-1.6165278	-3.2158727
C	2.4092277	-2.9345904	-2.8523648
O	2.1513441	-4.0135545	-2.5804988
Fe	-1.4801261	-2.5642966	-3.7854652
O	-1.4962581	-0.3686051	-5.7668546
O	-1.0189285	-4.4485546	-1.5581884
O	-4.1626424	-3.5797091	-4.3821861
O	0.3261371	-4.1690249	-5.4460052
C	-1.1992189	-3.7232349	-2.4238049
C	-3.1408212	-3.1318813	-4.1093757
C	-0.3207054	-3.4964036	-4.7801341
C	-1.4935038	-1.2253628	-5.0105212

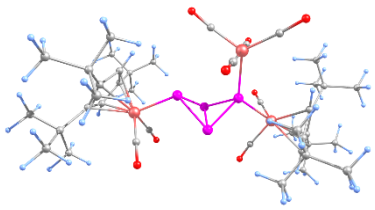

Table S20. Cartesian coordinates of the optimized geometry of **5*-3a** at the B3LYP/def2-TZVP level.

Atom	x	y	z
Fe	2.0793309	0.2736267	3.2246339
Fe	-2.9454652	0.1536534	-1.9354874
P	1.4461267	0.1572577	0.9430140
P	-0.4538325	1.2767035	0.5674032
P	-0.4940663	-0.9168433	0.6935399
P	-0.6107634	0.0703065	-1.3149180
O	0.9933693	-2.4011677	3.6251248
O	-0.4225520	1.4761262	4.1079041
O	-3.9536703	0.2289604	0.8024826
O	-2.5817427	3.0468184	-2.0644633
C	3.7617352	0.0315774	4.5668359
C	4.2273540	-0.1561367	3.1834256
C	3.9606979	1.0735218	2.5139471
C	3.3662949	2.0213627	3.3768867
C	3.2453352	1.3559104	4.6316242
C	-3.7003106	0.0281000	-3.9980492
C	-4.7941811	-0.1283596	-3.0365301
C	-4.4736863	-1.2981969	-2.2809072
C	-3.2540526	-1.8786047	-2.6994987
C	-2.7736602	-1.0252985	-3.7291100
C	3.9160851	-0.7646782	5.8818485
C	5.2303112	-0.2873230	6.5472521
C	3.9536284	-2.2955727	5.7563452
C	2.7577142	-0.4439439	6.8533606
H	2.7347631	0.6031129	7.1537048
H	2.8831592	-1.0323508	7.7639980
H	1.7891855	-0.6982313	6.4213024
H	6.2851106	-1.8517023	4.2178000
H	6.9277372	-0.4964844	3.2916414
H	7.0260852	-2.1379037	2.6505141
H	4.9804356	-3.3502840	1.9097934
H	3.4429125	-2.5166532	1.7111389
H	3.9786907	-3.0116746	3.3138677
H	5.9689091	-1.6395785	0.5673359
H	6.0120848	0.0618742	1.0144506
H	4.5083334	-0.6700083	0.4326210
H	4.4942409	5.2497822	3.1597258
H	5.3131053	3.7685587	2.6495824
H	4.9141924	4.0147545	4.3533317
H	1.7605800	3.3401481	1.4542124
H	3.4453858	3.3631932	0.9297926
H	2.6782408	4.8481227	1.4789434
H	2.1084249	5.2228148	3.8672349
H	2.4605442	4.0277206	5.1073516
H	1.1693593	3.7348735	3.9342465
H	-5.2338314	-0.1284647	-6.2651455
H	-3.6821799	-0.9240487	-6.5284407
H	-4.0564780	0.5818375	-7.3718678

C	0.5499548	1.0123147	3.7225367
C	1.4285125	-1.3579872	3.4421181
C	-3.4830765	0.2051753	-0.2375408
C	-2.7033387	1.9118084	-2.0236582
C	5.0475407	-1.2641209	2.4832598
C	6.3957579	-1.4472841	3.2150145
C	4.3127372	-2.6130285	2.3619364
C	5.3972284	-0.8394171	1.0403629
C	3.1837951	3.5085313	3.1029851
C	4.5627812	4.1730982	3.3314064
C	2.7409295	3.7722196	1.6555537
C	2.1689343	4.1502535	4.0623172
C	-3.5301863	0.8706164	-5.2810306
C	-4.1709523	0.0463093	-6.4267683
C	-4.1509102	2.2765023	-5.2718867
C	-2.0415300	1.0624168	-5.6294723
C	-6.1644504	0.5661532	-2.8512270
C	-7.0170918	0.3965582	-4.1285549
C	-6.9644328	-0.1152127	-1.7177994
C	-6.0672733	2.0544613	-2.4616637
C	-2.7834287	-3.2810296	-2.3393500
C	-3.5820384	-4.2529872	-3.2421788
C	-3.0777735	-3.6197714	-0.8687071
C	-1.2885590	-3.4792206	-2.6127902
H	4.1709819	1.2520047	1.4747209
H	2.8287977	1.8028224	5.5168129
H	-5.0899197	-1.6966705	-1.4951113
H	-1.8509509	-1.1714078	-4.2617259
H	5.2054397	0.7877098	6.7347227
H	6.1009047	-0.4980307	5.9269567
H	5.3681897	-0.7944307	7.5051808
H	4.0489070	-2.7247423	6.7559843
H	4.7969585	-2.6556958	5.1751182
H	3.0373653	-2.6909638	5.3198473
H	-5.2299215	2.2698024	-5.1546586
H	-3.9379289	2.7545136	-6.2299901
H	-3.7194661	2.9070255	-4.4950584
H	-1.9656862	1.6444936	-6.5495092
H	-1.5203763	0.1240499	-5.8048536
H	-1.5158628	1.6106922	-4.8497871
H	-8.0260736	0.7729158	-3.9462921
H	-7.0985869	-0.6570736	-4.4040766
H	-6.6173205	0.9362215	-4.9823882
H	-7.9178655	0.4025824	-1.6024173
H	-6.4507321	-0.0638532	-0.7570730
H	-7.1868593	-1.1601937	-1.9406654
H	-5.4841866	2.6470432	-3.1576901
H	-5.6194844	2.1628154	-1.4729728
H	-7.0705428	2.4850288	-2.4182933
H	-3.3924632	-4.0554057	-4.2991706
H	-4.6566115	-4.1661818	-3.0686519
H	-3.2871608	-5.2837360	-3.0327750
H	-2.7611486	-4.6429466	-0.6563311
H	-4.1431955	-3.5572917	-0.6386332
H	-2.5410807	-2.9566787	-0.1897526
H	-1.0310689	-3.2715666	-3.6526235
H	-1.0092471	-4.5143300	-2.4066833
H	-0.6821193	-2.8398995	-1.9757502
Fe	1.2570313	0.1055233	-2.7838171
O	2.0495609	-2.5627291	-1.8001284
O	0.4559895	2.8574232	-3.4897191
O	3.8892322	1.1411181	-1.9999444
O	1.0452196	-0.8854590	-5.5343646
C	0.7530049	1.7839815	-3.2249479
C	2.8431733	0.7431953	-2.2621013
C	1.0753207	-0.5020571	-4.4488239
C	1.7276620	-1.5331862	-2.1812251

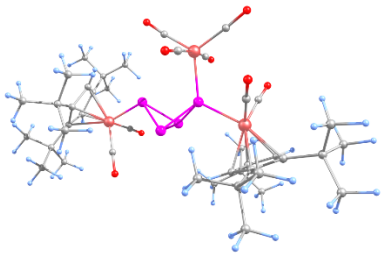

Table S21. Cartesian coordinates of the optimized geometry of **5*-3b** at the B3LYP/def2-TZVP level.

Atom	x	y	z
Fe	3.5295049	-0.5281371	0.0482690
Fe	-3.8170305	-0.5763168	0.1088743
P	1.4023294	-0.5729586	1.1139345
P	-0.0860733	-1.6643189	-0.1361774
P	-0.1414064	0.5350643	-0.0754119
P	-1.6211174	-0.6342449	1.1221477
O	2.4757279	0.7641573	-2.3398283
O	3.0908438	-3.1735008	-1.0914308
O	-4.4393120	-2.9633291	1.6742885
O	-4.3820718	1.3686919	2.2096111
C	5.4227152	0.5317340	0.0216523
C	4.5625359	1.1083579	1.0645625
C	4.3015611	0.0469752	1.9833248
C	4.9344569	-1.1510815	1.5898032
C	5.6061289	-0.8351090	0.3719703
C	-4.3780268	0.8459445	-1.4533333
C	-5.5164695	-0.0294668	-1.1337909
C	-5.0772557	-1.3491053	-1.4292737
C	-3.7570022	-1.3644434	-1.9522789
C	-3.3364638	-0.0134400	-1.9231443
C	6.2653077	1.1110390	-1.1368370
H	6.9913663	-0.8250303	-1.9179706
H	7.0447336	0.5020419	-3.0605812
H	5.4995186	-0.2556798	-2.6751094
H	5.9753379	3.5683014	0.7422490
H	6.0144278	2.9858473	2.4053579
H	5.0682684	4.4155714	1.9865481
H	2.9957093	4.2276495	0.6171167
H	2.2665210	2.6628274	0.2663089
H	3.6562770	3.2166805	-0.6596361
H	3.0092932	3.6049191	2.9171345
H	3.9111952	2.2401826	3.5648394
H	2.4148798	1.9711846	2.6545909
H	6.2385678	-2.9662169	4.1900785
H	5.6732228	-1.2927722	4.2158897
H	7.0311741	-1.7496740	3.1808081
H	3.0315251	-3.1553670	2.2672254
H	3.2799764	-2.0684359	3.6327413
H	3.9013777	-3.7136850	3.6977722
H	5.7785187	-4.4544802	2.2433686
H	6.6591962	-3.3333204	1.2136181
H	5.0262651	-3.8524529	0.7704477

C	7.6636163	1.4326772	-0.5536555
C	5.7195926	2.3716383	-1.8248403
C	6.4547792	0.0611675	-2.2551329
C	3.2323719	-2.1348895	-0.6306335
C	2.8670127	0.2744976	-1.3807665
C	-4.1572455	-2.0256770	1.0886257
C	-4.1461427	0.5952781	1.4042714
C	4.1244434	2.5529193	1.3955516
C	5.3749852	3.4270622	1.6376346
C	3.2152639	3.1962808	0.3307261
C	3.3188157	2.5786354	2.7131111
C	5.0817723	-2.4155169	2.4273621
C	6.0671049	-2.0815469	3.5726958
C	3.7423340	-2.8572748	3.0387660
C	5.6691482	-3.5746041	1.6064095
C	-4.2207010	2.3724136	-1.6377595
C	-4.5263913	2.6692448	-3.1272923
C	-5.1131488	3.2702582	-0.7671701
C	-2.7703495	2.8152641	-1.3576571
C	-7.0032966	0.2252753	-0.7857477
C	-7.6672020	0.9789908	-1.9605971
C	-7.7616386	-1.1144677	-0.6524586
C	-7.2490919	0.9727764	0.5382859
C	-3.1333891	-2.5481265	-2.6890697
C	-4.1273062	-2.9639255	-3.8007716
C	-2.9080195	-3.7548363	-1.7620327
C	-1.8159198	-2.1486908	-3.3692493
H	3.6852376	0.1416147	2.8595082
H	6.1926052	-1.5353613	-0.1953161
H	-5.6813497	-2.2301283	-1.3047630
H	-2.3678243	0.3273942	-2.2437769
H	8.1291384	0.5380383	-0.1365188
H	7.6123098	2.1813884	0.2364869
H	8.3157778	1.8177060	-1.3411906
H	6.4041434	2.6532433	-2.6277521
H	5.6477492	3.2240152	-1.1561298
H	4.7435127	2.1998923	-2.2769077
H	-5.5430582	2.3861978	-3.4001570
H	-3.8408459	2.1299091	-3.7830814
H	-4.4101157	3.7376416	-3.3230784
H	-6.1734924	3.1350384	-0.9584103
H	-4.8800517	4.3125258	-0.9938534
H	-4.9276102	3.1230447	0.2960041
H	-2.6881314	3.8907227	-1.5259838
H	-2.0422973	2.3337690	-2.0077804
H	-2.4845579	2.6173088	-0.3247454
H	-8.7426409	1.0546665	-1.7856908
H	-7.5175628	0.4432340	-2.9004071
H	-7.2840310	1.9884457	-2.0859636
H	-8.7990487	-0.9048440	-0.3876152
H	-7.3471766	-1.7455591	0.1355332
H	-7.7723544	-1.6797354	-1.5857399
H	-6.7306927	1.9217602	0.6071833
H	-6.9453896	0.3606741	1.3881043
H	-8.3180406	1.1715280	0.6442366
H	-4.3481812	-2.1269840	-4.4666769
H	-5.0700268	-3.3273637	-3.3881248
H	-3.6954415	-3.7677560	-4.4008861
H	-2.5336181	-4.6037276	-2.3386562
H	-3.8359938	-4.0683780	-1.2794874
H	-2.1795197	-3.5306273	-0.9837336
H	-1.9763156	-1.3553315	-4.1030085
H	-1.3996459	-3.0086428	-3.8977338
H	-1.0693057	-1.8095531	-2.6527521
Fe	-1.4389794	-0.7851245	3.4695660
O	-1.3308786	2.1645487	3.4613113
O	-1.3127797	-3.7088311	3.0746042
O	1.0460326	-0.8656359	5.0314980
O	-3.8968737	-0.9103587	5.0666305
C	-1.3759694	-2.5779373	3.2376883
C	0.0970917	-0.8340464	4.3823631
C	-2.9610782	-0.8590672	4.4013980
C	-1.3903513	1.0212588	3.4754706

Table S22. Cartesian coordinates of the optimized geometry of **5*-3c** at the B3LYP/def2-TZVP level.

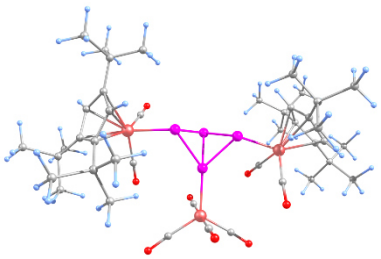

Atom	x	y	z
Fe	3.3124591	0.7247390	1.5080602
Fe	-2.9588402	-0.5477518	-2.1711958
P	1.0587145	0.1788362	1.0362914
P	0.7412533	-0.5179228	-1.0870453
P	-0.0742496	1.3967368	-0.4661375
P	-1.4067710	-0.3895112	-0.4031635
O	3.4767853	2.7499578	-0.5757370
O	4.2263550	-1.3205412	-0.3538017
O	-4.0615607	2.0389088	-1.4016930
O	-1.0151970	0.5283026	-4.0557560
C	4.5977713	1.7936628	2.9018357
C	3.2041270	1.9036460	3.3534719
C	2.7668436	0.5664926	3.5938101
C	3.7855023	-0.3719831	3.3257014
C	4.8992289	0.4032961	2.8854755
C	-3.1590727	-2.4586319	-3.2126827
C	-4.3134506	-1.6008934	-3.5041189
C	-4.9299550	-1.3473194	-2.2435996
C	-4.2509010	-2.0044248	-1.1831190
H	7.2342449	1.3237640	1.9568192
H	7.5537232	2.9828518	1.4941004
H	6.2834745	2.0782167	0.6720464
H	3.9129007	4.3480051	4.6376419
H	3.2003037	3.1889437	5.7583885
H	2.3080217	4.6388660	5.2910076
H	1.3922861	4.8949227	2.9790284
H	1.3960639	3.5484146	1.8427331
H	2.8634947	4.4733840	2.1188734
H	0.3436475	3.4622570	4.5611831
H	1.0661228	1.9877830	5.1943601
H	0.4054321	2.0256107	3.5492119
H	3.9517727	-2.9715512	5.5568582
H	3.0754813	-1.4467319	5.7335798
H	4.8346178	-1.4396937	5.5715067
H	2.3444439	-2.5506954	2.1989535
H	1.5911513	-2.0370217	3.7058216
H	2.4589720	-3.5690342	3.6377944
H	4.9305527	-3.6508252	3.3683940

C	-3.1594939	-2.6621399	-1.7985849
C	5.7517637	2.7971593	2.6771247
C	6.4968979	2.9277894	4.0286165
C	5.3621957	4.2026764	2.1940406
C	6.7576300	2.2504682	1.6386667
C	3.8367023	-0.5231454	0.3691155
C	3.3669154	1.9681126	0.2517436
C	-3.5920250	1.0389444	-1.6969753
C	-1.7683194	0.1129052	-3.3017073
C	2.3158218	3.0993751	3.7607210
C	2.9840349	3.8624326	4.9260120
C	1.9868344	4.0590565	2.6031342
C	0.9561022	2.5989319	4.2965219
C	3.7767633	-1.8503557	3.6951711
C	3.9181027	-1.9283278	5.2341223
C	2.4640134	-2.5359488	3.2828183
C	4.9581233	-2.6031190	3.0624937
C	-2.2061463	-3.3115954	-4.0795944
C	-2.9001106	-4.6803682	-4.2902372
C	-1.8245338	-2.7350041	-5.4518044
C	-0.8763891	-3.5740670	-3.3390900
C	-4.9835992	-1.1220586	-4.8122355
C	-5.4408832	-2.3438692	-5.6394599
C	-6.2628564	-0.3165906	-4.4944537
C	-4.1032603	-0.1920269	-5.6691762
C	-4.7673847	-2.1681841	0.2419045
C	-6.0502933	-3.0287979	0.1641172
C	-5.1174859	-0.8140891	0.8825407
C	-3.7465247	-2.8971779	1.1296130
H	1.7768703	0.3045338	3.9212082
H	5.8499405	-0.0092032	2.5989989
H	-5.8106334	-0.7439337	-2.1103676
H	-2.4304306	-3.2511220	-1.2717805
H	6.8734400	1.9598699	4.3642239
H	5.8517017	3.3251305	4.8119428
H	7.3487302	3.6030339	3.9193482
H	6.2736685	4.7892811	2.0618066
H	4.7401012	4.7401142	2.9032199
H	4.8514909	4.1790275	1.2323923
H	5.9180994	-2.1961483	3.3864860
H	4.9245186	-2.5771787	1.9731013
H	-3.8423127	-4.5825596	-4.8284578
H	-3.1090768	-5.1635361	-3.3339939
H	-2.2489081	-5.3410965	-4.8673504
H	-2.6755166	-2.6119670	-6.1150922
H	-1.1370171	-3.4276444	-5.9416249
H	-1.3111857	-1.7783462	-5.3630568
H	-0.2214471	-4.1628292	-3.9836856
H	-1.0104600	-4.1430705	-2.4196507
H	-0.3579941	-2.6469569	-3.0945535
H	-6.0234642	-2.0075067	-6.5000546
H	-6.0756483	-3.0023681	-5.0425531
H	-4.6098661	-2.9328613	-6.0189050
H	-6.7092509	0.0194775	-5.4315864
H	-6.0512466	0.5730482	-3.8992494
H	-7.0101020	-0.9177664	-3.9733620
H	-3.1452147	-0.6260011	-5.9324901
H	-3.9135010	0.7453778	-5.1453364
H	-4.6256171	0.0477262	-6.5985656
H	-5.8477999	-3.9960508	-0.3007303
H	-6.8308594	-2.5325385	-0.4159196
H	-6.4416454	-3.2108066	1.1677626
H	-5.5685701	-0.9727549	1.8646982
H	-5.8336018	-0.2519441	0.2800985
H	-4.2274692	-0.1987358	1.0170807
H	-3.5281164	-3.8981375	0.7503791
H	-4.1525849	-3.0107280	2.1370112
H	-2.8100897	-2.3433833	1.2051966
Fe	-0.1934749	3.4885831	-1.4091412
O	-2.0956134	4.2470886	0.7269742
O	1.7385494	2.5988066	-3.4684990
O	1.5788888	5.7026834	-0.6435984
C	-1.3657225	3.9522468	-0.1001667
C	0.9958763	2.9367512	-2.6729130
C	0.9126428	4.8075420	-0.9095300
O	-2.1766904	4.0733698	-3.4944097
C	-1.4217326	3.7994322	-2.6753620

4.6.5 Crystallographic details

[{Cp‴Fe(CO)$_2$}$_2$(μ$_3$,η$^{1:1:1:1}$-P$_4$){Cr(CO)$_4$}] (**2a**)

Compound **2a** crystalizes in the form of green-blackish needles from a saturated solution in *n*-pentane/CH_2Cl_2 upon storage at -28°C. A suitable crystal with dimensions 0.41 × 0.10 × 0.06 mm^3 was selected and mounted on a Xcalibur, AtlasS2, Gemini ultra diffractometer. The crystal was kept at a steady T = 123(1) K during data collection. The structure was solved with the ShelXT (Sheldrick, 2015) solution program using Olex2 (Dolomanov et al., 2009) as the graphical interface. The model was refined with ShelXL 2018/3 (Sheldrick, 2015) using full matrix least squares minimization on F^2. The asymmetric unit contains two molecules of **2a**, which display a cis- and trans-arrangement of the tert-butyl groups of the Cp‴ ligand, respectively, as well as one disordered CH_2Cl_2 molecule.

[{Cp‴Fe(CO)$_2$}$_2$(μ$_3$,η$^{1:1:1:1}$-P$_4$){Mo(CO)$_4$}] (**2b**)

Compound **2b** crystalizes in the form of orange-red needles from a saturated solution in *n*-pentane/CH_2Cl_2 upon storage at -28°C. A suitable crystal with dimensions 0.23 × 0.04 × 0.03 mm^3 was selected and mounted on a GV50, TitanS2 diffractometer. The crystal was kept at a steady T = 89.9(4) K during data collection. The structure was solved with the ShelXT 2018/2 (Sheldrick, 2018) solution program using Olex2 (Dolomanov et al., 2009) as the graphical interface. The model was refined with ShelXL 2018/3 (Sheldrick, 2015) using full matrix least squares minimization on F^2. The asymmetric unit contains two molecules of **2b**, which display a cis- and trans-arrangement of the tert-butyl groups of the Cp‴ ligand, respectively, as well as one disordered CH_2Cl_2 molecule.

[{Cp‴Fe(CO)$_2$}$_2$(μ$_3$,η$^{1:1:1:1}$-P$_4$){W(CO)$_4$}] (**2c**)

Compound **2c** crystalizes in the form of dark brown needles from a saturated solution in *n*-pentane/CH_2Cl_2 upon storage at -28°C. A suitable crystal with dimensions 0.26 × 0.07 × 0.03 mm^3 was selected and mounted on a Xcalibur, AtlasS2, Gemini ultra diffractometer. The crystal was kept at a steady T = 123 K during data collection. The structure was solved with the ShelXT 2014/5 (Sheldrick, 2014) solution program using Olex2 (Dolomanov et al., 2009) as the graphical interface. The model was refined with ShelXL 2018/3 (Sheldrick, 2015) using full matrix least squares minimization on F^2.The asymmetric unit contains two molecules of **2c**, which display a cis- and trans-arrangement of the tert-butyl groups of the Cp‴ ligand, respectively, as well as one disordered CH_2Cl_2 molecule.

[{Cp‴Fe(CO)$_2$}$_2$(μ$_3$,η$^{1:1:1:1}$-P$_4$){Au(PPh$_3$)}]$^+$[PF$_6$]$^-$ (**2d**)

Compound **2d** crystallizes as orange plates from THF/hexane mixtures. The crystals were heavily intergrown. A suitable crystal with dimensions 0.22 × 0.07 × 0.01 mm^3 was selected and mounted on a Xcalibur, Ruby, Gemini ultra diffractometer. The crystal was kept at a steady T = 123(1) K during data collection. The structure was solved with the olex2.solve (Bourhis et al., 2015) solution program using Olex2 (Dolomanov et al., 2009) as the graphical interface. The model was refined with ShelXL 2018/3 (Sheldrick, 2015) using full matrix least

squares minimisation on F^2. Even though, the largest single crystal that could be found was used, only a diffraction limit of 1.0 Å was obtained. Therefore, only very rough values can be obtained for the parameters of the molecular structure. The asymmetric unit contains one molecule of **2d**.

[{(Cp‴Fe(CO)$_2$)$_2$(μ$_3$,η$^{1:1:1:1}$-P_4)}$_2$Ag]$^+$[PF_6]$^-$ (**3**)

Compound **3** crystallizes as orange plates from THF/hexane mixtures. A suitable crystal with dimensions 0.51 × 0.19 × 0.05 mm^3 was selected and mounted on a Xcalibur, Ruby, Gemini ultra diffractometer. The crystal was kept at a steady T = 123(1) K during data collection. The structure was solved with the olex2.solve (Bourhis et al., 2015) solution program using Olex2 (Dolomanov et al., 2009) as the graphical interface. The model was refined with ShelXL 2018/3 (Sheldrick, 2015) using full matrix least squares minimisation on F^2. The asymmetric unit contains two molecules of **3** together with seven molecules of THF. The crystals were twinned by inversion.

[{Cp‴(CO)$_2$Fe}$_2$(μ$_4$,η$^{1:1:2:2}$-P_4){Co(CO)$_3$}$_2$] (**4**)

Compound **4** crystalizes in the form of dark brown needles from a saturated solution in CH_2Cl_2 upon storage at -28°C. A suitable crystal with dimensions 0.27 × 0.09 × 0.07 mm^3 was selected and mounted on an Oxford Diffraction Gemini Ultra diffractometer. The crystal was kept at a steady T = 123 K during data collection. The structure was solved with the SIR-97 (Altomare, 1999) solution. The model was refined with ShelXL 2018/3 (Sheldrick, 2015) using full matrix least squares minimisation on F^2. The asymmetric unit contains one molecule of **4** as well as one solvent molecule.

[{Cp‴Fe(CO)$_2$}$_2$(μ$_4$,η$^{1:1:1:3}$-P_4CO){Fe(CO)$_4$}{Fe(CO)$_3$}] (**5**)

Compound **5** crystalizes a saturated solution in toluene upon storage at -12°C . A suitable crystal with dimensions 0.12 × 0.08 × 0.02 mm^3 was selected and mounted on a STOE-IPDS diffractometer. The crystal was kept at a steady T = 123.15 K during data collection. The structure was solved with the olex2.solve (Bourhis et al., 2015) solution program using Olex2 (Dolomanov et al., 2009) as the graphical interface. The model was refined with ShelXL 2018/3 (Sheldrick, 2015) using full matrix least squares minimisation on F^2. The asymmetric unit contains one molecule of **5** as well as one solvent molecule.

Table S23. Overview of selected crystallographic parameters of the single crystal X-ray diffraction experiments performed for **2a**-**2d**.

	2a	**2b**	**2c**	**2d**
Formula	$C_{84.8}H_{117.6}Cl_{1.6}Cr_2Fe_4O_{16}P_8$	$C_{85}Cl_2Fe_4H_{118}Mo_2O_{16}P_8$	$C_{85}Cl_2Fe_4H_{118}O_{16}P_8W_2$	$C_{56}H_{73}AuF_6Fe_2O_4P_6$
$D_{calc.}$**/g cm^{-3}**	1.397	1.457	1.575	1.587
μ**/mm^{-1}**	8.647	8.953	11.140	10.472
Formula Weight	2024.86	2129.73	2305.55	1418.63
Colour	dark green	orange	dark brown	orange
Shape	block	needle	needle	plate
Size/mm^3	0.41×0.10×0.06	0.23×0.04×0.03	0.26×0.07×0.03	0.22×0.07×0.01
***T*/K**	123(1)	89.9(4)	123	123(1)
Crystal System	monoclinic	monoclinic	monoclinic	monoclinic
Space Group	*C*2/*c*	*I*2/*a*	*C*2/*c*	$P2_1/n$
***a*/Å**	47.5807(11)	42.0710(8)	47.552(2)	9.9443(7)
***b*/Å**	12.02710(14)	12.0572(3)	12.0517(3)	31.748(2)
***c*/Å**	41.8909(10)	40.7112(11)	42.166(2)	19.0838(12)
***α*/°**	90	90	90	90
***β*/°**	126.538(3)	109.898(2)	126.439(7)	99.739(7)
***γ*/°**	90	90	90	90
V/Å^3	19260.9(10)	19418.2(8)	19441(2)	5938.1(7)
Z	8	8	8	4
Z'	1	1	1	1
Wavelength/Å	1.54184	1.54184	1.54184	1.54178
Radiation type	Cu K_α	Cu K_α	Cu K_α	Cu K_α
Q_{min}**/°**	3.718	3.720	3.721	3.643
Q_{max}**/°**	66.410	74.008	66.380	51.531
Measured Refl's.	47023	52607	54192	11651
Ind't Refl's	16658	19176	16841	6205
Refl's with I > 2(I)	14371	15514	13828	4460
R_{int}	0.0409	0.0538	0.0693	0.0546
Parameters	1090	1063	1063	694
Restraints	13	0	0	0
Largest Peak	1.042	1.186	2.138	1.434
Deepest Hole	-0.894	-1.285	-1.550	-0.843
GooF	1.041	1.031	1.020	0.978
wR_2 **(all data)**	0.0986	0.1231	0.1310	0.1025
wR_2	0.0934	0.1140	0.1220	0.0891
R_1 **(all data)**	0.0482	0.0630	0.0636	0.0824
R_1	0.0390	0.0478	0.0503	0.0480

Table S24. Overview of selected crystallographic parameters of the single crystal X-ray diffraction experiments performed for **3**, **4** and **5**.

	3	**4**	**5**
Formula	$C_{90.8}H_{145.6}AgF_6Fe_4O_{11.7}P_9$	$C_{45}H_{60}Cl_2Co_2Fe_2O_{10}P_4$	$C_{49.5}H_{62}Fe_4O_{12}P_4$
***D*$_{calc.}$/ g cm^{-3}**	1.370	1.498	1.435
***μ*/mm^{-1}**	7.676	11.713	1.199
Formula Weight	2148.46	1185.27	1196.27
Colour	orange	brown	brown
Shape	plate	needle	needle
Size/mm^3	0.51×0.19×0.05	0.27×0.09×0.07	0.12×0.08×0.02
***T*/K**	123(1)	123	123.15
Crystal System	monoclinic	monoclinic	triclinic
Flack Parameter	0.176(3)	-0.012(3)	-
Hooft Parameter	0.179(2)	0.000(3)	-
Space Group	*Cc*	*Cc*	*P*-1
***a*/Å**	17.91660(10)	10.0351(2)	11.656(2)
***b*/Å**	37.5514(2)	20.2508(5)	15.514(3)
***c*/Å**	17.34270(10)	26.2400(5)	17.863(4)
***α*/°**	90	90	66.07(3)
***β*/°**	116.7650(10)	99.668(2)	78.41(3)
***γ*/°**	90	90	70.06(3)
V/Å^3	10417.95(13)	5256.7(2)	2768.2(13)
Z	4	4	2
Z'	1	1	1
Wavelength/Å	1.54178	1.54184	0.71073
Radiation type	Cu K$_α$	Cu K$_α$	MoK□
***Q*$_{min}$/°**	3.172	3.417	1.863
***Q*$_{max}$/°**	66.577	66.738	24.914
Measured Refl's.	40334	11828	18291
Ind't Refl's	13176	5836	8946
Refl's with I > 2(I)	13032	5277	6306
***R*$_{int}$**	0.0422	0.0328	0.0484
Parameters	1298	604	741
Restraints	527	2	227
Largest Peak	0.787	0.545	0.503
Deepest Hole	-0.452	-0.351	-0.461
GooF	1.033	0.984	0.891
***wR*$_2$ (all data)**	0.0810	0.0744	0.0971
***wR*$_2$**	0.0807	0.0731	0.0918
***R*$_1$ (all data)**	0.0319	0.0345	0.0595
***R*$_1$**	0.0316	0.0300	0.0402

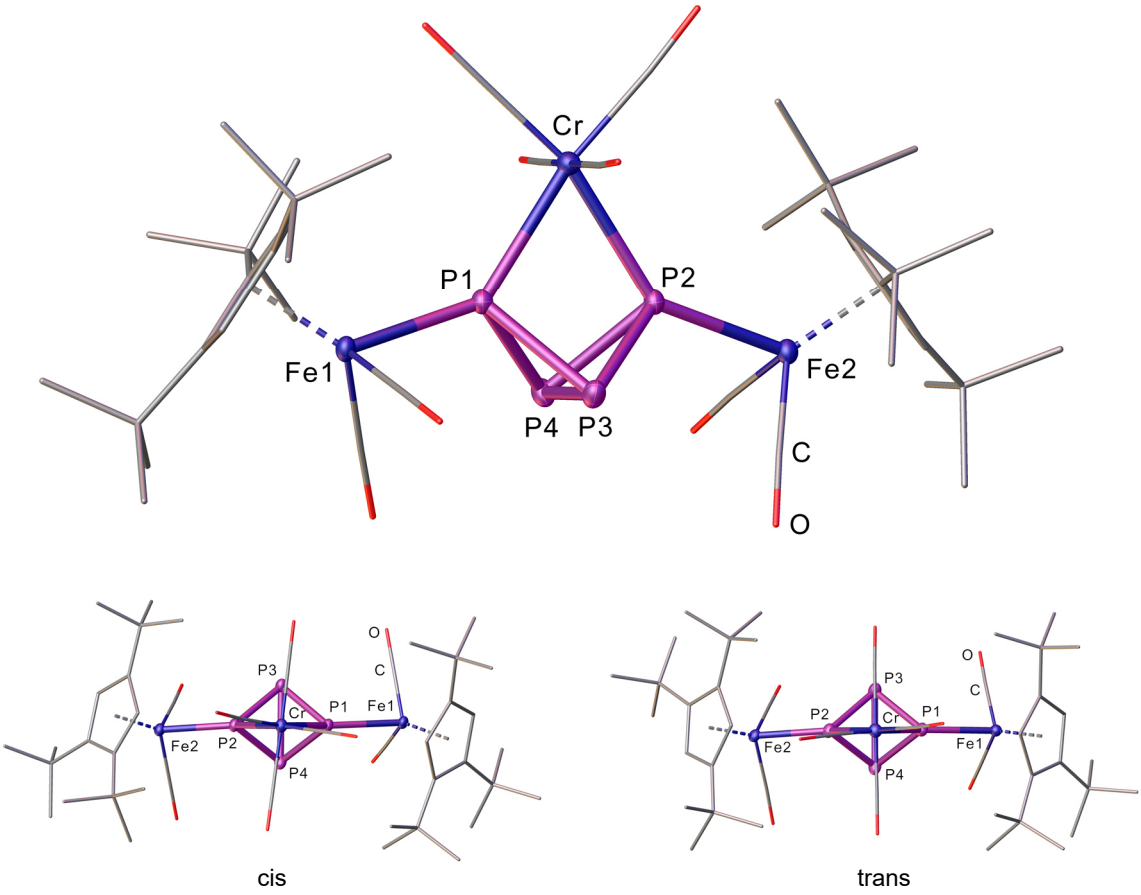

Figure S17. Molecular structure of the two isomers of **2a** in the solid state; for clarity H atoms and solvent molecules are omitted; thermal ellipsoids drawn at 50% probability (molecular structures of **2b** and **2c** are structurally identical)

Table S25. Selected bond lengths [Å] and angles [°] of both isomers of **2a**, **2b** and **2c** in the solid state.

		2a M =Cr		**2b** M = Mo		**2c** M = W	
		cis	trans	cis	trans	cis	trans
d [Å]	**Fe1–P1**	2.3042(8)	2.3167(8)	2.2958(11)	2.3064(12)	2.2929(17)	2.3009(18)
	Fe2–P2	2.3063(8)	2.3155(8)	2.2952(10)	2.3010(12)	2.2924(16)	2.3049(16)
	M–P1	2.4709(8)	2.4682(9)	2.6085(10)	2.5724(11)	2.6030(15)	2.5817(16)
	M–P2	2.4904(8)	2.4869(8)	2.5877(9)	2.5934(10)	2.5916(14)	2.5989(14)
	P1–P3	2.2243(10)	2.2116(10)	2.2238(12)	2.2320(14)	2.208(2)	2.215(2)
	P1–P4	2.2309(10)	2.2273(10)	2.2070(13)	2.2121(14)	2.227(2)	2.230(2)
	P2–P3	2.2213(10)	2.2260(11)	2.2250(13)	2.2273(14)	2.232(2)	2.227(2)
	P2–P4	2.2072(9)	2.2203(10)	2.2303(14)	2.2321(15)	2.226(2)	2.216(2)
	P1··P2	2.731(10)	2.745(10)	2.777(10)	2.799(10)	2.777(10)	2.786(10)
	P3–P4	2.2055(10)	2.2071(11)	2.2036(14)	2.2073(15)	2.204(2)	2.206(2)
α [°]	**P1–M–P2**	66.80(2)	67.27(3)	64.61(3)	65.62(3)	64.62(5)	65.07(5)
	P1–P3–P2	75.81(3)	76.41(4)	77.25(4)	77.76(5)	77.40(7)	77.69(8)
	P1–P4–P2	75.96(3)	76.21(3)	77.48(5)	78.07(5)	77.15(7)	77.60(7)
	P3–P1–P4	59.34(3)	59.63(3)	59.65(4)	59.56(5)	59.60(7)	59.50(7)
	P3–P2–P4	59.74(3)	59.52(4)	59.29(4)	59.34(5)	59.26(7)	59.54(7)

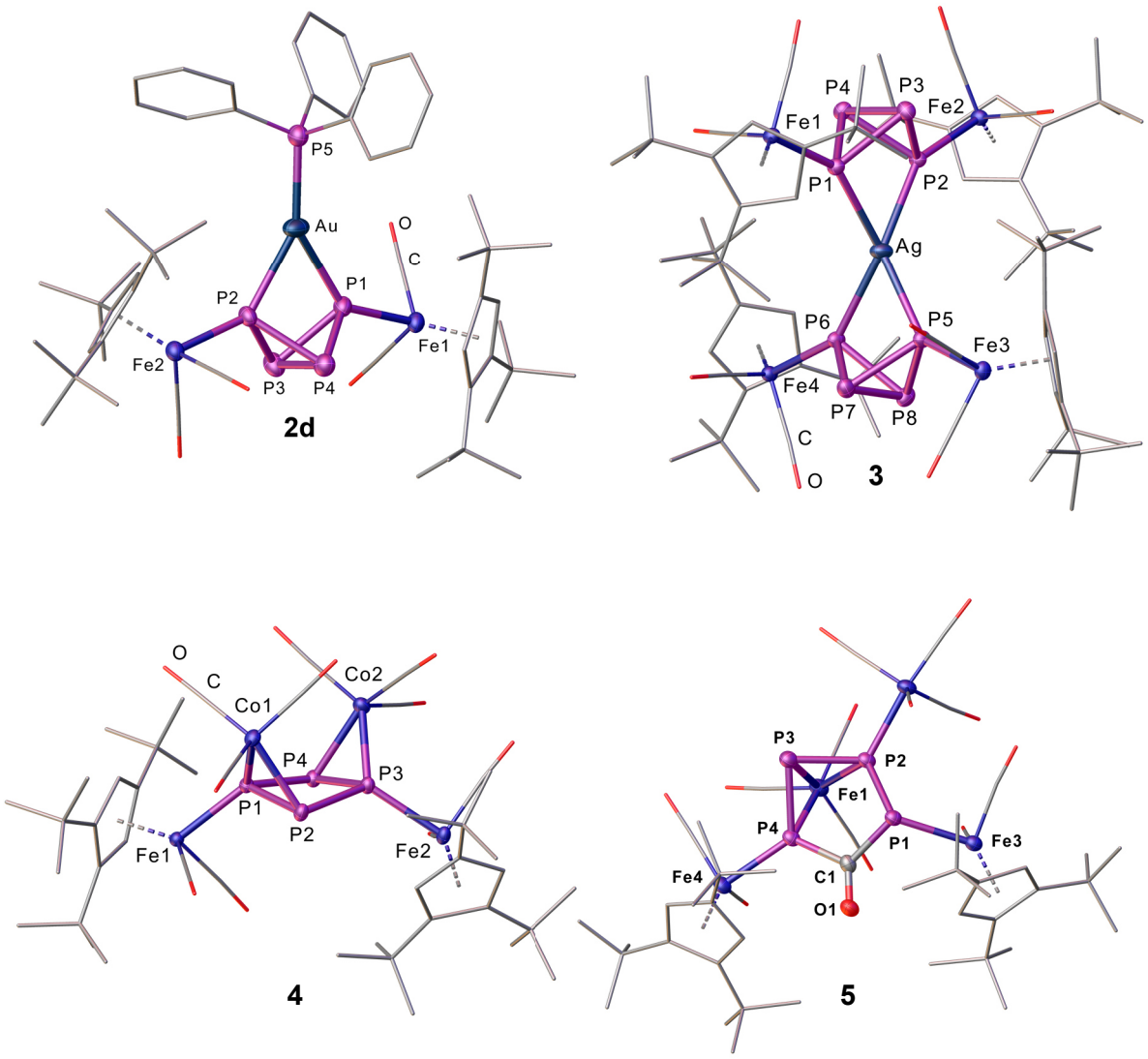

Figure S18. Molecular structure of the cationic fragments of **2d** and **3** as well as **4** and **5** in the solid state; for reasons of clarity H atoms and solvent molecules are omitted; thermal ellipsoids drawn at 50% probability level

Table S26. Selected bond lengths [Å] and angles [°] of **2d** in the solid state; due to the low diffraction limit of the crystallographic experiment, the parameters are not reliable.

d / Å				α / °	
Fe1–P1	2.281(3)	**P1–P3**	2.204(3)	**P1–Au–P2**	68.16(7)
Fe2–P2	2.270(3)	**P1–P4**	2.210(3)	**P1–Au–P5**	146.84(8)
Au–P1	2.480(2)	**P2–P3**	2.220(3)	**P2–Au–P5**	144.65(8)
Au–P2	2.557(2)	**P2–P4**	2.223(3)	**P1–P3–P2**	79.31(11)
Au–P5	2.292(2)	**P1··P2**	2.823	**P1–P4–P2**	79.10(11)
		P3–P4	2.183(3)	**P3–P1–P4**	59.27(11)
				P3–P2–P4	58.85(10)

Table S27. Selected bond lengths [Å] and angles [°] of **3** in the solid state.

d / Å				α / °			
Ag–P1	2.6340(9)	**P1–P3**	2.2194(14)	**P1–Ag–P2**	67.07(3)	**P1–P3–P2**	81.12(4)
Ag–P2	2.5884(9)	**P1–P4**	2.2189(13)	**P5–Ag–P6**	66.07(3)	**P1–P4–P2**	81.06(4)
Ag-P5	2.6109(9)	**P2–P3**	2.2181(13)	**P1–Ag–P5**	130.22(3)	**P3–P1–P4**	58.91(4)
Ag-P6	2.6161(9)	**P2–P4**	2.2213(13)	**P1–Ag–P6**	129.34(3)	**P3–P2–P4**	58.89(4)
P1-Fe1	2.3011(11)	**P3-P4**	2.1824(13)	**P2–Ag–P5**	137.19(3)	**P5–P7–P6**	79.95(5)
P2-Fe2	2.2987(11)	**P5–P7**	2.2242(14)	**P2–Ag–P6**	139.69(3)	**P5–P8–P6**	79.83(4)
P5-Fe3	2.3035(11)	**P5–P8**	2.2198(13)			**P7–P5–P8**	58.58(5)
P6-Fe4	2.3032(11)	**P6–P7**	2.2112(13)			**P7–P6–P8**	58.75(5)
P1··P2	2.885	**P6–P8**	2.2214(13)				
P5··P6	2.850	**P7-P8**	2.1742(15)				

Table S28. Selected bond lengths [Å] and angles [°] of **4** in the solid state.

d / Å				α / °			
Co1–P1	2.2666(15)	**Fe2–P3**	2.2877(15)	**P1–Co1–P2**	56.07(5)	**P2–P1–P4**	91.22(7)
Co1–P2	2.2759(15)	**P1–P4**	2.2924(17)	**P3–Co2–P4**	56.24(5)	**P1–P2–P3**	87.10(6)
Co2–P3	2.2441(15)	**P1–P2**	2.1351(18)	**Co1–P1–Fe1**	125.65(6)	**P2–P3–P4**	91.53(7)
Co2–P4	2.2872(15)	**P2–P3**	2.2804(17)	**Co2–P3–Fe2**	121.80(6)	**P1–P4–P3**	86.77(6)
Fe1–P1	2.2958(15)	**P3–P4**	2.1360(18)	**Co1–P1–P2**	62.18(5)	**P3–P1–P2–P4**	13.3(9)
				Co1–P1–P4	119.23(6)		

Table S29. Selected bond lengths [Å] and angles [°] of **5** in the solid state.

d / Å				α / °			
P1–P2	2.2114(15)	**Fe1–P2**	2.3205(15)	**C1–P1–P2**	94.17(13)	**P1–P2–Fe1**	115.36(5)
P2–P3	2.1623(14)	**Fe1–P3**	2.4079(13)	**C1–P1–Fe3**	112.48(12)	**P2–P3–P4**	85.45(6)
P3–P4	2.1876(15)	**Fe3–P1**	2.3202(12)	**P3–P2–P1**	103.44(6)	**P2–P3–Fe1**	60.75(5)
P4–C1	1.909(4)	**Fe4–P4**	2.2824(14)	**P3–P2–Fe2**	116.61(5)	**P4–P3–Fe1**	60.24(5)
P1–C1	1.855(4)	**Fe2–P2**	2.2865(14)	**P1–P2–Fe2**	113.86(5)	**C1–P4–P3**	108.05(12)
		Fe1–P4	2.3139(13)	**P3–P2–Fe1**	64.87(4)	**C1–P4–Fe4**	118.02(11)
				P3–P4–Fe1	64.61(4)	**P1–C1–P4**	115.18(19)

4.6.6 References

[1] C. Schwarzmaier, A. Y. Timoshkin, G. Balázs, M. Scheer, *Angew. Chem. Int. Ed.* **2014**, *53*, 9077-9081.

[2] R. B. King, A. Frozalia, *Inorg. Chem.* **1966**, *5*, 1837.

[3] V. Riera, J, Ruiz, *J. Chem. Soc. Dalton Trans*. **1990**, *1*, 1607-1611.

[4] (a) E. Speyer, H. Wolf, *Ber. Dtsch. Chem. Ges*. **1927**, *60*, 1424.
(b) D. F. Keely, R. E. Johnson, *J. Inorg. Nucl. Chem.* **1959**, *11*, 33.

[5] (a) P. Szabo, L. Marko, G. Bor, *Chem. Techn.* **1961**, *13*, 549.
(b) I. Wender, H. W. Sternberg, S. Metlin, M. Orchin, *Inorg. Synth.* **1957**, *5*, 190.

[6] TopSpin 3.0, Bruker BioSpin GmbH

[7] (a) F. Furche, R. Ahlrichs, C. Hättig, W. Klopper, M. Sierka, F. Weigend, *WIREs Comput. Mol. Sci.* **2014**, *4*, 91-100.
(b) R. Ahlrichs, M. Bär, M. Häser, H. Horn, C. Kölmel, *Chem. Phys. Lett.* **1989**, *162*, 165-169.
(c) O. Treutler, R. Ahlrichs, *J. Chem. Phys.* **1995**, *102*, 346-354.
(d) TURBOMOLE V6.4, a development of University of Karlsruhe and Forschungszentrum Karlsruhe GmbH, http://www.turbomole.com.

[8] (a) K. Eichkorn, O. Treutler, H. Oehm, M. Häser, R. Ahlrichs, *Chem. Phys. Lett.* **1995**, *242*, 652-660.
(b) K. Eichkorn, F. Weigend, O. Treutler, R. Ahlrichs, *Theor. Chem. Acc.* **1997**, *97*, 119.

[9] (a) A. D. Becke, *J. Chem. Phys.* **1993**, *98*, 5648-5652.
(b) C. Lee, W. Yang, R. G. Parr, *Phys. Rev. B* **1988**, *37*, 785-789.
(c) A. D. Becke, *Phys. Rev. A* **1988**, *38*, 3098-3100.
(d) S. H. Vosko, L. Wilk, M. Nusair, *Can. J. Phys.* **1980**, *58*, 1200-1211.
(e) J. C. Slater, *Phys. Rev.* **1951**, *81*, 385-390.

[10] (a) A. Schäfer, C. Huber, R. Ahlrichs, *J. Chem. Phys.* **1994**, *100*, 5829.
(b) K. Eichkorn, F. Weigend, O. Treutler, R. Ahlrichs, *Theor. Chem. Acc.* **1997**, *97*, 119.
(c) F. Weigend, R. Ahlrichs, *Phys. Chem. Chem. Phys.* **2005**, *7*, 3297.
(d) F. Weigend, *Phys. Chem. Chem. Phys.* **2006**, *8*, 1057.

[11] (a) K. Eichkorn, O. Treutler, H. Ohm, M. Häser, R. Ahlrichs, *Chem. Phys. Lett.* **1995**, *242*, 652-660.
(b) M. Sierka, A. Hogekamp, R. Ahlrichs, *J. Chem. Phys.* **2003**, *118*, 9136-9148.

[12] F. Weigend, *Phys. Chem. Chem. Phys.* **2006**, *8*, 1057-1065.

[13] NBO 6.0. E. D. Glendening, J. K. Badenhoop, A. E. Reed, J. E. Carpenter, J. A. Bohmann, C. M. Morales, C. R. Landis, F. Weinhold (Theoretical Chemistry Institute, University of Wisconsin, Madison, WI, **2013**); http://nbo6.chem.wisc.edu/

[14] (a) R. F. W. Bader, *Atoms in Molecules: A Quantum Theory*, Oxford University Press, **1994**.
(b) R. F. W. Bader, *Chem. Rev.* **1991**, *91*, 893-928.

[15] (a) T. Lu, F. Chen, *J. Comput. Chem.* **2012**, *33*, 580-592.
(b) http://sobereva.com/multiwfn

4.7 Author contributions

Rebecca Grünbauer

- Synthesis and characterization of compounds **2a**, **2b** and **2c**.
- Preparation of manuscript (including figures, schemes, tables and supplementary information) except for paragraphs on the topic of DFT calculations and Figures S11, S12, S13, S14 and S15.

Christoph Schwarzmaier

- Synthesis and characterization of compounds **2d** and **3**.

  The synthesis and characterization of compounds **2d** and **3** was already performed within the scope of the Ph. D. thesis of Christoph Schwarzmaier *(University of Regensburg,* **2012**) and the results are also included therein.

Miriam Eberl

- Synthesis and characterization of compounds **4**, **5** and **5***.
- Preparation of Figures S11, S12, S13, S14 and S15.

  The synthesis and characterization of compounds **5*** and **5** was already performed within the scope of the diploma thesis of Miriam Eberl *(University of Regensburg,* **2006**) and the synthesis and characterization of compound **4** was already performed within the scope of the Ph. D. thesis of Miriam Eberl *(University of Regensburg,* **2011**). The results are also included in the respective theses.

Gábor Balázs

- Execution of DFT calculations.
- Preparation of manuscript (including figures, schemes, tables and supplementary information) for paragraphs on the topic of DFT calculations.

Manfred Scheer

- Supervision of project.

5. Reactivity of P_4 butterfly compounds towards NHCs: Generation of a novel metal bridged P_2 dumbbell complex

Rebecca Grünbauer, Stephan Reichl, Gábor Balázs and Manfred Scheer

5.1 Abstract

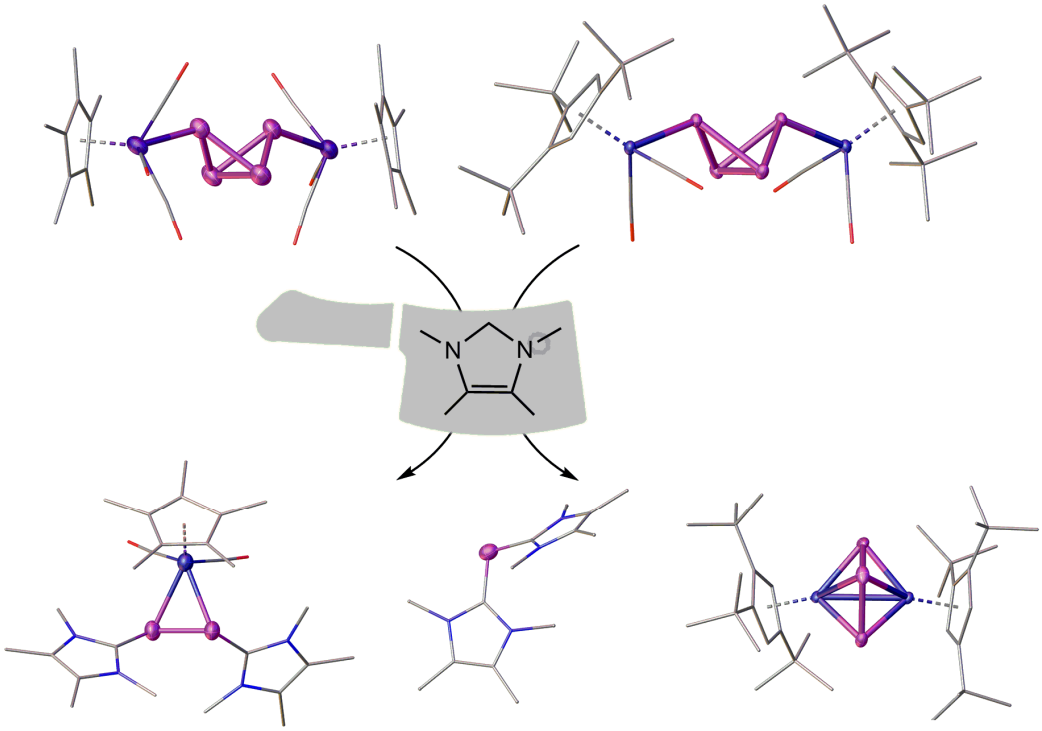

*Herein, we report on a novel reactivity of [{Cp'''Fe(CO)$_2$}$_2$(μ,η$^{1:1}$-P$_4$)] (**A**, Cp''' = C$_5$H$_2$^{t}Bu$_3$) and [{Cp*Cr(CO)$_3$}$_2$(μ,η$^{1:1}$-P$_4$)] (**B**, Cp* = C$_5$(CH$_3$)$_5$) towards the N-heterocyclic carbene IMe (1,3,4,5-tetramethyl-imidazol-2-ylidene). Depending on the reaction temperature, the reaction of **A** with IMe selectively affords either [P(IMe)$_2$][Fe(CO)$_2$Cp'''] (**1**) or [P(IMe)$_2$][{Cp'''Fe}$_2$(μ,η$^{3:3}$-P$_3$)] (**2**). In contrast, the reaction of **B** with IMe yields [P(IMe)$_2$][Cr(CO)$_3$Cp*] (**3**) and [{Cp*Cr(CO)$_2$}(η^2-P$_2$IMe$_2$)][Cr(CO)$_3$Cp*] (**4**) simultaneously. Compound **2** is an anionic diiron complex containing an allylic P$_3$ ligand, whereas **4** represents a novel cationic metal bridged P$_2$ dumbbell compound. In **4** the P$_2$ dumbbell is bridged by an unsaturated [Cr(CO)$_2$Cp*] fragment accompanied by the additional end-on coordination of two IMe ligands. Compounds **1** and **2** as well as the crystalline mixture of **3** and **4** could be characterized by NMR spectroscopy and ESI-MS spectrometry alongside with single crystal X-ray diffraction analysis.*

5.2 Introduction

The reactivity of polyphosphorus (P_n) ligand complexes (n≤4) has been intensively studied over the last decades.[1] The ultimate goal of these studies is to develop a more sustainable, economical and safer generation of phosphorus containing compounds on an academic and an industrial scale, respectively. One common feature of all polyphosphorus ligands is the vast opportunity for coordination originating from the accessible lone pairs on every P atom. Due to this coordination potential, P_n ligands are mostly stabilized in the coordination sphere of unsaturated organometallic[1a-b] or main group[1c-d] moieties. However, in most cases the resulting P_n ligand complexes nevertheless display additional electron lone pairs rendering them available for further coordination processes. Within this field, the tetraphospha-*bicyclo*[1.1.0]butane structural motif is of major interest as it represents the P_4 scaffold obtained after the first reductive P–P bond cleavage during the activation of the P_4 tetrahedron.[2] [{Cp‴Fe(CO)$_2$}$_2$(μ,η$^{1:1}$-P_4)] (**A**, Cp‴ = $C_5H_2{}^tBu_3$) and [{Cp*Cr(CO)$_3$}$_2$(μ,η$^{1:1}$-P_4)] (**B**, Cp* = $C_5(CH_3)_5$), two prominent examples for the class of so called P_4 butterfly compounds (due to the intrinsic geometry of the central P_4 unit) are accessible in remarkably high yields (>95%).[2c] Consequently, **A** and **B** are excellent starting materials to study the reactivity of the P_4 butterfly unit towards various Lewis acids.[3-7] Within these studies, our group was able to demonstrate the successful coordination of the intact P_4 butterfly moiety as well as rearrangement and fragmentation processes (Scheme 1).

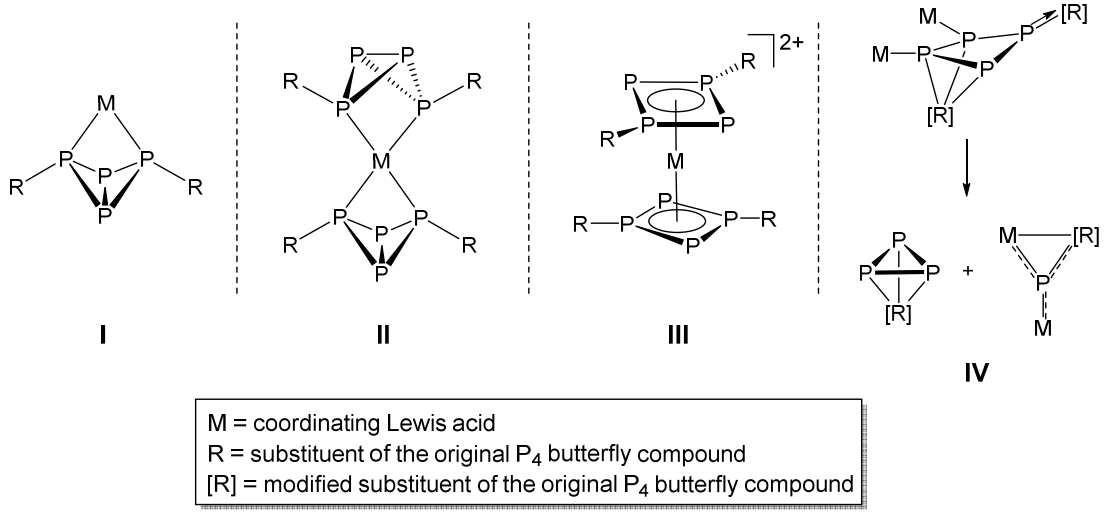

Scheme 1. Structural motifs obtained after coordination, rearrangement and fragmentation of the P_4 butterfly complex upon the reaction with various Lewis acids.

Early investigations concerning the coordination chemistry of the P_4 butterfly unit with monovalent coinage metal salts afforded a tetraphosphametalla-*tricyclo*[1.1.1.0^{2,4}]pentane type **I** compound (Scheme 1) and a homoleptic spiro complex with two orthogonally coordinated P_4 butterfly ligands (Scheme 1, type **II**).[3] Herein, the geometric properties of the P_4 butterfly scaffold mainly stay unaltered while the wing tip P atoms coordinate towards the Lewis acidic fragment in a chelating fashion. Next to this bidentate coordination, a planar isomerization of the P_4 butterfly unit yielding a planar 6π-aromatic R_2P_4 ligand can be observed, when reacting **A** with [Fe(CH$_3$CN)$_6$][PF$_6$]$_2$ (Scheme, type **III**).[4] In contrast, the quantitative formation of bidentate

coordination products according to type **I** is observed, if **A** and **B** are reacted with $FeBr_2$·dme (dme = 1,2-dimethoxyethane).[4,5] Consequently, the reaction pathway is strongly depended on the nature of the Lewis acid and its intrinsic acidity. Lastly, the reaction of **A** with tetracarbonyl fragments of Cr, Mo and W (obtained from $[M(CO)_4(nbd)]$; nbd = norbornadiene) selectively afforded type **I** compounds.[6] For the reaction of **B** with $[W(CO)_4(nbd)]$ an analog type **I** complex was obtained, while the reaction with $[Cr(CO)_4]$ and $[Mo(CO)_4]$ fragments resulted in rearrangement yielding a bend *cyclo*-P_4 moiety which undergoes subsequent P_1/P_3-fragmentation under special reaction conditions (Scheme 1, type **IV**).[7]

Therefore, the reactivity of the P_4 butterfly complexes towards Lewis acids is well investigated yielding expected as well as surprising and intriguing new products. Consequently, the question arises whether the opposite reaction pathway, the reaction of P_4 butterfly compounds with nucleophiles, is feasible as well. An example for a polyphosphorus complex, whose reactivity towards nucleophiles was intensively studied, is $[Cp^*Fe(\eta^5\text{-}P_5)]$.[8] A common observation upon the reaction with nucleophiles is that the fivefold symmetry of the *cyclo*-P_5 ligand is broken by the nucleophilic addition resulting in a bend η^4-P_5 envelope unit (Scheme 2, type **V**). Depending on the reaction conditions and the nature of the attacking nucleophile a bridging of two pentaphosphaferrocene units could be observed as well (Scheme 2, type **VI**).

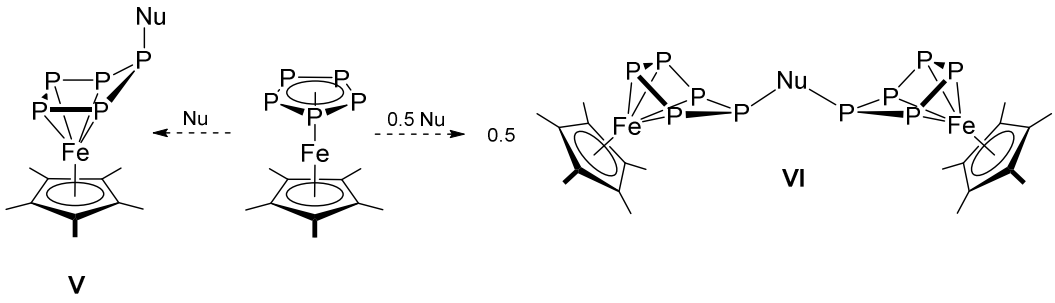

Scheme 2. Products obtained from the reaction of $[Cp^*Fe(\eta^5\text{-}P_5)]$ with various nucleophiles.

Intrigued by these results, this work focuses on the reaction of the P_4 butterfly complexes **A** and **B** with various nucleophiles. Hereby, special emphasis is laid on *N*-heterocyclic carbenes (NHCs) as they have proven to be a powerful reagent in the stabilization of labile compounds as well as versatile ligands in catalytic applications since their first synthetic appearance reported by *Arduengo et al.* in 1991.[9] Generally, NHC ligands can be employed for the stabilization of unsubstituted main group element moieties (e.g. formal C(0), Si(0) or Ge(0) species).[9b] The first compounds similar to phosphorus-NHC adducts were reported in 1964: twofold coordinated P atoms interpreted as phosphacyanines.[10] However, 2-chlorobenzothiazolium of 2-chloroquinolinium salts were utilized as starting materials in the generation of these compounds and not the classical NHCs used nowadays. Within the phosphorus chemistry, one special field of application for NHCs is the stabilization of the gaseous P_2 allotrope. In contrast to its heavier homolog N_2 is highly reactive and prone to aggregation.[11] In 2008, *Robinson et al.* reported on the first NHC stabilized P_2 dumbbells for which a bisphosphinidene structure was proclaimed.[12] Consequently, the two P atoms are connected via a P–P single bond and each P atoms displays two additional electron lone pairs. This observation is a drastic contrast in comparison to the P≡P triple bond present in the free P_2 dumbbell.

5.3 Results & Discussion

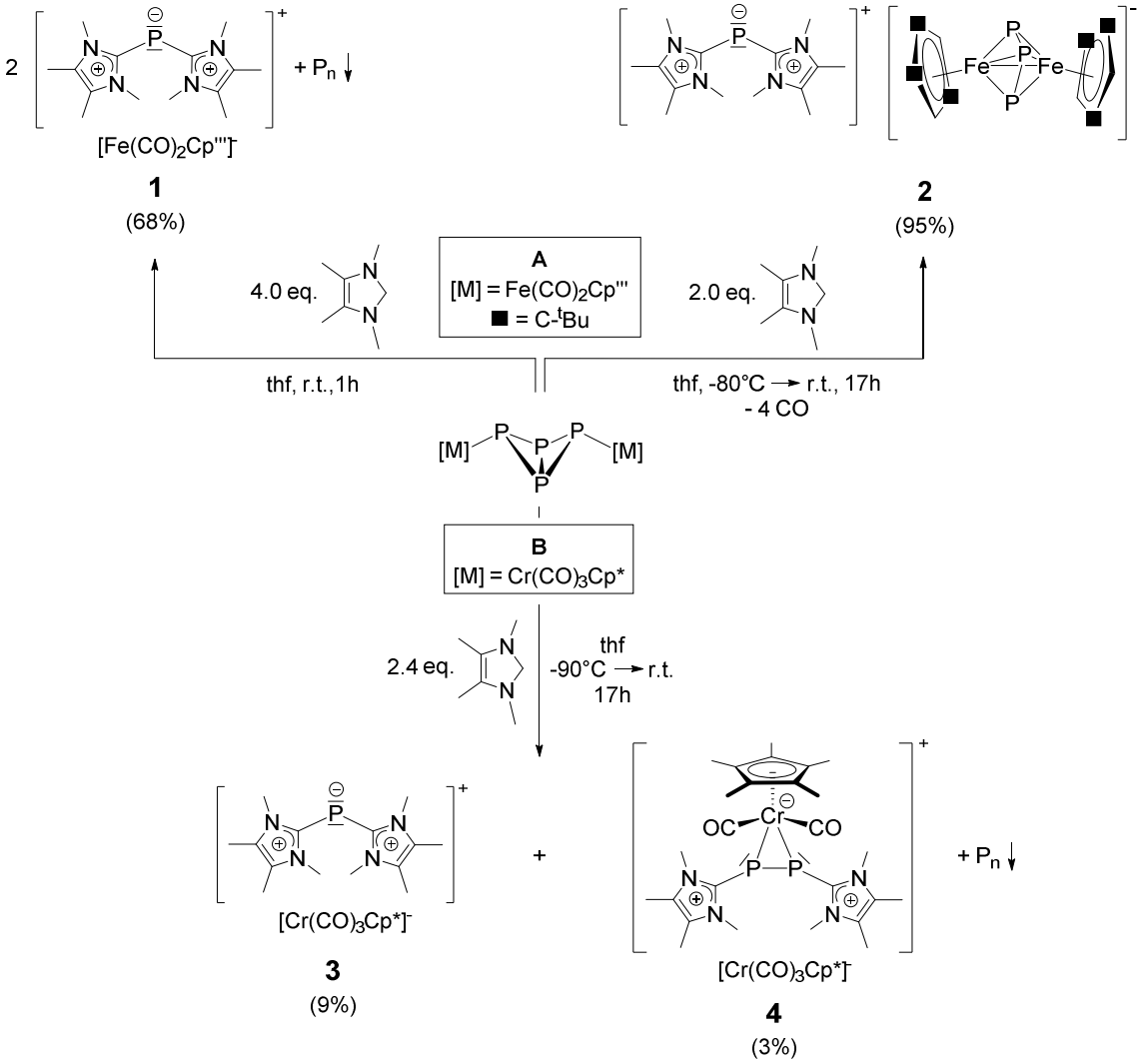

Scheme 3. Reactions of **A** and **B** with IMe at different reaction conditions.

Initial studies showed that reactions of the P_4 butterfly compounds **A** and **B** with nucleophiles like $LiNMe_2$, $LiCH_2SiMe_3$, $KCHPh_2$ at various reaction conditions result in either uncontrollable decomposition of the starting materials or no conversion at all. Additionally, if sterically demanding NHCs like IDipp (1,3-bis(2,6-diisopropylphenyl)imidazol-2-ylidene) are reacted with **A** or **B**, no reaction of the starting materials was detected by NMR spectroscopic methods. However, when employing the rather small NHC IMe (1,3,4,5-tetramethylimidazol-2-ylidene) a reproducible reaction outcome was found. When reacting **A** with IMe at room temperature, $[P(IMe)_2][Fe(CO)_2Cp''']$ (**1**, Scheme 3) is obtained selectively alongside insoluble red precipitate (most likely polyphosphorus aggregates). In contrast, $[P(IMe)_2][\{Cp'''Fe\}_2(\mu,\eta^{3:3}\text{-}P_3)]$ (**2**, Scheme 3) is afforded exclusively, if the reaction is performed at -80 °C. The monophosphorus cation $[P(IMe)_2]^+$ has been reported with various anions and is thoroughly investigated. However, the fact that the reaction of **A** with IMe affords different anions depending on the reaction temperature is intriguing. This suggest, that **2** represents the kinetically favored product, whereas **1** is the thermodynamically favored compound. Through the addition of

IMe, one P atom of **A** is abstracted affording the $[P(IMe)_2]^+$ cation. At low temperatures the remaining P_3 scaffold of the former P_4 butterfly unit rearranges under carbonyl extrusion yielding the $[\{Cp'''Fe\}_2(\mu,\eta^{3:3}\text{-}P_3)]^-$ anion of **2**, which incorporates a bridging allylic P_3 unit. At higher temperatures, the organometallic substituent of **A** evolves into the $[Fe(CO)_2Cp''']^-$ anion of **1**, while the residual P atoms of the P_4 butterfly unit aggregate and form the insoluble precipitate.

When **B** is reacted with IMe, the two products $[P(IMe)_2][Cr(CO)_3Cp^*]$ (**3**, Scheme 3) and $[\{Cp^*Cr(CO)_2\}\text{-}(\eta^2\text{-}P_2IMe_2)][Cr(CO)_3Cp^*]$ (**4**, Scheme 3) are obtained simultaneously next to insoluble yellow precipitate (most likely polyphosphorus aggregates). Compound **3** is another representative of the known $[P(IMe)_2]^+$ cation whereas, to the best of our knowledge, **4** is a representative of a novel structural motif: the first P_2 dumbbell stabilized by two terminal NHCs and one bridging organometallic fragment. Compound **3** is isostructural to **1** and afforded analogously: one P atom of the P_4 butterfly unit of **B** is abstracted by two IMe molecules affording the $[P(IMe)_2]^+$ cation, while the organometallic substituent of **B** evolves into the $[Cr(CO)_3Cp^*]^-$ anion and the remaining P atoms aggregate forming a polyphosphorus precipitate and P_4. However, during the formation of **4** a rearrangement occurs after the initial abstraction of one P atom from the P_4 butterfly unit. The residual phosphorus scaffold reacts with two molecules of IMe affording an NHC substituted P_2 dumbbell. The P_2 dumbbell is additionally stabilized by the coordination towards a $\{Cp^*Cr(CO)_2\}$ fragment obtained from the substituent of the starting material **B**. Again, polyphosphorus precipitate and P_4 can be detected as byproducts of this reaction. They arise as aggregates formed from the redundant P atoms extruded from the P_4 butterfly moiety during the concurrent formations of **3** and **4**.

Previous experiments showed that **B** is more likely to decompose or rearrange in comparison to **A**. For example, when solutions of **A** or **B** are stirred at room temperature, a quantitative decomposition of **B** resulting in $[Cp^*Cr(CO)_2(\eta^3\text{-}P_3)]$ is detected by ^{31}P NMR spectroscopy, whereas for **A** no significant decomposition or fragmentation can be detected. With a dissociation energy of 142.91 $kJ\cdot mol^{-1}$, the cleavage of the Fe–P bonds in **A** is considerably disfavored in comparison to the corresponding fragmentation of **B** (67.47 $kJ\cdot mol^{-1}$).[5] Consequently, the $\{Cp'''Fe(CO)_2\}$ substituent is less likely to detach, rearrange and reattach to a modified P_n moiety. However, the detachment of the organometallic substituent of **B** and the rearrangement affording a canopying $\{Cp^*Cr(CO)_2\}$ fragment is essential to the formation of **4**. Consequently, the fact that the organometallic fragment of **A** is less likely to rearrange might explain why no iron analog to **4** can be observed for the reaction of **A** with IMe.

As **3** and **4** are formed simultaneously and due to very similar properties concerning solubility and crystallization as well as the fast decomposition during chromatographic workup, analytical investigations could only be performed for a mixture of crystals of **3** and **4**. Moreover, each manipulation of the reaction mixture leads to the additional formation of insoluble yellow precipitate. Hence, intricate workup leads to the depletion of the obtained amounts of **3** and **4**.

Compounds **1** and **3** crystalize in the triclinic space group $P\bar{1}$ as clear orange and yellow plates, respectively. In contrast, **2** crystalizes in the form of dark pink blocks in the monoclinic space group $P2_1/n$. One molecule of **1** and **2** is present in the respective asymmetric unit, while for **3** two cationic and two anionic entities can be found in the asymmetric unit (Fig. 1).[13] The $[P(IMe)_2]^+$ cation incorporated by **1**, **2** and **3** is known and could be previously characterized in the presence of different counter anions.[14] As expected, the bond lengths and angles determined by single crystals X-ray diffraction for **1**, **2** and **3** comply well with the previously reported values for the $[P(IMe)_2]^+$ cation (Table 1). However, a couple of distinctive features of **1**, **2** and **3** can

be noted. Since the structural parameters are recorded in the solid state, it can be stated that the bond lengths and angles of $[P(IMe)_2]^+$ are highly dependent on packing effects and influenced by the corresponding anions. Compared to the other representatives, the $[P(IMe)_2]^+$ cation in **2** displays the most unique structural parameters. With 102.65(10)°, the C–P–C angle of **2** is the largest of all reported $[P(IMe)_2]^+$ cations. This indicates that the elaborate $[\{Cp'''Fe\}_2(\mu,\eta^{3:3}\text{-}P_3)]^-$ counter ion of **2** has a strong influence on the structure of the $[P(IMe)_2]^+$ cation in the solid state.

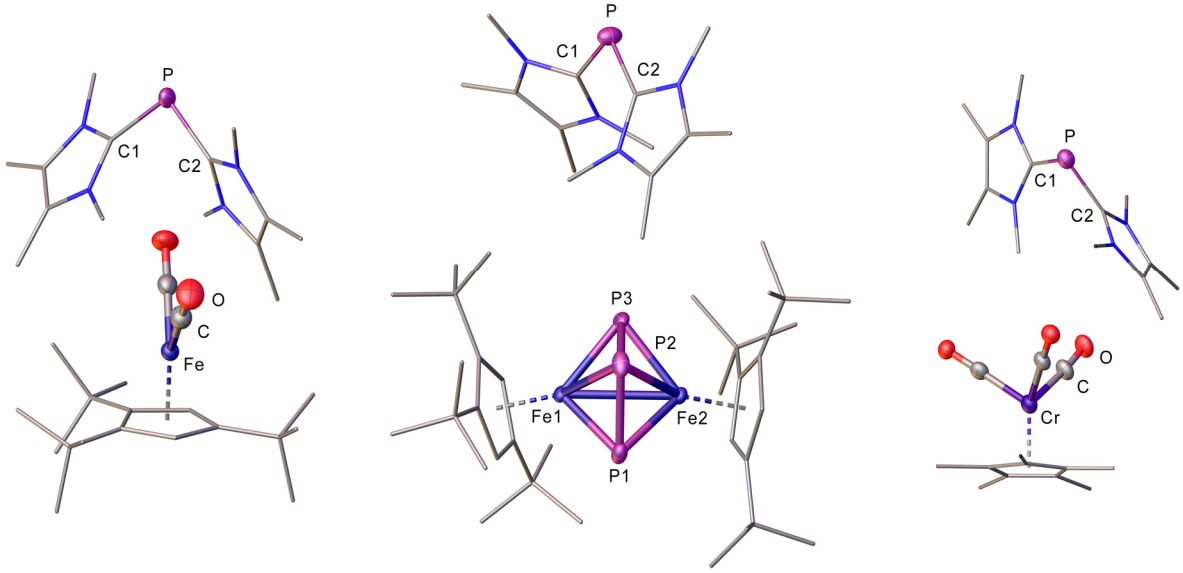

1 **2** **3**

Figure 1. Molecular structure of **1**, **2** and **3** in the solid state; H atoms are omitted for clarity and CO as well as Cp ligands are drawn in the wire frame model; thermal ellipsoids are drawn at 50% probability.

Table 1. Comparison of structural parameters of the $[P(IMe)_2]^+$ cation in the solid state in respect to different anions.

	anion	P–C [Å]		C–P–C [°]	Twist angle [°][1]	
1	$[Fe(CO)_2Cp''']^-$	1.8049(17)	1.8054(18)	95.79(8)	42.10(8)	44.75(8)
2	$[\{Cp'''Fe\}_2(\mu,\eta^{3:3}\text{-}P_3)]^-$	1.802(2)	1.797(2)	102.65(10)	26.08(10)	49.42(10)
3[2]	$[Cr(CO)_3Cp^*]^-$	1.805(13) 1.817(13)	1.787(11) 1.792(12)	98.3(6) 96.9(6)	35.9(7) 36.3(7)	44.9(7) 46.7(7)
	$[Cp'''Co(\eta^3\text{-}P_3)]^-$	1.8033(18)	1.7941(17)	98.74(8)	38.9(6)	42.7(7)
	$[\{Cp^*Mo\}_2(\mu,\eta^{3:3}\text{-}P_3)(\mu,\eta^{2:2}\text{-}P_2)]^-$	1.801(7)	1.801(7)	97.4(3)	45.1(6)	49.7(8)
	Br^-	1.8002(13)	1.8032(13)	98.63(6)	38.8	42.8
	I^-	1.796(1)	1.804(2)	96.3(1) 98.2(1)	42.7(1)	43.5(1)
	$[BPh_4]^-$	1.801(2)	1.812(2)	98.30(10)	44.7	59.0
	$[(TerN)_2P]^-$ [3]	1.790(2)	1.801(2)	96.96(7)	40.2	46.3

[1] Distortion angle between the $PC^{Carbene}_2$ plane and the planes spanned by the NHC ring systems
[2] Preliminary values due to poor single crystal X-ray diffraction data
[3] Ter = 2,6-bis(2,4,6-trimethyl-phenyl)phenyl

An interesting parameter for the characterization of the $[P(IMe)_2]^+$ cation is the twist angle describing the degree of distortion of the two NHC ligands in respect to the plane spanned by the central P atom and the two carbene C atoms. Two notably different twist angles are recorded for **2** (26.08(10)° and 49.42(10)°) as well as **3** (35.9(7)°/36.3(7)° and 44.9(7)°/46.7(7)°). Again, the strongly deviating twist angles are a result of the asymmetric environment in the crystal lattice. Since the $[\{Cp'''Fe\}_2(\mu,\eta^{3:3}\text{-}P_3)]^-$ counter ion of **2** is sterically more intricate than the $[Cp^*Cr(CO)_3]^-$ counter ion of **3**, the effect is more notably for **2** resulting in an even stronger deviation of the correlated parameters.

The $[\{Cp'''Fe\}_2(\mu,\eta^{3:3}\text{-}P_3)]^-$ anion found in **2** represents the reduced version of the neutral $[\{Cp'''Fe\}_2(\mu,\eta^{3:3}\text{-}P_3)]$ (**C**): the first binuclear complex incorporating a triphosphaallyl unit.[15] However, whereas **C** is highly symmetric, **2** is not symmetric indicating that the reduction reduces the allylic character of the bridging P_3 ligand in the solid state (Table 2). With 2.1601(8) Å and 2.1897(8) Å, the P–P bonds in **2** are shortened in comparison to an ordinary P–P single bond (2.209(5) Å).[16] Yet, they are slightly elongated in comparison to the respective P–P bonds in **C** (2.148(1) Å). The Fe–Fe distance found in **2** is given at 2.8236(4) Å and therefore remarkably elongated in comparison to the corresponding bond in **C** (2.589(1) Å).[17] In addition, the Fe1–P–Fe2 angles in **2** are widened in comparison to the parameters in **C** (Table 2). Consequently, the formal reduction of **C** to **2** results in an enlargement of the structural scaffold. In contrast, the P–P–P angle of **2** (95.21(3)°) is slightly smaller than the angle reported for the neutral compound **C** (100.71(7)°).

Table 2. Comparison of structural parameters of the $[\{Cp'''Fe\}_2(\mu,\eta^{3:3}\text{-}P_3)]^-$ anion found in **2** and the neutral $[\{Cp'''Fe\}_2(\mu,\eta^{3:3}\text{-}P_3)]$ (**C**) in the solid state.

	d / Å						**α / °**	
	2	**C**		**2**	**C**		**2**	**C**
Fe1–P1	2.1942(6)	2.225(1)	**P1–P2**	2.1601(8)	2.148(1)	**Fe1–P1–Fe2**	79.94(2)	71.51(4)
Fe1–P2	2.4221(6)	2.2446(1)	**P2–P3**	2.1897(8)	2.148(1)	**Fe1–P2–Fe2**	71.315(18)	63.92(4)
Fe1–P3	2.1931(6)	2.225(1)	**Fe1–Fe2**	2.8236(4)	2.589(1)	**Fe1–P3–Fe2**	80.06(2)	71.51(4)
Fe2–P1	2.2015(6)	2.225(1)				**P1–P2–P3**	95.21(3)	100.71(7)
Fe2–P2	2.4217(6)	2.2446(1)						
Fe2–P3	2.1971(6)	2.225(1)						

The ^{1}H NMR spectra of **1**, **2** and **3** display the expected signals for the freely rotating Cp ligands of the anions, the methyl groups attached to the N atoms and the methyl groups located on the unsaturated back bone of IMe, respectively. Additionally, the ^{31}P NMR spectra of **1**, **2** and **3** confirm the previously reported signal for $[P(IMe_2)]^+$, a singlet at δ = -114 ppm (recorded in thf-d_8). Moreover, the ^{31}P NMR spectrum of **2** reveals two additional sets of signals attributed to the $[\{Cp'''Fe\}_2(\mu,\eta^{3:3}\text{-}P_3)]^-$ anion: a doublet at δ = 638.6 ppm (P1 and P3) and a triplet at δ = -384.1 ppm (P2, labeling according to Fig. 1). Simulation of the ^{31}P NMR spectrum of **2** confirmed a $^1J_{PP}$ coupling constant of 352.6 Hz. Hence, a P–P bond order in between a single and a double bond can be stated in compliance with the single crystal X-ray diffraction data. In the ESI-MS spectra of **1**, **2** and **3** the molecular peaks for the $[P(IMe)_2]^+$ cation and the accompanying anions are recorded in the positive and negative mode of operation, respectively.

After layering a solution obtained from the reaction of **B** with 2.4 eq. IMe with *n*-pentane, **4** crystallizes alongside **3** in the form of brown blocks in the monoclinic space group $P2_1/n$ (Fig. 2). However, the crystals break easily and the debris cannot be distinguished from crystalline **3** under the microscope. Hence, an optical separation of **3** and **4** could not be achieved. In the solid state the P–P bond length of the central P_2 dumbbell of **4** amounts to 2.1246(8) Å. It is elongated in comparison to the corresponding P–P bond in [{CpCr(CO)$_2$}$_2${μ,η$^{2:2}$-P_2}] (2.060(1) Å), in which the P_2 dumbbell is coordinated by two {CpCr(CO)$_2$} fragments forming a tetrahedron.[18] However, it is shorter than a regular P–P single bond, given at 2.209(5) Å.[16] Consequently, a bond order in between a P–P single and P=P double bond can be proposed for the central P_2 unit in **4**. In contrast, solely NHC stabilized P_2 dumbbells L:P–P:L (with L = IDipp or IMes (1,3-bis(2,4,6-trimethylphenyl)imidazol-2-ylidene)) incorporate P–P bond lengths in the range of a regular P–P single bond (L = IDipp: 2.2052(10) Å; L = IMes: 2.1897(11) Å).[12] Additionally, the two P–C bonds in **4** (1.835(3) Å and 1.842(3) Å) are slightly elongated in comparison to the distances reported for L:P–P:L (L = IDipp: 1.7504(17) Å; L = IMes: 1.754(3) Å) indicating a weaker interaction comparable to a P–C single bond. One outstanding observation about the molecular structure of **4** is the fact that the {Cp*Cr(CO)$_2$} fragment is canopying the P_2 dumbbell in an asymmetrical fashion. The central Cr atom is shifted slightly towards one of the P atoms which results in two different P–Cr bond lengths of 2.3954(7) Å and 2.4480(7) Å as well as two differing P–P–Cr angles of 65.26(3)° and 62.71(2)°. The IMe ligands are arranged in a trans-conformation and with torsion angles of 93.98(8)° and 93.37(8)° they are nearly perpendicular in respect to the central CrP_2 plane.

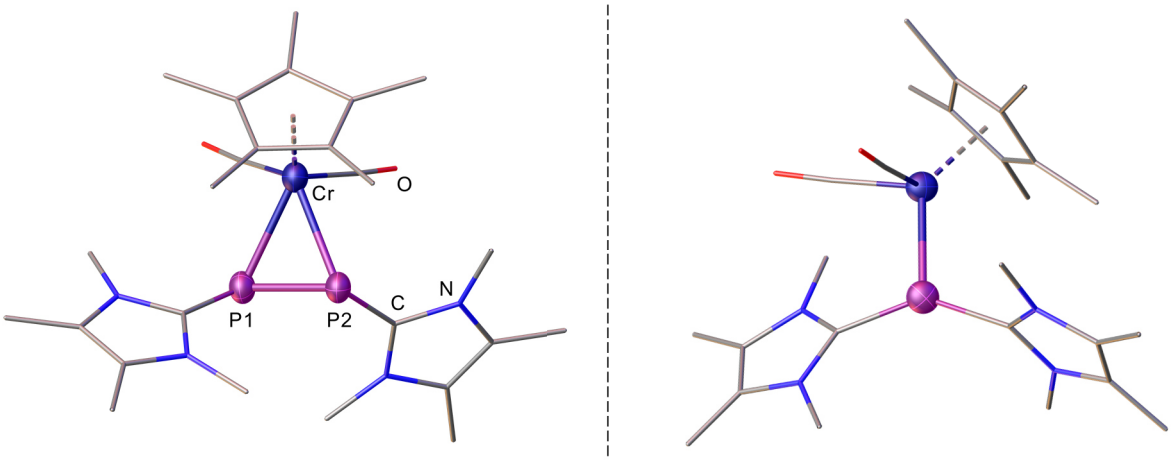

Figure 2. Molecular structure of the cationic fragment of **4** in the solid state (left: front view; right: side view); H atoms are omitted for clarity and CO as well as Cp* ligands are drawn in the wire frame model (only one part of the disordered Cp* ligand is depicted); thermal ellipsoids are drawn at 50% probability.

Five singlets can be detected in the ^{1}H NMR spectrum of **4** at δ = 1.83 ppm, 2.18 ppm, 2.24 ppm, 3.85 ppm and 4.06 ppm (recorded in thf-d_8). Due to the intrinsic asymmetry of **4**, which is introduced by the sloping coordination mode of the {Cp*Cr(CO)$_2$} fragment, the methyl groups of the two IMe ligands are no longer magnetically equivalent, consequently affording four distinct singlets next to the signal attributed to the Cp* ligand. Due to the asymmetric coordination sphere, two doublets at δ = -52.0 ppm and δ = -82.1 ppm are recorded in the ^{31}P NMR spectrum of **4** for the inequivalent P atoms. This confirms that the P_2 dumbbell maintains the asymmetrical η^2-coordination towards the {Cp*Cr(CO)$_2$} fragment in solution. The $^1J_{PP}$ coupling

constant of **4** (338 Hz) is larger than the one recorded for [IMesP–PIDipp] ($^1J_{PP}$ = 249 Hz) for which a P–P single bond is proposed.[19] However, the P=P double bond incorporating $[IMesP–PIDipp]^{2+}$ displays a $^1J_{PP}$ coupling constant of 543 Hz.[19] Consequently, for **4** a P–P bond order in between a single and a double bond is reasonable. Finally, ESI^+-MS and ESI^--MS experiments exclusively afforded the molecular peaks for the $[\{Cp^*Cr(CO)_2\}(\eta^2\text{-}P_2IMe_2)]^+$ cation and the $[Cr(CO)_3Cp^*]^-$ anion, respectively.

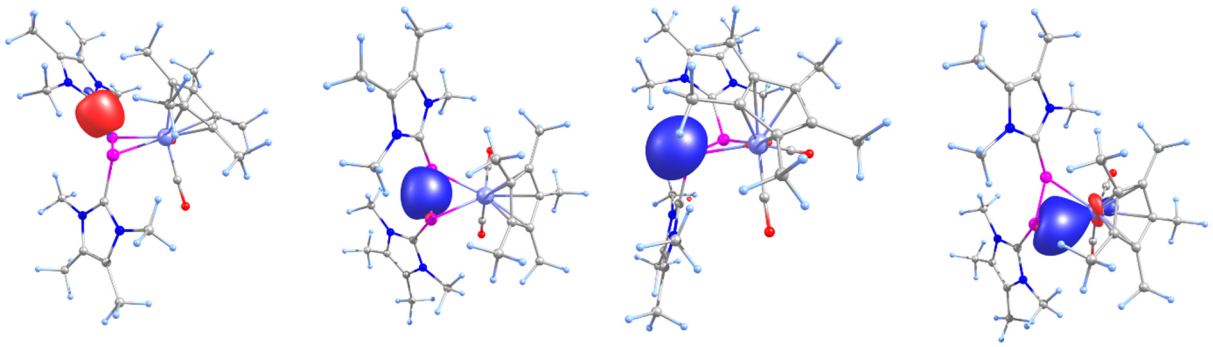

C–P bond | P–P bond | lone pair of electrons on P atom | Cr–P bond

Figure 3. Selected localized molecular orbitals of **4**.

To gain further insight in the electronic structure of **4**, the compound has been investigated by DFT calculations at the B3LYP/def2-TZVP level. The natural population analysis (NPA) shows that the Cr atom is negatively charged (−0.86), while the Cp* ligand and the CO groups are slightly positively charged (0.15 and 0.36, respectively) resulting in an overall negative charge of −0.35 for the $\{Cp^*Cr(CO)_2\}$ fragment. The central P_2 unit and the two NHC fragments bear a positive charge of 0.37, 0.51 and 0.47, respectively, resulting in a $\{P_2IMe_2\}$ fragment with an overall positive charge of 1.35. The Wiberg Bond Index (WBI) of the P–P bond (1.14) confirms only a weak double bond character, while the WBIs of the C–P bonds (0.98 and 1.01) are characteristic for single bonds. The NBO analysis illustrates the presence of only one lone pair of electrons on each P atom in an approximate $sp^{0.5}$ hybrid orbital, alongside to two weakly polarized Cr–P bonds in which the P atoms participate with almost pure p orbitals (sp^{11} and $sp^{7.2}$). This description of the electronic structure of **4** is in line with the localized molecular orbitals. In Fig. 3 the localized molecular orbitals corresponding to the C–P bond, the P–P bond, the lone pair of electrons on the P atom and the Cr–P bond are depicted.

The AIM analysis of the electron density in **4** allowed the detection of bond critical points (BCPs) along the P–P and Cr–P bonds (Fig. 4). The locations of BCPs corresponding to the Cr–P bonds point towards a metallacyclopropane-like bonding. However, the relatively high ellipticity at the BCPs 1-3 (P_2Cr core) indicates a deformation of the electron density in this plane, hence the presence of a P–P double bond.

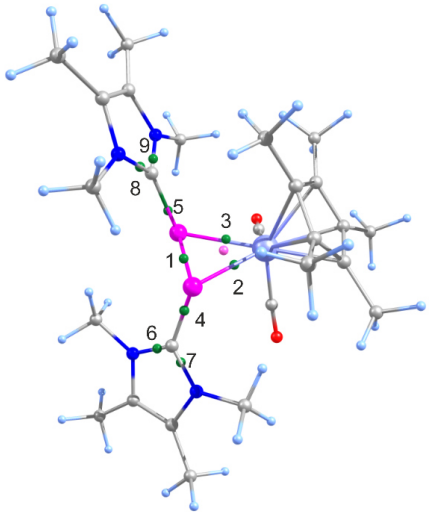

Figure 4. Locations and labeling of selected Bond Critical Points (BCP, green) and Ring Critical Points (RCP, violet) in the electron density of **4**.

Although, the Laplacian of the electron density is positive at the BCPs corresponding to the Cr–P bonds, the relatively high electron density and high energy density at the BCPs clearly shows the Cr–P bonds (Fig. 5). Additionally, the ratio of the potential-energy density $|V_c|$ and the kinetic-energy density G_c at the bond critical point for the P–P and P–C bonds are characteristic for covalent interactions ($|V|/G > 2$), while those of the Cr–P bonds are characteristic for intermediate interactions between typical covalent and closed shell, for which the $|V|/G$ ratio lies between 1 and 2. Based on this results the electronic structure of **4** can be described with the Lewis formula shown in Scheme 3.

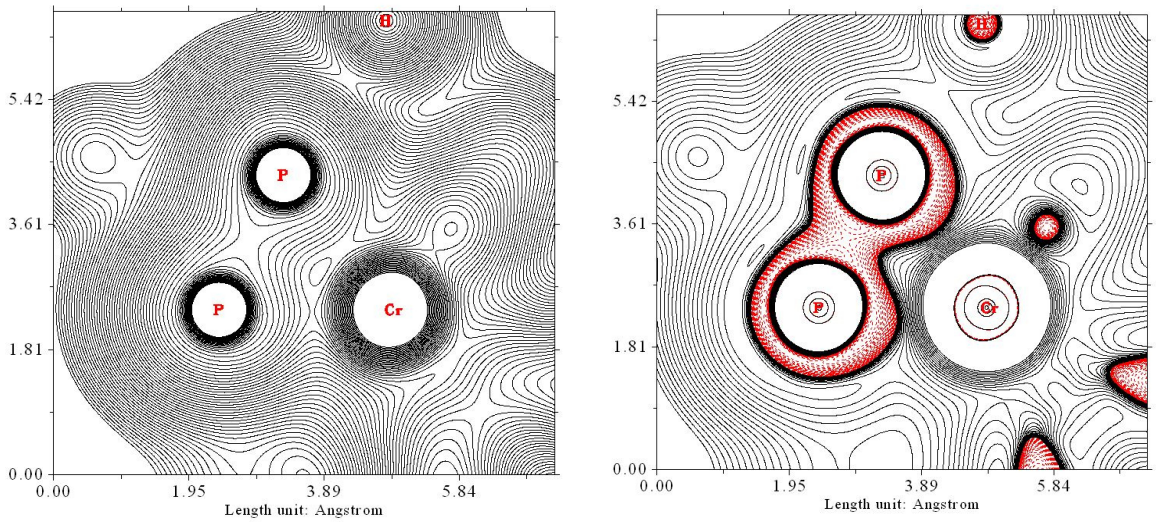

Figure 5. Electron density (left) and the Laplacian of the electron density (right) in the P_2Cr plane in **4**.

One compelling difference in the composition of the $[\{Cp^*Cr(CO)_2\}(\eta^2\text{-}P_2IMe_2)]^+$ cation of **4** in comparison to the $[P(IMe)_2]^+$ cation found in **1**, **2** and **3** is the intrinsic phosphorus-NHC ratio. Whereas a 1:2 ratio is found in

$[P(IMe)_2]^+$, a 1:1 ratio is presented in $[\{Cp^*Cr(CO)_2\}(\eta^2\text{-}P_2IMe_2)]^+$. Therefore, it can be assumed that the formation of **3** would be favored over the synthesis of **4**, if the amount of IMe reacted with **B** is increased. ^{31}P NMR spectroscopic studies validated this proposed effect of stoichiometry variation in the starting materials on the product ratio (cf. Si Fig. S3). ^{31}P NMR spectra were recorded for the reaction of **B** with increasing amounts of IMe and the relative integrals of the observed signals corresponding to **B**, **3** and **4** are given in Table 3. A continuous increase in the formation of **3** can be monitored upon addition of additional IMe, whereas no **4** can be detected anymore, when adding more than 4.0 eq. of IMe. For an optimized yield of **4** (approx. 3% in crystalline yield), 2.4 eq. of IMe proved to be the ideal amount of the starting material even though traces of **B** are still detectable. Smaller amounts of IMe still afford the formation of the desired products **3** and **4**, however considerable amounts of **B** are not converted. Moreover, when using 6.0 eq. of IMe or more, additional side products could be observed in the ^{31}P NMR spectrum of which none could be identified so far.

Table 3. Relative integrals of the signals obtained from the experimental ^{31}P NMR spectra of reactions of **B** with varying equivalents of IMe (recorded in thf with C_6D_6 capillary at 300 K).

eq. IMe	relative integrals I_{rel}		
	B	**3**	**4**
1.0	52.4%	10.4%	3.5%
2.0	23.2%	38.2%	5.7%
4.0	2.0%	52.2%	4.2%
6.0*	-	86.3%	-

* formation of reasonable amounts of side products is detected.

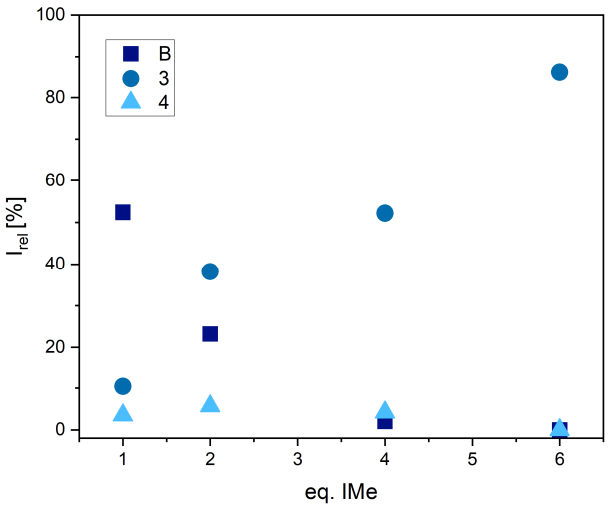

5.4 Conclusion

In summary, the reaction of the P_4 butterfly compound **A** with IMe selectively affords either $[P(IMe)_2][Fe(CO)_2Cp''']$ (**1**) or $[P(IMe)_2][\{Cp'''Fe\}_2(\mu,\eta^{3:3}\text{-}P_3)]$ (**2**) depending on the reaction temperature. In addition, the reaction of the chromium analog **B** with IMe afforded $[IMe_2P][Cr(CO)_3Cp^*]$ (**3**) and $[\{Cp^*Cr(CO)_2\}(\eta^{2}\text{-}P_2IMe_2)][Cr(CO)_3Cp^*]$ (**4**). Next to the known $[P(IMe)_2]^+$ cation found in **1**, **2** and **3**, the anionic entity of **2** incorporates an allylic P_3 ligand in a bridging $\mu,\eta^{3:3}$-coordination mode. Moreover, the cationic P_2 dumbbell in **4** represents a novel class of products accessible from the versatile starting material **B**. In **4** the P_2 dumbbell is stabilized by two NHC molecules and one canopying organometallic $\{Cp^*Cr(CO)_2\}$ fragment, a coordination array which was not reported on so far. Comprehensive DFT calculations delineate a weak double bond character for the P_2 dumbbell with one localized lone pair of electrons on each P atom while the $\{Cp^*Cr(CO)_2\}$ fragment bears a formal negative charge. Consequently, the P_4 butterfly chemistry is not limited to the previously reported bidentate coordination pattern but offers a great variety towards different reagents.

5.5 References

[1] (a) B. M. Cossairt, N. A. Piro, C. C. Cummins, *Chem. Rev.* **2010**, *110*, 4164-4177.
(b) M. Caporali, L. Gonsalvi, A. Rossin, M. Peruzzini, *Chem. Rev.* **2010**, *110*, 4178-4235.
(c) M. Scheer, G. Balázs, A. Seitz, *Chem. Rev.* **2010**, *110*, 4236-4256.
(d) N. A. Giffin, J. D. Masuda, *Coord. Chem. Rev.* **2011**, *255*, 1342-1359.

[2] (a) O. J. Scherer, G. Schwarz, G. Wolmershäuser, *Z. Anorg. Allg. Chem* **1996**, *622*, 951-957.
(b) O. J. Scherer, T. Hilt, G. Wolmershäuser, *Organometallics* **1998**, *17*, 4110-4112.
(c) C. Schwarzmaier, A. Y. Timoshkin, G. Balázs, M. Scheer, *Angew. Chem. Int. Ed.* **2014**, *53*, 9077-9081.

[3] C. Schwarzmaier, S. Heinl, G. Balázs, M. Scheer, *Angew. Chem. Int. Ed. Engl.* **2015**, *54*, 13116-13121.

[4] J. Müller, S. Heinl, C. Schwarzmaier, G. Balázs, M. Keilwerth, K. Meyer, M. Scheer, *Angew. Chem. Int. Ed. Engl.* **2017**, *56*, 7312-7317.

[5] R. Grünbauer, *Master thesis*, University of Regensburg (Regensburg), **2016**.

[6] Cf. chapter 4 of this thesis.

[7] Cf. chapter 3 of this thesis.

[8] (a) E. Mädl, M.V.Butovskii, G. Balázs, E. V. Peresypkina, A. V. Virovets, M. Seidl, M. Scheer, *Angew. Chem. Int. Ed* **2014** ,*53*, 7643-7646.
(b) E. Mädl, *Ph. D. thesis*, University of Regensburg (Regensburg), **2016**.

[9] (a) A. J. Arduengo, R. L. Harlow, M. Kline, *J. Am. Chem. Soc.* **1991**, *113*, 361-363.
(b) V. Nesterov, D. Reiter, P. Bag, P. Frisch, R. Holzner, A. Porzelt, S. Inoue, *Chem. Rev.* **2018**, *118*, 9678-9842.

[10] K. Dimroth, P. Hoffmann, *Angew. Chem. Int. Ed. Engl.* **1964**, *3*, 384−384.

[11] A. F. Holleman, N. Wiberg, E. Wiberg, *Lehrbuch für Anorganische Chemie*, 102. Edition, de Gryter, **2007**, 746-749.

[12] L. Y. Goh, C. K. Chu, R. C. S. Wong*, J. Chem. Soc, Dalton Trans.* **1989**, *1*, 1951-1956.

[13] It has to be noted that only preliminary data can be given for the single crystal X-ray diffraction analysis of **3** as only crystals of poor quality could be obtained.

[14] (a) **Br^-/$[BPh_4]^-$:** C. L. B. Macdonald, J. F. Binder, A. Swidan, J. H. Nguyen, S. C. Kosnik, B. D. Ellis*, Inorg. Chem.* **2016**, *55*, 7152-7166.
(b) **I^-:** M. Cicac-Hudi, J. Bender, S. H. Schlindwein, M. Bispinghoff, M. Nieger, H. Grützmacher, G. Gudat, *Eur. J. Inorg. Chem.* **2016**, 649-658.
(c) **$[(TerN)_2P]^-$**: A. Hinz, A. Schulz, A. Villinger, *Chem. Commun.* **2016**, *52*, 6328-6331.
(d) **$[Cp'''Co(\eta^3\text{-}P_3)]^-$ / $[\{Cp^*Mo\}_2(\mu,\eta^{3:3}\text{-}P_3)(\mu,\eta^{2:2}\text{-}P_2)]^-$**: M. Piesch, S. Reichl, M. Seidl, G. Balázs, M. Scheer, *Angew. Chem.* **2019**, *131*, 16716-16721; *Angew. Chem. Int. Ed.* **2019**, *58*, 16563-16568.

[15] M. Scheer, S. Deng, O. J. Scherer, M. Sierka, *Angew. Chem. Int. Ed.* **2005**, *44*, 3755-3758.

[16] (a) A. Simon, H. Borrmann, H. Craubner, *Phosphorus Sulfur Silicon Relat. Elem.* **1987**, *30*, 507-510.
(b) H.Okudera, E. Dinnebier Robert, A. Simon, *Z.Kristallogr.* **2005**, *220*, 259.

[17] Supplementary DFT calculations to elucidate the nature of the Fe–Fe interaction are still pending and could not be completed within the scope of this thesis.

[18] L. Y. Goh, C. K. Chu, R. C. S. Wong*, J. Chem. Soc, Dalton Trans.* **1989**, *1*, 1951-1956.

[19] A. Doddi, D. Bockfeld, M.-K. Zaretzke, C. Kleeberg, T. Bannenberg, M. Tamm, *Dalton Trans.* **2017**, *46*, 15859-15864.

5.6 Supplementary information

5.6.1 General remarks

All experiments were carried out under an atmosphere of dry argon or nitrogen using glovebox and Schlenk techniques. Residues of oxygen and water were removed from the inert gas by passing it over a BASF R 3-11 ($CuO/MgSiO_3$) catalyst, concentrated H_2SO_4 and finally granulated silica gel. Dry solvents were collected from a Braun SPS Apparatus and degassed prior to use. The deuterated solvents thf-d_8 was degassed and dried by stirring with Na/K alloy, followed by distillation.

The starting materials [{Cp‴Fe(CO)$_2$}$_2$(μ,η$^{1:1}$-P_4)] (**A**)[1], [{Cp*Cr(CO)$_3$}$_2$(μ,η$^{1:1}$-P_4)] (**B**)[2], IMe[3], IDipp[4] and $KCHPh_2$[5] were prepared according to literature procedures. $LiNMe_2$ and $LiCH_2SiMe_3$ are commercially available and were used without further modification.

NMR spectra were recorded at the NMR department of the University Regensburg using a Bruker Advance 300 or 400 spectrometer. Samples are referenced against TMS (^{1}H) or 85% H_3PO_4 (^{31}P) as external standards. Chemical shifts (δ) are reported in ppm and coupling constants (*J*) in Hz. The spectra were processed using the TopSpin 3.5 software (Bruker) and the WIN-DAISY module of this software was used to perform simulations.[6]

Mass spectrometry was performed by the MS department of the University Regensburg. ESI-MS spectra were recorded on a Q-TOF 6540 UHD (Agilent) spectrometer. The observed fragments were assigned according to the mass/charge (m/z) ratio and the isotope pattern.

5.6.2 Syntheses

Synthesis of [P(IMe)$_2$][Cp‴Fe(CO)$_2$] (1)

A colourless solution of IMe (149.0 mg, 1.2 mmol, 4.0 eq) in 10 mL thf is added to a red solution of **A** (244.3 mg, 0.3 mmol, 1.0 eq) in 10 mL thf. Thereby, the red colour intensified and a red solid is formed. The solution is stirred for one hour and subsequently the solvent is removed under reduced pressure. The orange residue is washed with cold toluene (3 x 10 mL, -30 °C), dissolved again in thf and stored at room temperature. Compound **1** is obtained in the form of dark orange plates suitable for single crystal X-ray diffraction analysis after three days.

Analytical data for 1

Yield 255.2 mg (0.41 mmol, 68 %).

^{1}H NMR (thf-d_8, 300 K): δ [ppm] = 1.13 (s, 9H, $C_5H_2{}^tBu_3$), 1.31 (s, 18H, $C_5H_2{}^tBu_3$), 2.25 (s, 12H, N-CH_3), 3.44 (s, 12H, C-CH_3), 3.93 (s, 2H, $C_5H_2{}^tBu_3$).

^{31}P{^{1}H} NMR (thf-d_8, 300 K): δ [ppm] = -114.6 (s, 1P, [P(IMe)$_2$]$^+$).

^{31}P NMR (thf-d_8, 300 K):	δ [ppm] = -114.6 (s, 1P, [P(IMe)$_2$]$^+$).
ESI$^-$-MS (dme)	m/z = 345.15 [Fe(CO)$_2$Cp‴]$^-$ (100%).
ESI$^+$-MS (dme)	m/z = 279.18 [P(IMe)$_2$]$^+$ (100%).
IR (solid)	$\tilde{\nu}_{CO}$ [cm^{-1}] = 1836.63 (m), 1767.95 (m).

Synthesis of [P(IMe)$_2$][{Cp‴Fe}$_2$(μ,η$^{3:3}$-P$_3$)] (2)

A red solution of **A** (760.6 mg, 0.8 mmol, 1.0 eq) in thf is cooled to -80°C. A -80 °C cold solution of IMe (198.7 mg, 1.6 mmol, 2.0 eq) in 10 mL thf is added. The mixture is stirred overnight and allowed to reach room temperature. Thereby, the colour changes to reddish-purple. The solvent is removed *in vacuo*. A dark red solution is extracted with toluene (3 x 10 mL) from the residue. The solvent is reduced under reduced pressure and stored at 8 °C. Compound **2** can be obtained in the form of dark red blocks suitable for single crystal X-ray diffraction analysis after one week.

Analytical data for 2

Yield	720.0 mg (0.76 mmol, 95 %).
^{1}H NMR (thf-d_8, 300 K)	δ [ppm] = 1.43 (s, 9H, C$_5$H$_2$^{t}Bu$_3$), 1.58 (s, 18H, C$_5$H$_2$^{t}Bu$_3$), 1.84 (s, 12H, N-CH$_3$), 2.88 (s, 12H, C-CH$_3$), 3.82 (s, 2H, C$_5$H$_2$^{t}Bu$_3$).
^{31}P{^{1}H} NMR (tol-d_8, 300 K)	δ [ppm] = 638.6 (d, 2P, $^1J_{AX}$ = 352.6 Hz, P$_A$), -114.2 (s, 1P, [P(IMe)$_2$]$^+$), -348.1 (t, 1P, $^1J_{AX}$ = 352.6 Hz, P$_x$).
^{31}P NMR (tol-d_8, 300 K)	δ [ppm] = 638.6 (d, 2P, $^1J_{AX}$ = 352.6 Hz, P$_A$), -114.2 (s, 1P, [P(IMe)$_2$]$^+$), -348.1 (t, 1P, $^1J_{AX}$ = 352.6 Hz, P$_x$).
ESI$^-$-MS (dme)	m/z = 671.24 [{Cp‴Fe}$_2$(μ,η$^{3:3}$-P$_3$)]$^-$ (100%).
ESI$^+$-MS (dme)	m/z = 279.18 [P(IMe)$_2$]$^+$ (100%).
Elemental Analysis	calcd. for [C$_{48}$H$_{82}$N$_4$P$_4$Fe$_2$] (950.78 g·mol^{-1}) C 60.64, H 8.69, N 5.89; found: C 61.08, H 8.05, N 5.97.

Synthesis of [P(IMe)$_2$][Cr(CO)$_3$Cp*] (3) and [{Cp*Cr(CO)$_2$}(η^2-P$_2$IMe$_2$)][Cr(CO)$_3$Cp*] (4)

An orange-brown solution of **B** (66 mg, 0.1 mmol, 1.0 eq.) in thf (5 mL) and a colorless solution of IMe (30 mg, 0.24 mmol, 2.4 eq.) in thf (5 mL) are cooled to -90 °C. Slowly, the solution of IMe is added to the solution of **B** while stirring. The solution is brought to room temperature overnight and hereby a color change to a dark brown solution and the formation of yellow precipitate is observed. The brown solution is filtered via a canula, diluted with additional 5 mL of thf and layered with n-pentane. After a few days two kinds of crystals suitable for single crystal X-ray diffraction are obtained: small yellowish blocks of **3** and dark brown blocks of **4**.

Crystalline Yield of the mixture of 3 and 4 14.0 mg

For product ratio of 3:1 (as found in by NMR spectroscopic studies): **3**: 11.2 mg (0.009 mmol, 9%).

4: 2.8 mg (0.003 mmol, 3%).

Analytical data for 3

^{1}H NMR (thf-d_8, 300K)	δ[ppm] = 1.83 (s, 15H, Cp*), 2.24 (s, 12H, N-C<u>H</u>$_3$), 3.44 (s, 12H, C-C<u>H</u>$_3$).
^{31}P NMR (thf-d_8, 300K)	δ[ppm] = -114.8 (s, 1P, [<u>P</u>(IMe)$_2$]$^+$).
^{31}P{^{1}H} NMR (thf-d_8, 300K)	δ[ppm] = -114.8 (s, 1P, [<u>P</u>(IMe)$_2$]$^+$).
ESI$^-$-MS (CH_3CN)	m/z = 271.04 [Cr(CO)$_3$Cp*]$^-$ (100%).
ESI$^+$-MS (CH_3CN)	m/z = 279.18 [P(IMe)$_2$]$^+$ (100%).

Analytical data for 4

^{1}H NMR (thf-d_8, 300K)	δ[ppm] = 1.83 (s, 15H, Cp*), 2.18 (s, 6H, N-C<u>H</u>$_3$), 2.24 (s, 12H, N-C<u>H</u>$_3$), 3.85 (s, 6H, C-C<u>H</u>$_3$), 4.06 (br, s, 6H, C-C<u>H</u>$_3$).
^{31}P NMR (thf-d_8, 300K)	δ[ppm] = -52.0 (d, $^{1}J_{PP}$ = 388 Hz, 1P), -82.1 (d, $^{1}J_{PP}$ = 388 Hz, 1P).
^{31}P{^{1}H} NMR (thf-d_8, 300K)	δ[ppm] = -52.0 (d, $^{1}J_{PP}$ = 388 Hz, 1P), -82.1 (d, $^{1}J_{PP}$ = 388 Hz, 1P).
ESI$^-$-MS (CH_3CN)	m/z = 271.04 [Cr(CO)$_3$Cp*]$^-$ (100%).
ESI$^+$-MS (CH_3CN)	m/z = 533.20 [{Cp*Cr(CO)$_2$}(η^2-P$_2$IMe$_2$)]$^+$ (100%).

5.6.3 NMR spectroscopic experiments

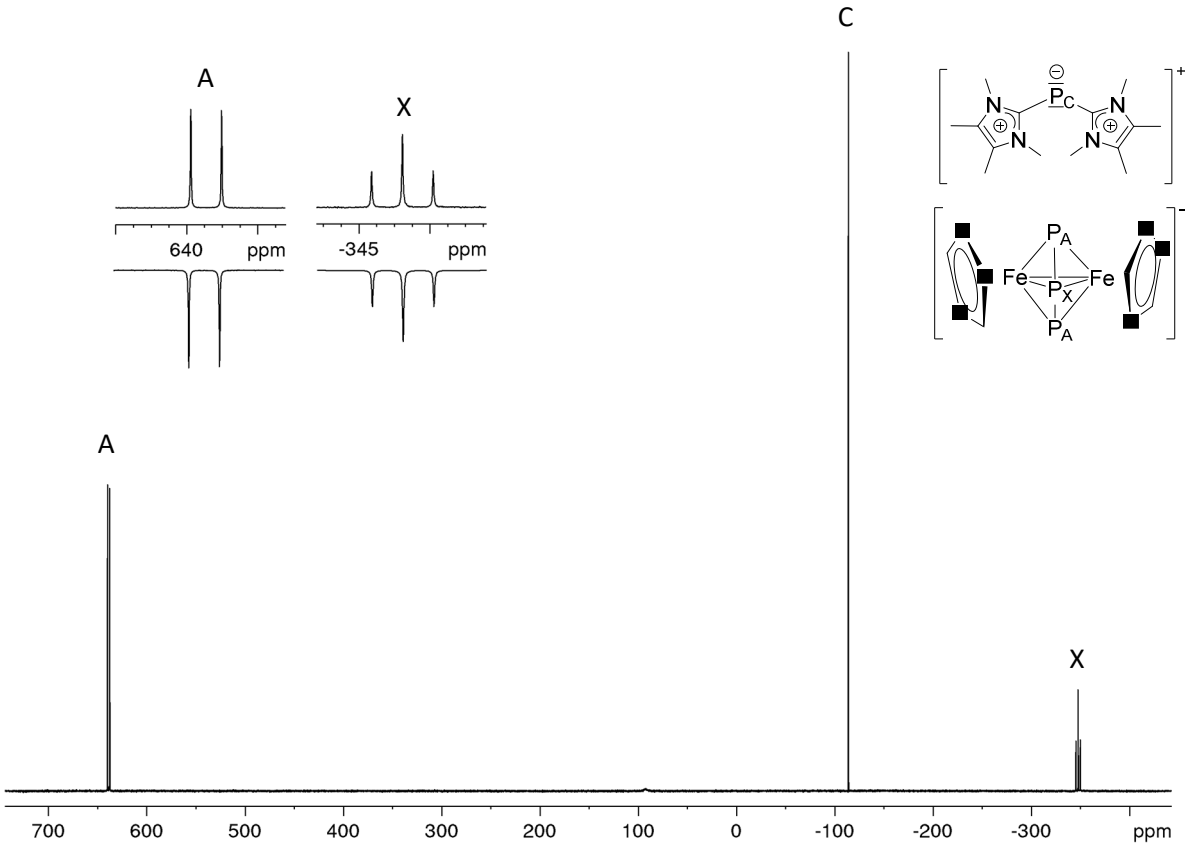

Figure S1. $^{31}P\{^1H\}$ NMR spectrum of **2** (recorded in thf-d_8 at 300 K); inset: comparison of experimental (top) and (simulated) $^{31}P\{^1H\}$ NMR spectrum of the anionic entity of **2**.

The simulation of the $^{31}P\{^1H\}$ NMR spectrum of the anionic entity of **2** was carried out on the basis of an A_2X spin system with a C_1 symmetry.

Table S1. Experimental and simulated values for the chemical shifts and coupling constants in the $^{31}P\{^1H\}$ NMR spectrum of **2** (recorded in thf-d_8 at 300 K).

experimental values				**simulated values**			
δ_A	638.6 ppm	$^1J_{AX}$	254 Hz	δ_A	638.6 ppm	$^1J_{AX}$	352.6 Hz
δ_X	-384.1 ppm			δ_X	-348.1 ppm		

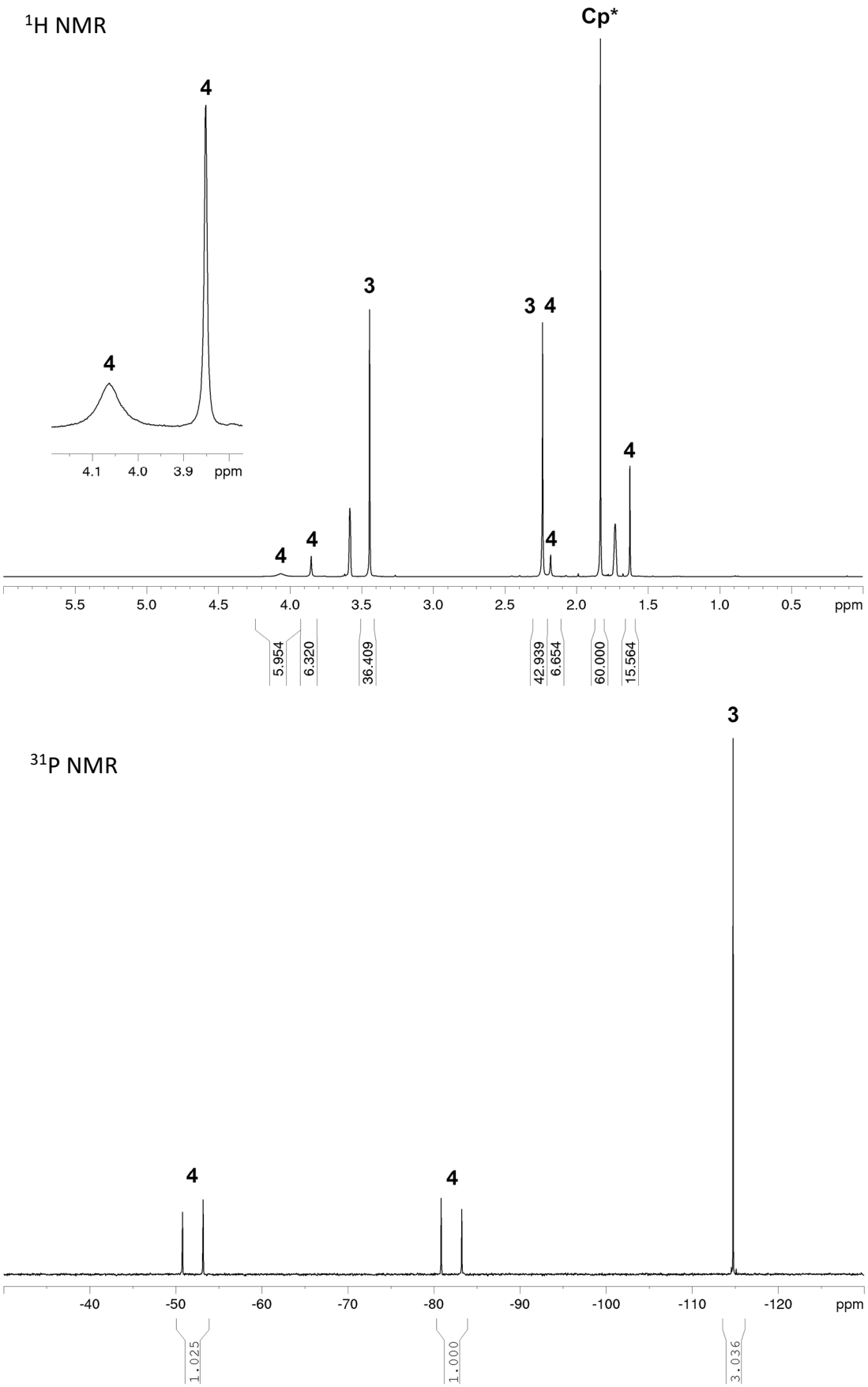

Figure S2. Experimental ^{1}H NMR (top) and ^{31}P NMR (bottom) spectrum of the crystal mixture of **3** and **4** (ratio 3/1, recorded in thf-d_8 at 300 K).

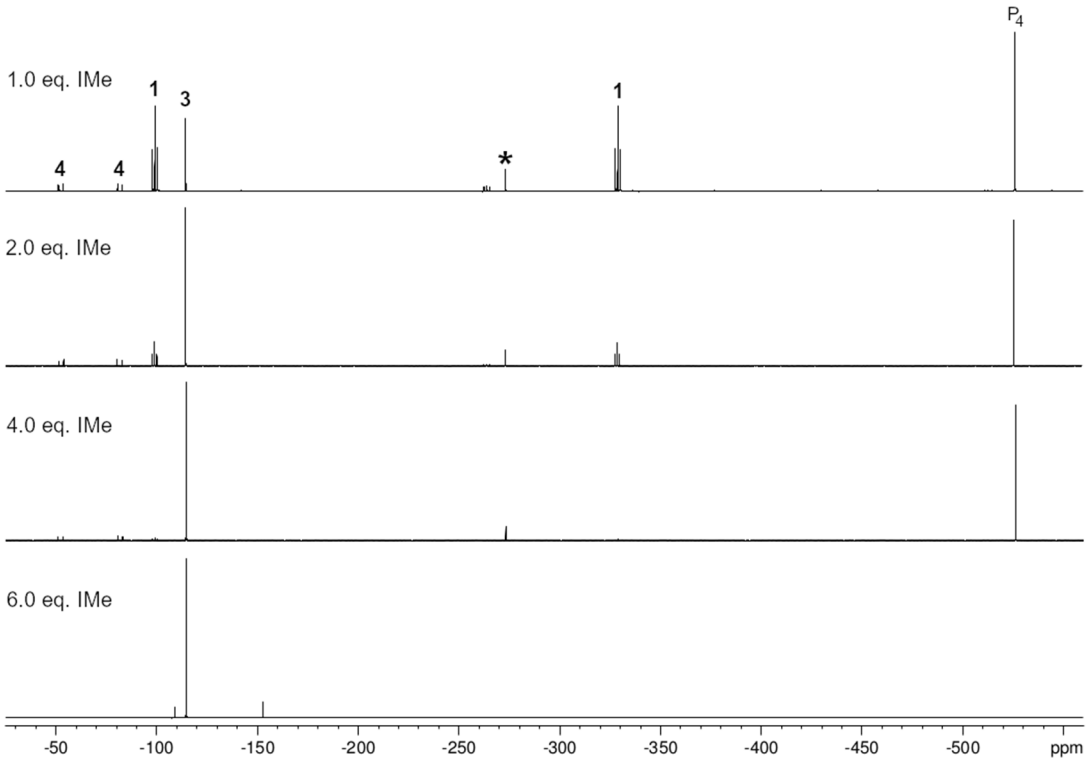

Figure S3. Experimental $^{31}P\{^1H\}$ NMR spectra of the reaction solution obtained from the reaction of **B** with various equivalents of IMe in thf (recorded with C_6D_6 capillary at 300 K; peak marked with asterisk is attributed to the common side product [Cp*Cr(CO)$_2$(η^3-P$_3$)]).

5.6.4 DFT calculations

The geometry of the molecules has been optimized using the TURBOMLE program package[7] at the RI-[8]B3LYP[9] level together with the def2-TZVP basis set for all atoms.[10] To speed up the calculations, the Coulomb part was evaluated by using the Multipole Accelerated Resolution of Identity method (MARI-*J*)[11] along with optimized auxiliary basis sets on all atoms.[12] The natural bond orbital analysis (NBO) has been performed with NBO 6.0[13] on the wave function obtained at the B3LYP/def2-TZVP level of theory. The topological analysis of the electron density obtained from the DFT calculations, according to the Atoms in Molecules theory[14] has been performed with the MultiWFN program (version 3.6).[15]

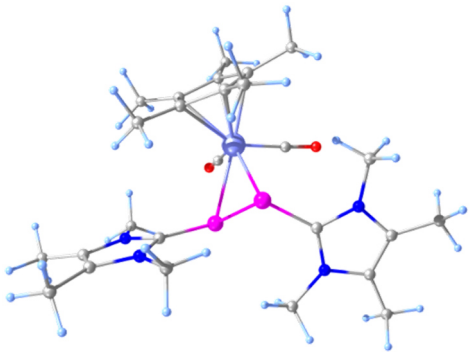

Table S2. Cartesian coordinates of the optimized geometry of **4** at the B3LYP/def2-TZVP level. E = -3110.31259080507 a.u.)

Atom	x	y	z	Atom	x	y	z
Cr	2.169143400	0.017355100	1.185933300	H	1.574044000	1.563552900	-2.466059400
P	-0.061701000	-0.001879400	2.237046400	H	0.275974300	1.683664200	-3.670178800
P	-0.052956500	0.034879300	0.083201200	H	0.328345700	0.310336400	-2.554672800
N	-1.453430900	2.666767800	0.034608300	C	2.756086700	1.578064000	2.799516300
N	-0.250691400	-2.444639900	3.649602500	C	-2.906015100	-4.632987000	2.370336000
N	-1.728437900	-2.410116400	2.078091400	H	-3.925860900	-4.264946900	2.508870000
N	-0.322523100	2.118529900	-1.721696400	H	-2.794044400	-5.523257400	2.985616600
O	2.516394500	-2.829156100	2.010026900	H	-2.799395600	-4.937252800	1.326689600
O	2.776562500	-1.100895200	-1.528502600	C	2.644441100	2.234659500	1.542602000
C	-0.630184900	1.710997500	-0.462395300	C	-2.605639500	-1.993149500	0.989414000
C	-0.706333600	-1.700086000	2.614728100	H	-2.659084200	-0.910852700	0.964051000
C	-1.647815600	3.678659300	-0.905401500	H	-3.599075600	-2.397227300	1.168941600
C	-0.933144800	3.334277600	-2.009191600	H	-2.234823300	-2.348836800	0.029151700
C	-1.886860100	-3.618712600	2.754836500	C	-0.768343600	4.036517200	-3.311380700
C	-0.958814700	-3.635480100	3.748129600	H	0.282179400	4.234754500	-3.535477300
C	4.283693500	0.611921100	1.364548700	H	-1.286223100	4.993030100	-3.287857800
C	3.754509300	0.566798600	2.688876500	H	-1.183180500	3.459145600	-4.141399100
C	2.351721000	-1.730017900	1.687230600	C	4.312787700	-0.249574800	3.815947000
C	-2.502398000	4.866512000	-0.634008100	H	3.582732600	-0.410604500	4.609077600
H	-3.534581100	4.583333600	-0.414188400	H	5.167509400	0.263540700	4.267544000
H	-2.519857800	5.521844700	-1.502137400	H	4.661080300	-1.226251200	3.481415600
H	-2.132113100	5.449439000	0.212896900	C	2.080649600	2.009602700	4.064036900
C	2.512417900	-0.677422900	-0.488803500	H	1.063819000	2.361233500	3.891222800
C	-2.126323200	2.672529000	1.327530600	H	2.639662300	2.831366200	4.523420300
H	-1.772011300	1.837343500	1.922046100	H	2.031093400	1.206542500	4.798515200
H	-3.204830200	2.591707800	1.185477000	C	3.975123900	2.177611900	-0.695200100
H	-1.908420900	3.601339900	1.853514100	H	4.307442100	1.390528100	-1.371580800
C	3.594921600	1.647841200	0.654631900	H	4.798563900	2.892607200	-0.601013900
C	0.783475800	-2.047808000	4.596230500	H	3.148395000	2.705366200	-1.171317800
H	1.278478200	-1.157856300	4.223835800	C	5.477269000	-0.150253100	0.872199400
H	1.517779500	-2.843966500	4.695111500	H	5.546256700	-1.136540400	1.330642400
H	0.337094200	-1.834084600	5.568112800	H	6.400095300	0.387504100	1.112593900
C	-0.652263900	-4.662916000	4.779351900	H	5.455617000	-0.291799300	-0.208060400
H	0.362267600	-5.053087500	4.667355600	C	1.842381400	3.473114400	1.280979500
H	-1.340604700	-5.500797300	4.692767300	H	1.577014600	3.576675700	0.229113200
H	-0.745234700	-4.261835800	5.791402300	H	2.414651200	4.365005400	1.557230900
C	0.518711300	1.376589300	-2.657150700	H	0.922010300	3.492217300	1.865208000

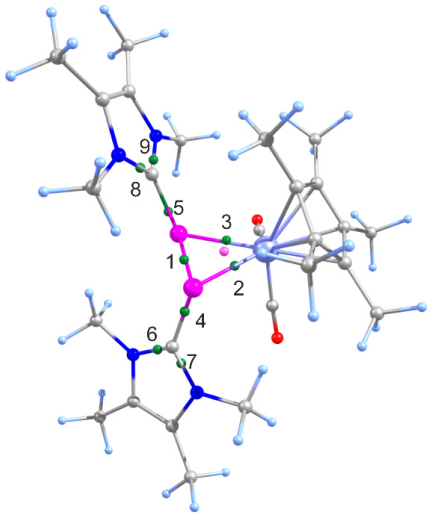

Table S3. Properties of selected critical points in the electron density of **4**. ρ(r) = electron density at CP; $\nabla^2\rho(r)$ = Laplacian of electron density; H(r) = energy density; G(r) = Lagrangian kinetic energy; V(r) = potential energy density; ε(r) = ellipticity of electron density at CP (ε(r) = [$\lambda_1(r)/\lambda_2(r)$]-1; where λ_1 and λ_2 are the lowest and the second lowest eigenvalues of Hessian matrix of ρ, respectively); η(r) = eta index (η(r) = $|\lambda_1(r)|/\lambda_3(r)$, where λ_1 and λ_3 are the lowest and the highest eigenvalues of Hessian matrix of ρ, respectively); Bond degree, BD = H(BCP)/ ρ (BCP) (the more positive the BD, the weaker the interaction). Labeling according to Fig. 4.

	ρ(r)	$\nabla^2\rho(r)$	H(r)	G(r)	V(r)	|V|/G	ε(r)	η(r)	BD (H/R)
BCP-1	0.122	-0.145	-0.069	0.033	-0.101	3.118	0.399	1.548	-0.566
BCP-2	0.059	0.098	-0.016	0.040	-0.056	1.390	0.331	0.263	-0.265
BCP-3	0.055	0.117	-0.013	0.042	-0.055	1.306	0.334	0.182	-0.235
BCP-7	0.331	-1.009	-0.511	0.259	-0.769	2.975	0.224	1.962	-1.542
BCP-6	0.330	-1.002	-0.505	0.254	-0.759	2.985	0.223	1.972	-1.532
BCP-4	0.142	0.003	-0.119	0.119	-0.238	1.993	0.185	0.537	-0.838
BCP-5	0.141	0.001	-0.117	0.118	-0.235	1.998	0.234	0.551	-0.835
BCP-8	0.329	-0.998	-0.502	0.253	-0.755	2.987	0.216	1.968	-1.528
BCP-9	0.329	-1.008	-0.499	0.247	-0.746	3.020	0.212	1.997	-1.519
RCP	0.051	0.114	-0.011	0.040	-0.051	1.284	-	-	-

5.6.5 Crystallographic details

$[P(IMe)_2][Fe(CO)_2Cp'''] (\mathbf{1})$

Compound **1** crystalizes in the form of dark orange plates from a saturated solution in thf at room temperature after 3 days. A suitable crystal with dimensions 0.29 × 0.20 × 0.08 mm^3 was selected and mounted on a Xcalibur, AtlasS2, Gemini ultra diffractometer. The crystal was kept at a steady T = 123(1) K during data collection. The structure was solved with the ShelXT 2018/2 (Sheldrick, 2018) solution program using Olex2 (Dolomanov et al., 2009) as the graphical interface. The model was refined with ShelXL 2018/3 (Sheldrick, 2015) using full matrix least squares minimisation on F^2. The asymmetric unit contains one molecule of **1**.

$[P(IMe)_2][\{Cp'''Fe\}_2(\mu,\eta^{3:3}\text{-}P_3)] (\mathbf{2})$

Compound **2** crystalizes in the form of dark red blocks from a saturated solution in toluene after one week. A suitable crystal with dimensions 0.42 × 0.16 × 0.05 mm^3 was selected and mounted on a GV50, TitanS2 diffractometer. The crystal was kept at a steady T = 123.01(10) K during data collection. The structure was solved with the ShelXT 2018/2 (Sheldrick, 2018) solution program using Olex2 (Dolomanov et al., 2009) as the graphical interface. The model was refined with ShelXL 2018/3 (Sheldrick, 2015) using full matrix least squares minimisation on F^2. The asymmetric unit contains one molecule of **2**.

$[P(IMe)_2][Cr(CO)_3Cp^*] (\mathbf{3})$

Compound **3** crystalizes in the form of clear yellow blocks after layering a saturated reaction solution in thf with n-pentane after a few days. A suitable crystal with dimensions 0.10 × 0.05 × 0.04 mm^3 was selected and mounted on a GV50, TitanS2 diffractometer. The crystal was kept at a steady T = 123.1(3) K during data collection. The structure was solved with the ShelXT 2018/2 (Sheldrick, 2018) solution program using Olex2 (Dolomanov et al., 2009) as the graphical interface. The model was refined with ShelXL 2018/3 (Sheldrick, 2015) using full matrix least squares minimisation on F^2. Due to poor quality of the obtained crystals only preliminary values can be given for the structural parameters. The asymmetric unit contains two anionic and cationic fragments of **3**.

$[\{Cp^*Cr(CO)_2\}(\eta^2\text{-}P_2IMe_2)][Cr(CO)_3Cp^*] (\mathbf{4})$

Compound **4** crystalizes in the form of dark brown blocks after layering a saturated reaction solution in thf with n-pentane after a few days. A suitable crystal with dimensions 0.17 × 0.14 × 0.10 mm^3 was selected and mounted on a GV50, TitanS2 diffractometer. The crystal was kept at a steady T = 123.00(16) K during data collection. The structure was solved with the ShelXT 2018/2 (Sheldrick, 2018) solution program using Olex2 (Dolomanov et al., 2009) as the graphical interface. The model was refined with ShelXL 2018/3 (Sheldrick, 2015) using full matrix least squares minimisation on F^2.The asymmetric unit contains one molecule of **4**.

Table S4. Selected parameters for the single crystal X-ray diffraction experiments of **1**, **2**, **3** and **4**.

	1	**2**	**3**	**4**
Formula	$C_{33}H_{53}FeN_4O_2P$	$C_{48}H_{82}Fe_2N_4P_4$	$C_{54}H_{78}Cr_2N_8O_6P_2$	$C_{39}H_{54}Cr_2N_4O_5P_2$
$D_{calc.}$/ g cm^{-3}	1.203	1.269	1.266	1.318
m/mm^{-1}	4.198	6.156	4.047	5.399
Formula Weight	624.61	950.75	1101.18	824.80
Colour	orange	dark pink	yellow	dark brown
Shape	plate	block	plate	block
Size/mm^3	0.29×0.20×0.08	0.42×0.16×0.05	0.10×0.05×0.04	0.17×0.14×0.10
T/K	123(1)	123.01(10)	123.1(3)	123.00(16)
Crystal System	triclinic	monoclinic	triclinic	monoclinic
Space Group	$P\bar{1}$	$P2_1/n$	$P\bar{1}$	$P2_1/n$
a/Å	10.8194(4)	13.7995(2)	8.9241(12)	14.7956(3)
b/Å	12.5965(6)	22.0551(3)	18.0574(17)	8.60807(16)
c/Å	15.1388(6)	16.5807(2)	18.8286(14)	32.9425(6)
α/°	106.563(4)	90	106.662(7)	90
β/°	98.875(3)	99.5490(10)	91.003(9)	97.7244(16)
γ/°	113.707(4)	90	95.628(9)	90
V/Å^3	1723.64(14)	4976.40(12)	2889.4(5)	4157.52(13)
Z	2	4	2	4
Z'	1	1	1	1
Wavelength/Å	1.54184	1.54184	1.54184	1.54184
Radiation type	CuK_a	CuK_a	Cu K_a	Cu K_α
Q_{min}/°	4.151	3.365	4.035	3.467
Q_{max}/°	72.873	74.005	62.387	75.267
Measured Refl's.	12167	20961	49308	35858
Ind't Refl's	6639	9772	9187	8355
Refl's with I > 2(I)	6295	9039	3895	7041
R_{int}	0.0194	0.0395	0.3119	0.0616
Parameters	387	579	676	679
Restraints	0	57	0	314
Largest Peak	0.530	0.713	0.809	0.479
Deepest Hole	-0.232	-1.177	-0.775	-0.459
GooF	1.030	1.063	1.088	1.040
wR_2 **(all data)**	0.0887	0.1239	0.4240	0.1261
wR_2	0.0871	0.1203	0.3433	0.1180
R_1 **(all data)**	0.0363	0.0520	0.2256	0.0548
R_1	0.0339	0.0488	0.1401	0.0456

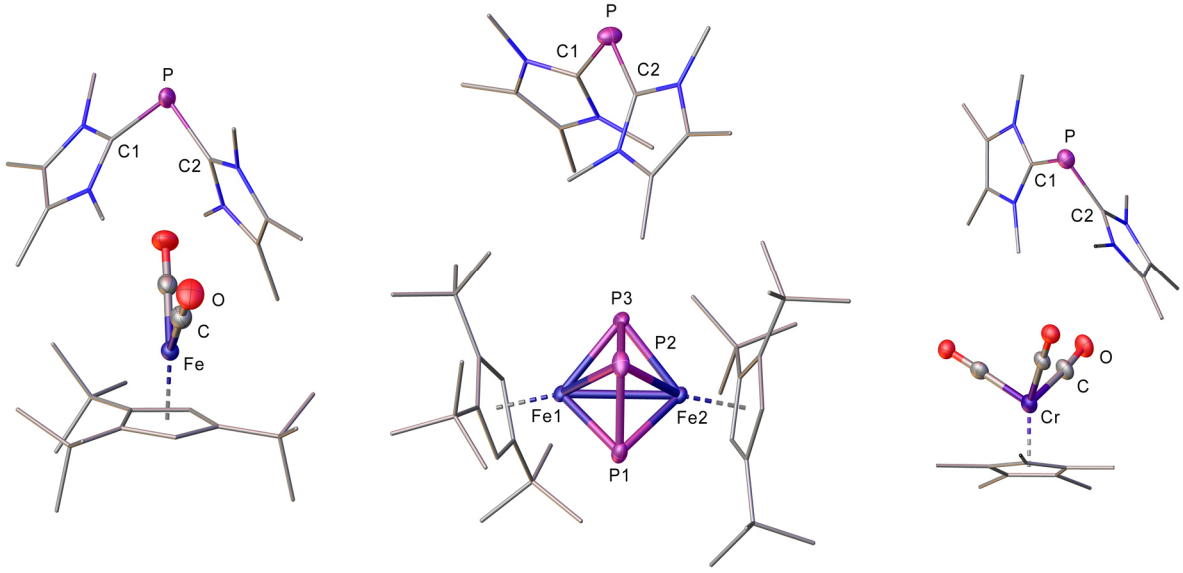

1 **2** **3**

Figure S4. Molecular structure of **1**, **2** and **3** in the solid state; H atoms are omitted for clarity and CO as well as Cp ligands are drawn in the wire frame model; thermal ellipsoids are drawn at 50% probability.

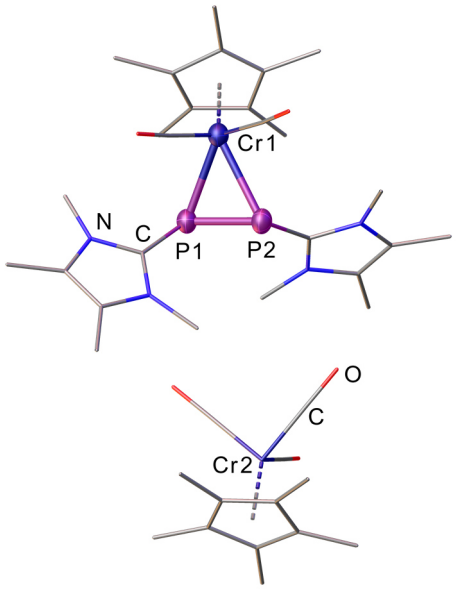

Figure S5. Molecular structure of **4** in the solid state; H atoms are omitted for clarity and CO as well as Cp* ligands are drawn in the wire frame model (only one part of the disordered Cp* ligand is depicted); thermal ellipsoids are drawn at 50% probability.

Table S5. Selected bond lengths [Å] and angles [°] of the $[P(IMe)_2]^+$ cation of **1**, **2** and **3** in the solid state.

	P–C [Å]		C–P–C [°]	Twist angle [°][1]	
1	1.8049(17)	1.8054(18)	95.79(8)	42.10(8)	44.75(8)
2	1.802(2)	1.797(2)	102.65(10)	26.08(10)	49.42(10)
3[2]	1.805(13) 1.817(13)	1.787(11) 1.792(12)	98.3(6) 96.9(6)	35.9(7) 36.3(7)	44.9(7) 46.7(7)

[1] Distortion angle between the $PC^{Carbene}_2$ plane and the planes spanned by the NHC ring systems.
[2] Preliminary values due to poor single crystal X-ray diffraction data.

Table S6. Selected bond lengths [Å] and angles [°] of the $[\{Cp'''Fe\}_2(\mu,\eta^{3:3}\text{-}P_3)]^-$ anion of **2** in the solid state.

	d / Å			α / °	
Fe1–P1	2.1942(6)	**Fe2–P3**	2.1971(6)	**Fe1–P1–Fe2**	79.94(2)
Fe1–P2	2.4221(6)	**P1–P2**	2.1601(8)	**Fe1–P2–Fe2**	71.315(18)
Fe1–P3	2.1931(6)	**P2–P3**	2.1897(8)	**Fe1–P3–Fe2**	80.06(2)
Fe2–P1	2.2015(6)	**Fe1–Fe2**	2.8236(4)	**P1–P2–P3**	95.21(3)
Fe2–P2	2.4217(6)				

Table S7. Selected bond lengths [Å] and angles [°] of **4** in the solid state.

	d / Å		α / °		
Cr1–P1	2.3954(7)	**P1–Cr1–P2**	52.02(2)	**P1–Cr1–P2–C8**	93.98(8)
Cr1–P2	2.4480(7)	**P2–P1–Cr1**	65.26(3)	**P2–Cr1–P1–C1**	93.37(8)
P1–P2	2.1246(8)	**P1–P2–Cr1**	62.71(2)		
P1–C	1.842(3)	**C1–P1–Cr1**	114.09(8)		
P2–C	1.835(3)	**C8–P2–Cr1**	112.90(8)		

5.6.6 References

[1] C. Schwarzmaier, A. Y. Timoshkin, G. Balázs, M. Scheer, Angew. Chem. Int. Ed. 2014, 53, 9077-9081.
[2] (a) R. B. King, *J. Organomet. Chem.* **1967**, *8*, 139-148.
(b) P. Leoni, A. Landi, M. Pasquali, *J. Organomet. Chem.* **1987**, *321*, 365-369.
(c) T. J. Jaeger, M. C. Baird, *Organometallics* **1988**, *7*, 2074-2076.
(d) C. Schwarzmaier, A. Y. Timoshkin, G. Balázs, M. Scheer, *Angew. Chem. Int. Ed.* **2014**, *53*, 9077-9081.
[3] N. Kuhn, T. Kratz, *Syntheses* **1993**, *6*, 561-562.
[4] A. J. Arduengo, R. Krafczyk, R. Schmutzler, H. A. Craig, J. R. Goerlich, W. J. Marschall, M. Unverzagt, *Tetrahedron* **1999**, *55*, 14523-14534.

[5] M. Schlosser, J. Hartmann, *Angew. Chem.* **1973**, *85*, 544-545; *Angew. Chem. Int. Ed. Engl.* **1973**, *12*, 508-509.
[6] TopSpin 3.0, Bruker BioSpin GmbH
[7] (a) F. Furche, R. Ahlrichs, C. Hättig, W. Klopper, M. Sierka, F. Weigend, *WIREs Comput. Mol. Sci.* **2014**, *4*, 91-100.
(b) R. Ahlrichs, M. Bär, M. Häser, H. Horn, C. Kölmel, *Chem. Phys. Lett.* **1989**, *162*, 165-169.
(c) O. Treutler, R. Ahlrichs, *J. Chem. Phys.* **1995**, *102*, 346-354.
(d) TURBOMOLE V6.4, a development of University of Karlsruhe and Forschungszentrum Karlsruhe GmbH, http://www.turbomole.com.
[8] (a) K. Eichkorn, O. Treutler, H. Oehm, M. Häser, R. Ahlrichs, *Chem. Phys. Lett.* **1995**, *242*, 652-660.
(b) K. Eichkorn, F. Weigend, O. Treutler, R. Ahlrichs, *Theor. Chem. Acc.* **1997**, *97*, 119.
[9] (a) A. D. Becke, *J. Chem. Phys.* **1993**, *98*, 5648-5652.
(b) C. Lee, W. Yang, R. G. Parr, *Phys. Rev. B* **1988**, *37*, 785-789.
(c) A. D. Becke, *Phys. Rev. A* **1988**, *38*, 3098-3100.
(d) S. H. Vosko, L. Wilk, M. Nusair, *Can. J. Phys.* **1980**, *58*, 1200-1211.
(e) J. C. Slater, *Phys. Rev.* **1951**, *81*, 385-390.
[10] (a) A. Schäfer, C. Huber, R. Ahlrichs, *J. Chem. Phys.* **1994**, *100*, 5829.
(b) K. Eichkorn, F. Weigend, O. Treutler, R. Ahlrichs, *Theor. Chem. Acc.* **1997**, *97*, 119.
(c) F. Weigend, R. Ahlrichs, *Phys. Chem. Chem. Phys.* **2005**, *7*, 3297.
(d) F. Weigend, *Phys. Chem. Chem. Phys.* **2006**, *8*, 1057.
[11] (a) K. Eichkorn, O. Treutler, H. Ohm, M. Häser, R. Ahlrichs, *Chem. Phys. Lett.* **1995**, *242*, 652-660.
(b) M. Sierka, A. Hogekamp, R. Ahlrichs, *J. Chem. Phys.* **2003**, *118*, 9136-9148.
[12] F. Weigend, *Phys. Chem. Chem. Phys.* **2006**, *8*, 1057-1065.
[13] NBO 6.0. E. D. Glendening, J. K. Badenhoop, A. E. Reed, J. E. Carpenter, J. A. Bohmann, C. M. Morales, C. R. Landis, F. Weinhold (Theoretical Chemistry Institute, University of Wisconsin, Madison, WI, **2013**); http://nbo6.chem.wisc.edu/
[14] (a) R. F. W. Bader, *Atoms in Molecules: A Quantum Theory*, Oxford University Press, **1994**.
(b) R. F. W. Bader, *Chem. Rev.* **1991**, *91*, 893-928.
[15] (a) T. Lu, F. Chen, *J. Comput. Chem.* **2012**, *33*, 580-592.
(b) http://sobereva.com/multiwfn.

5.7 Author contributions

Rebecca Grünbauer

- Synthesis and characterization of compounds **3** and **4**.
- Performance of additional studies concerning the reactivity of **A** and **B** towards $LiNME_2$, $LiCH_2SiMe_3$, $KCHPh_2$ and IDipp.
- Preparation of manuscript (including figures, schemes, tables and supplementary information) except for paragraphs on the topic of DFT calculations.

Stephan Reichl

- Synthesis and characterization of compounds **1** and **2**.

Gábor Balázs

- Execution of DFT calculations.
- Preparation of manuscript (including figures, schemes, tables and supplementary information) for paragraphs on the topic of DFT calculations.

Manfred Scheer

- Supervision of project.

6. The P_4 butterfly complex $[\{Cp^*Cr(CO)_3\}_2(\mu,\eta^{1:1}\text{-}P_4)]$: a starting material for P_4 transfer processes

Rebecca Grünbauer and Manfred Scheer

6.1 Abstract

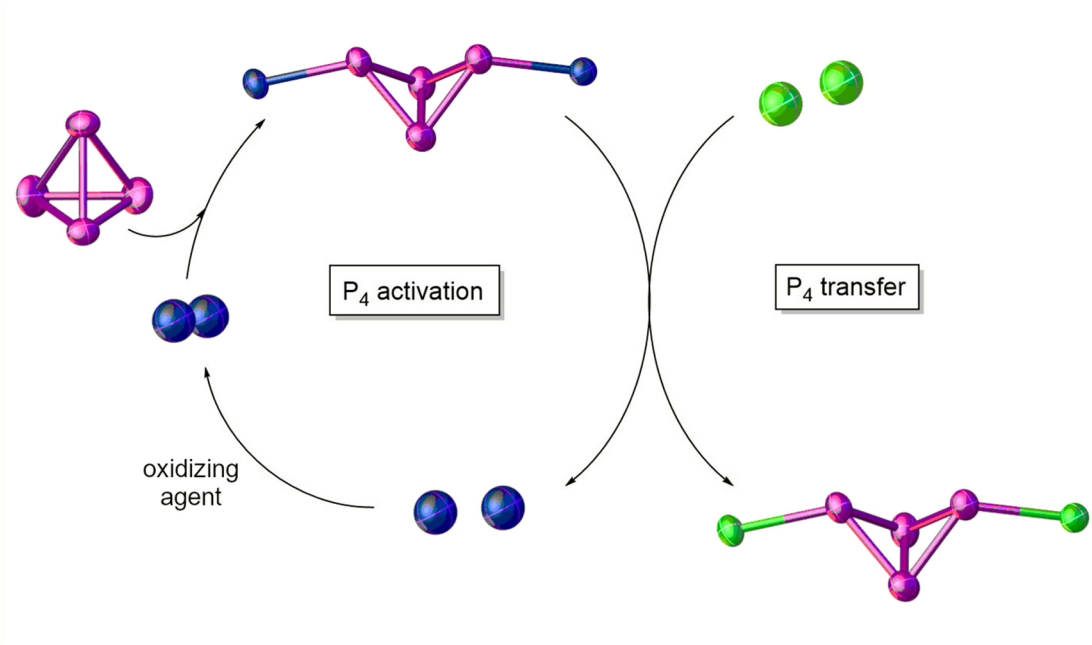

*Herein, we report on a novel reactivity of $[\{Cp^*Cr(CO)_3\}_2(\mu,\eta^{1:1}\text{-}P_4)]$ ($Cp^* = C_5(CH_3)_5$; **1**), which utilizes the selective cleavage of the two P–Cr bonds in **1** to initiate a substituent exchange yielding new P_4 butterfly species. By means of NMR and IR spectroscopy studies, the successful generation of $[\{Cp'''Fe(CO)_2\}_2(\mu,\eta^{1:1}\text{-}P_4)]$ ($Cp''' = C_5H_2{}^tBu_3$; **A**) and $[Cp'''_2(\mu,\eta^{1:1}\text{-}P_4)]$ (**B**) via the novel P_4 butterfly transfer route originating from **1** could be confirmed. For this purpose, **1** was reacted with 2.0 eq. of $K[Cp'''Fe(CO)_2]$ or NaCp''', respectively, and a quantitative conversion of **1** could be detected alongside the formation of 2.0 eq. of the $[Cp^*Cr(CO)_3]^-$ anion. Moreover, various syntheses of novel organometallic and organic P_4 butterfly compounds were examined and first results show that the generation of different compounds is conceivable. However, the isolation and stabilization of these sensitive molecules proves to be a major challenge.*

6.2 Introduction

The activation of small molecules like CO, N_2 or P_4 is currently of great scientific interest as the understanding of the underlying mechanistic steps could solve many fundamental issues, e. g. uneconomical and hazardous synthetic processes on an industrial scale.[1] In the field of P_4 activation, compounds incorporating a tetraphospha-*bicyclo*[1.1.0]butane motif are formed in the first step of the activation of the P_4 tetrahedron.[2] The so called P_4 butterfly compounds can serve as starting materials in the investigation of the reactivity of polyphosphorus ligand complexes and can therefore provide more insight in the mechanisms behind the first essential steps of P_4 activation. Due to the expanding understanding of these processes, the generation of phosphorus containing compounds is expected to eventually become more economical, less hazardous and more selective.

Most commonly, P_4 butterfly units are stabilized through coordination towards unsaturated organometallic fragments via the wing tip P atoms. The first example for a compound incorporating such a P_4^{2-} structural motif was reported by *Lindsell* and *Ginsberg* in 1971: [(PPh$_3$)$_2$RhCl(η$^{1:1}$-P_4)].[3] At first it was reported that within this complex an intact P_4 tetrahedron coordinates towards the {(PPh$_3$)$_2$RhCl} fragment in a η^2-coordination mode. However, subsequent ^{31}P NMR spectroscopic experiments specified a complete cleavage of the P–P bond affording a chelating P_4 butterfly ligand. In contrast, bridging P_4 butterfly complexes are stabilized by two (organometallic) substituents. The most famous representative of this class of P_4 butterfly compounds is the complex [{Cp^{R}Fe(CO)$_2$}$_2$(μ,η$^{1:1}$-P_4)] (Cp^R = Cp″ ($C_5H_3{}^tBu_2$) or Cp‴ ($C_5H_2{}^tBu_3$, **A**)), which was first obtained by *Scherer* et al.[4] Interestingly, our group was able to optimize the synthesis of **A**, which can be quantitatively obtained by reacting the dimeric [Cp‴Fe(CO)$_2$]$_2$ with elemental P_4 at ambient conditions.[5] The vast reaction potential of **A** has been intensively studied under photolytic[4a] and thermolytic[4b] reaction conditions and the improved synthesis of **A** initiated investigations concerning its coordination potential.[5,6]

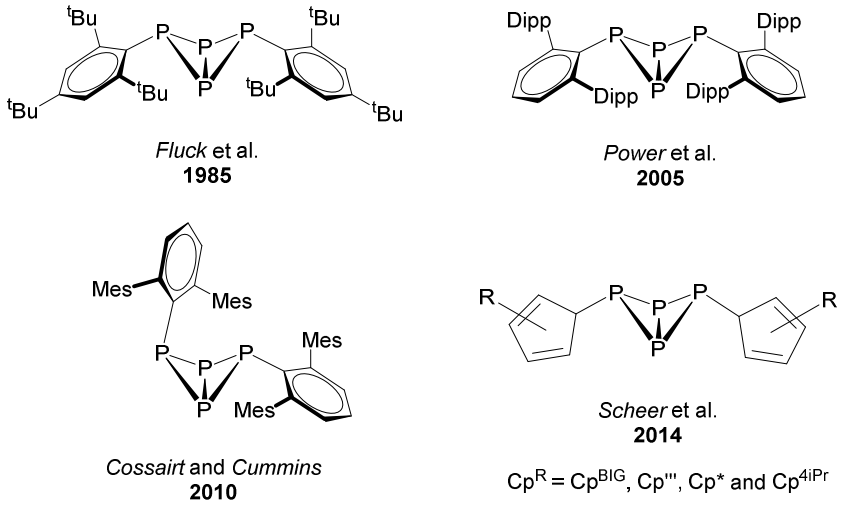

Scheme 1. Overview of neutral *organo*-P_4 butterfly compounds (Dipp = 2,6-^{i}Pr$_2$C$_6$H$_3$, Mes = 2,4,6-(CH$_3$)$_3$C$_6$H$_2$, Cp^{BIG} = C$_5$(4-^{n}BuC$_6$H$_4$)$_5$, Cp‴ = C$_5$H$_2{}^t$Bu$_3$, Cp* = C$_5$(CH$_3$)$_5$, Cp^{4iPr} = C$_5$H^{i}Pr$_4$).

Next to investigations concerning P_4 butterfly compounds that are stabilized by organometallic fragments, the scientific community shares great interest in the synthesis of P_4 butterfly units with organic substituents. Only

a few of them are known so far and therefore the need for an easy synthetic access to novel "*organo*-P_4 butterfly" complexes is obvious (Scheme 1). After theoretical suggestions that a [$C_2(\mu,\eta^{1:1}\text{-}P_4)$] motif is thermodynamically stable[7], *Fluck et al.* were the first to report on the successful synthesis of the bright orange [$Mes^*_2(\mu,\eta^{1:1}\text{-}P_4)$] ($Mes^*$ = 2,4,6-^{t}Bu$_3$C$_6$H$_2$) in 1985 (Scheme 1).[8] Implying different sterically demanding ligands, the group of *Power* was able to isolate [$Ar^{Dipp}_2(\mu,\eta^{1:1}\text{-}P_4)$] ($Ar^{Dipp}$ = 2,6-(2,6-^{i}Pr$_2$C$_6$H$_3$)$_2$C$_6$H$_3$, Scheme 1) while *Cummins* and *Cossairt* reported on the synthesis of [$Dmp_2(\mu,\eta^{1:1}\text{-}P_4)$] (Dmp = 2,6-(2,4,6-(CH$_3$)$_3C_6H_2$)$_2C_6H_3$, Scheme 1).[9] One common feature of all these compounds is the fact that the P_4 unit is connected to an aromatic substituent via a sp^2 hybridized carbon atom. However, our group was able to demonstrate that a substitution via a sp^3 hybridized carbon atom is possible as well by synthetizing various [$Cp^R_2(\mu,\eta^{1:1}\text{-}P_4)$] compounds that incorporate cyclopentadienyl ligands (Cp^R = Cp^{BIG} (C$_5$(4-^{n}Bu-C$_6$H$_4$)$_5$, Cp* (C$_5$(CH$_3$)$_5$), Cp‴ (C$_5$H$_2$^{t}Bu$_3$), Cp^{4iPr} (C$_5$H^{i}Pr$_4$); Scheme 1).[10] [$Cp^{BIG}_2(\mu,\eta^{1:1}\text{-}P_4)$] was obtained by reacting P_4 with Cp^{BIG} radicals, which were generated from the reaction of $NaCp^{BIG}$ with CuBr. For Cp ligands that do not generate comparingly stable radical species (e.g. Cp* , Cp‴ and Cp^{4iPr}), another reaction pathway starting from $FeBr_3$, MCp^R (M = Li or Na) and P_4 was implied as the supporting Fe^{II}/Fe^{III} redox system enables the formation of a $Cp^{\cdot}$ radical from a Cp^- anion.

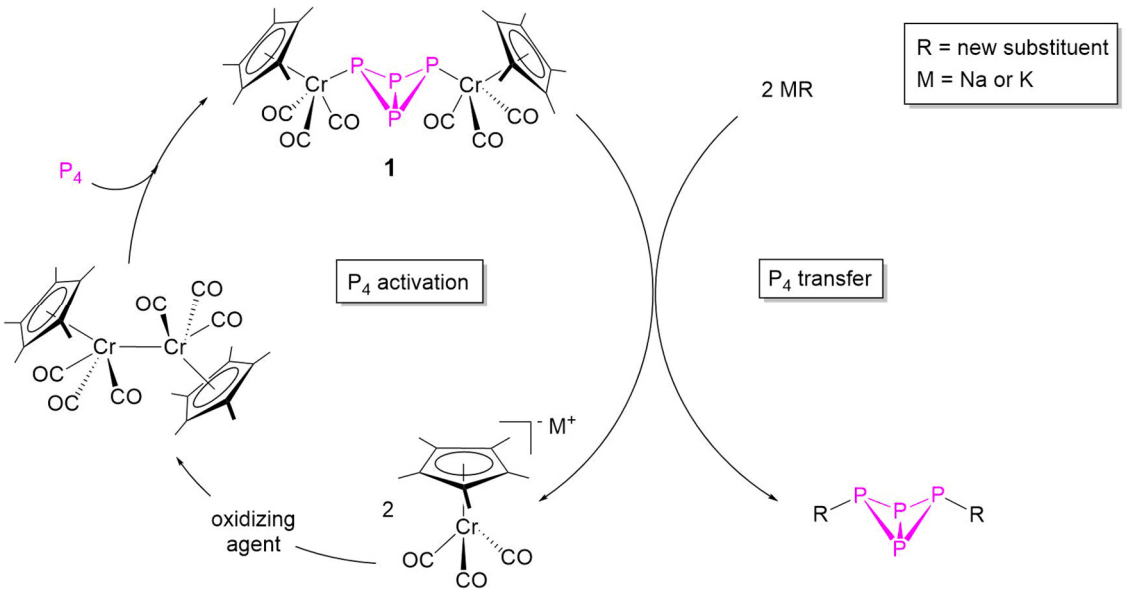

Scheme 2. Proposed P_4 activation/transfer reaction mechanism starting from **1**.

Previous experiments and theoretical calculations delineate that the Cr–P bonds in [{Cp*Cr(CO)$_3$}$_2(\mu,\eta^{1:1}\text{-}P_4)$] (**1**, dissociation energy: 67.47 kJ·mol^{-1}) are easily cleaved in comparison to the Fe–P bonds in **A** (dissociation energy: 142.91 kJ·mol^{-1}).[11] Hence, the question arose whether it is possible to utilize this remarkable feature of **1**. Therefore, the idea to specifically break the P–Cr bonds of **1** and attach new ligands on the resulting naked P_4 butterfly motif came to mind. This straightforward substituent exchange might grant a foothold in the generation of a plethora of unprecedented P_4 butterfly compounds that cannot be obtained from a more classical approach (e.g. reacting P_4 with the corresponding dimer of the substituent like in the classical synthetic approach to obtain **A**, *vide supra*). Moreover, if the released chromium substituent of **1** could be isolated from the reaction mixture, the chromium dimer [Cp*Cr(CO)$_3$]$_2$ could be recovered with the help of a

suitable oxidizing agent. [Cp*Cr(CO)$_3$]$_2$ could once again be reacted with P_4 to obtain **1** initiating another cycle of the P_4 activation / P_4 transfer procedure (Scheme 2). Consequently, the unique reactivity of **1** could introduce a synthetic pathway not only towards the generation of unprecedented P_4 butterfly compounds but also in terms of chemical efficiency as it might eventually enable a semi-catalytic transfer of P_4 butterfly moieties.

6.3 Results and Discussion

6.3.1 Organometallic substituents

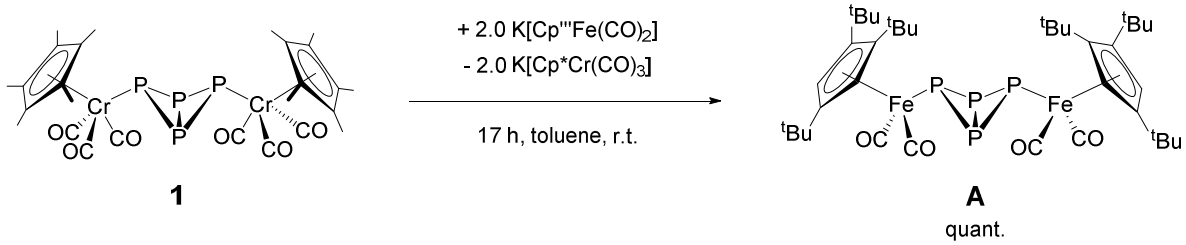

Scheme 3. Successful substituent transfer starting from **1** yielding **A**.

To test out the proposed substituent transfer, **1** was reacted successfully with 2.0 eq. of K[Cp‴Fe(CO)$_2$] quantitatively yielding the known **A** and 2.0 eq. of K[Cp*Cr(CO)$_3$] after 17 hours (Scheme 3). NMR and IR spectroscopy confirmed the quantitative formation of **A** without any side reactions (cf. SI). Consequently, it can be stated that the proposed substituent transfer deriving from **1** is generally possible. A red solution of **A** could be isolated from the crude reaction mixture upon the extraction with *n*-hexane leaving behind K[Cp*Cr(CO)$_3$] as a yellow solid. The clean separation of the two reaction products due to different solubilities is a great starting point for the desired recovery of [Cp*Cr(CO)$_3$]$_2$ to ultimately achieve a semi-catalytic P_4 activation/transfer procedure.

The successful substituent transfer converting the chromium P_4 butterfly complex **1** into the iron P_4 butterfly complex **A** is a compelling incentive to expand the investigations towards the generation of novel P_4 butterfly compounds. Therefore, various organometallic reagents were reacted with **1** in accordance to the successful reaction with K[Cp‴Fe(CO)$_2$]. Hereby, one approach towards the generation of novel P_4 butterfly complexes was to incorporate smaller Cp ligands like the unsubstituted Cp and the symmetrical Cp* (e.g. reacting **1** with K[CpFe(CO)$_2$] and K[Cp*Fe(CO)$_2$]).[12] Another approach was to react **1** with K[Cp′Mo(CO)$_3$], K[CpW(CO)$_3$] and Na[Cp‴W(CO)$_3$] in order to obtain P_4 butterfly complexes of the heavier homologs of chromium. However, all of the employed reagents gave the same result. In the ^{31}P NMR spectra of the reaction mixtures no signals corresponding to the starting material **1** or newly formed P_4 butterfly compounds could be obtained. On the contrary, an almost quantitative conversion affording P_4 was recorded alongside the occasional formation of small amounts of [Cp*Cr(CO)$_2$(η^3-P$_3$)], a common byproduct of all manipulations of **1**. Moreover, IR spectroscopic investigations confirmed that for the reactions of **1** with K[CpFe(CO)$_2$] and K[Cp*Fe(CO)$_2$] the corresponding [Cp^{R}Fe(CO)$_2$]$_2$ dimers (Cp: $\tilde{\nu}_{CO}$ [cm^{-1}] = 1952, 1937, 1783; Cp*: $\tilde{\nu}_{CO}$ [cm^{-1}] = 1959, 1924, 1755

cm^{-1}; both recorded in toluene) can be detected in the reaction mixture. Additionally, bands corresponding to $K[Cp^*Cr(CO)_3]$ could be identified as well ($\tilde{\nu}_{CO}$ [cm^{-1}] = 1994, 1873; recorded in toluene).

This observation confirms that the initial step in the P_4 transfer process, the cleavage of the Cr–P bonds of **1** affording $[Cp^*Cr(CO)_3]^-$, occurred effectively. Consequently, unsubstituted P_4 butterfly moieties are expected to be present in the reaction solution available for the coordination towards the newly introduced organometallic fragments forming novel P_4 butterfly compounds. However, the newly obtained P_4 butterfly compounds (e.g. $[\{CpFe(CO)_2\}_2(\mu,\eta^{1:1}\text{-}P_4)]$) are most likely thermodynamically very unstable, instantly decomposing to afford P_4 and the corresponding organometallic dimer (e.g. $[CpFe(CO)_2]_2$; Scheme 4).

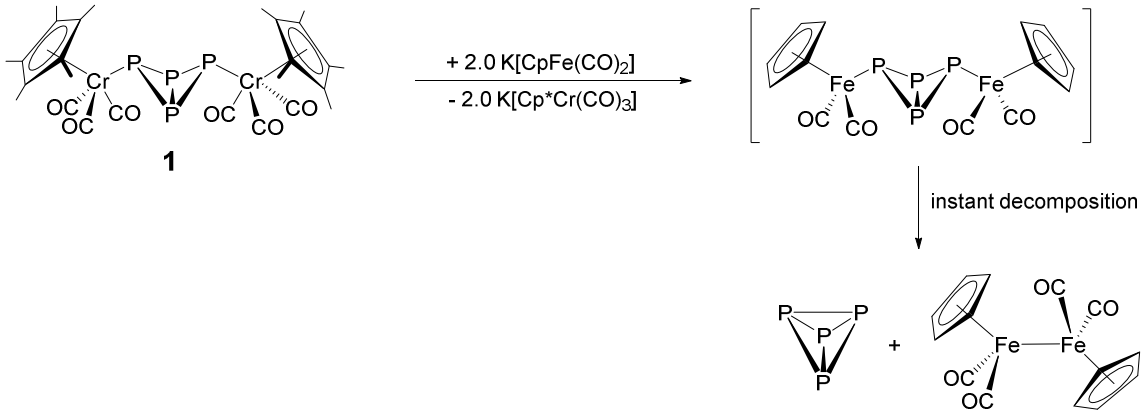

Scheme 4. Proposed reaction of **1** with $K[CpFe(CO)_2]$ as an example of the instant decomposition of the newly obtained P_4 butterfly compounds of the substituent transfer experiments.

Unfortunately, no method could be established to stabilize, obtain, isolate and eventually characterize the expected novel P_4 butterfly complexes due to their presumed instability. Yet, the detection of the expected decomposition products $K[Cp^*Cr(CO)_3]$, $[CpM(CO)_x]_2$ and P_4 suggest the instant fragmentation of the newly formed P_4 butterfly compounds.

Most likely, the smaller cyclopentadienyl ligands (Cp, Cp* and Cp′) cannot provide the stabilization introduced by the steric hindrance of the Cp‴ ligand of the $[Fe(CO)_2Cp'''']$ fragment, which is apparently essential to the stability of **A**. Therefore, P_4 butterfly compounds incorporating the smaller Cp derivatives appear to be not accessible via this novel P_4 butterfly transfer reaction pathway. Additionally, the implementation of the heavier transition elements Mo and W did not result in the formation of the desired novel P_4 butterfly compounds as well. For molybdenum and tungsten no P_4 butterfly compounds are known so far. $[\{CpM(CO)_2\}_2\{\mu,\eta^{2:2}\text{-}P_2\}]$ and $[CpM(CO)_2(\eta^3\text{-}P_3)]$ (M = Mo, W) are the only species obtained from reacting P_4 with $[CpM(CO)_2]_2$ or $[CpM(CO)_3]_2$ (M = Mo, W) under thermolytic conditions.[13] Consequently, molybdenum and tungsten substituted P_4 butterfly compounds might not be thermodynamically stable but decompose instantly.

6.3.2 Organic substituents

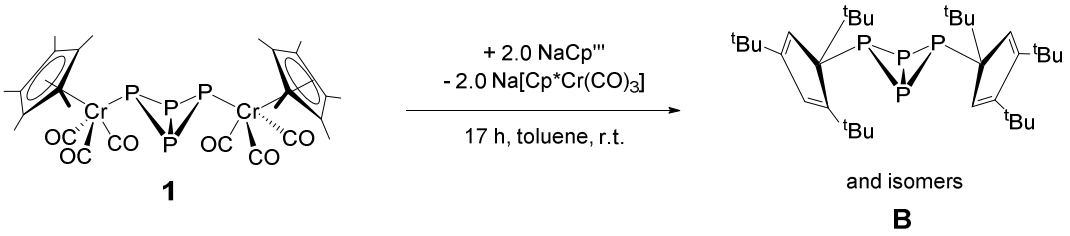

Scheme 5. Successful substituent transfer starting from **1** yielding **B**.

Next to the formation of novel organometallic P_4 butterfly complexes, the unique reactivity of **1** could be the ideal starting point for an alternative synthetic pathway in the generation of *organo*-P_4 butterfly compounds. To test this hypothesis, **1** was reacted with two equivalents of NaCp‴, proposing the formation of the already known [Cp‴$_2$(μ,η$^{1:1}$-P_4)] (**B**) by means of the above discussed P_4 butterfly transfer processes. Through ^{31}P NMR spectroscopy a successful reaction and moreover an improved selectivity in comparison to the original synthesis, incorporating $FeBr_3$, NaCp‴ and P_4, could be detected.[10] In the previous synthetic approach the isomer depicted in Scheme 5 was obtained in approx. 35% yield alongside three other constitutional isomers varying in the arrangement of the ^{t}Bu substituents of the Cp‴ ligands. In contrast, the depicted isomer of **B** could be identified as the main product from the substituent transfer originating from **1** with a relative amount of 84% in respect to all obtained isomers of **B**. The ABMN spin system of the depicted isomer of **B** affords four elaborate multiplets in the corresponding ^{31}P NMR spectrum, which could be further examined by simulation. In comparison to the ^{31}P NMR chemical shifts given in literature[10], the signals in the ^{31}P NMR spectrum recorded for the reaction of **1** with 2.0 eq. NaCp‴ are slightly shifted (Table 1). One explanation for this observation could be the interference of a paramagnetic chromium compound present in the reaction solution.

Table 1. Comparison of the previously reported ^{31}P NMR spectrum of the depicted isomer of **B** and the corresponding signals in the simulated ^{31}P NMR spectrum from the reaction of **1** with 2.0 eq. NaCp‴ (both recorded in C_6D_6 at 300 K).

		P_A	P_B	P_M	P_N
δ [ppm]	reported[10]	-154.6	-162.5	-324.8	-352.1
	recorded	-126.6	-132.0	-312.4	-343.2
J [Hz]	reported[10]	191 (AM) 175 (AN) 317 (AB)	175 (BN) 191 (BM) 317 (AB)	191 (AM) 175 (BM) 173 (MN)	175 (BN) 191 (AN) 173 (MN)
	recorded	187 (AM) 208 (AN) 348 (AB)	169 (BN) 195 (BM) 348 (AB)	187 (AM) 195 (BM) 177 (MN)	169 (BN) 207 (AN) 177 (MN)

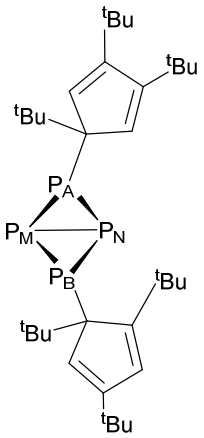

Motivated by the successful synthesis of **B**, the reaction of **1** with NaCp* was analogously studied to investigate, if this synthetic route can be applied to obtain *organo*-P_4 butterfly complexes with sterically less demanding substituents as well. Surprisingly, an immediate conversion of **1** accompanied by the quantitative formation of P_4 could be observed in the ^{31}P NMR spectrum suggesting that if [$Cp^*_2(\mu,\eta^{1:1}\text{-}P_4)$] is formed, it decomposes instantly. This was not to be expected as previous reports proved that [$Cp^*_2(\mu,\eta^{1:1}\text{-}P_4)$] is a stable compound.[10] Variable temperature $^{31}P\{^1H\}$ NMR spectroscopy delineates that lowering the reaction temperature does not facilitate the formation of the desired product (cf. SI). Below 223 K no conversion of the starting material can be detected. When the sample is heated above this temperature a constant increase in P_4 can be detected without the formation of a novel P_4 butterfly intermediate. Consequently, a rapid decomposition of an instable reaction product, which cannot be detected on an NMR time scale, affording P_4 can be stated.

Hence, the above discussed reaction of **1** with alkali cyclopentadienyl compounds is not a universal reaction pathway for the formation of novel *organo*-P_4 butterfly compounds. Consequently, a different class of reactive organic substituents was studied. Therefore, Ph_3CCl and Ph_2CHCl, respectively, were reacted with $AlCl_3$ to afford the reactive cations Ph_3C^+ and Ph_2CH^+, respectively. In a second step, these activated carbon species were reacted with **1** in order to perform the abstraction of the [$Cp^*Cr(CO)_3$] fragment and the subsequent P–C bond formation.

First experiments on an NMR spectroscopic scale gave promising results. For the reactions of **1** with 2.0 eq. of $Ph_3CCl/AlCl_3$ and $Ph_2CHCl/AlCl_3$, respectively, two triplets assignable to new P_4 butterfly species could be detected in the $^{31}P\{^1H\}$ NMR spectra, respectively ($[Ph_3C]^+$: δ [ppm] = 16.2 (t, $^1J_{PP}$ = 238 Hz, 2P), -313.6 (t, $^1J_{PP}$ = 238 Hz, 2P), Fig. 1; $[Ph_2CH]^+$: δ [ppm] = 25.4 (t, $^1J_{PP}$ = 273 Hz, 2P), -301.2 (t, $^1J_{PP}$ = 273 Hz, 2P)). However, the apparently quantitative formation of these new compounds is not reproducible and upscaling of the reaction lead to major difficulties. For example, reasonable amounts of byproducts like [$Cr(CO)_3Cp^*X$] (X = CO or Cl) and [$Cp^*_2Cr_2Cl_3$] could be isolated from the reaction mixture and characterized. Additionally, a blue fluorescent oil could be extracted from the crude reaction mixture of the reaction of **1** with $Ph_2CHCl/AlCl_3$. This suggest that a deprotonation of Ph_2CH^+ followed by a dimerization affording $Ph_2C{=}CPh_2$ occurred. To rule out that $AlCl_3$ is the culprit of the side reactions, alternative chloride abstractors like $TlPF_6$ were used and the reaction was repeated in the presence of a base (NBU). Unfortunately, no conversion could be detected at all when adding these reagents.

Another approach to eliminate the side effects of $AlCl_3$ on the reaction, was reacting **1** with $[Ph_3C][BF_4]$ instead of utilizing Ph_3CCl and $AlCl_3$. Surprisingly, a different $^{31}P\{^1H\}$ NMR spectrum compared to the one obtained after the reaction of **1** with $Ph_3CCl/AlCl_3$ was recorded (Fig. 1). Instead of two triplets assignable to a new P_4 butterfly species, the reaction of **1** with $[Ph_3C]^+[BF_4]^-$ afforded two multiples at δ = 66.6 ppm and δ = 82.8 ppm in the $^{31}P\{^1H\}$ NMR spectrum. The splitting patterns of these multiplets are very similar to the ones of the signals reported for the 6π-aromatic P_4R_2 ligand found in [$\{(Cp'''Fe(CO)_2)_2(\mu_3,\eta^{1:1:4}\text{-}P_4)\}_2Fe][PF_6]_2$ ($\delta(^{31}P\{^1H\}$ NMR) = 91.7 ppm and 114.3 ppm).[6c] Consequently, it can be proposed that no substituent transfer on the intact P_4 butterfly moiety occurred but some sort of rearrangement of the central P_4 scaffold arose. Unfortunately, all attempts to crystalize, isolate or further characterize the intriguing reaction product failed. In order to increase the accessibility of the product an excess of [$Cr(CO)_4$(nbd)] (nbd = norbornadiene) was added to the reaction mixture assuming that a coordination of the newly formed P_4 ligand motif towards [$Cr(CO)_4$] fragments would facilitate crystallization. $^{31}P\{^1H\}$ NMR experiments confirmed the successful coordination of [$Cr(CO)_4$] fragments as a remarkable upfield shift of approx. 130 ppm and a change in the

splitting pattern of the detected signal could be observed resulting in a very broad multiplet with a chemical shift of δ = -57.3 ppm. However, the resulting product appears to be a brown oil not feasible for further investigation. Furthermore, the reaction was performed analogously with $[Ph_3C]^+[B(C_6F_5)_4]^-$ in order to promote crystallization by anion exchange. However, only a quantitative conversion to P_4 could be detected in the ^{31}P NMR spectrum of this reaction. Additionally, the reaction was performed with **A** as well, as the lower solubility of the Cp‴ ligand in comparison to the Cp* ligand facilitates isolation. However, no conversion could be detected for the reaction of **A** with $[Ph_3C]^+[BF_4]^-$ by NMR spectroscopic experiments. Consequently, **1** is once again the more intriguing starting material due to its increased and more unique reactivity. However, the insufficiency of means to isolate the obtained products in a major setback.

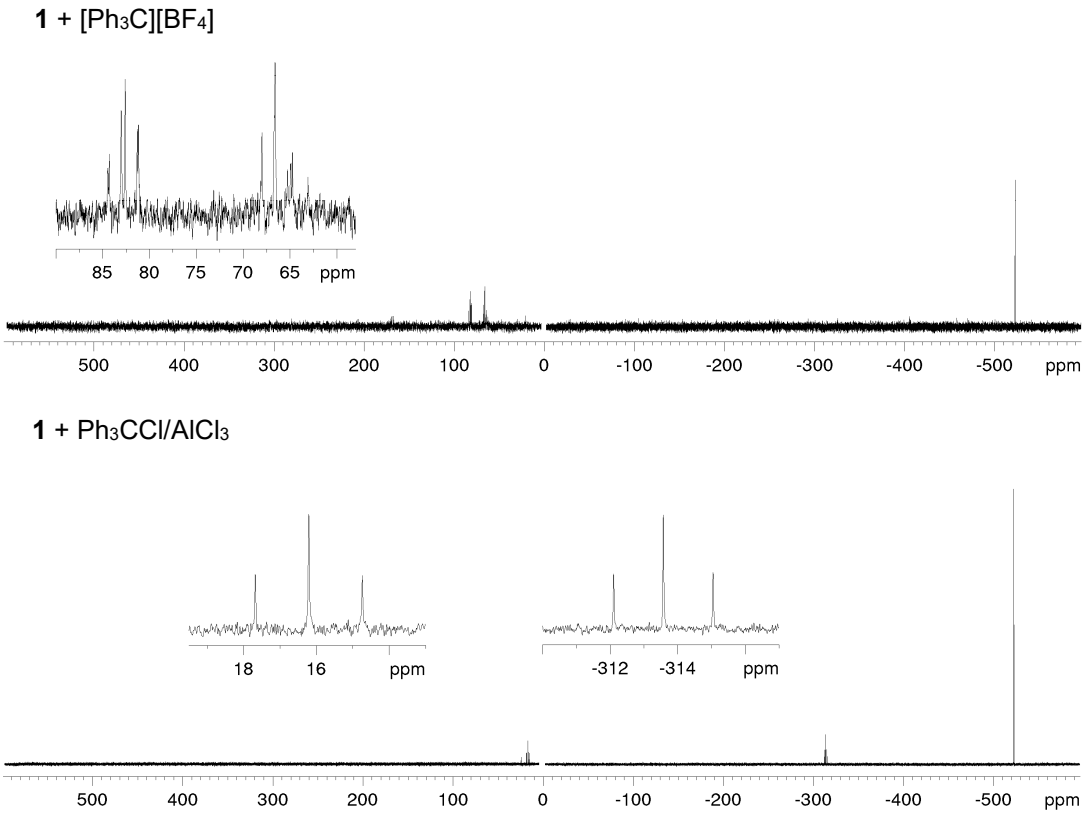

Figure 1. $^{31}P\{^1H\}$ NMR spectra of the crude reaction mixtures of the reaction of **1** with 2.0 eq. $[Ph_3C]^+[BF_4]^-$ (top) and the reaction of **1** with 2.0 eq. $Ph_3CCl/AlCl_3$ (bottom; both recorded in CD_2Cl_2 at 300 K).

6.4 Conclusion

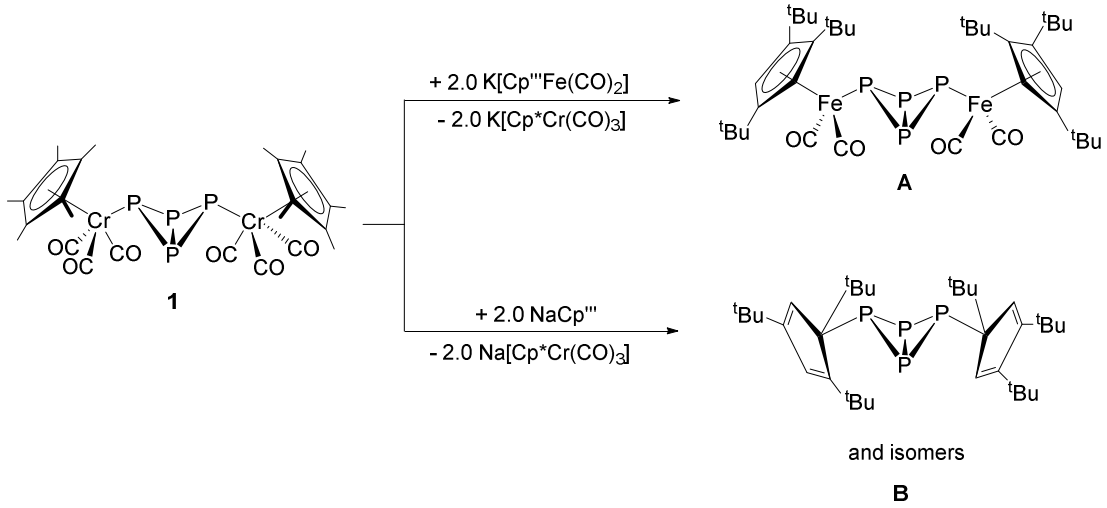

Scheme 6. Successful substituent transfer reactions starting from **1**.

In conclusion, the rather weak P–Cr bonds in **1** enable an unprecedent reactivity pathway for P_4 butterfly compounds by allowing selective substituent transfer. Although first results were very promising, the substituent exchange starting from **1** could not produce any novel P_4 butterfly compounds so far. However, the fact that already known P_4 butterfly compounds could be obtained by this reaction pathway is affirming (Scheme 6). **A** and **B** could be obtained from this novel synthetic pathway and in the case of **B** even an increase in selectivity could be observed compared to the literature procedure. Maybe fine tuning the reaction conditions, improving the steric demand of the substituents or the implementation of more thermodynamically stable substituents could promote the successful generation of novel P_4 butterfly compounds from the novel reactivity we found for **1**. Control experiments showed, that **A** does not display this kind of reactivity further manifesting that **1** is the more diverse reagent compared to the traditional P_4 butterfly compound **A**. Moreover, the clean separation of K[Cp*Cr(CO)$_3$] in the successful P_4 butterfly transfer from **1** to **A** is the first step to recover the released chromium substituent and eventually retrieve [Cp*Cr(CO)$_3$]$_2$ to start another cycle in the semi-catalytic P_4 activation/transfer process.

6.5 References

[1] (a) N. Hazari, Chem. *Soc. Rev.* **2010**, *39*, 4044-4056.
(b) I. Mellone, F. Bertini, L. Gonsalvi, A. Guerriero, M. Peruzzini, *Chimia* **2015**, *69*, 331-338.
(c) Z. Turner, *Inorganics* **2015**, *3*, 597.
(d) R. A. Henderson, *Trans. Met. Chem.* **1990**, *15*, 330-336.
(e) V. P. Indrakanti, J. D. Kubicki, H. H. Schobert, *Energy Environ. Sci.* **2009**, *2*, 745-758.
(f) X. Yin, J. R. Moss, *Coord. Chem. Rev.* **1999**, *181*, 27-59.

[2] (a) B. M. Cossairt, N. A. Piro, C. C. Cummins, *Chem. Rev.* **2010**, *110*, 4164-4177.
(b) M. Caporali, L. Gonsalvi, A. Rossin, M. Peruzzini, *Chem. Rev.* **2010**, *110*, 4178-4235.
(c) M. Scheer, G. Balázs, A. Seitz, *Chem. Rev.* **2010**, *110*, 4236-4256.
(d) N. A. Giffin, J. D. Masuda, *Coord. Chem. Rev.* **2011**, *255*, 1342-1359.

[3] A. P. Ginsberg, W. E. Lindsell, *J. Am. Chem. Soc.* **1971**, *93*, 2082-2084.

[4] (a) O. J. Scherer, G. Schwarz, G. Wolmershäuser, *Z. Anorg. Allg. Chem* **1996**, *622*, 951-957.
(b) O. J. Scherer, T. Hilt, G. Wolmershäuser, *Organometallics* **1998**, *17*, 4110-4112.

[5] C. Schwarzmaier, S. Heinl, G. Balázs, M. Scheer, *Angew. Chem. Int. Ed. Engl.* **2015**, *54*, 13116-13121.

[6] (a) M. Eberl, *Ph.D. thesis*, University of Regensburg (Regensburg), **2011**.
(b) C. Schwarzmeier, *Ph.D. thesis*, University of Regensburg (Regensburg), **2012**.
(c) J. Müller, S. Heinl, C. Schwarzmaier, G. Balázs, M. Keilwerth, K. Meyer, M. Scheer, Angew. Chem. Int. Ed. 2017, 56, 7312 – 7317.

[7] (a) W. Schoeller, C. Lerch, *Inorg. Chem.* **1983**, *22*, 2992-2998
(b) W. W. Schoeller, V. Staemmler, P. Rademacher, E. Niecke, *Inorg. Chem.* **1986**, *25*, 4382-4385

[8] Riedel, R., Hausen, H.-D. and Fluck, E., *Angew. Chem. Int. Ed. Engl.* **1985**, *24*, 1056-1057.

[9] (a) A. R. Fox, R. J. Wright, E. Rivard, P.P.Power, *Angew. Chem. Int Ed.* **2005**, *44*, 7729-7733.
(b) B. M. Cossairt, C. C. Cummins, *New. J. Chem.* **2010**, *35*, 1533 – 1536.

[10] S. Heinl, S. Reisinger, C. Schwarzmaier, M. Bodensteiner, M. Scheer, *Angew. Chem. Int. Ed.* **2014**, *53*, 7639 – 7642.

[11] (a) Cf. other chapters of this thesis.
(b) R. Grünbauer, *Master thesis*, University of Regensburg (Regensburg), **2016**.

[12] [{Cp*Fe(CO)$_2$}$_2$(μ,η$^{1:1}$-P_4)] was proposed by ^{31}P NMR spectroscopy (δ[ppm] = -46.5 (t, $^1J_{AB}$ = 185 Hz, 2P, P_A), -337.5 (t, $^1J_{AB}$ = 185 Hz, 2P, P_B); recorded in a thf reaction solution), however it decomposes during workup and could therefore not be structurally characterized yet: L. Weber, U. Sonnenberg, *Chem. Ber.* **1991**, *124*, 725-728.

[13] (a) O. J. Scherer, H. Sitzmann, G. Wolmershäuser, *J. Organomet. Chem.* **1984**, *268*, C9.
(b) O. J. Scherer, H. Sitzmann, G. Wolmershäuser, *Angew. Chem. Int. Ed. Engl.* **1985**, *24*, 351.
(c) L. Y. Goh, C. K. Chu, R. C. S. Wong, *J. Chem. Soc. Dalton Trans.* **1989**, *1*, 1951-1956.

6.6 Supplementary Information

6.6.1 General remarks

All experiments were performed under an inert gas atmosphere of dry argon or nitrogen using standard Schlenk and Glovebox techniques. Residues of oxygen and water were removed from the inert gas by passing it over a BASF R 3-11 ($CuO/MgSiO_3$) catalyst, concentrated H_2SO_4 and finally granulated silica gel. Dry solvents were collected from a Braun SPS Apparatus and degassed prior to use. The deuterated solvents C_6D_6 and CD_2Cl_2 were degassed and dried by stirring with Na/K alloy and CaH_2, respectively, followed by distillation. After the distillation, CD_2Cl_2 was additionally stored over molecular sieve (3 Å) which had previously been dried for four hours under high vacuum at 100 °C.

NMR spectra were recorded at the NMR department of the University Regensburg using a Bruker Advance 300 or 400 spectrometer. Samples are referenced against TMS (^1H, ^{13}C) or 85% H_3PO_4 (^{31}P) as external standards. Chemical shifts [δ] are reported in ppm and coupling constants [*J*] in Hz. The spectra were processed using the TopSpin 3.5 software (Bruker) and the WIN-DAISY module of this software was used to perform simulations.[1] IR spectra were recorded on a FT-IR spectrometer from DIGILAB (FTS 800) for diluted solutions sealed between KBr plates.

The starting materials [{Cp*Cr(CO)$_3$}$_2$(μ,η$^{1:1}$ -P$_4$)] (**1**)[2], NaCp*[3], NaCp‴[4], [Cr(CO)$_4$(nbd)][5] were prepared according to literature procedures. For Na[Cp‴Fe(CO)$_2$], K[CpFe(CO)$_2$], K[Cp*Fe(CO)$_2$] K[Cp′Mo(CO)$_3$], K[CpW(CO)$_3$] and Na[Cp‴W(CO)$_3$] the synthesis was performed as a variation of the instructions for the preparation of the respective Cp compounds.[6] [Ph$_3$C][BF$_4$], [Ph$_3$C][B(C$_6$F$_5$)$_4$], Ph$_3$CCl, Ph$_2$CHCl, AlCl$_3$, TlPF$_6$ and 1,8-Diazabicyclo[5.4.0]undec-7-ene (DBU) are commercially available and were used without further modification.

6.6.2 Organometallic substituents

6.6.2.1 Experimental setup

To an orange-brown solution of **1** (20 mg, 0.03 mmol, 1.0 eq.) in 5 mL toluene a solution of 2.0 eq. K[Cp^{R}M(CO)$_x$] (0.06 mmol) in toluene (5 mL) was added dropwise. No immediate color change could be observed, and the reaction mixture was stirred overnight at room temperature. Subsequently, the solution was concentrated and transferred to an NMR tube with a C_6D_6 capillary.

For the reaction with Na[Cp‴Fe(CO)$_2$] the solvent was removed from the reaction mixture under reduced pressure affording a mixture of yellow and red solid. By extraction with *n*-hexane a red solution (**A**) could be separated from the yellow residue (Na[Cp*Cr(CO)$_3$]). The solvent from the extract was subsequently removed *in vacuo*.

Experimental data

^{31}P{^{1}H} NMR (toluene with C_6D_6 capillary, 300 K))

Na[Cp‴Fe(CO)$_2$] δ[ppm] = -82.5 (t, $^1J_{AB}$ = 186 Hz, 2P, **A**), -324.7 (t, $^1J_{AB}$ = 186 Hz, 2P, **A**).

K[CpFe(CO)$_2$]	δ[ppm] = -512.6 (s, P_4).
K[Cp*Fe(CO)$_2$]	δ[ppm] = -512.6 (s, P_4).
K[Cp'Mo(CO)$_3$]	δ[ppm] = -95.0 (t, $^1J_{AB}$ = 196 Hz, 2P, **1**), -273.6 (s, 1.2P, [Cp*Cr(CO)$_2$(η^3-P_3)]), -327.2 (t, $^1J_{AB}$ = 196 Hz, 2P, **1**), -522.6 (s, 21.7P, P_4).
K[CpW(CO)$_3$]	δ[ppm] = -273.6 (s, 1.2P, [Cp*Cr(CO)$_2$(η^3-P_3)]), -522.8 (s, 21.7 P, P_4).
Na[Cp‴W(CO)$_3$]	δ[ppm] = -95.0 (t, $^1J_{AB}$ = 196 Hz, 2P, **1**), -273.5 (s, 0.5P, [Cp*Cr(CO)$_2$(η^3-P_3)]), -327.4 (t, $^1J_{AB}$ = 196 Hz, 2P, **1**), -522.2 (s, 2.7P, P_4).

IR (toluene)

Na[Cp‴Fe(CO)$_2$]	$\tilde{\nu}_{CO}$ [cm^{-1}] = 2000 (s), 1990 (s), 1949(s), 1942 (s), 1765 (w).
K[CpFe(CO)$_2$]	$\tilde{\nu}_{CO}$ [cm^{-1}] = 1995 (s), 1952 (w), 1936 (s), 1914 (m), 1874 (s), 1782 (s), 1726 (m, br).
K[Cp*Fe(CO)$_2$]	$\tilde{\nu}_{CO}$ [cm^{-1}] = 1994 (m), 1972 (w), 1959 (w), 1924 (s), 1873 (s), 1755 (m), 1727 (w).

6.6.2.2 IR spectroscopic experiments

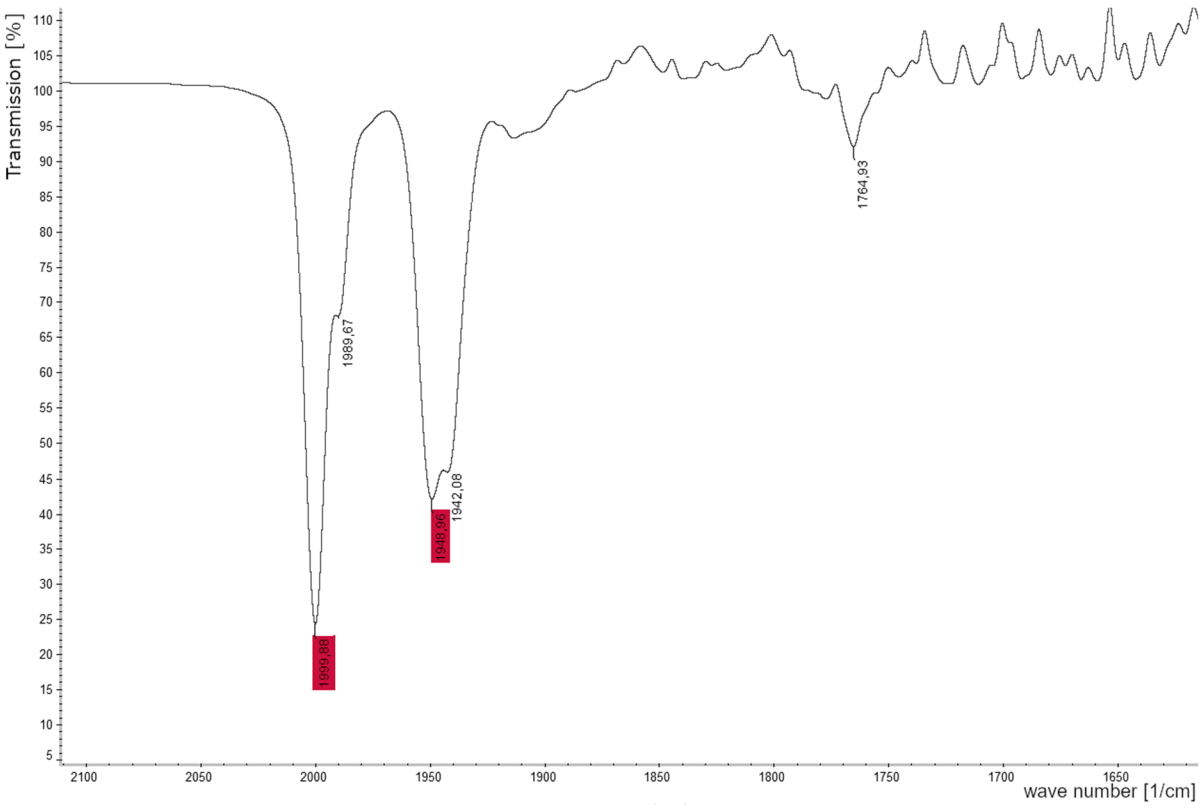

Figure S1. IR spectrum of the red solution extracted with *n*-hexane from the crude reaction product of the reaction of **1** with 2.0 eq. Na[Cp‴Fe(CO)$_2$] (recorded in toluene); the bands corresponding to **A** are marked red.

The yellow residue from this reaction of **1** with 2.0 eq. Na[Cp‴Fe(CO)$_2$] could not be taken up in any solvent appropriate for measuring IR in reasonable amounts. Therefore, no IR spectrum for Na[Cp*Cr(CO)$_3$] could be recorded.

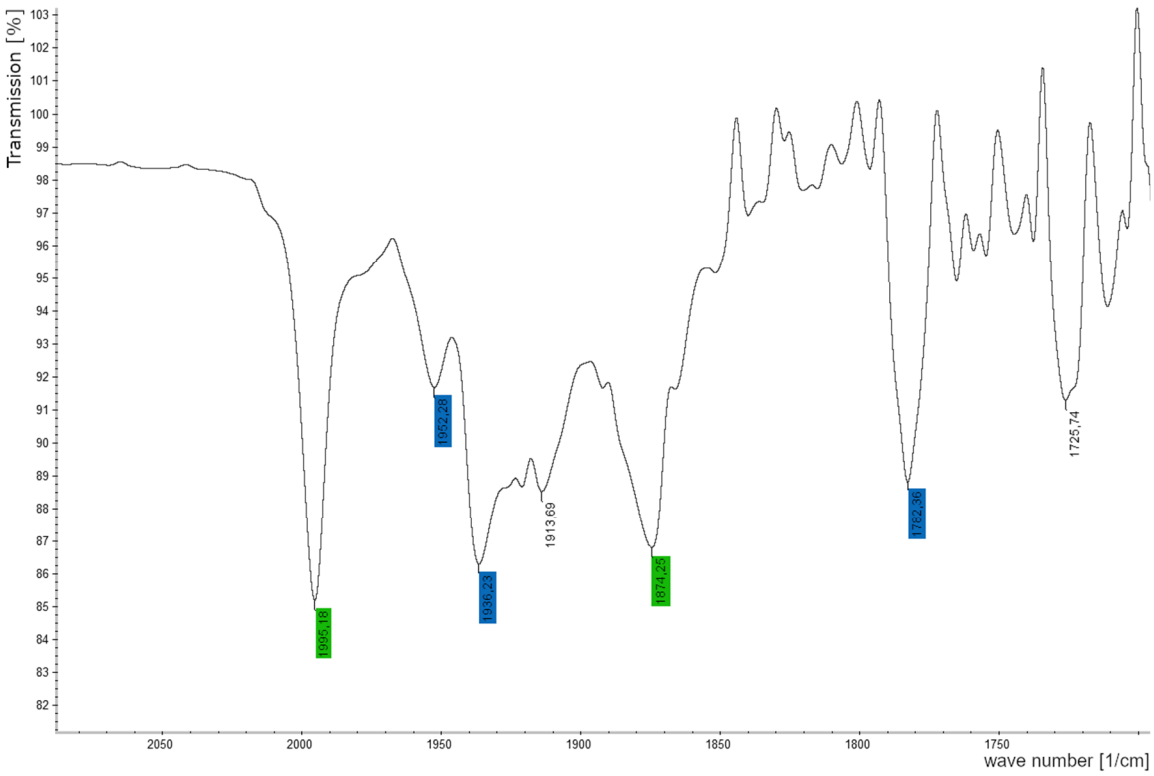

Figure S2. IR spectrum of the solid obtained from the reaction of **1** with 2.0 eq. $K[CpFe(CO)_2]$ (recorded in toluene); the bands corresponding to $[CpFe(CO)_2]_2$ (blue) and $K[Cp^*Cr(CO)_3]$ (green) are marked

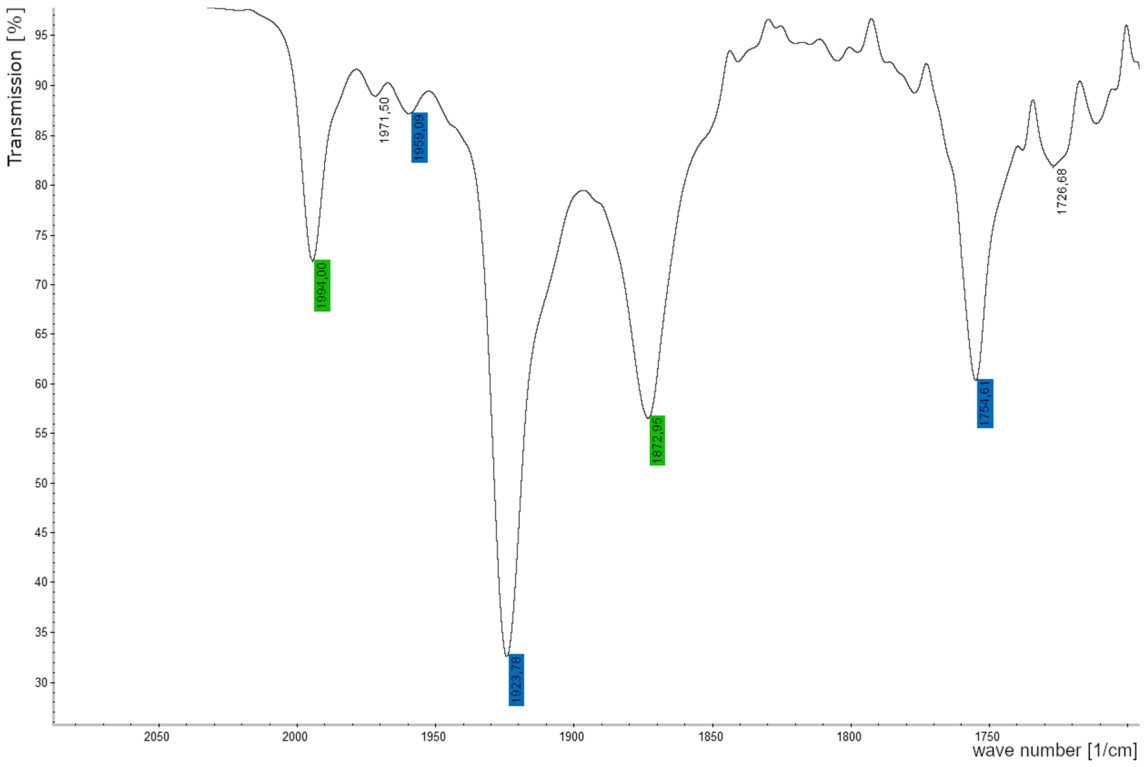

Figure S3. IR spectrum of the solid obtained from the reaction of **1** with 2.0 eq. $K[Cp^*Fe(CO)_2]$ (recorded in toluene); the bands corresponding to $[Cp^*Fe(CO)_2]_2$ (blue) and $K[Cp^*Cr(CO)_3]$ (green) are marked.

6.6.2.3 NMR spectroscopic experiments

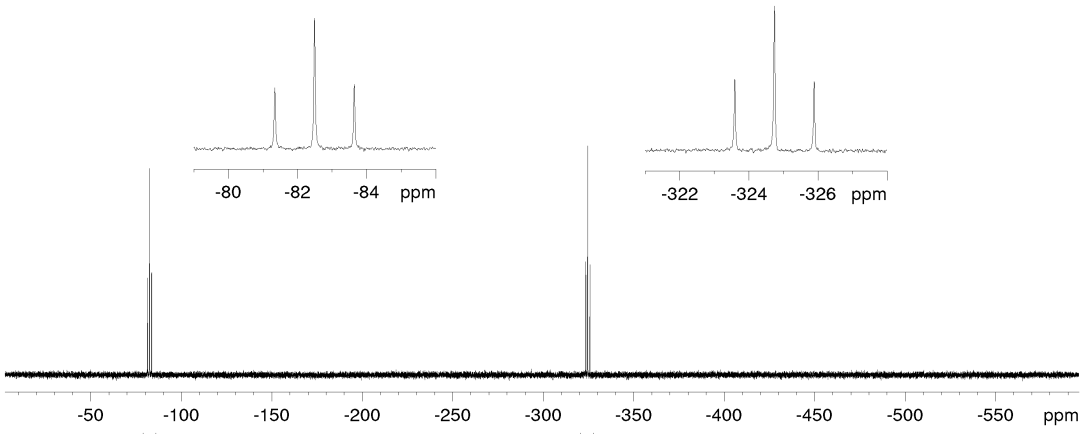

Figure S4. $^{31}P\{^1H\}$ NMR spectrum of the crude reaction mixture of the reaction of **1** with 2.0 eq. Na[Cp‴Fe(CO)$_2$] (recorded in toluene with C_6D_6 capillary at 300 K).

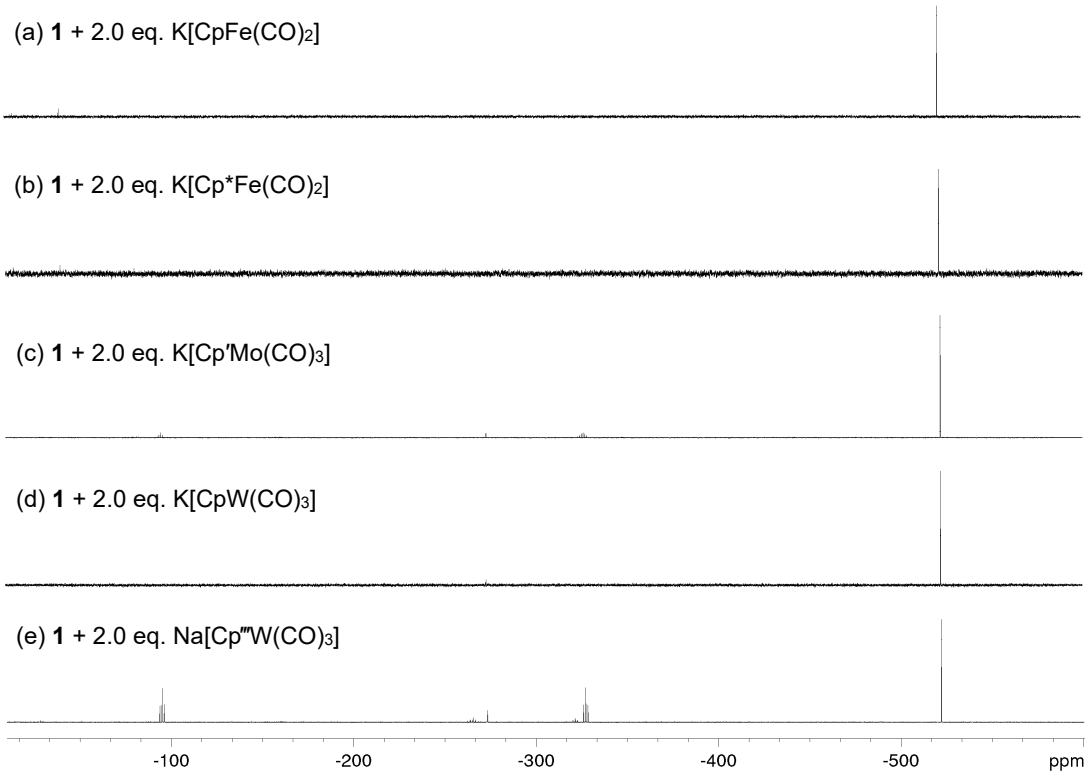

Figure S5. $^{31}P\{^1H\}$ NMR spectra of the crude reaction mixture of 1.0 eq. **1** with 2.0 eq. of different organometallic reagents (recorded in toluene with C_6D_6 capillary at 300 K).

6.6.3 Organic substituents

6.6.3.1 Experimental setup

Reaction of 1 with $NaCp^R$

An orange-brown solution of 1.0 eq. **1** (17 mg, 0.03 mmol or 25 mg, 0.04 mmol, respectively) in 5 mL toluene is added dropwise to a suspension of 2.0 eq. $NaCp^R$ (Cp‴: 13 mg, 0.05 mmol; Cp*: 12 mg, 0.08 mmol) in 5 mL toluene. No immediate color change is observed and the reaction mixture is stirred overnight at room temperature. Subsequently, the solvent is removed *in vacuo* yielding yellow and brown solid, respectively.

Experimental data

NaCp‴

^{1}H NMR (C_6D_6, 300 K) δ[ppm] = 1.07 (s, 19.9H, Cp*), 1.15 (s, 14.0H, ^{t}Bu), 1.17 (s, 20.6H, ^{t}Bu), 1.25 (s, 22.9H, ^{t}Bu), 1.30 (s, 14.1H, ^{t}Bu), 1.35 (s, 18.4H, ^{t}Bu), 1.36 (s, 18.3H, ^{t}Bu), 1.71 (s, 12.8H, ^{t}Bu), 2.96 (s, 2.4H, CH), 3.09 (s, 3.0H, CH), 3.89 (q, $^1J_{HH}$ = 6.8 Hz, 3.4H, CH), 5.76 (m, 1.0H, CH), 5.96 (t, $^1J_{HH}$ = 1.8 Hz, 2.3H, CH), 6.42 (m, 4.7H, CH).

^{31}P{^{1}H} NMR (C_6D_6, 300 K) δ[ppm] = -99.1 (t, $^1J_{PP}$ = 193 Hz, 0.04P), -123.6 to -135.4 (m, 2P, P_A and P_B), -157.8 (m, 0.1P), -269.4 (s, [Cp*Cr(CO)$_2$(η^3-P$_3$)], 0.3P), -312.4 (dt, $^1J_{MN}$ = 170 Hz, $^1J_{AM}$ = $^1J_{BM}$ = 190 Hz, 1P, P_M), -328.5 (t, $^1J_{PP}$ = 194 Hz, 0.1P), -332.0 (t, $^1J_{PP}$ = 190 Hz, 0.5P), -334.8 (t, $^1J_{PP}$ = 183 Hz, 0.1P), -343.1 (dt, $^1J_{MN}$ = 170 Hz, $^1J_{AN}$ = $^1J_{BN}$ = 206 Hz, 1P, P_N), -520.6 (s, 3P, P_4).

NaCp*

^{31}P{^{1}H} NMR (C_6D_6, 300 K) δ[ppm] = -269.9 (s, 1P, [Cp*Cr(CO)$_2$(η^3-P$_3$)]), -520.4 (s, 17P, P_4).

Reaction of 1 with NaCp* for VT NMR experiments

An orange-brown solution of **1** (25 mg, 0.04 mmol, 1.0 eq.) in 2 mL CD_2Cl_2 and a yellow suspension of NaCp* (12 mg, 0.08 mmol, 1.0 eq.) in 2 mL CD_2Cl_2 are cooled to -80°C. Subsequently, **1** is added to the suspension of NaCp* dropwise. The resulting mixture is transferred to a chilled NMR tube and placed in a tempered NMR spectrometer recording ^{1}H and ^{31}P{^{1}H} NMR spectra in intervals of 20°C .

Experimental data

^{31}P{^{1}H} NMR (CD_2Cl_2, 193 K) δ[ppm] = -92.7 (t, $^1J_{PP}$ = 198 Hz, 2P, **1**), -326.8 (t, $^1J_{PP}$ = 198 Hz, 2P, **1**), -516.6 (s, 0.5P, P_4).

^{31}P{^{1}H} NMR (CD_2Cl_2, 213 K) δ[ppm] = -93.2 (t, $^1J_{PP}$ = 198 Hz, 2P, **1**), -326.7 (t, $^1J_{PP}$ = 198 Hz, 2P, **1**), -518.0 (s, 0.5P, P_4).

^{31}P{^{1}H} NMR (CD_2Cl_2, 233 K) δ[ppm] = -93.6 (t, $^1J_{PP}$ = 198 Hz, 2P, **1**), -326.8 (t, $^1J_{PP}$ = 198 Hz, 2P, **1**), -519.3 (s, 0.5P, P_4).

^{31}P{^{1}H} NMR (CD_2Cl_2, 253 K) δ[ppm] = -94.7 (t, $^1J_{PP}$ = 198 Hz, 2P, **1**), -327.6 (t, $^1J_{PP}$ = 198 Hz, 2P, **1**), -521.1 (s, 0.6P, P_4).

^{31}P{^{1}H} NMR (CD_2Cl_2, 273 K) δ[ppm] = -95.2 (t, $^1J_{PP}$ = 198 Hz, 2P, **1**), -327.8 (t, $^1J_{PP}$ = 198 Hz, 2P, **1**), -522.2 (s, 0.9P, P_4).

^{31}P{^{1}H} NMR (CD_2Cl_2, 300 K) δ[ppm] = -95.2 (t, $^1J_{PP}$ = 198 Hz, 2P, **1**), -327.4 (t, $^1J_{PP}$ = 198 Hz, 2P, **1**), -522.8 (s, 2.5P, P_4).

Reaction of 1 with $Ph_2CXCl/AlCl_3$ (X = Ph or H)

A colorless solution of 2.0 eq. Ph_2CXCl (X = Ph : 10 mg, 0.04 mmol; X = H, 0.06 mL of a 1:10 diluted solution in toluene, 0.04 mmol) in toluene (5 mL) is added dropwise to a colorless suspension of 2.0 eq. $AlCl_3$ (5 mg, 0.04 mmol). The now orange solution is stirred for 5 min before adding a brownish solution of 1.0 eq. **1** (12 mg, 0.02 mmol) in 5 mL toluene. No immediate color change is observed and the resulting mixture is stirred overnight while the color changes to green. The solvent is removed *in vacuo* yielding greenish-brown solids.

Experimental data

$Ph_2CHCl/AlCl_3$

^{31}P{^{1}H} NMR (CD_2Cl_2, 300 K) δ[ppm] = 25.4 (t, $^1J_{PP}$ = 273 Hz, 2P), -301.2 (t, $^1J_{PP}$ = 273 Hz, 2P), -522.8 (s, 0.2P, P_4).

$Ph_3CCl/AlCl_3$

^{31}P{^{1}H} NMR (CD_2Cl_2, 300 K) δ[ppm] = 16.2 (t, $^1J_{PP}$ = 238 Hz, 2P), -313.6 (t, $^1J_{PP}$ = 238 Hz, 2P), -522.8 (s, 7.5P, P_4).

Reaction of 1 with $[Ph_3C][BF_4]$ and subsequent addition of $[Cr(CO)_4(nbd)]$

An orange-brown solution of 1.0 eq. **1** (12 mg, 0.02 mmol) in toluene (5 mL) is added to a yellow suspension of 2.0 eq. $[Ph_3C][BF_4]$ (12 mg, 0.04 mmol) in toluene (5 mL). No immediate color change is observed and the resulting reaction mixture is stirred overnight. The solvent is removed from the now greenish brown solution under reduced pressure affording a brownish solid.

^{31}P NMR (CD_2Cl_2, 300 K) δ[ppm] = 82.8 (m, 2P), 66.6 (m, 2P), -522.9 (s, P_4).

^{31}P{^{1}H} NMR (CD_2Cl_2, 300 K) δ[ppm] = 82.8 (m, 2P), 66.6 (m, 2P), -522.9 (s, P_4).

In a second step the obtained brownish solid is taken up in CH_2Cl_2 (5 mL) and a solution of 1.0 eq. $[Cr(CO)_4(nbd)]$ (39 mg, 0.02 mmol) in CH_2Cl_2 (5 mL) is added to the reaction mixture. No immediate color change is observed and the solution is stirred overnight. The solvent is removed *in vacuo* yielding a green solid.

$^{31}P\{^1H\}$ NMR (CD_2Cl_2) δ[ppm] = -53.9 to - 60.6 (m, 4P), -522.1 (s, 4P, P_4).

6.6.3.2 NMR spectroscopic experiments

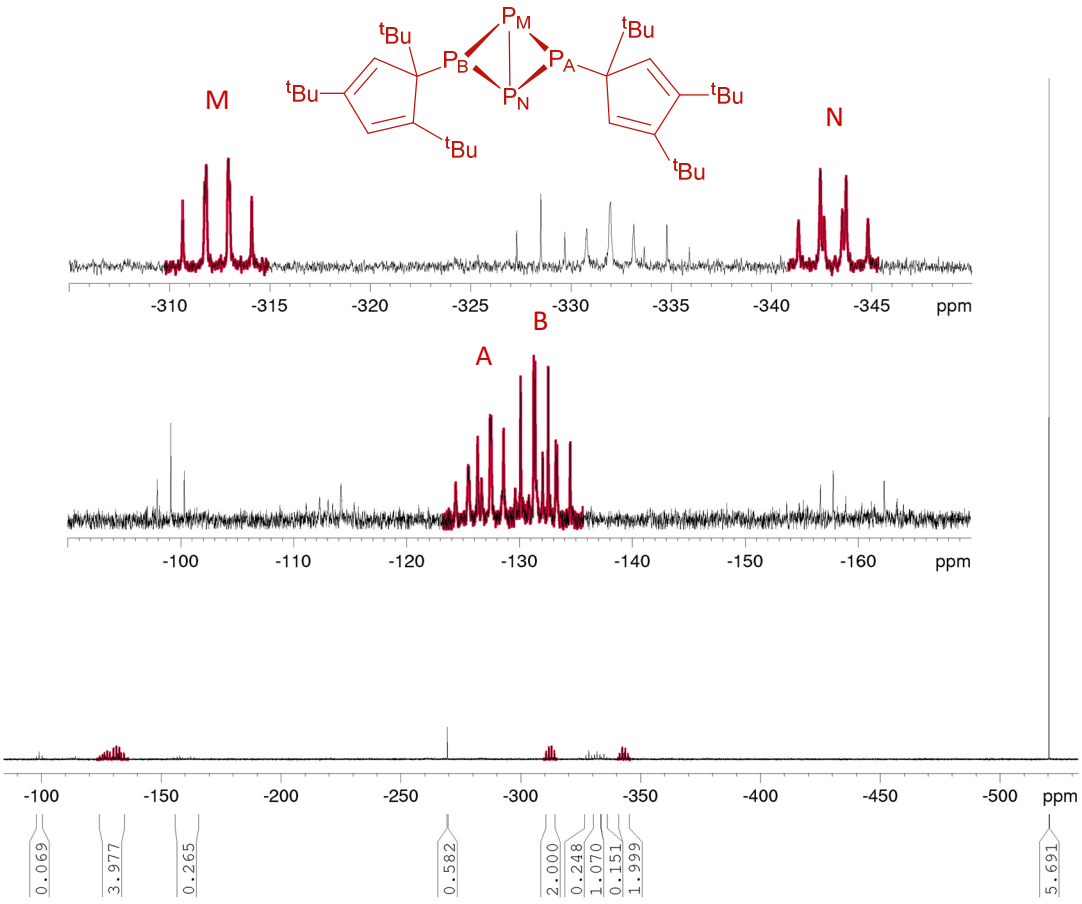

Figure S6. Crude $^{31}P\{^1H\}$ NMR spectrum of the reaction mixture of 1.0 eq. **1** and 2.0 eq. NaCp‴ (recorded in C_6D_6 at 300K); signals for predominant isomer of **B** are marked red.

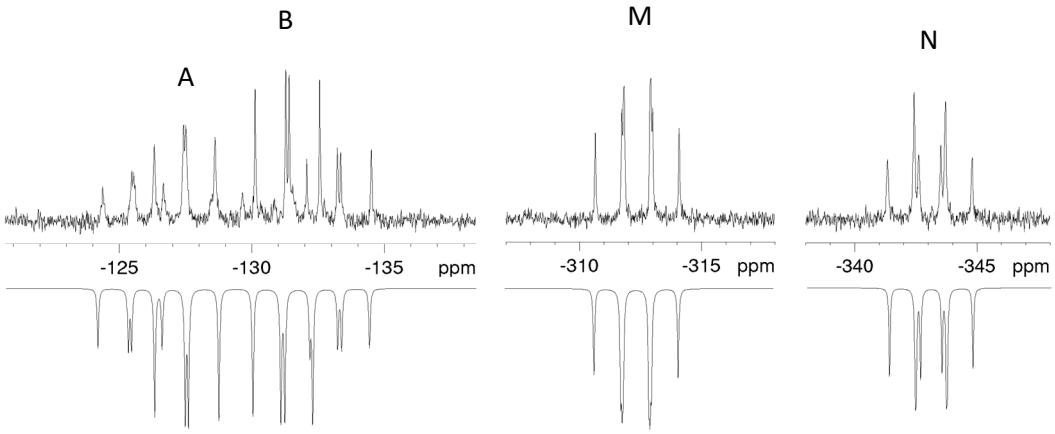

Figure S7. Experimental (top, recorded in C_6D_6 at 300K) and simulated (bottom) $^{31}P\{^1H\}$ NMR spectrum of the major isomer of **B**.

The simulation of the $^{31}P\{^1H\}$ NMR spectrum of **B** was carried out on the basis of an ABMN spin system with a C_1 symmetry.

Table S1. Experimental and simulated values for the chemical shifts and coupling constants in the $^{31}P\{^1H\}$ NMR spectrum of the major isomer of **B**.

experimental values				**simulated values**			
δ_A	-127.1 ppm	$^1J_{AB}$	-	δ_A	-126.56 ppm	$^1J_{AB}$	347.66 Hz
δ_B	-132.0 ppm	$^1J_{AM}$	190 Hz	δ_B	-132.02 ppm	$^1J_{AM}$	186.79 Hz
δ_M	-312.4 ppm	$^1J_{BM}$	190 Hz	δ_M	-312.39 ppm	$^1J_{BM}$	195.01 Hz
δ_N	-343.1 ppm	$^1J_{AN}$	206 Hz	δ_N	-343.17 ppm	$^1J_{AN}$	207.49 Hz
		$^1J_{BN}$	206 Hz			$^1J_{BN}$	169.09 Hz
		$^1J_{NM}$	170 Hz			$^1J_{NM}$	177.33 Hz

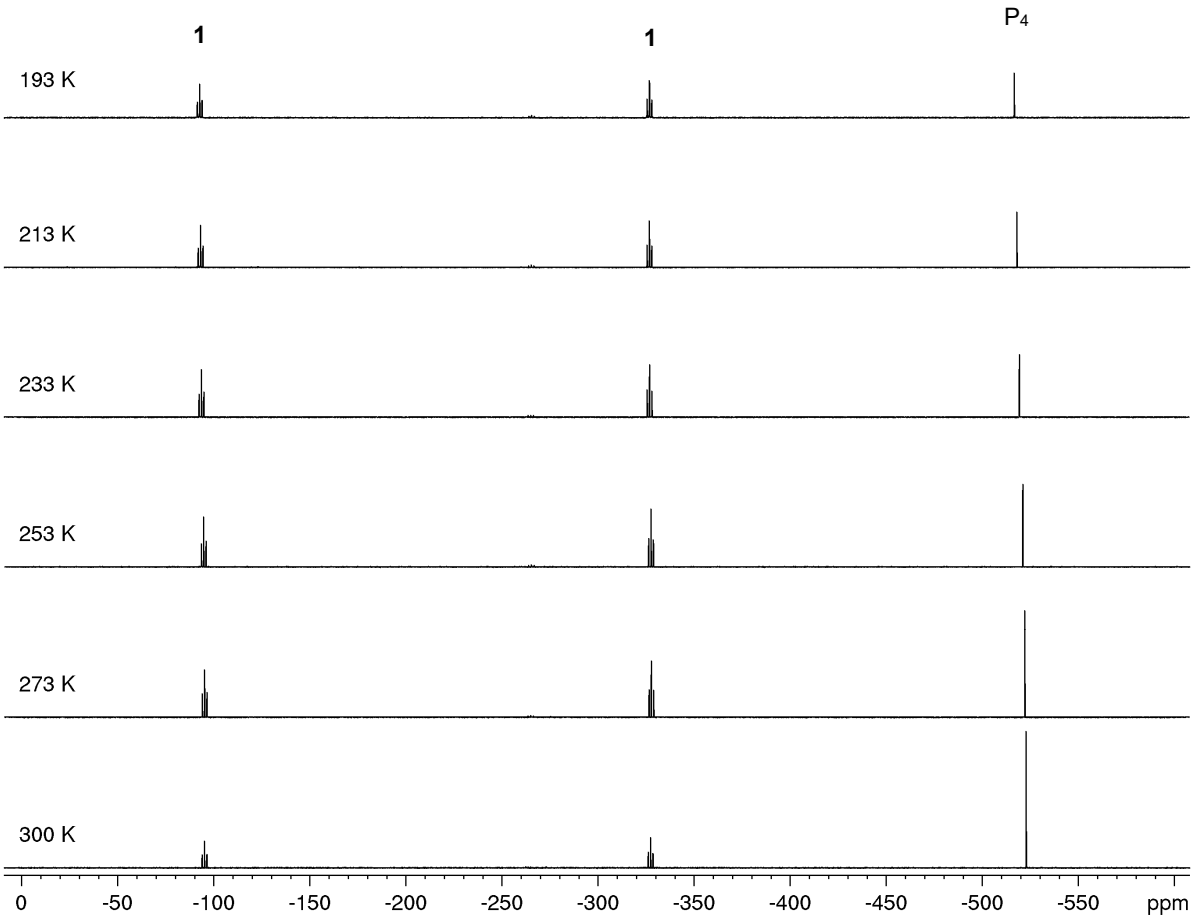

Figure S8. VT $^{31}P\{^{1}H\}$ NMR spectra of the reaction of **1** with 2.0 eq. NaCp* (recorded in CD_2Cl_2).

The amount of P_4 present in the $^{31}P\{^{1}H\}$ NMR spectra at 193 K can be attributed to decomposition during the transfer of the sample.

Table S2. Relative integral of the signal attributed to P_4 in the VT $^{31}P\{^{1}H\}$ NMR spectra of the reaction of **1** with 2.0 eq. NaCp* (recorded in CD_2Cl_2).

T	193 K	213 K	233 K	253 K	273 K	300 K
I_{rel} (P_4)	19.4 %	19.3 %	19.7 %	23.0 %	30.0 %	55.6 %

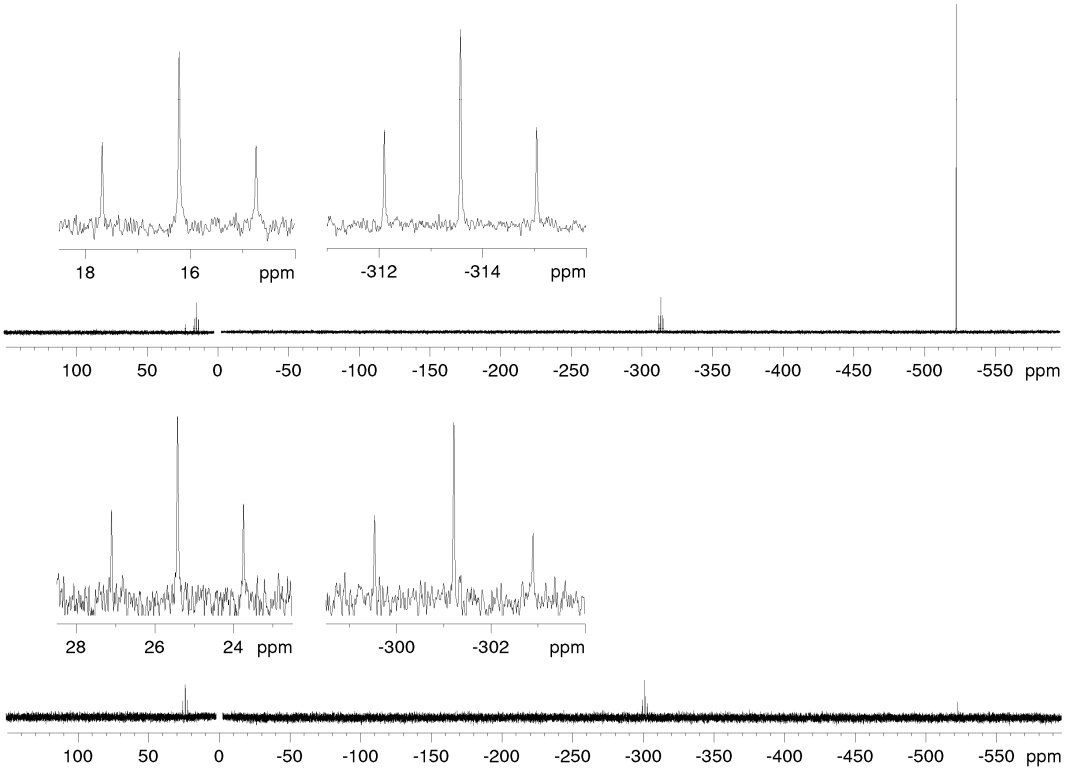

Figure S9. Crude $^{31}P\{^1H\}$ NMR spectra of the reaction of **1** with $Ph_3CCl/AlCl_3$ (top) and with $Ph_2CHCl/AlCl_3$ (bottom; both recorded in CD_2Cl_2 at 300K).

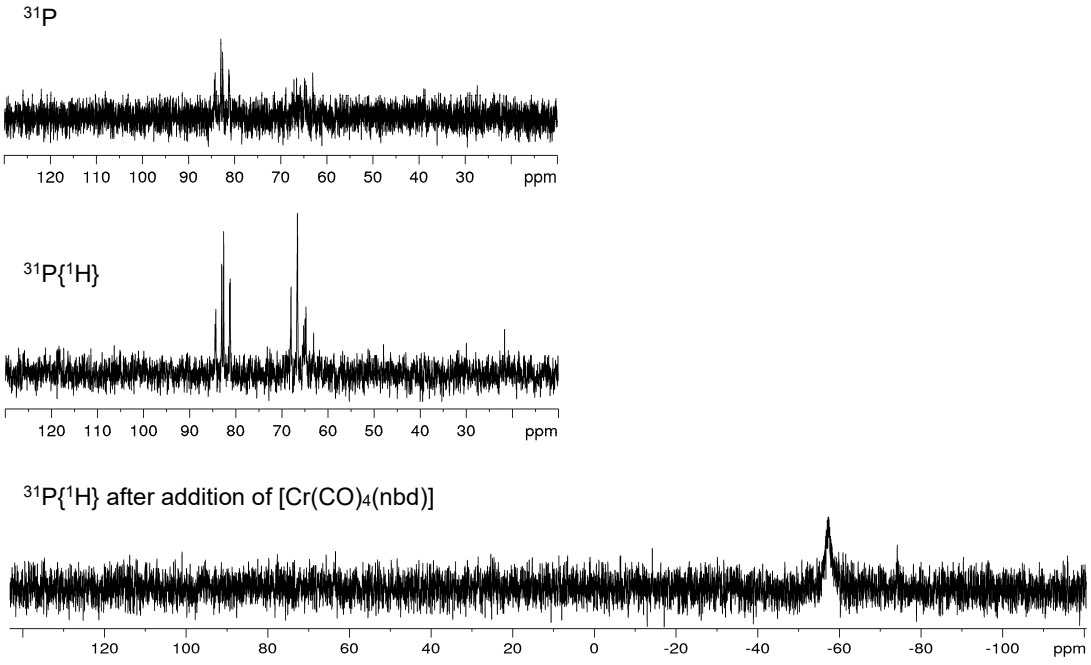

Figure S10. ^{31}P (top) and $^{31}P\{^1H\}$ (middle) NMR spectra of the reaction of **1** with $[Ph_3C][BF_4]$ and the $^{31}P\{^1H\}$ NMR spectra after the subsequent addition of [Cr(CO)$_4$(nbd)] (bottom; all recorded in CD_2Cl_2 at 300K).

6.6.4 References

[1] TopSpin 3.0, Bruker BioSpin GmbH.

[2] (a) R. B. King, *J. Organomet. Chem.* **1967**, *8*, 139-148.
(b) P. Leoni, A. Landi, M. Pasquali, *J. Organomet. Chem.* **1987**, *321*, 365-369.
(c) T. J. Jaeger, M. C. Baird, *Organometallics* **1988**, *7*, 2074-2076.
(d) C. Schwarzmaier, A. Y. Timoshkin, G. Balázs, M. Scheer, *Angew. Chem. Int. Ed.* **2014**, *53*, 9077-9081.

[3] (a) D. Feitler, G. M. Whitesides, *Inorg. Chem.* **1976**, *15*, 466.
(b) W. A. H. Herrmann, W. Kachler, H. Biersack, I. Bernal, M. Creswick, *Chem. Ber.* **1981**, *114*, 3558.

[4] C. G. Venier, E. W. Casserly, J. Am. Chem. Soc. 1990, 112, 2808-2809.

[5] R. B. King, A. Frozalia, *Inorg. Chem.* **1966**, *5*, 1837.

[6] (a) E. O. Fischer, W. Hafner, H. O. Stahl. *Z. anorg. allg. Chem.* **1955**, *282*, 47-62.
(b) T. S. Piper, G. Wilkinson, *J. Inorg. Nucl. Chem.* **1956**, *3*, 104-124.

6.7 Author Contributions

Rebecca Grünbauer	• Performance of all reported experiments and characterizations. • Preparation of manuscript (including figures, schemes, tables and supplementary information).
Manfred Scheer	• Supervision of project.

7.Thesis treasury - Synthesis of $[\{(Cp^*Cr(CO)_3)_2(\mu_3,\eta^{1:1:4}\text{-}P_4)\}_2Fe][PF_6]_2$

Rebecca Grünbauer and Manfred Scheer

7.1 Abstract

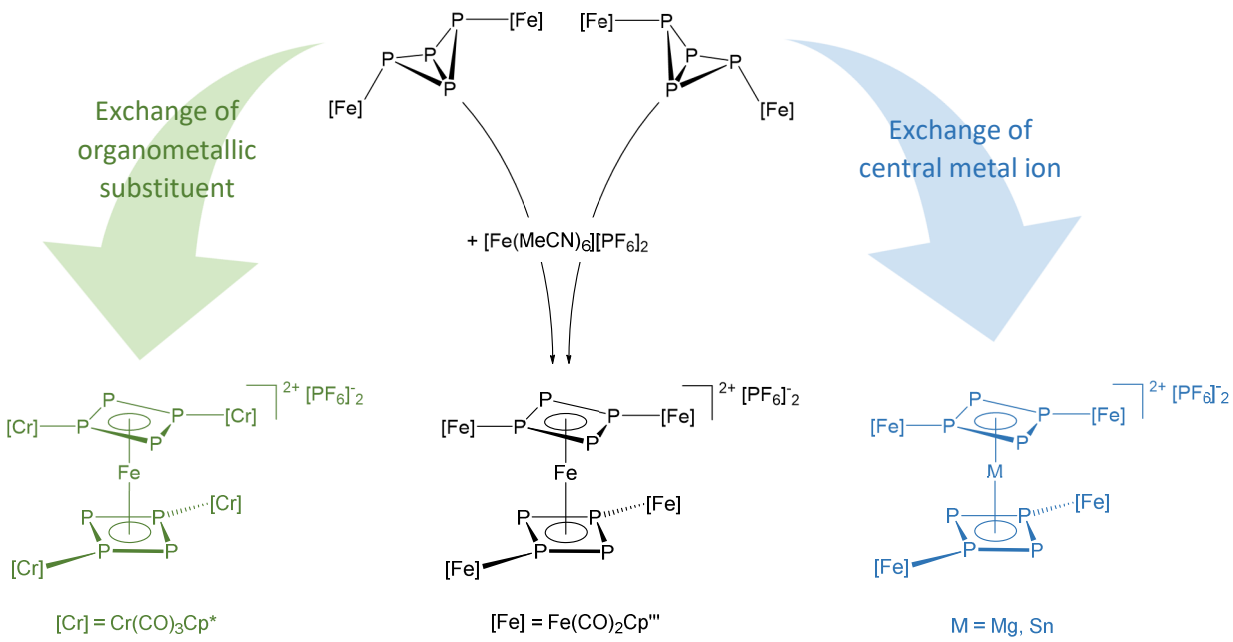

*Intrigued by the previously reported synthesis of $[\{(Cp'''Fe(CO)_2)_2(\mu_3,\eta^{1:1:4}\text{-}P_4)\}_2Fe][PF_6]_2$ (**1**), the aim of this work was to expand this field of research by synthetizing novel main group and transition metal analoga. Herein, the synthesis of $[\{(Cp^*Cr(CO)_3)_2(\mu_3,\eta^{1:1:4}\text{-}P_4)\}_2Fe][PF_6]_2$ (**2**), the chromium analog of **1** is reported. Single crystal X-ray diffraction analysis and $^{31}P\{^1H\}$ NMR spectroscopy revealed that the molecular structure of **2** is almost identical to **1**, the first fully characterized carbon free sandwich complex incorporating two 6π-aromatic $P_4[Fe]_2$ ligands. In contrast, all attempts to obtain cyclo-P_4 sandwich complexes of main group elements were not successful.*

7.2 Introduction

Recent studies delineate, that the P_4 butterfly compounds [{Cp‴Fe(CO)$_2$}$_2$(μ,η$^{1:1}$-P_4)] (**A**, Cp‴ = $C_5H_2{}^tBu_3$) and [{Cp*Cr(CO)$_3$}$_2$(μ,η$^{1:1}$-P_4)] (**B**, Cp* = $C_5(CH_3)_5$) are promising starting materials in the synthesis of bidentate coordination products as well as the generation of novel P_n ligand complexes (*vide infra*). Hitherto, various examples in which P_4 butterfly compounds act as chelating ligands are known.[1] Moreover, early studies reported the synthesis of novel P_n ligand complexes by exposing **A** to thermolytic[2] and photolytic[3] reaction conditions. Additionally, the novel rearrangement processes reported in the other chapters of this work underline the importance of P_4 butterfly compounds in the generation of unprecedented P_n ligand containing compounds. One outstanding example for a novel P_n scaffold obtained from a P_4 butterfly compound is [{(Cp‴Fe(CO)$_2$)$_2$(μ$_3$,η$^{1:1:4}$-P_4)}$_2$Fe][PF_6]$_2$ (**1**): the first fully characterized carbon free sandwich complex incorporating two 6π-aromatic P_4[Fe]$_2$ ligands.[4] By reacting **A** with a "naked" Fe^{2+} ion found in [Fe(MeCN)$_6$][PF_6]$_2$, the selective cleavage of the bond between the two bridgehead P atoms in the P_4 butterfly unit is induced eventually affording the cyclic ligands. This unique reaction behavior is utterly intriguing, prompting us to further investigate this reaction behavior. One approach to broaden the library of *cyclo*-P_4 sandwich complexes is the modification of the sandwiched metal ion in order to achieve the generation of main group P_4 sandwich complexes. Another approach is to react the chromium P_4 butterfly **B** with [Fe(MeCN)$_6$][PF_6]$_2$.

7.3 Results and Discussion

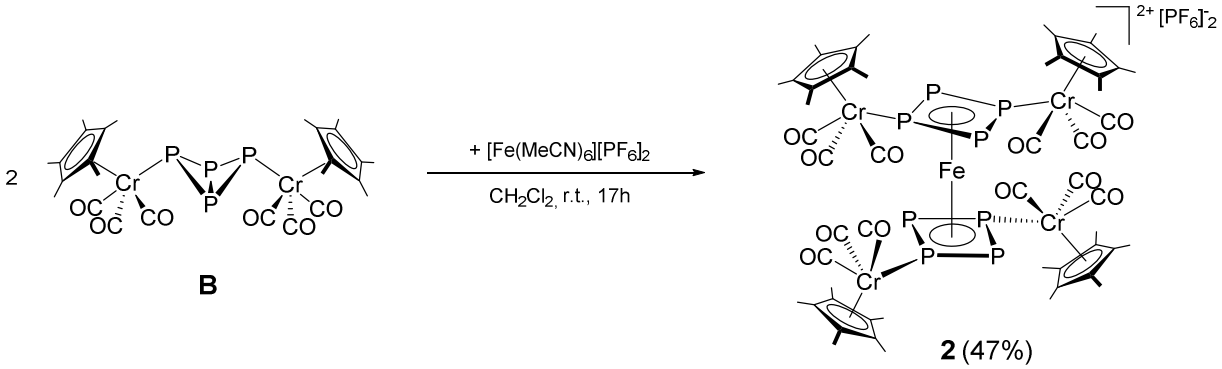

Scheme 1. Reaction of **B** with [Fe(MeCN)$_6$][PF_6]$_2$ affording **2**.

Unfortunately, the reactions of **A** with [Mg(MeCN)$_6$][PF_6]$_2$, [Sn(MeCN)$_6$][PF_6]$_2$ and [Sn(MeCN)$_6$][Tef]$_2$ (Tef = [Al(OC(CF_3)$_3$)$_4$]$^-$) did not afford the desired main group P_4 sandwich complexes. Although a conversion of the starting material could be detected by ^{31}P NMR spectroscopy, no conclusions can be drawn for the composition of the obtained products. They appear to be paramagnetic in solution and can therefore not be detected in the ^{31}P NMR spectra. Moreover, all crystallization attempts failed. In contrast, the successful reaction of **B** with [Fe(MeCN)$_6$][PF_6]$_2$ afforded [{(Cp*Cr(CO)$_3$)$_2$(μ$_3$,η$^{1:1:4}$-P_4)}$_2$Fe][PF_6]$_2$ (**2**), the chromium analog of **1** (Scheme 1). Analog to **1**, the molecular structure of **2** can be described as a sandwich complex incorporating two parallel 6π-aromatic *cyclo*-P_4 ligands (Fig.1). **2** crystallizes in the form of black needles in the orthorhombic space group *Fddd*. Compound **2** is excellently soluble in polar solvents like CH_3CN or CH_2Cl_2 and insoluble in non-polar solvents like *n*-hexane.

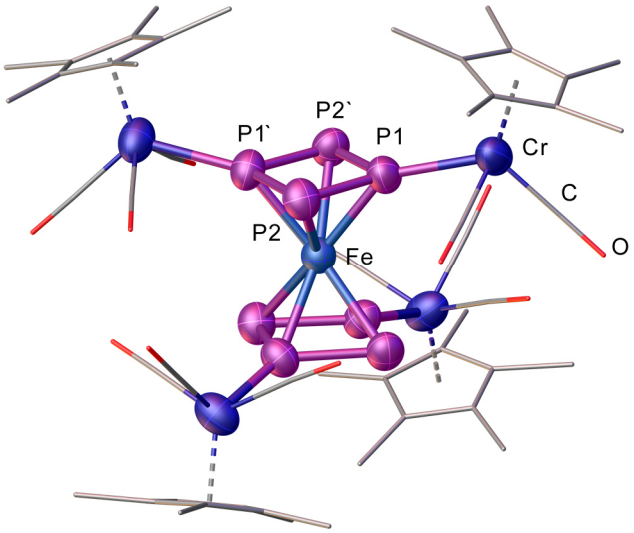

Figure 1. Molecular structure of the cation of **2** in the solid state; for clarity H atoms, the counter ion and solvent molecules are omitted; thermal ellipsoids drawn at 50% probability.

Table 1: Selected bond lengths [Å] and angles [°] of **1** and **2** in the solid state.

	d / Å			α / °	
	1	**2**		**1**	**2**
Fe–P1	2.2255(9)	2.263(2)	**P1–P2–P1′**	82.76(4) 82.88(4)	81.68(13)
Fe–P2	2.2317(9)	2.388(2)			
P1–P2	2.1406(10)	2.136(4)	**P2–P1–P2′**	97.11(4) 97.24(4)	98.31(13)
P1–P2′	2.1547(10)	2.151(3)			
$Cent_{PPPP}$–Fe	1.7648(7) 1.7759(7)	1.767(1)	**torsion along $Cent_{PPPP}$–Fe-$Cent_{PPPP}$**	60	68

Due to poor crystal quality, only preliminary values can be given for the single crystal X-ray diffraction analysis of **2** which depict an identical structure to **1**. The molecular structure of **2** in the solid state is highly symmetric with the asymmetric unit containing one quarter of the $[\{(Cp^*Cr(CO)_3)_2(\mu_3,\eta^{1:1:4}\text{-}P_4)\}_2Fe]^{2+}$ cation and one half of a $[PF_6]^-$ anion. With 2.136(4) Å and 2.151(3) Å, respectively, the P–P bonds inside the *cyclo*-P_4 unit are shortened compared to a classical P–P single bond (2.209(5) Å).[5] The P–P bond lengths of the $[P_4Fe_2]$ ligand are comparable to the respective bonds found in the $Cs_2P_4{\cdot}2NH_3$ anion (2.146(1) Å and 2.1484(9) Å).[6] However, analog to **1**, the P–P–P angles of the *cyclo*-P_4 motif of **2** (81.68(13)° and 98.31(13)°) differ from an ideal square geometry due to the steric influence of the organometallic substituents. The distance of the centroid of the *cyclo*-P_4 ligand and the central Fe^{2+} ion ($Cent_{PPPP}$–Fe = 1.767(1) Å) is marginally elongated in comparison to the hypothetical $[Fe(P_4)_2]^{2-}$ ion (1.739 Å)[7] and compares well with the value found for **1** (1.7648(7) Å / 1.7759(7) Å). The repulsion of the organometallic substituents in **1** and **2** is likely to cause this widening of the sandwich structure. Both, **1** and **2** display a rotation of the parallel *cyclo*-P_4 motifs along the $Cent_{PPPP}$–Fe–$Cent_{PPPP}$ axis (**1**: 60° / **2**: 68°). In contrast, DFT calculations predicted a staggered conformation of the unsubstituted $[Fe(P_4)_2]^{2-}$ *cyclo*-P_4-sandwich dianion.[7] Again, the deviation from this proposed D_{4d}

symmetry, might be explained by the steric repulsion of the carbonyl and Cp ligands of the organometallic substituents.

As expected, only one singlet (δ = 2.08 ppm) can be detected in the ^{1}H NMR spectrum of **2** as all Cp* ligands are magnetically equivalent and rotate freely in solution. Similar to **1**, an AA′BB′ spin system can be deduced for **2** from the corresponding ^{31}P{^{1}H} NMR spectrum. Two multiplets attributed to the unsubstituted P atoms (δ_B = 90.9 ppm, P2 according to Fig. 1) and organometallically substituted P atoms (δ_A = 113.3 ppm, P1 according to Fig. 1), respectively, could be detected and confirmed by simulation.

From a reaction of **B** with $[Fe(MeCN)_6][PF_6]_2$ some crystals of $[Cp^*Cr(CO)_3][PF_6]_2$ could be identified as a side product by single crystal X-ray diffraction experiments. This underlines the previously observed fragility of the Cr–P bond in **B** in comparison to the Fe–P bond in **A** for which no analog side reaction was witnessed.[8]

Reactions with **1** and **2** as starting materials appear to be very promising due to the unique molecular structure of the *cyclo*-P_4 sandwich complexes. Analogously to the substituent exchange observed for **B**[8], **2** was reacted with $K[Cp'''Fe(CO)_3]$ in order to obtain **1** and $K[Cp^*Cr(CO)_2]$. Although a conversion of the starting materials could be observed, neither the desired or novel products could be identified or characterized yet.

7.4 Conclusion

In conclusion, it was possible to obtain the homoleptic *cyclo*-P_4 sandwich complex **2**, the chromium analog of the previously reported **1**. Preliminary single crystal X-ray diffraction analysis of **2** depicts an almost identical molecular structure of the central *cyclo*-P_4 sandwich scaffold. In contrast, experiments with main group element salts were not successful yet, denying the desired formation of main group *cyclo*-P_4 sandwich compounds. Moreover, subsequent conversions of **1** and **2** were not successful either but bear great potential for novel reaction pathways.

7.5 References

[1] (a) C. Schwarzmaier, S. Heinl, G. Balázs, M. Scheer, *Angew. Chem. Int. Ed. Engl.* **2015**, *54*, 13116-13121.
(b) M. Eberl, Ph.D. thesis, University of Regensburg (Regensburg), **2011**.
(c) C. Schwarzmeier, Ph.D. thesis, University of Regensburg (Regensburg), **2012**.

[2] O. J. Scherer, T. Hilt, G. Wolmershäuser, *Organometallics* **1998**, *17*, 4110-4112.

[3] O. J. Scherer, G. Schwarz, G. Wolmershäuser, *Z. Anorg. Allg. Chem* **1996**, *622*, 951-957

[4] J. Müller, S. Heinl, C. Schwarzmaier, G. Balázs, M. Keilwerth, K. Meyer, M. Scheer, *Angew. Chem. Int. Ed.* **2017**, *56*, 7312-7317.

[5] (a) A. Simon, H. Borrmann, H. Craubner, *Phosphorus Sulfur Silicon Relat. Elem.* **1987**, *30*, 507-510.
(b) H. Okudera, E. Dinnebier Robert, A. Simon, *Z. Kristallogr.,* **2005**, *220*, 259.

[6] F. Kraus, J. C. Aschenbrenner, N. Korber, *Angew. Chem. Int. Ed.* **2003**, *42*, 4030-4033; *Angew. Chem.* **2003**, *115*, 4162 – 4165.

[7] Z. Li, C. Zhao, L. Chen, *J. Mol. Struct.* THEOCHEM **2007**, *810*, 1-6.

[8] c.f. chapter 6 of this thesis

7.6 Supplementary information

7.6.1 General remarks

All experiments were carried out under an atmosphere of dry argon or nitrogen using glovebox and Schlenk techniques. Residues of oxygen and water were removed from the inert gas by passing it over a BASF R 3-11 ($CuO/MgSiO_3$) catalyst, concentrated H_2SO_4 and finally granulated silica gel. Dry solvents were collected from a Braun SPS Apparatus and degassed prior to use. The deuterated solvent CD_2Cl_2 was degassed and dried by stirring with CaH_2 followed by distillation. After the distillation, CD_2Cl_2 was stored over molecular sieve (3 Å) which had previously been dried for four hours under high vacuum at 100 °C.

$[\{Cp'''Fe(CO)_2\}_2(\mu,\eta^{1:1}\text{-}P_4)]$ (**A**)[1], $[\{Cp^*Cr(CO)_3\}_2(\mu,\eta^{1:1}\text{-}P_4)]$ (**B**)[2], $[Fe(MeCN)_6][PF_6]_2$[3], $[Mg(MeCN)_6][PF_6]_2$[4], $[Sn(MeCN)_6][PF_6]_2$[5] and $[Sn(MeCN)_6][Tef]_2$[5] were prepared according to literature procedures.

NMR spectra were recorded at the NMR department of the University Regensburg using a Bruker Advance 300 or 400 spectrometer. Samples are referenced against TMS (^1H) or 85% H_3PO_4 (^{31}P) as external standards. Chemical shifts (δ) are reported in ppm and coupling constants (*J*) in Hz. The spectra were processed using the TopSpin 3.5 software (Bruker) and the WIN-DAISY module of this software was used to perform simulations.[6]

7.6.2 Synthesis

An orange-brown solution of **B** (66 mg, 0.10 mmol, 2.0 eq.) in CH_2Cl_2 (5 mL) is added to colorless solution of $[Fe(CH_3CN)_6(PF_6)_2]$ (30 mg, 0.05 mmol, 1.0 eq.) in CH_2Cl_2 (5 mL). The resulting mixture is stirred at room temperature overnight and a color change towards red can be observed. The solvent is subsequently removed under reduced pressure affording a brown solid. To obtain pure **2**, the solid was taken up in 15 mL CH_2Cl_2 and layered with *n*-hexane. After one week, black needles suitable for single crystal X-ray analysis could be obtained.

Analytical data for 2

Yield	40 mg (0.24 mmol, 47%).
^{1}H NMR (CD_2Cl_2, 300 K)	δ[ppm] = 2.08 (s, 60H, Cp*).
^{31}P NMR (CD_2Cl_2, 300 K)	δ[ppm] = -143.9 (sept, 5P, PF_6), 90.9 (m, $^1J_{AB}$ = 349.48 Hz, $^1J_{AB'}$ = 367.46 Hz, $^1J_{A'B}$ = 369.08, $^1J_{A'B'}$ = 369.98 Hz, $^2J_{AA'}$ = 9.92 Hz, 2P, P_A and $P_{A'}$), 113.3 (m, $^1J_{AB}$ = 349.48 Hz, $^1J_{AB'}$ = 367.46 Hz, $^1J_{A'B}$ = 369.08, $^1J_{A'B'}$ = 369.98 Hz, $^2J_{BB'}$ = 14.89 Hz, 2P, P_B and $P_{B'}$).
^{31}P{^{1}H} NMR (CD_2Cl_2, 300 K)	δ[ppm] = -143.9 (sept, 5P, PF_6), 90.9 (m, $^1J_{AB}$ = 349.48 Hz, $^1J_{AB'}$ = 367.46 Hz, $^1J_{A'B}$ = 369.08, $^1J_{A'B'}$ = 369.98 Hz, $^2J_{AA'}$ = 9.92 Hz, 2P, P_A and $P_{A'}$), 113.3 (m, $^1J_{AB}$ = 349.48 Hz, $^1J_{AB'}$ = 367.46 Hz, $^1J_{A'B}$ = 369.08, $^1J_{A'B'}$ = 369.98 Hz, $^2J_{BB'}$ = 14.89 Hz, 2P, P_B and $P_{B'}$).

7.6.3 NMR spectroscopic experiments

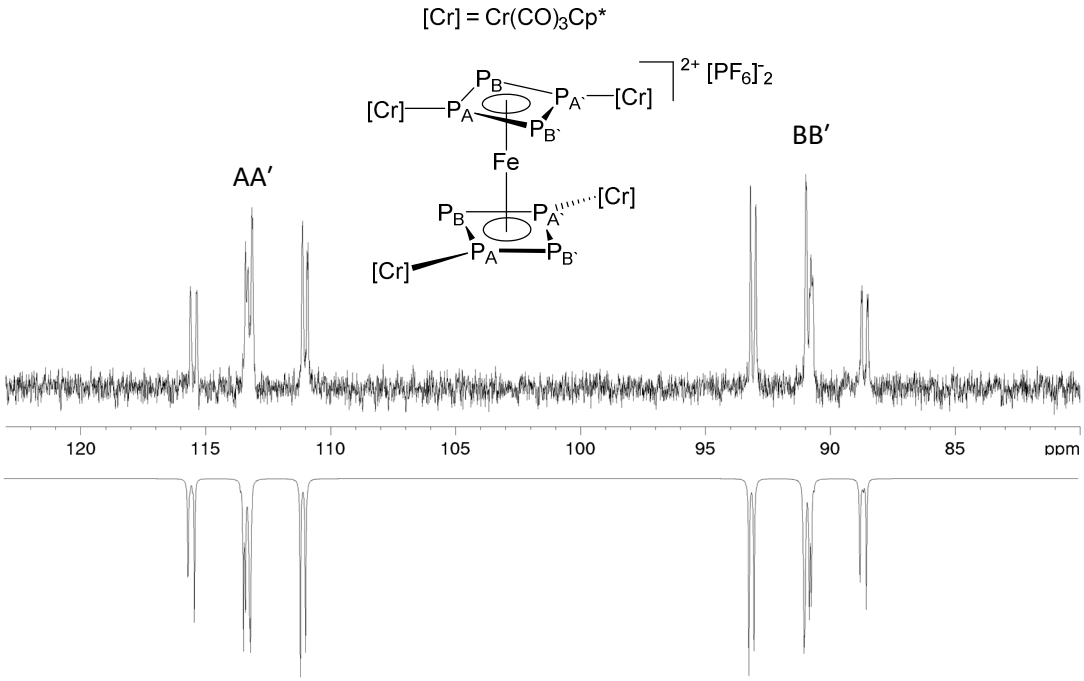

Figure S1. Experimental (top, recorded in CD_2Cl_2 at 300 K) and simulated (bottom) $^{31}P\{^1H\}$ NMR spectrum of **2** in CD_2Cl_2

Table S1. Experimental and simulated values for the chemical shifts and coupling constants in the $^{31}P\{^1H\}$ NMR spectrum of **2** (recorded in CD_2Cl_2 at 300 K).

experimental values				simulated values			
δ_A	113.3 ppm	$^1J_{AB}$	- Hz	δ_A	113.15 ppm	$^1J_{AB}$	349.48 Hz
$\delta_{A'}$	113.3 ppm	$^1J_{AB'}$	- Hz	$\delta_{A'}$	113.15 ppm	$^1J_{AB'}$	367.46 Hz
δ_B	90.9 ppm	$^1J_{A'B}$	- Hz	δ_B	90.95 ppm	$^1J_{A'B}$	369.08 Hz
$\delta_{B'}$	90.9 ppm	$^1J_{A'B`}$	- Hz	$\delta_{B'}$	90.95 ppm	$^1J_{A'B'}$	369.98 Hz
		$^2J_{AA'}$	- Hz			$^2J_{AA'}$	9.92 Hz
		$^2J_{BB'}$	- Hz			$^2J_{BB'}$	14.89 Hz

The simulation of the $^{31}P\{^1H\}$ NMR spectrum of **2** was carried out on the basis of an AA′XX′ spin system with a C_1 symmetry.

7.6.4 Crystallographic details

Compound **2** crystalizes in the form of dark needles after layering a saturated reaction solution in CH_2Cl_2 with *n*-hexane after a few days. A suitable crystal with dimensions 0.25 × 0.20 × 0.03 mm^3 was selected and mounted on a GV50, TitanS2 diffractometer. The crystal was kept at a steady T = 123.0(2) K during data collection. The structure was solved with the ShelXT 2018/2 (Sheldrick, 2018) solution program using Olex2 (Dolomanov et al., 2009) as the graphical interface. The model was refined with ShelXL 2018/3 (Sheldrick, 2015) using full matrix least squares minimization on F^2. The asymmetric unit contains one quarter of the $[\{(Cp^*Cr(CO)_3)_2(\mu_3,\eta^{1:1:4}\text{-}P_4)\}_2Fe]^{2+}$ cation and one half of a $[PF_6]^-$ anion.

Table S2: Selected parameters for the single crystal X-ray diffraction experiment of **2**.

Formula	$C_{52}H_{60}Cr_4F_{12}FeO_{12}P_{10}$	***Z***	8
$D_{calc.}$ **/ g cm^{-3}**	1.619	***Z'***	0.25
***m*/mm^{-1}**	9.661	**Wavelength/Å**	1.54184
Formula Weight	1678.55	**Radiation type**	Cu K_a
Colour	dark brown	Q_{min}/°	3.208
Shape	plate	Q_{max}/°	65.074
Size/mm^3	0.25×0.20×0.03	**Measured Refl's.**	9235
***T*/K**	123.0(2)	**Ind't Refl's**	2906
Crystal System	orthorhombic	**Refl's with I > 2(I)**	1780
Space Group	*Fddd*	R_{int}	0.1031
***a*/Å**	22.301(3)	**Parameters**	402
***b*/Å**	23.444(2)	**Restraints**	622
***c*/Å**	26.347(4)	**Largest Peak**	0.838
***a*/°**	90	**Deepest Hole**	-0.596
***b*/°**	90	**GooF**	1.086
***g*/°**	90	wR_2 **(all data)**	0.3140
V/Å^3	13774(3)	wR_2	0.2654
		R_1 **(all data)**	0.1385
		R_1	0.1024

7.6.5 References

[1] C. Schwarzmaier, A. Y. Timoshkin, G. Balázs, M. Scheer, Angew. Chem. Int. Ed. 2014, 53, 9077-9081.

[2] (a) R. B. King, *J. Organomet. Chem.* **1967**, *8*, 139-148.
(b) P. Leoni, A. Landi, M. Pasquali, *J. Organomet. Chem.* **1987**, *321*, 365-369.
(c) T. J. Jaeger, M. C. Baird, *Organometallics* **1988**, *7*, 2074-2076.
(d) C. Schwarzmaier, A. Y. Timoshkin, G. Balázs, M. Scheer, *Angew. Chem. Int. Ed.* **2014**, *53*, 9077-9081.

[3] J. K. Clegg, J. Cremers, A. J. Hogben, B. Breiner, M. M. J. Smulders, J. D. Thoburn, J. R. Nitschke, *Chem. Sci.* **2013**, *4*, 68-76.

[4] E. N. Keyzer, H. F. J. Glass, Z. Liu, P. M. Bayley, S. E. Dutton, C. P. Grey, D. S. Wright, *J. Am. Chem. Soc.* **2016**, *138*, 8682-8685.

[5] M. Schleep, C. Hettich, D. Kratzert, H. Scherer, I. Krossing, *Chem. Commun.* **2017**, *53*, 10914-10917.

[6] TopSpin 3.0, Bruker BioSpin GmbH

7.7 Author contributions

Rebecca Grünbauer	• Synthesis and characterization of compound **2**. • Additional experiments concerning the reactions of **A** with $[Mg(MeCN)_6][PF_6]_2$, $[Sn(MeCN)_6][PF_6]_2$ and $[Sn(MeCN)_6][Tef]_2$ and the reactivity of **2**. • Preparation of manuscript (including figures, schemes, tables and supplementary information).
Manfred Scheer	• Supervision of project.

8. Conclusion

In summary, various synthetic opportunities originating from compounds incorporating the tetraphospha-*bicyclo*[1.1.0]butane ("P_4 butterfly") structural motif were illuminated in this thesis. The isolobal compounds [{Cp‴Fe(CO)$_2$}$_2$(μ,η$^{1:1}$-P_4)] (**A,** Cp‴ = $C_5H_2{}^tBu_3$) and [{Cp*Cr(CO)$_2$}$_3$(μ,η$^{1:1}$-P_4)] (**B**, Cp* = $C_5(CH_3)_5$) were chosen as starting materials for reactivity investigations concerning the central P_4 butterfly moiety. The results reported herein validated that the different substituents in **A** and **B** can have a significant influence on the respective reaction behavior. On the one hand, previous reports state that similar products are obtained when reacting **A** and **B** with small Lewis acidic salts.[1] On the other hand, major differences in reactivity were detected when reacting the related **A** and **B** with different metal carbonyls or nucleophiles within the scope of this thesis (*vide infra*).

In general, the reactivity of **B** is more diverse than the reactivity of **A**. The dissociation of the P–Cr bond in **B** (dissociation energy: 67.47 kJ·mol^{-1}) is reasonably less endothermic than the cleavage of the corresponding P–Fe bond in **A** (dissociation energy: 142.91 kJ·mol^{-1}).[1c] Thus, **B** is expected to be a more promising starting material for fragmentation, rearrangement and substituent exchange processes ultimately affording novel polyphosphorus ligand complexes. Supporting this proposal, a variety of selective rearrangement processes and discrete fragmentation routes could be observed in the scope of this thesis in addition to straightforward coordination processes (*vide infra*).

8.1 Reactivity of [{Cp*Cr(CO)$_3$}$_2$(μ,η$^{1:1}$-P_4)] towards Lewis acidic tetracarbonyl moieties of Cr, Mo and W

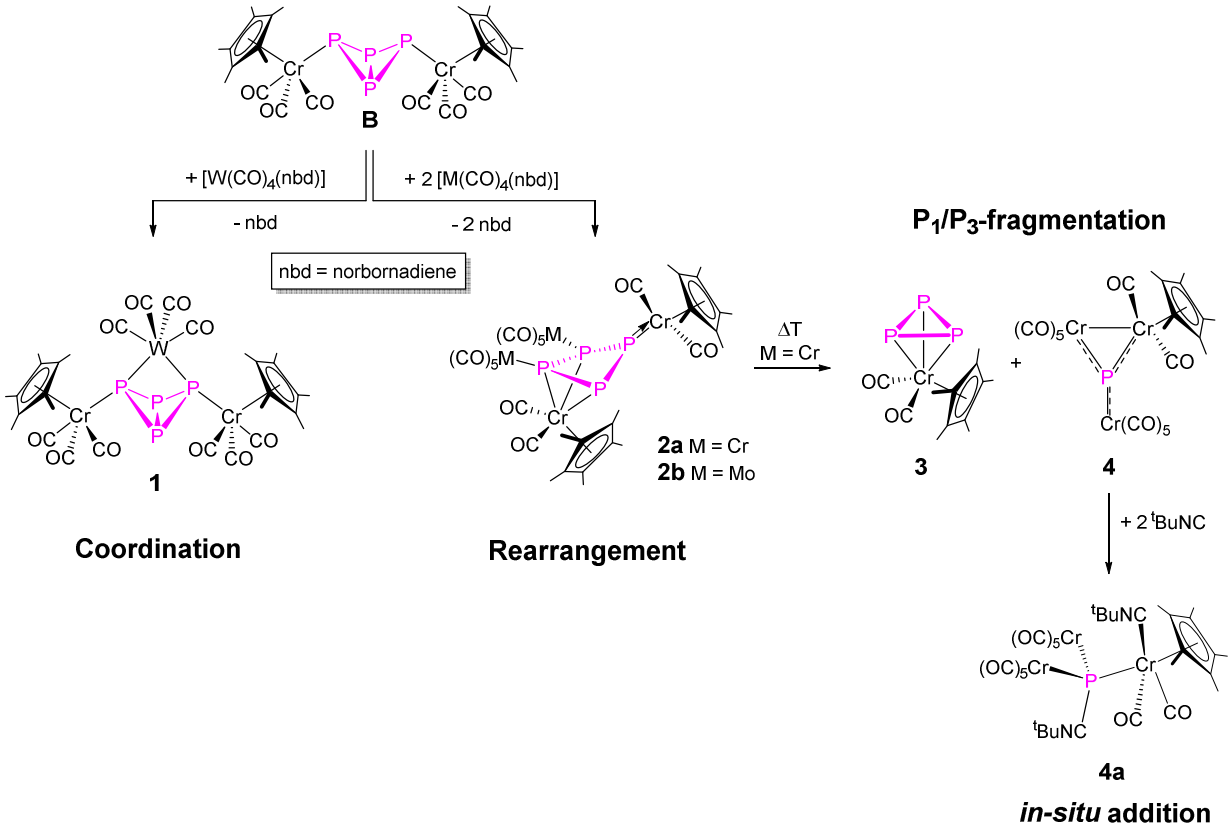

Scheme 1. Reactions of **B** with [M(CO)$_4$(nbd)] (M = Cr, Mo, W).

When **B** is reacted with [M(CO)$_4$(nbd)] (M = Cr, Mo, W; nbd = norbornadiene) two different reaction pathways can be observed depending on the nature of the employed metal. The chelating adduct [{Cp*Cr(CO)$_3$}$_2$(μ_3,$\eta^{1:1:1:1}$-P$_4$){W(CO)$_4$}] (**1**), which contains a bidentate P$_4$ butterfly ligand, is afforded from the reaction of **B** with a Lewis acidic [W(CO)$_4$] fragment. In contrast, reactions of **B** with tetracarbonyl fragments of Cr and Mo result in the step-wise formation of the monosubstituted [{Cp*Cr(CO)$_2$}$_2$(μ_3,$\eta^{3:1:1}$-P$_4$){M(CO)$_5$}] (**2a′**: M = Cr; **2b′**: M = Mo) and the disubstituted [{Cp*Cr(CO)$_2$}$_2$(μ_4,$\eta^{3:1:1:1}$-P$_4$){M(CO)$_5$}$_2$] (**2a**: M = Cr; **2b**: M = Mo), which contain a folded *cyclo*-P$_4$ unit in an unpreceded coordination sphere. Carbonyl rearrangement processes leave **2′** and **2** with [Cp*Cr(CO)$_2$] substituents, inducing an electron deficit on the Cr atoms. In order to repeal the electronic imbalance, one of the Cr atoms is coordinated in a η^3-fashion by one plane of the folded P$_4$ unit, while a formal double bond can be observed between the other Cr atom and the adjacent P atom. The central *cyclo*-P$_4$ structural motif, which displays a folding angle of approx. 136°, is additionally stabilized by one or two [M(CO)$_5$] fragments obtained from the released CO ligands and intrinsic [M(CO)$_4$] fragments (M = Cr, Mo). This step-wise stabilization of the deltoid *cyclo*-P$_4$ scaffold can be monitored excelently by ^{31}P NMR spectroscopy.

Additionally, an unprecedented P$_1$/P$_3$-fragmentation of **2a** yielding the *cyclo*-P$_3$ complex [Cp*Cr(CO)$_2$-(η^3-P$_3$)] (**3**) and the as yet unknown phosphinidene complex [Cp*Cr-(CO)$_2$(Cr(CO)$_5$)$_2$(μ_3-P)] (**4**) could be monitored by ^{31}P NMR spectroscopy (Fig. 1). The proposed identity of **4** was validated by an *in-situ* reaction with ^{t}BuNC, which yielded [{Cp*Cr(CO)$_2$(^{t}BuNC)}P-{Cr(CO)$_5$}$_2$(^{t}BuNC)] (**4a**). The formation of Lewis acid-Lewis base pairs is a common feature for phosphinidenes and the process is accompanied by a drastic change in the ^{31}P NMR chemical shift. Upon addition of ^{t}BuNC, a change in the ^{31}P NMR chemical shift from δ = 1124 ppm (attributed to the planar coordination geometry in **4**) to δ = -166 ppm (attributed to the pseudo-tetragonal coordination environment found in **4a**) could be observed. Similarly, the reaction of the phosphinidene complex [Cp*P{W(CO)$_5$}$_2$] with ^{t}BuNC affords the Lewis acid/base adduct [Cp*P{W(CO)$_5$}$_2$(^{t}BuNC)] accompanied by the extreme change of the ^{31}P NMR chemical shift from δ = 1076.5 ppm to δ = −73.1 ppm.[2] Supporting DFT calculations validated the identities of **4** and **4a**, confirming the proposed selective P$_1$/P$_3$ fragmentation originating from **2**. Consequently, the rearrangement/fragmentation process originating from **B** introduces a novel pathway towards the generation of novel chromium P$_n$ ligand complexes.

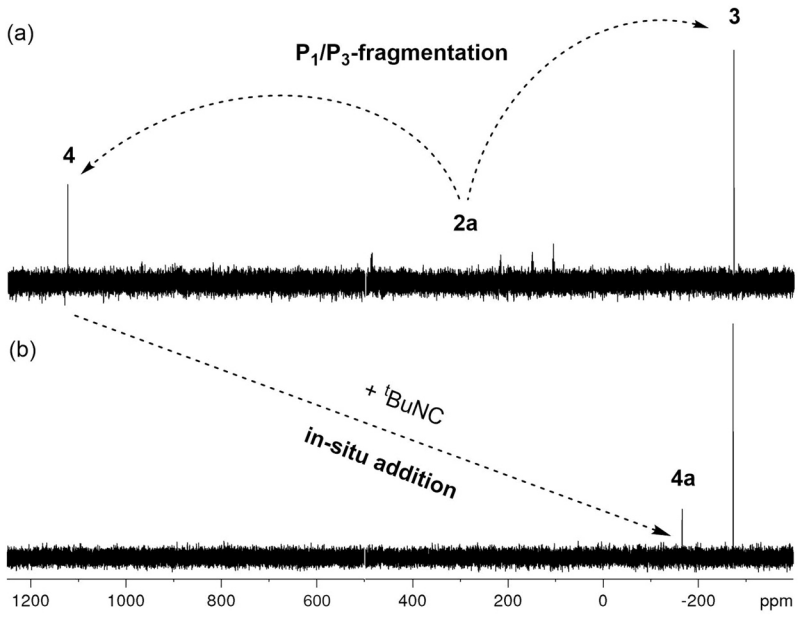

Figure 1. ^{31}P{^{1}H} NMR spectra (recorded in thf with C$_6$D$_6$ capillary at 300 K) of the fragmentation of **2a** yielding **3** and **4** (a) and the *in-situ* reaction with ^{t}BuNC affording **4a** (b).

8.2 Reactivity of [{Cp‴Fe(CO)$_2$}$_2$(μ,η$^{1:1}$-P$_4$)] towards different Lewis acids

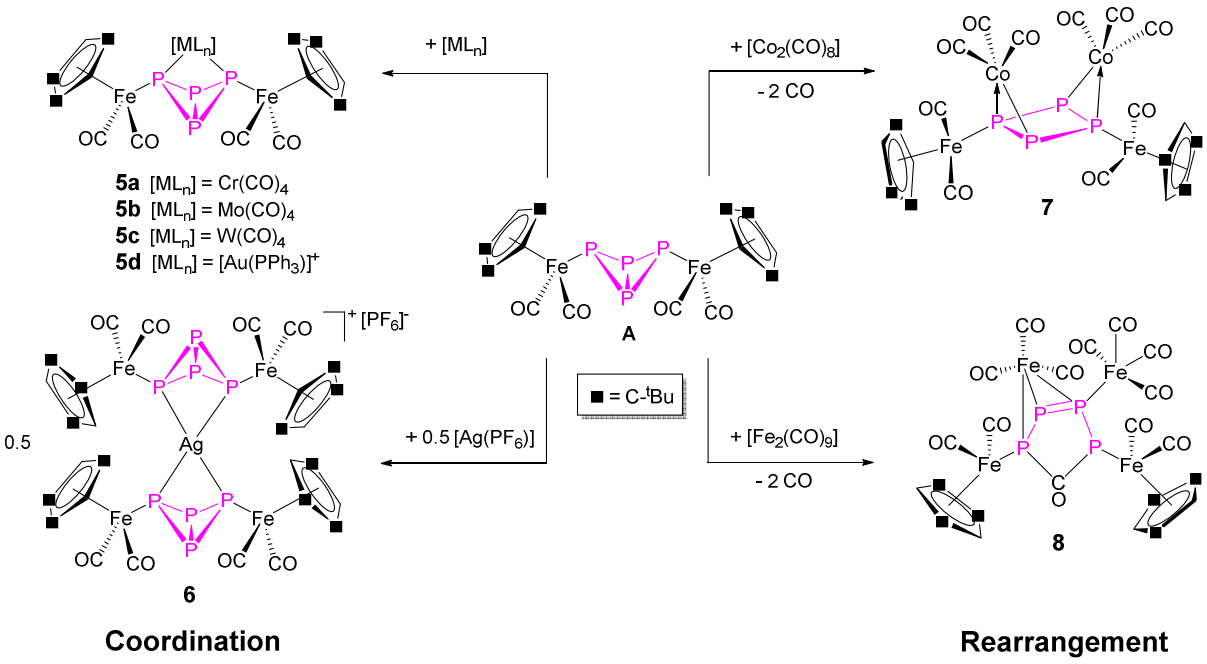

Scheme 2. Coordination and rearrangement products obtained from **A**.

The reactivity of **A** towards Lewis acids is strongly influenced by the nature of the Lewis acid itself. For rather weak Lewis acids like coinage metal salts a bidentate coordination of **A** via the two wing tip P atoms of the intact P$_4$ butterfly unit was observed previously.[1a] Within this thesis, the synthesis of [{Cp‴Fe(CO)$_3$}$_2$-(μ$_3$,η$^{1:1:1:1}$-P$_4$){M(CO)$_4$}] (M = Cr (**5a**), Mo (**5b**), W (**5c**)) and [{Cp‴Fe(CO)$_2$}$_2$(μ$_3$,η$^{1:1:1:1}$-P$_4$){AuPPh$_3$}][PF$_6$] (**5d**) is reported by reacting **A** with [M(CO)$_4$(nbd)] (M = Cr, Mo, W; nbd = norbornadiene) or [(Ph$_3$P)Au(tht)][PF$_6$] (tht = tetrahydrothiophene), respectively (Scheme 2). Compounds **5a-d** are obtained as a result from a ligand exchange of the weakly coordinating nbd and tht ligands with the more strongly donating P$_4$ butterfly moiety affording analog compounds to the previously reported Lewis acid-P$_4$ butterfly adducts.[1a] Additionally, the reaction of **A** with [AgPF$_6$] affords [{(Cp‴Fe(CO)$_2$)$_2$(μ$_3$,η$^{1:1:1:1}$-P$_4$)}$_2$Ag][PF$_6$] (**6**), a heteroleptic spiro complex with a pseudotetrahedral coordination geometry. The structural scaffold of **A** remains basically unaltered by the coordination process, resulting in very small bite angles of approx. 64° for **5** and **6**. One outstanding feature of **5c** in comparison to the other obtained P$_4$ butterfly ligand complexes is the unexpected solvent dependency of the NMR spectra. Hitherto, such a degree of solvent dependency is unknown for P$_n$ ligand complexes but could be observed for biologically active phosphate groups due to the dynamic formation of hydrogen bridges induced by polar solvents.[3] Experimental ^{31}P{^{1}H} NMR spectra of **5c** in mixtures of CH_2Cl_2 and *n*-pentane clearly illustrate the linear dependency of the ^{31}P{^{1}H} NMR chemical shifts in respect to the polarity of the solvent (Fig. 2). These observations suggest a highly dynamic coordination between the P$_4$ butterfly ligand **A** and the [W(CO)$_4$] fragment in solution, which is strongly influenced by the polarity of the solvent.

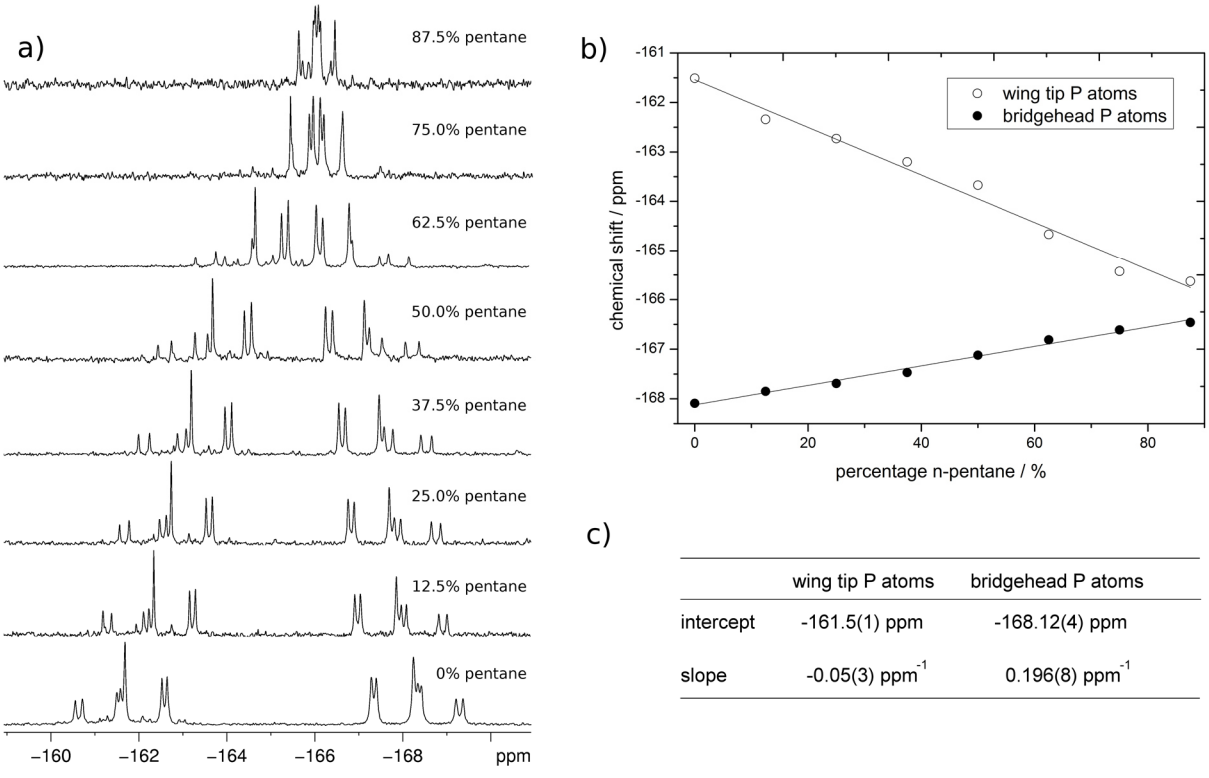

	wing tip P atoms	bridgehead P atoms
intercept	-161.5(1) ppm	-168.12(4) ppm
slope	-0.05(3) ppm^{-1}	0.196(8) ppm^{-1}

Figure 2. (a) $^{31}P\{^1H\}$ NMR spectra of **5c** in CH_2Cl_2/*n*-pentane mixtures with increasing *n*-pentane percentage (recorded with C_6D_6-capillary at 300 K); (b) chemical shift of the recorded $^{31}P\{^1H\}$ NMR spectra compared with the *n*-pentane percentage of the responding solutions; (c) parameters of the linear fits displayed in (b)

In contrast to the previously described coordination of the intact P_4 butterfly moiety, the reactions of **A** with $[Co_2(CO)_8]$ and $[Fe_2(CO)_9]$ induce a rearrangement of the P_4 unit. The reactions of **A** with these more reactive Lewis acids yield $[\{Cp'''(CO)_2Fe\}_2(\mu_4,\eta^{1:1:2:2}\text{-}P_4)\{Co(CO)_3\}_2]$ (**7**, Scheme 2) and $[\{Cp'''Fe(CO)_2\}_2(\mu_4,\eta^{1:1:1:3}\text{-}P_4CO)\{Fe(CO)_4\}\{Fe(CO)_3\}]$ (**8**, Scheme 2), respectively. During the formation of **7**, the P–P bond between the former bridgehead P atoms of **A** is selectively cleaved, affording an almost planar *cyclo*-P_4 moiety that is asymmetrically capped by two $[Co(CO)_3]$ fragments. Taking the rearrangement process one step further, one carbonyl group inserts into the *cyclo*-P_4 scaffold during the formation of **8**, resulting in a tetraphosphole structural motif. However, **8** is obtained from the reaction of **A** with $[Fe_2(CO)_9]$ only after additional rearrangement processes occur during the chromatographic work up or crystallization. A combination of IR and NMR spectroscopy, mass spectrometry and DFT calculations suggest that $[\{Cp'''Fe(CO)_2\}_2(\mu_4,\eta^{1:1:1:2}\text{-}P_4)\{Fe(CO)_4\}\{Fe(CO)_3\}]$ (**8′**) is initially formed from the reaction of **A** with $[Fe_2(CO)_9]$ and acts as an intermediate in the generation of **8**. Compound **8′** represents an intact molecule of **A** which coordinates towards a $[Fe(CO)_4]$ fragment in a terminal η^1-coordination mode while a second a $[Fe(CO)_3]$ fragment is coordinated in a chelating η^2-fashion.

Consequently, **A** has once again proven to be a valuable bidentate ligand in the generation of new chelating Lewis acid-P_4 butterfly adducts. Moreover, the conversion with more reactive Lewis led to the desired surge from mere coordination compounds towards original polyphosphorus ligand complexes.

8.3 Reactivity of P_4 butterfly compounds towards nucleophiles

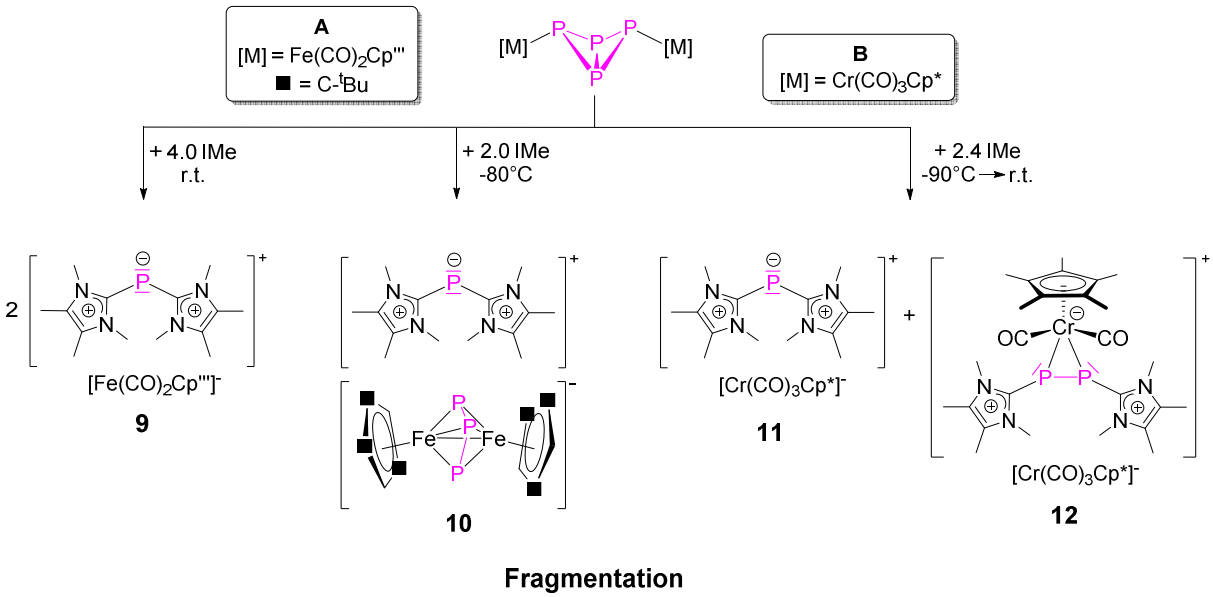

Scheme 3. Reactions of **A** and **B** with IMe under different reaction conditions.

While the reactivity of neutral P_4 butterfly complexes towards different Lewis acids has been the topic of previous reports[1] and parts of this thesis, no investigations concerning their reactivity towards nucleophiles have been published to the best of our knowledge. Therefore, **A** and **B** were reacted with the rather small *N*-heterocyclic carbene IMe (1,3,4,5-tetramethylimidazol-2-ylidene) to initiate the study of this hitherto unexplored reaction pathway.

The reaction of **A** with IMe is highly temperature depended. If the reaction is performed at room temperature, $[P(IMe)_2][Fe(CO)_2Cp''']$ (**9**) is obtained selectively alongside a red precipitate (most likely polyphosphorus aggregates). In contrast, performing the reaction at -80 °C affords $[P(IMe)_2][\{Cp'''Fe\}_2(\mu,\eta^{3:3}\text{-}P_3)]$ (**10**) as the exclusive product. The temperature driven formation of the anion suggests that **10** represents the kinetic product of the reaction while **9** is the thermodynamically favored product. If the reaction is repeated for **B**, two distinct products can be isolated simultaneously: $[P(IMe)_2][Cr(CO)_3Cp^*]$ (**11**) and $[[\{Cp^*Cr(CO)_2\}(\eta^2\text{-}P_2IMe_2)][Cr(CO)_3Cp^*]$ (**12**). The $[P(IMe)_2]^+$ cation found in **9**, **10** and **11** is well established and the evaluation of the molecular structure in the solid state depicts that the counter ion has only a marginal influence on the overall structural parameters of the cation. The $[\{Cp'''Fe\}_2(\mu,\eta^{3:3}\text{-}P_3)]^-$ anion of **10** can be formally described as a reduced version of $[\{Cp'''Fe\}_2(\mu,\eta^{3:3}\text{-}P_3)]$, the first binuclear complex which bears an allylic $\mu\text{-}P_3$ unit.[4] By comparison, the formal reduction results in the partial resolution of the allylic system and a notable widening of the structural scaffold. Intriguingly, **12** represents the first P_2 dumbbell that is stabilized by one bridging organometallic fragment as well as two NHC ligands in a trans conformation. The $\{Cr(CO)_2Cp^*\}$ fragment is coordinated by the P_2 dumbbell in an asymmetrical η^2-coordination mode, resulting in an AA′ spin system in the ^{31}P NMR spectrum. Comprehensive DFT calculations delineate a formal negative charge of the $\{Cp^*Cr(CO)_2\}$ fragment and a weak double bond character of the P_2 dumbbell with one localized lone pair of electrons on each P atom.

A variation in the stoichiometry of the reaction of **B** with IMe strongly influences the product distribution of **11** and **12** due to the intrinsic phosphorus/carbene ratios of the two products. By increasing the amount of IMe present in the reaction solution, the product distribution is clearly shifted towards **11** accompanied by the formation of byproducts and an increased amount of insoluble precipitate (Fig. 3).

In summary, the successful reactions of **A** and **B** with IMe are very intriguing and pave the way for further investigations of the reactivity of P_4 butterfly compounds towards nucleophiles. Especially the formation of **12**, a novel type of P_2 ligand complex, is an incentive to study this novel reaction pathway.

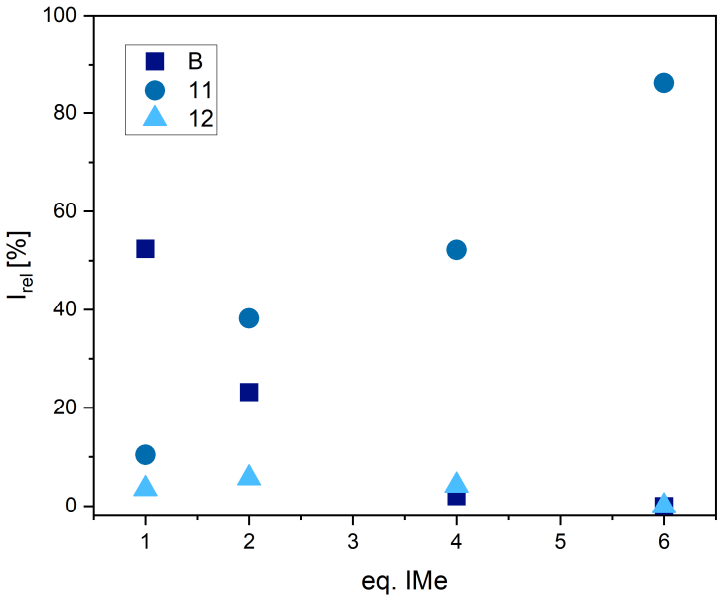

Figure 3. Relative integrals of the signals attributed to **B**, **11** and **12** in the experimental ^{31}P NMR spectra (recorded in thf with C_6D_6 capillary at 300 K) of reactions of **B** with varying equivalents of IMe in respect to the amount of IMe present in the reaction solution.

8.4 [{Cp*Cr(CO)$_3$}$_2$(μ,η$^{1:1}$-P$_4$)] as a starting material of P$_4$ butterfly transfer processes

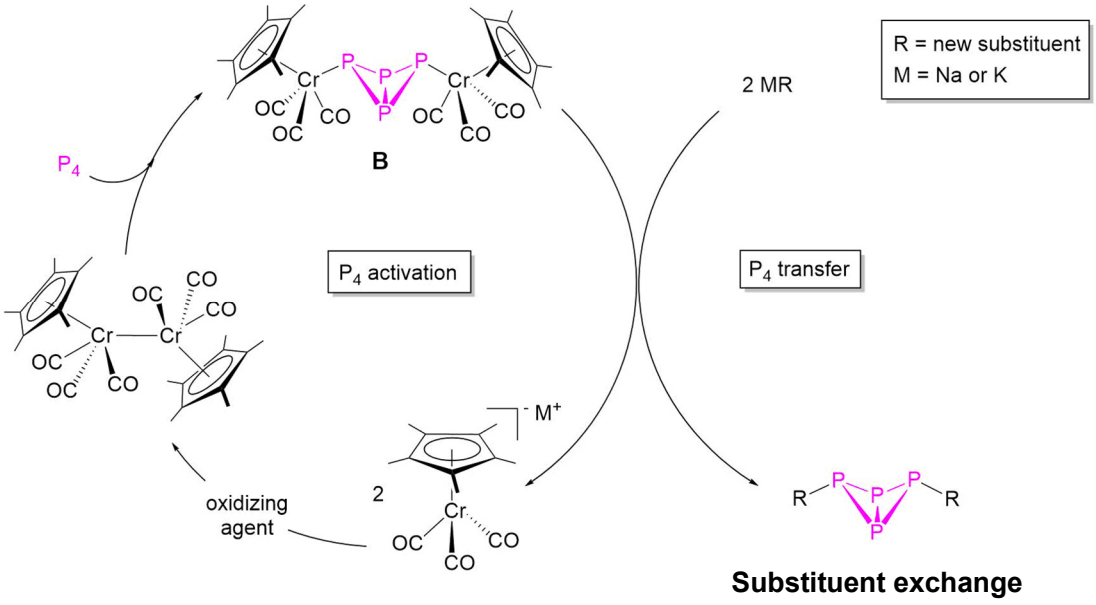

Scheme 4. Proposed P_4 activation/transfer reaction mechanism starting from **B**.

All reactions reported for P_4 butterfly compounds thus far focus on the transformation of the central P_4 unit affording either chelating coordination products or novel P_n ligand complexes. In contrast, little to no interest was taken in the transformation of the adjacent organic or organometallic substituents of the P_4 butterfly compounds. However, the rather labile P–Cr bond in **B** introduces a unique opportunity to investigate this as yet untouched field of research. As this bond represents the weakest link in **B**, the connection of the central P_4 butterfly motif towards the substituents is expected to be cleaved selectively under very mild reaction conditions. Consequently, an uncoordinated P_4 butterfly motif is a reasonable intermediate species available for the subsequent attachment towards newly introduced substituents. Hence, novel P_4 butterfly compounds might be obtained. Moreover, the isolation of the released $[Cp^*Cr(CO)_3]$ fragments of **B** might enable the recovery of the corresponding $[Cp^*Cr(CO)_3]_2$ dimer after conversion with a suitable reagent. Subsequently, $[Cp^*Cr(CO)_3]_2$ could be reacted with white phosphorus affording **B** and thereby closing the semi-catalytic P_4 activation/transfer cycle (Scheme 4).

The reaction of **B** with 2.0 eq. of $K[Cp'''Fe(CO)_2]$ or $NaCp'''$, respectively, affords the known P_4 butterfly compounds **A** and $[Cp'''_2(\mu,\eta^{1:1}\text{-}P_4)]$ (**13**), respectively, alongside 2.0 eq. of $K[Cp^*Cr(CO)_3]$. Consequently, it could be confirmed that **B** can be transformed into different known P_4 butterfly compounds via the suggested substituent exchange route. These encouraging results obviously shift the focus of attention towards the generation of novel P_4 butterfly compounds that hitherto could not be obtained via conventional synthetic pathways. However, from the reactions of **B** with various organometallic ($K[CpFe(CO)_2]$, $K[Cp^*Fe(CO)_2]$, $K[Cp'Mo(CO)_3]$, $K[CpW(CO)_3]$ and $Na[Cp'''W(CO)_3]$) and organic ($NaCp^*$, $[Ph_3C]^+$ and $[Ph_2CH]^+$) reagents no novel P_4 butterfly compounds could be obtained. Instead, IR and NMR spectroscopy depict a quantitative consumption of **B**, followed by the formation of a novel (P_4 butterfly) compound that instantly decomposes. However, the spectroscopic methods confirmed that the initial P–Cr bond cleavage occurred selectively supporting the utilization of **B** as a unique starting material in the novel substituent exchange pathway. However, as only known P_4 butterfly compounds could be obtained from this reaction pathway so far, further investigation must be carried out concerning the ideal reaction parameters and the stability of the desired products to ultimately obtain novel P_4 butterfly compounds.

8.5 Generation of a new chromium substituted *cyclo*-P_4 sandwich complex

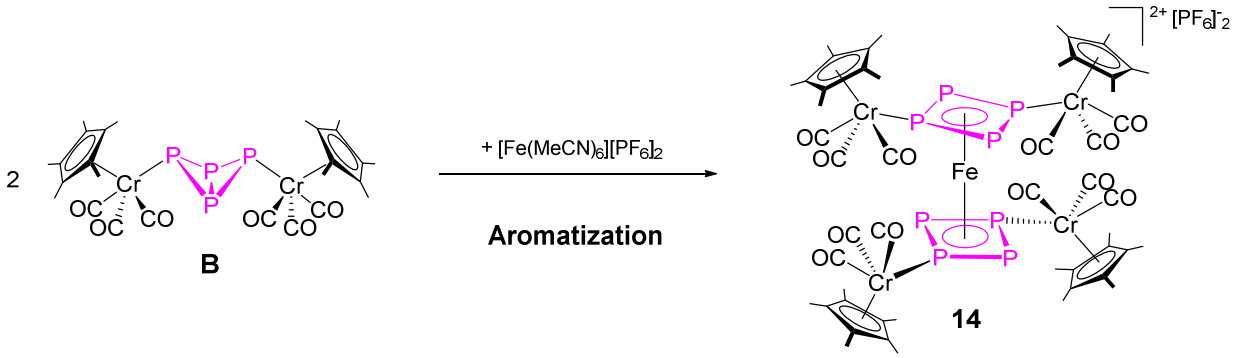

Scheme 5. Reaction of **B** with $[Fe(MeCN)_6][PF_6]_2$ affording **14**.

Since previous studies showed that reacting **A** with 0.5 eq. of $[Fe(MeCN)_6][PF_6]_2$ results in the formation of $[\{(Cp'''Fe(CO)_2)_2(\mu_3,\eta^{1:1:4}\text{-}P_4)\}_2Fe][PF_6]_2$ (**14′**)[1b], the analogous reaction was performed with **B** (Scheme 5). NMR spectroscopy and single crystal X-ray diffraction analysis confirmed that the isolobal compound $[\{(Cp^*Cr(CO)_3)_2(\mu_3,\eta^{1:1:4}\text{-}P_4)\}_2Fe][PF_6]_2$ (**14**) is obtained from the reaction of **B** with 0.5 eq. $[Fe(MeCN)_6][PF_6]_2$ and the structural parameters of **14** are very similar to those reported for **14′**. Hence, the isomerization process transforming **A** into a 6π-aromatic *cyclo*-P_4 ligand ultimately affording the *cyclo*-P_4 sandwich complex **14′** can be replicated for the analog chromium P_4 butterfly complex **B**.

In summary, the results presented in this thesis delineate various synthetic pathways originating from the P_4 butterfly structural motif. Next to coordination processes originating from the intact tetraphospha-*bicyclo*[1.1.0]butane structural motif numerous rearrangement, fragmentation and planarization pathways are described within this thesis. Consequently, the P_4 butterfly unit is a promising device in the synthesis of novel P_n ligands and irreplaceable for investigations concerning P_4 activation.

8.6 References

[1] (a) C. Schwarzmaier, S. Heinl, G. Balázs, M. Scheer, *Angew. Chem.* **2015**, *127*, 13309-13314; *Angew. Chem. Int. Ed. Engl.* **2015**, *54*, 13116-13121.
(b) J. Müller, S. Heinl, C. Schwarzmaier, G. Balázs, M. Keilwerth, K. Meyer, M. Scheer, *Angew. Chem.* **2017**, *129*, 7418-7423; *Angew. Chem. Int. Ed.* **2017**, *56*, 7312-7317.
(c) R. Grünbauer, *Master Thesis*, University of Regensburg (Regensburg), **2016**.

[2] (a) M. Scheer, E. Leiner, P. Kramkowski, M. Schiffer, G. Baum, *Chem. Eur. J.* **1998**, *4*, 1917-1923.
(b) M. Seidl, M. Schiffer, M. Bodensteiner, A. Y. Timoshkin, M. Scheer, *Chem. Eur. J.* **2013**, *19*, 13783-13791.

[3] (a) D. B. Lerner, W. J. Becktel, R. Everett, M. Goodman, D. R. Kearns, *Biopolymers* **1984**, *23*, 2157-2172.
(b) R. Streck, A. J. Barnes, *Spectrochimica Acta Part A* **1999**, *55*, 1059-1076.

[4] M. Scheer, S. Deng, O. J. Scherer, M. Sierka, *Angew. Chem. Int. Ed.* **2005**, *44*, 3755-3758.

9. Appendices

9.1 List of abbreviations

General abbreviations

Å	Angstroem, 1 Å = $1 \cdot 10^{-10}$ m
AIM	Atoms in Molecules
Ar^{Dipp}	2,6-(2,6-$^{i}Pr_2C_6H_3)_2C_6H_3$
BCP	bond critical points
butterfly	*bicyclo*[1.1.0]butane
°C	degree Celsius
CAAC	cyclic alkyl-(amino)carbene
cHex	*cyclo*-hexane, C_6H_{11}
Cp	cyclopentadienyl, C_5H_5
Cp′	1-*tert*-butylcyclopentadienyl, $C_5H_4{}^{t}Bu$
Cp″	1,3-di-*tert*-butylcyclopentadienyl, $C_5H_3{}^{t}Bu_2$
Cp‴	1,2,4-tris-*tert*-butylcyclopentadienyl, $C_5H_2{}^{t}Bu_3$
Cp*	pentamethylcyclopentadienyl, $C_5(CH_3)_5$
Cp^{BIG}	penta-4-*n*-butylphenylcyclopentadienyl, $C_5(4\text{-}{}^{n}BuC_6H_4)_5$
Cp^{4iPr}	1,2,3,4-tetra-*iso*-propylcyclopentadienyl, $C_5H{}^{i}Pr_4$
Cp^{R}	cyclopentadienyl derivative (specified in text)
d	day(s)
DBU	1,8-diazabicyclo[5.4.0]undec-7-ene
DFT	density functional theory
Dipp	2,6-diisopropylphenyl, 2,6-$(CH(CH_3)_2)_2C_6H_3$
dme	1,2-dimethoxyethane
Dmp	2,6-(2,4,6-$(CH_3)_3C_6H_2)_2C_6H_3$
dppe	bis(diphenylphosphino)ethane
dppm	1,2-bis(diphenylphosphino)methane
DTA	Differential Thermal Analysis
E	group 15 element (specified in text)
e^{-}	electron(s)
et al.	et alii (“and others”),
eV	electronvolt, 1 eV = $1.60217657(4) \cdot 10^{-19}$ J
EI-MS	electron ionization mass spectroscopy
eq.	equivalent(s)
ESI-MS	electron spray ionization mass spectroscopy
Fig.	Figure
LIFDI-MS	liquid injection field desorption ionization mass spectroscopy
h	hour(s)
HOMO	highest occupied molecular orbital
IDipp	1,3-bis(2,6-diisopropylphenyl)imidazol-2-ylidene
IMe	1,3,4,5-tetramethylimidazol-2-ylidene
IMes	1,3-bis(2,4,6-trimethylphenyl)imidazol-2-ylidene
^{i}Pr	*iso*-propyl, $CH(CH_3)_2$
K	degree Kelvin
L	ligand (specified in text)

LA	Lewis acid
LB	Lewis base
LUMO	lowest unoccupied molecular orbital
M	metal (specified in text)
$[M^+]$	molecular ion
Me	methyl, CH_3
Menthyl	2-CH_3,6-^{i}Pr-C_6H_9
Mes*	2,4,6-^{t}Bu$_3$C$_6$H$_2$
m/z	mass to charge ratio
nbd	norbornadiene, *bicyclo*[2.2.1]hepta-2,5-diene
^{n}Bu	*n*-butyl, C_4H_9
NBO	natural bond orbital
NHC	*N*-heterocyclic carbene
np_3	tris(2-diphenylphosphinoethyl)amine
NPA	Natural Population Analysis
Nu	nucleophile (specified in text)
Ph	Phenyl, C_6H_5
R	(organic) substituent (specified in text)
RCP	ring critical points
r.t.	room temperature
sMes	2,4,6-^{t}Bu$_3$C$_3$H$_2$
T	temperature
Tef	$[Al(OC(CF_3)_3)_4]^-$
Ter	2,6-(2,4,6-$(CH_3)_3C_6H_2)_2C_6H_3$
TMS	*tetra*-methylsilane, $Si(CH_3)_4$
^{t}Bu	*tert*-butyl, $C(CH_3)_3$
thf	tetrahydrofurane, C_4H_8O
tht	tetrahydrothiophene
VE	valence electrons
VT	variable temperature
WBI	Wiberg Bond Index
X-ray	Röntgen radiation

Interpretation of NMR spectra

br	broad signal
d	doublet
δ	chemical shift
Hz	Hertz = s^{-1}
J	coupling constant
m	multiplet
NMR	nuclear magnetic resonance
ppm	parts per million
s	singlet
t	triplet
v	resonance frequency

Interpretation of IR spectra

br	broad signal
IR	infrared spectroscopy
m	medium
s	strong
$\tilde{\nu}$	wavenumber
w	weak

9.2 List of numbered compounds

A $[(np_3)Ni(\eta^1\text{-}P_4)]$

B $[Ag(\eta^2\text{-}P_4)_2][Al(OC(CF_3)_3)_4]$

C $[(PPh_3)_2RhCl(\eta^{1:1}\text{-}P_4)]$

D″ $[\{Cp''Fe(CO)_2\}_2(\mu,\eta^{1:1}\text{-}P_4)]$

D‴ $[\{Cp'''Fe(CO)_2\}_2(\mu,\eta^{1:1}\text{-}P_4)]$

D* $[\{Cp^*Cr(CO)_3\}_2(\mu,\eta^{1:1}\text{-}P_4)]$

E $[\{sMes\}_2(\mu,\eta^{1:1}\text{-}P_4)]$

F $[Cp^*Nb(CO)_2(\eta^4\text{-}P_4)]$

G $[\{Zr(PhP\text{-}(CH_2SiMe_2NSiMe_2CH_2)_2\text{-}PPh)\}_2(\mu,\eta^{4:4}\text{-}P_4)]$

H $[(^{menthyl}CAAC)_2P_4]$

I $[(^{cHex}CAAC)_3P_4]$

J $[CH_3C(CH_2PPh_2)_3Co(\eta^3\text{-}P_3)]$

K $[\{CH_3C(CH_2PPh_2)_3Ni\}_2(\mu,\eta^{3:3}\text{-}P_3)](BF_4)_2$

L $[\{CpMo(CO)_2\}_2(\mu,\eta^{2:2}\text{-}P_2)]$

M $[(^{cHex}CAAC)_2P_2]$

N $[\{CpMn(CO)_2\}_2(\mu_3,\eta^{1:1:1}\text{-}P)_2\{Fe_2(CO)_6\}]$

O_{Mo} $[PMo(Me_3SiNCH_2CH_2)_3N]$

O_W $[PW(Me_3SiNCH_2CH_2)_3N]$

P $[PMo(N(^tBu)Ar)_3]$

Q $[\{Cp^*Cr\}_2(\mu,\eta^{5:5}\text{-}P_5)]$

R $[Cp^*Fe(\eta^5\text{-}P_5)]$

S $[Ti(\eta^5\text{-}P_5)_2]^{2-}$

T $[\{Cp^*Mo\}_2(\mu,\eta^{6:6}\text{-}P_6)]$

U $[\{Cp^*Ti\}_2(\mu,\eta^{3:3}\text{-}P_6)]$

D_A $[\{Cp''Fe(CO)\}(\mu,\eta^{2:1}\text{-}P_4)\{Fe(CO)_2Cp''\}]$

D_B $[\{Cp''Fe\}(\mu,\eta^{4:1}\text{-}P_4)\{Fe(CO)_2Cp''\}]$

D_C $[\{Cp''Fe\}(\eta^4\text{-}P_4Fe(CO)Cp'')]$

D_D $[\{Cp''Fe\}_2(\mu,\eta^{4:4}\text{-}P_4)]$

D_E $[\{Cp'''Fe\}_2(\mu,\eta^{4:4}\text{-}P_4)]$

D_F $[Cp'''Fe(\eta^5\text{-}P_5)]$

D_G $[\{Cp'''Fe\}_2(\mu,\eta^{2:2}\text{-}P_2)\mu\text{-}CO]$

D_H $[\{Cp'''Fe\}_2(\mu\text{-}P)_2]$

D_I $[Cp'''Fe(\eta^5\text{-}P_3C_2Ph_2)]$

D_J $[\{Cp'''Fe(CO)_n\}_3P_{11}]$

D_K $[Cp'''Fe(\eta^5\text{-}P_4C^tBu)]$

D_L $[Cp'''Fe(\eta^5\text{-}P_3(C^tBu)_2)]$

D_M $[\{Cp'''Fe\}_2(\mu,\eta^{3:3}\text{-}P_3)]$

D_N $[\{Cp'''Fe(CO)_2\}_2(\mu_3,\eta^{1:1:1:1}\text{-}P_4)\{Cu(CH_3CN)\}][BF_4]$

D_O $[\{(Cp'''Fe(CO)_2)_2(\mu_3,\eta^{1:1:1:1}\text{-}P_4)\}_2Cu][BF_4]$

D_P $[\{Cp'''Fe(CO)_2\}\{Cp'''Fe(CO)\}(\mu_4,\eta^{1:1:1:1:2}\text{-}P_4)\{CuI\}]_2$

D_Q $[\{Cp'''Fe(CO)_2\}_2(\mu_3,\eta^{1:1:1:1}\text{-}P_4)\{FeBr_2\}]$

D_R $[\{(Cp'''Fe(CO)_2)_2(\mu_3,\eta^{1:1:4}\text{-}P_4)\}_2Fe][PF_6]_2$

9.3 Acknowledgements

Finally, I would like to express my gratitude to:

- Prof. Dr. Manfred Scheer for providing good working conditions and his interest in my academic and personal progress.
- Dr. Gábor Balázs for many valuable pieces of advice and numerous DFT calculations.
- The “Fonds der Chemischen Industrie” for a Ph. D. scholarship.
- Dr. Michael Bodensteiner, Dr. Stefanie Gärtner and their team of the X-ray diffraction analysis department for help with any X-ray related problem.
- Dr. Ilya Shenderovich, Anette Schramm, Georgine Stühler and Fritz Kastner for the measurement of my NMR spectra.
- Josef Kirmeier and Wolfgang Söllner for recording my mass spectra.
- Helmut Schüller, Barbara Baumann and Wilhelmine Krutina for the elemental analyses.
- The team of the Glasbläser and Werkstätten for repairing things quickly.
- Dr. Michael Seidl for the final review of my X-ray diffraction data.
- Dr. Dirk Herrmann for proofreading parts of this thesis.
- Barbara Bauer for help with any (administrative) problem.
- My friends and family for their enduring support especially during the hard and trying times.
- Jana: without you, this time would have been a lot darker.